Seismic Performance of Steel Plate Girder Bridges with Integral Abutments

Publication No. FHWA-HIF-11-043 **August 2011**

U.S. Department of Transportation
Federal Highway Administration

1. Report No	2. Government Accession No.	3. Recipient's Catalog No.
FHWA-HIF-11-043	XXX	XXX

4. Title and Subtitle	5. Report Date
Seismic Performance of Steel Plate Girder Bridges with Integral Abutments	August 2011
	6. Performing Organization Code XXX
7. Authors	8. Performing Organization Report No.
Ahmad M. Itani and Gokhan Pekcan	UNR/CCEER-10-08
9. Performing Organization Name and Address Department of Civil and Environmental Engineering University of Nevada, Reno, Nevada 89557-0208 Fax: A. Itani: (775) 784-1362, e-mail: itani@unr.edu	10. Work Unit No. (TRAIS) XXX
	11. Contract or Grant No. XXX
12. Sponsoring Agency Name and Address FHWA Office of Bridge Technology 1200 New Jersey Ave SE Washington DC 20590	13. Type of Report and Period Covered XXX
	14. Sponsoring Agency Code XXX

15. Supplementary Notes

The research and development project herein were performed in the Center for Civil Engineering Earthquake Research at the University of Nevada, Reno. The project was sponsored by the Federal Highway Administration. The opinions expressed in this report are those of the authors and do not necessarily reflect the views of the University of Nevada, Reno, the Sponsor, or the individuals whose names appear in this report.

16. Abstract

This report presents the results of a pilot study on the seismic behavior and response of steel bridges with integral abutments. Analytical investigations were conducted on computational models of steel bridges with integral abutments to determine their seismic behavior as a system and to develop seismic design guidelines. The effect of the superstructure flexibility due to inadequate embedment length was investigated using 3D finite element models. This flexibility, modeled as translational and rotational springs, proved to have significant effect on the overall bridge dynamic characteristics in terms of periods and critical mode shapes. Lateral and longitudinal load paths and the seismic response were investigated using modal pushover and nonlinear time history analyses. A limited investigation on the effect of skew was conducted on a single-span integral abutment bridge. A procedure for incorporating the system level damping due to the yielding and inelastic responses of various components was proposed for use in the seismic analysis. Based on the analytical investigations and available experimental research, guidelines for the seismic analysis and design of integral abutment bridges were developed.

17. Key Words	18. Distribution Statement
Integral Abutment, Seismic Design, Steel Bridges, Piles, Soil-Structure Interaction, Earthquake Engineering	No restrictions. This document is available to the public through the National Technical Information Service, Springfield VA 22161

19. Security Classif. (of this Report)	20. Security Classif. (of this page)	21. No. of Pages	22. Price
Unclassified	Unclassified	165	$XXX.XX

FOREWORD

Integral abutment bridges designed without the use of expansion joints are gaining wider acceptance, because they cost less to build and require less effort to maintain. They have a track record of good in-service performance. However, there is a lack of seismic design guidelines and information in seismic behavior and response of steel plate girder bridges with integral abutments. This FHWA sponsored pilot study performed computer model analysis to investigate factors that are expected to affect the behavior and response of steel bridges. The study finds that the performance of steel bridges with integral abutments may be better than the convention seat-type abutment bridges. Based on the results, guidelines are proposed for the design and computer modeling of steel bridges with integral abutments, and for analytical modeling of the nonlinear response of steel piles used for the abutments.

This report will be of interest to the researchers and bridge engineers involved in the design and analysis of steel plate girder bridges.

M. Myint Lwin, Director

Office of Bridge Technology

Notice

This document is disseminated under the sponsorship of the U.S. Department of Transportation in the interest of information exchange. The U.S. Government assumes no liability for the use of the information contained in this document. This report does not constitute a standard, specification, or regulation.

The U.S. Government does not endorse products or manufacturers. Trademarks or manufacturers' names appear in this report only because they considered essential to the objective of the document.

Quality Assurance Statement

The Federal Highway Administration (FHWA) provides high-quality information to serve Government, industry, and the public in a manner that promotes public understanding. Standards and policies are used to ensure and maximize the quality, objectivity, utility, and integrity of its information. FHWA periodically reviews quality issues and adjusts its programs and processes to ensure continuous quality improvement.

SI* (MODERN METRIC) CONVERSION FACTORS

APPROXIMATE CONVERSIONS TO SI UNITS

Symbol	When You Know	Multiply By	To Find	Symbol
		LENGTH		
in	inches	25.4	millimeters	mm
ft	feet	0.305	meters	m
yd	yards	0.914	meters	m
mi	miles	1.61	kilometers	km
		AREA		
in^2	square inches	645.2	square millimeters	mm^2
ft^2	square feet	0.093	square meters	m^2
yd^2	square yard	0.836	square meters	m^2
ac	acres	0.405	hectares	ha
mi^2	square miles	2.59	square kilometers	km^2
		VOLUME		
fl oz	fluid ounces	29.57	milliliters	mL
gal	gallons	3.785	liters	L
ft^3	cubic feet	0.028	cubic meters	m^3
yd^3	cubic yards	0.765	cubic meters	m^3
		NOTE: volumes greater than 1000 L shall be shown in m^3		
		MASS		
oz	ounces	28.35	grams	g
lb	pounds	0.454	kilograms	kg
T	short tons (2000 lb)	0.907	megagrams (or "metric ton")	Mg (or "t")
		TEMPERATURE (exact degrees)		
°F	Fahrenheit	5 (F-32)/9 or (F-32)/1.8	Celsius	°C
		ILLUMINATION		
fc	foot-candles	10.76	lux	lx
fl	foot-Lamberts	3.426	$candela/m^2$	cd/m^2
		FORCE and PRESSURE or STRESS		
lbf	poundforce	4.45	newtons	N
lbf/in^2	poundforce per square inch	6.89	kilopascals	kPa

APPROXIMATE CONVERSIONS FROM SI UNITS

Symbol	When You Know	Multiply By	To Find	Symbol
		LENGTH		
mm	millimeters	0.039	inches	in
m	meters	3.28	feet	ft
m	meters	1.09	yards	yd
km	kilometers	0.621	miles	mi
		AREA		
mm^2	square millimeters	0.0016	square inches	in^2
m^2	square meters	10.764	square feet	ft^2
m^2	square meters	1.195	square yards	yd^2
ha	hectares	2.47	acres	ac
km^2	square kilometers	0.386	square miles	mi^2
		VOLUME		
mL	milliliters	0.034	fluid ounces	fl oz
L	liters	0.264	gallons	gal
m^3	cubic meters	35.314	cubic feet	ft^3
m^3	cubic meters	1.307	cubic yards	yd^3
		MASS		
g	grams	0.035	ounces	oz
kg	kilograms	2.202	pounds	lb
Mg (or "t")	megagrams (or "metric ton")	1.103	short tons (2000 lb)	T
		TEMPERATURE (exact degrees)		
°C	Celsius	1.8C+32	Fahrenheit	°F
		ILLUMINATION		
lx	lux	0.0929	foot-candles	fc
cd/m^2	$candela/m^2$	0.2919	foot-Lamberts	fl
		FORCE and PRESSURE or STRESS		
N	newtons	0.225	poundforce	lbf
kPa	kilopascals	0.145	poundforce per square inch	lbf/in^2

*SI is the symbol for the International System of Units. Appropriate rounding should be made to comply with Section 4 of ASTM E380.
(Revised March 2003)

TABLE OF CONTENTS

LIST OF FIGURES

LIST OF TABLES

ACKNOWLEDGEMENT

Partial funding for the study presented in this report was provided by the Federal Highway Administration (FHWA) through a contract (DTFH61-07-D-00004 – Task Order 003) with HDR Engineering, Inc. The authors would also like to acknowledge Mr. Edward Wasserman, Mr. Vasant Mistry and Dr. Brian Kozy of FHWA; and Mr. John Yadlosky of HDR Engineering, Inc. for their valuable comments and feedback. Also, the valuable help of Prof. Edwin Burdette and Prof. Qiuhong Zhao of University of Tennessee at Knoxville are acknowledged.

DISCLAIMER

EXECUTIVE SUMMARY

This report presents the results of a pilot study on the seismic behavior and response of steel bridges with integral abutments. Analytical investigations were conducted on computational models of steel bridges with integral abutments to determine their seismic behavior as a system and to develop seismic design guidelines. The effect of the superstructure flexibility due to inadequate embedment length was investigated using 3D finite element models. This flexibility, modeled as translational and rotational springs, proved to have significant effect on the overall bridge dynamic characteristics in terms of periods and critical mode shapes. Lateral and longitudinal load paths and the seismic response were investigated using modal pushover and nonlinear time history analyses. A limited investigation on the effect of skew was conducted on a single-span integral abutment bridge. A procedure for incorporating the system level damping due to the yielding and inelastic responses of various components was proposed for use in the seismic analysis. Based on the analytical investigations and available experimental research, guidelines for the seismic analysis and design of integral abutment bridges were developed.

A 3D finite element model of a typical girder-abutment connection was developed to establish the stiffness properties of the nonlinear springs used to represent the connection flexibility. These springs, along with springs that define the abutment-soil and soil-pile interactions, were utilized in global 3D bridge computational models to determine their effect on the overall bridge structural dynamics. This investigation has shown that the typical girder embedment length is insufficient to ensure a rigid connection. It was shown that the connection flexibility increased the vibration period of the main transverse translation mode up to 50%. As such, a procedure for calculating the minimum required girder-abutment embedment length to achieve a rigid connection was developed.

The seismic load paths in the longitudinal and transverse directions of a three-span integral abutment bridge were determined using pushover analysis for the dominant translational modes. In the longitudinal direction, a large percentage (72%) of the seismic force was resisted by the abutment-soil passive resistance. In the transverse direction, the overall response was governed by the soil-pile interaction. About 40% of the transverse seismic force was resisted by the soil-pile interaction for each abutment. This shows that the columns in integral abutment bridges were subjected to low seismic forces, thus limiting their damage during seismic events.

A limited investigation on the effect of skew was conducted on a single-span bridge with integral abutments to determine the effect of skew on the dynamic properties and seismic load path. Three models were developed: a) no skew, b) 45-degree skew, and c) 60-degree skew. The results of the analyses showed that the variation of the skew angle caused significant changes in the bridge dynamic characteristics in terms of periods and

mode shapes. It was also shown that the translational modes in the skew bridge are highly coupled between the longitudinal and the transverse translations.

The effectiveness of steel bridges with integral abutments in high seismic zones was also investigated. Three global computational models of three span bridges were developed: (a) integral abutment bridge with piles that have strong axis parallel to abutment axis (3SIAB-PSA), (b) integral abutment bridge with pile strong axis perpendicular to abutment axis (3SIAB-PWA), and (c) seat-type abutment bridge (3SSAB). Nonlinear time history analyses were performed using a suite of artificially generated ground motions matching the AASHTO design spectrum.

The following observations and conclusions were made based on the comparison of the responses of 3SIAB-PSA and 3SIAB-PWA:

- The 3SIAB-PSA performed better than 3SIAB-PWA in terms of the nonlinear response of piles. Thus, the pile strong axis should be oriented parallel to the abutment axis in seismic zones.

- Due to the pile axis orientation, the abutments in 3SIAB-PWA were stiffer in the transverse direction than those in 3SIAB-PSA. This increased the seismic demands at the abutments of 3SIAB-PWA.

- The pile axis orientation was insignificant in the longitudinal direction because this response was dominated by the abutment-soil interaction.

The following observations and conclusions were made based on the comparison of the responses of the integral abutment bridges (3SIAB-PSA and 3SIAB-PWA) and the seat-type abutment bridge (3SSAB):

- The seismic performances of the integral abutment bridges were better than the seat-type abutment bridge in terms of overall displacements and column forces.

- Large displacements were observed in 3SSAB in the longitudinal and transverse directions. The longitudinal displacement in 3SSAB was almost twice the displacement of the integral abutment bridges. Thus, a relatively large seat width should be provided for the seat type bridge due to these large displacements.

- In 3SSAB, all of the seismic forces in the transverse direction were resisted by the columns only. Thus, these columns will experience large inelastic activity (damage) after an earthquake which may require their replacement or bridge removal after severe ground motions.

Seismic design guidelines were developed based on the analytical investigations and available experimental research. The guidelines include the calculation of the embedment lengths, evaluation of pile displacement capacity, and system damping. In

addition, guidelines for analytical modeling of the nonlinear response of steel piles were presented. A pile displacement capacity that produces 10% radian rotation is recommended based on the available experimental research. It was noted that because of the confinement provided by the soil, the piles can sustain large ductility demand as long as the pile has sufficient embedment length into the abutment.

It was shown that a typical girder-abutment connection introduces flexibility in the system, and sufficient embedment length is required to make the rigid connection assumption valid. Thus, equations for determining the required minimum embedment length of steel girders into the abutment to ensure connection rigidity were proposed. These equations were also used to determine the embedment length of piles into the abutment to develop their plastic flexural capacity.

A procedure for evaluating the system level damping was developed. This procedure accounts for the yielding and inelastic response of various components such as abutment-soil interaction, soil-pile interaction, pile inelasticity, and column inelasticity. The system level damping was evaluated in the main longitudinal and transverse translation modes based on pushover analysis. The calculated damping should be applied to these two modes only while performing response spectrum analysis. A detailed example is presented in a step-by-step procedure to illustrate the use of the recommended design guidelines.

Chapter 1 INTRODUCTION

Recent earthquakes in California and Japan exposed the vulnerability of steel plate girder superstructures to seismic loads (Caltrans 1992; Astaneh-Asl et al. 1994; Bruneau et al. 1996). Various components of steel superstructures such as support cross frames, shear connectors, and bearings were damaged during these events. The observed damage showed that the aforementioned components are in the seismic load path and should be designed and detailed to withstand large cyclic deformations. Furthermore, experimental, analytical and field investigations have shown that adequate seismic performance of bridges depends on the presence of a reliable seismic load path and adequate detailing. Along this load path, specific elements may be designed and detailed to yield at a prescribed level, thus limiting the seismic forces on bridges regardless of the magnitude of the earthquake ground motions.

The seismic response of bridges with integral abutments is mainly dominated by the abutment-soil interaction in the longitudinal direction and soil-pile interaction in the transverse direction. This response will reduce the seismic demand on the piers and their footing. However, it will place larger demand on the piles of the integral abutments since they will be subjected to large cyclic deformations. With proper seismic design of the pile anchorage and seismic detailing of steel piles (b/t ratio and Kl/r), it is expected that these piles will perform adequately under the design level earthquake (return period of 1000 years). This pile behavior was proven experimentally by quasi-static cyclic testing of large scale steel piles that were used for the retrofit of California long span bridges (Astaneh-Asl et al. 1998) and by field experiments (Burdette et al. 2000; 2004; 2007).

In steel bridges with integral abutments, the inelastic action of the piles that are detailed for large cyclic deformation will limit the seismic forces on the components along the load path (Itani and Sedarat 2000). Preliminary analytical investigations by Itani and Sedarat (2000) have shown that the seismic response of the piles will limit the seismic force on bridge columns in the longitudinal and transverse directions.

However, there is a lack of information on the seismic system response of steel bridges with integral abutments. This information will enable bridge engineers to assess the benefit of using integral abutments in high seismic zones. To understand their seismic response, experimental and analytical investigations should be performed. This study presents a pilot investigation on the seismic behavior of integral abutment bridges using local and global computational models.

The objectives of this research are to:

- Establish realistic boundary conditions for steel girder-abutment connection and determine its effect on the overall seismic behavior of integral abutment bridges.

- Investigate the longitudinal and lateral behavior of straight and skew steel bridges with integral abutments.
- Establish the seismic response of steel bridges with integral abutments under large earthquake ground motions.
- Develop preliminary guidelines for the seismic design of steel bridges with integral abutments.

To achieve the above objectives five research tasks have been completed and presented in the subsequent chapters of this report:

- Task 1: Literature Review
- Task 2: Mathematical Models for Steel Girder Bridges with Integral Abutments
- Task 3: Seismic Load Path in Straight and Skew Bridges
- Task 4: Seismic Response of Steel Bridges with Integral Abutments
- Task 5: Seismic Design Guidelines and Design Example

1.1 GENERAL

Integral abutment bridges (IABs) are jointless bridges where the deck is continuous and connected monolithically to abutment wall with a rigid connection. Typically, a line of vertical piles under the abutment wall is used to carry vertical bridge loads and provide restraint for thermal loading. The rationale for integral abutments is presented by Wasserman (2007) and Wasserman and Walker (1996). A typical and common detail of a steel girder superstructure with integral abutment is shown in Figure 1-1.

Throughout the US, integral abutment bridges are becoming a design choice for short to moderate spans (Civjan et al. 2007). Integral abutment bridges designed and constructed in a variety of configurations have typically performed well under service loading (Soltani and Kukreti 1992; Burke 1993; Kunin and Alampalli 2000; Arockiasamy et al. 2004; Conboy and Stoothoff 2005).

A 2004 survey of the US DOTs practices, policies, and design criteria was reported at the 2005 FHWA Integral Abutment and Jointless Bridge Conference by Maruri and Petro (2005). The survey included questions regarding the number of integral abutments designed, built and in service, the criteria used for design and construction, span lengths, total bridge length, skew and curvature limitations, as well as reported problems experienced with jointless bridge construction.

In the 2004 survey, 77% of the responding agencies indicated that they would design integral and semi-integral abutments whenever possible. The approximate numbers of IAB designed and built since 1995 and in service are shown in Table 1-1. The maximum span and total bridge lengths are shown in Table 1-2 for steel and prestressed concrete bridges. Also, some states specify the limit of horizontal abutment movement as shown in Table 1-3.

According to the 39 agencies who responded to the survey (Table 1-1), there are approximately 13,000 jointless bridges on public highways; 9,000 equipped with fully integral abutments, and 4,000 with semi-integral abutments (integral superstructure/backwall connections that move according to the thermal demands, but independent of the vertical load support system). The aggregate number of jointless bridges is twice the number reported in a similar survey for a previous Integral Abutment Jointless Bridge Conference held in 1995. Analysis of the survey found that there was a lack of uniformity in usage and ranges of applicability. For instance, 59 percent of responding agencies had over 50 jointless bridges in service, 31 percent had 101 to 500 in service, 3 percent had 501 to 1000, and 15 percent had over 1000 such bridges in service.

Permissible lengths for jointless prestressed concrete girder bridges ranged from 45.7 m to 358 m, allowable skews from 15^{o} to 70^{o}, and no limit on curvatures was reported. State Route 50 over Happy Hollow Creek in Tennessee is an example of the upper limits of an integral abutment jointless bridge that can be achieved. The structure is 358 m in length on a 4.5^{o} curve. Reported steel girder bridge lengths range from 36.6 m to 167.7 m.

Yannotti et al (2006) reported on the integral abutment design practice in New York State as follows:

1. Bridge Length: less than 198.1 m (650 ft) without limitation on individual span length
2. Maximum Skew: maximum 45^{o}
3. Abutment reveal: less than 1.5 m (5 ft) which is the dimension from the bottom of the girder to the finished grade under the bridge at the abutment stem.
4. Curvature: Curved integral bridge is not permitted.
5. Maximum Bridge Grade: Maximum 5%
6. Steel H-piles or cast-in-place concrete piles are used; however cast-in-place concrete piles may only be used when the total bridge length is less than 48.8 m (160 ft).
7. Steel H-piles are oriented with the strong axis parallel to the girders so that bending occurs about the weak axis of the pile to allow easy accommodation of the bridge movement.
8. Piles must be driven a minimum of 6.1 m (20 ft) and are placed in pre-augured 3.0 m (10 ft) deep holes if the bridge length exceeds 30.5 m (100 ft).
9. Wing walls are separated from abutment stems when their length exceeds 4.0 m (13 ft) to minimize the bending moment caused by passive earth pressures.
10. Piles are designed to carry vertical loads equally and there is no explicit requirement to consider bending moment in piles.

FHWA and NHI (National Highway Institute) published LRFD Design Example for Steel Girder Superstructure Bridge (FHWA 2003b) and Comprehensive Design Example for Prestressed Concrete Girder Superstructure Bridge with Commentary (FHWA 2003a). A

reference in these examples is made to the selection of the type of abutment including integral abutment and semi-integral abutment, and worked examples are provided. American Iron and Steel Institute (AISI) and National Steel Bridge Alliance (NSBA) also published a manuscript titled “Integral Abutment for Steel Bridges” as part of the Highway Structures Design Handbook (Wasserman and Walker 1996).

1.2 ADVANTAGES AND LIMITATIONS OF INTEGRAL ABUTMENT BRIDGES

Integral abutment bridges cost less to construct and require less maintenance than equivalent bridges with expansion joints. In addition to reduction in construction cost and future maintenance costs, integral abutments also provide for efficiencies in the overall structure design. Integral abutment bridges have numerous attributes and few limitations. Some of the more important attributes are summarized below (Mistry, 2000):

- Simple Design: Abutments and piers of a continuous bridge are each supported by a single row of piles attached to the superstructures. Therefore, a continuous frame with a single horizontal member and two or more vertical members can be used for analysis and design purposes.
- Jointless construction: Is the primary attribute of the integral abutment bridges that has numerous advantages.
- Resistance to pressure: The jointless construction of integral bridges distributes longitudinal pavement pressures over a total superstructure area substantially greater than that of the approach pavement cross-section.
- Rapid construction: One row of vertical piles is usually used. The back wall can be cast simultaneously. Expansion joints and bearings are not needed. The normal delays and the costs associated with bearings and joints installation, adjustment, and anchorages are eliminated. Tolerance problems are reduced or eliminated.
- Ease in constructing embankments: Most embankments are made by large earth moving and compaction equipment.
- No cofferdams: Integral abutments are generally built with capped pile piers or drilled-shaft piers that do not require cofferdams.
- Simple forms: Since pier and abutment pile caps are usually of a simple rectangle shape they require simple forms.
- Reduced removal of existing elements: Integral abutment bridges can be built around the existing foundations without requiring the complete removal of existing substructures.
- Simple beam seats: Preparation of load surface for seat width can be simplified or eliminated in integral bridge construction.
- Greater end span ratio ranges: Integral abutment bridges are more resistant to uplift. Integral abutment weight acts as counterweights. Thus, a smaller end span to interior span ratio can be used without providing for expensive hold-downs to expansion bearings.

- Improved ride quality: Smooth jointless construction improves vehicular riding quality and diminishes vehicular impact stress levels.
- Design efficiency: Design efficiencies are achieved in substructure design. Longitudinal and transverse loads acting upon the superstructure may be distributed over more number of supports.
- Improved Load distribution: Loads are given broader distribution through the continuous and full-depth end diaphragm.
- Added redundancy and capacity for seismic events: Integral abutments provide added redundancy and capacity. Joints in seat-type abutment bridges introduce a potential collapse mechanism into the overall bridge structure. Integral abutments eliminate the most common cause of damage to bridges in seismic events which is loss of girder support. Integral abutments have consistently performed well in actual seismic events and significantly reduced or avoided problems such as back wall and bearing damage, associated with seat type jointed abutments. Jointless design is preferable for highly seismic regions.

However, limitations in the use of integral abutments include:

1. Need for approach slabs.
2. Joints at the end of the approach slab
3. Uncertainty of the pile flexural stresses in the loaded piles.
4. Imposed limits by some DOTs on the length and skew of the bridge.

In addition to primary loads such as gravity, wind, and seismic loads, integral abutment bridges are also subjected to secondary effects that include creep and shrinkage, thermal gradients, differential settlement and differential deflections, and pavement relief pressures when moisture and sustained high temperatures trigger pavement growth. Under static and/or dynamic loading conditions, soil-pile and abutment-soil interaction has been known to have significant effect on the overall performance and response of integral abutment bridges. This is discussed in more detail within the context of seismic response characteristics and with reference to published research.

1.3 SEISMIC RESPONSE CHARACTERISTICS: EXPERIMENTAL AND ANALYTICAL STUDIES

With respect to seismic performance, the benefits of integral abutment bridges over seat-type abutment bridges are: increased redundancy, larger damping due to nonlinear cyclic soil-pile-structure interaction, smaller displacements, and elimination of unseating potential. As such, integral abutment bridges are expected to have improved seismic performance compared to bridges with seat-type abutments (Hoppe and Gomez 1996; Itani and Sedarat 2000).

The soil–structure interaction in integral abutment bridges is one of the main sources of uncertainties and one of the most complex issues. This interaction is inherently nonlinear and depends on the magnitude and nature of the abutment, soil, and pile

deformations (translational, rotational). Limited experimental and analytical research has been conducted (e.g.: England et al. 2000; Faraji et al. 2001; Burdette et al. 1999; 2004; Fennema et al. 2005; Khodair and Hassiotis 2005; Hassiotis et al. 2006), and only quasi-static loading conditions were considered in these experimental studies. The most notable studies that involved field testing of piles were by Burdette et al. (2000; 2004; 2007), and Hassiotis et al. (2006).

In a two-phase experimental investigation funded by the Tennessee Department of Transportation, Burdette et al. (2000; 2007) investigated experimentally the lateral response of piles. The first phase consists of H-piles and in the second phase, additional tests were conducted with H-piles along with precast, prestressed concrete piles. These experimental investigations provided data for the soil-pile interaction and pile capacity.

The above experimental studies concluded that the current AASHTO and AISC interaction equations (axial load and moment) for the design of steel H-piles had limited applicability and in most cases are inappropriate (Ingram et al, 2003). Another important area of concern was the interface between the embedded pile and the abutment. It was found that the typical 1-ft embedment of the pile into the abutment had sufficient strength to allow thermal movement before inelastic action is developed in the piles. No significant cracking of the pile-abutment interface was observed contrary to earlier reports by other researchers that the concrete would severely spall before displacement approached 1 in. It was also found that the amount of cracking associated with lateral deflections depends on the stiffness of the soil and is more extensive in stiffer soils. However, even in extremely stiff soil conditions the cracking did not lead to loss of integrity of the interface.

There are limited but significant analytical studies that considered explicitly the seismic response characteristics of integral abutment bridges at a system level (e.g. Goel, 1997; Dehne and Hassiotis, 2003). The main objective of the study by Goel (1997) was to measure the vibration properties of a two-span concrete bridge from its motions recorded during actual earthquake events. Data was used in conjunction with an analytical model to investigate how the abutment participation affected the vibration properties of integral abutment bridges. Hence, it was noted that the abutment flexibility was an important element in earthquake design of integral abutment bridges. In particular, a more flexible abutment would lead to higher deformation demands on other components along the lateral load path.

Modeling the contribution of bridge abutments to overall bridge seismic response has been the focus of a significant research effort in the past decade. Many recent studies have shown how the abutment response significantly influences the response of short- and medium-length bridges. Some of these studies are based on sensitivity analyses using deterministic bridge models with varying abutment characteristics and capacities, and a relatively small number of earthquake ground motions. Realistic and accurate modeling of the abutment-soil interaction becomes even more important in the case of

integral abutment bridges. One of the major uncertainties in the design of integral abutment bridges is the soil response behind the abutments and next to the foundation piles during thermal expansion and seismic loads. This soil response along with the soil-pile interaction is inherently nonlinear and handling such interaction has become the main issue in integral abutment bridges.

Itani and Sedarat (2000) investigated the dynamic characteristics of integral abutment and seat-type abutment bridges. Simplified global models using space frame elements were developed for this purpose. It was shown that the period of the dominant longitudinal mode of integral abutment bridges was considerably shorter than the bridge with bearings at the abutments due to relatively high longitudinal stiffness of the abutments. It was observed that the transverse response of the bridge with integral abutments was extremely sensitive to the assumed restraint at the abutment.

Faraji et al. (2001) developed a three-dimensional finite-element model of an integral abutment bridge. The model consisted of a grillage model of the deck, abutment, beam-column elements to model the piles, and soil springs with nonlinear p-y properties to model the soil-pile-abutment-structure interaction. Although this study focused on loading cases due to differential temperature, remarks were made such that further studies are needed to consider the impact of pre-augering holes for the H-piles and backfilling with loose granular fill, the impact of skew alignments on the forces and moments at the abutment/superstructure joint, and the seismic response of long-span skew and nonskew integral abutment bridges. These studies would lead to a better theoretical understanding of the behavior of skew and nonskew, long-span integral abutment bridges during gravity, thermal, and seismic loadings.

1.4 GENERAL REMARKS REGARDING MODELING OF INTEGRAL ABUTMENT BRIDGES

A limited number of studies were found in the literature survey that investigated the seismic response characteristics at the component or subsystem level using a full 3D finite element as a tool. Khodair and Hassiotis (2005) developed and used a full 3D finite element mesh for the soil-pile-abutment interaction with appropriate boundary conditions. However, the composite connection at the abutment of integral abutment bridges was not the focus and therefore was not included in the study. An excerpt from the paper published is given below:

> *A 3D FE model was developed to study the nonlinear soil–pile interaction using the finite element software, ABAQUS/Standard (Hibbit, Karlsson & Sorenson [11]).*
>
> *The FE model includes the study of HP piles embedded in a single layer of sand confined within the corrugated galvanized steel sleeves. Each pile is modeled using eight-nodded solid continuum elements. The boundary conditions on the top of the pile ensure rigid translations and rotations. In*

the FE model two boundary conditions were imposed: (1) restraining all degrees of freedom associated with the nodes below a depth of 5.18 m from the top of the pile, due to the embedment of the pile into plain concrete below that depth, and (2) restraining all degrees of freedom along the perimeter of the sand sleeve representing the crushed stone used for backfilling (Figs. 11 and 12).

The rigid connection at the top of the pile was implemented through tying the top surface of the pile to the bottom surface of the abutment to ensure maintaining zero slope at the top of the pile, and hence full fixation of the piles into the abutment walls. The non-linear response of the soil was also modeled using solid continuum elements. The sand–pile interaction was modeled using surface-to-surface contact algorithm in ABAQUS/Standard (6.3.3). Two surfaces have been identified; the exterior surface of the pile was modeled as the master surface and the interior surface of the sand as the slave. The tangential contact between the pile and the surrounding sand was defined using a friction coefficient estimated by the tangent of the friction angle between the two materials.

Shamsabadi and Kapuskar (2010) investigated the seismic behavior of a skewed highway bridge with integral abutments in California using 3D nonlinear finite element model. In this study, nonlinear springs were used to model the soil-abutment interaction at the boundary between the end of the bridge and the abutment backfill. Comparisons of the analytical results and measured bridge response data showed that the 3D model is adequate in capturing the bridge seismic response.

1.5 TYPICAL ABUTMENT DETAILS OF INTEGRAL ABUTMENT BRIDGES WITH STEEL GIRDERS

Figure 1-2 and Figure 1-3 show the typical abutment detail used by the Wyoming and New York Departments of Transportations, respectively. In Figure 1-2, the piles are typically oriented with the strong axis perpendicular to the abutment axis or parallel to longitudinal direction of the bridge. The pile extends 12 in. (or more) into the abutment cap. The cap is tied to the end diaphragm and slab via #4 U-shaped stirrups and the #6 L-bar extending into the deck. The ends of the girders are completely encased in the concrete, and there are holes in the web through which the #5 bars extend near the back face of the abutment.

Other typical integral abutment details that have been used successfully are shown in Figure 1-4 and Figure 1-5 (Wasserman and Walker 1996). These typical details will be used to establish the local and global computational models of integral abutment bridges.

1.6 CONCLUSION

Based on the above literature review, it was revealed that little information is available on the seismic response of steel bridges with integral abutments. Furthermore, there is a paucity of information on modeling the soil-structure interaction between the abutment and soil, the pile and soil, the connection between the superstructure and the abutment, and the connection between the pile and the abutment. The common thread between most of the analytical and experimental studies that were reviewed is the local behavior between the piles and the base of the abutments, and does not cover the overall response of this type of bridge system during severe ground motions.

Table 1-1 Jointless bridges designed and built since 1995.

	Designed since 1995	**Built since 1995**	**In service (total)**
Full Integral	7,000	8,900	13,000
Semi-Integral	5,700	6,400	9,000
Deck Extension	1,600	1,600	4,000
Integral Piers	1,100	1,100	3,900

Table 1-2 Maximum span and bridge lengths of integral abutment bridges

Classification		**Steel Girder Bridge**	**Prestressed Concrete Bridge**
Maximum Span (m)	Full Integral	19.8 – 91.4	18.3 – 61.0
	Semi-Integral	19.8 – 61.0	27.4 – 61.0
	Deck Extension	24.4 – 61.0	27.4 – 61.0
	Integral Piers	30.5 – 91.4	36.6 – 61.0
Total Length (m)	Full Integral	45.7 – 198.1	45.7 – 358.1
	Semi-Integral	27.4 – 152.4	27.4 – 999.7
	Deck Extension	61.0 – 137.2	61.0 – 228.6
	Integral Piers	45.7 – 304.8	91.4 – 121.9

Table 1-3 Limits of horizontal abutment movement imposed by CA and TN DOTs

State DOT	With approach slab	Without approach slab	Remarks
California	± 25.4 mm (± 1.0 in)	± 12.7 mm (± 0.5 in)	At top of abutment
Tennessee	± 25.4 mm (± 1.0 in)	---	At pile cap

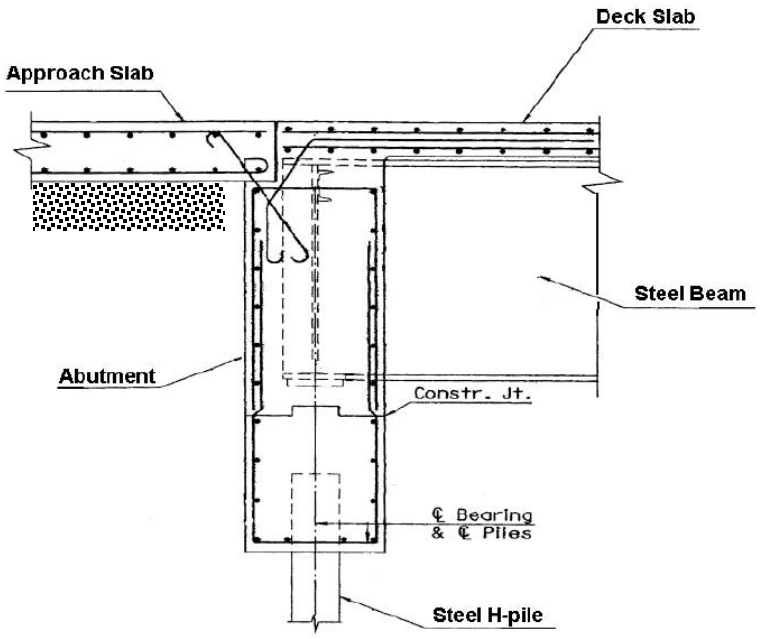

Figure 1-1 Typical integral abutment detail

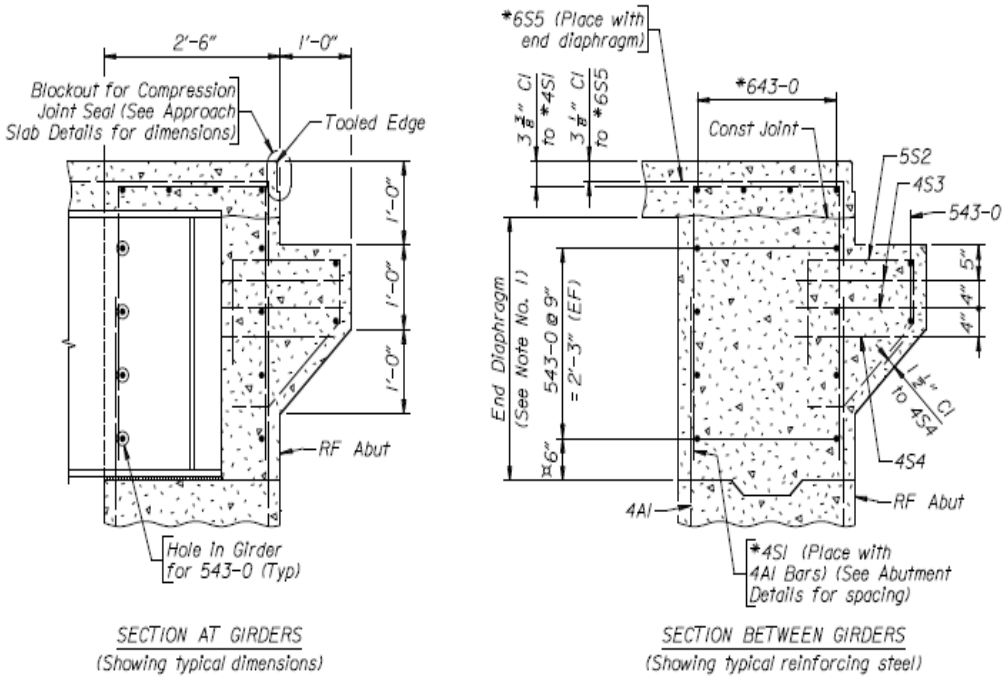

Figure 1-2 Typical IAB details from Wyoming DOT

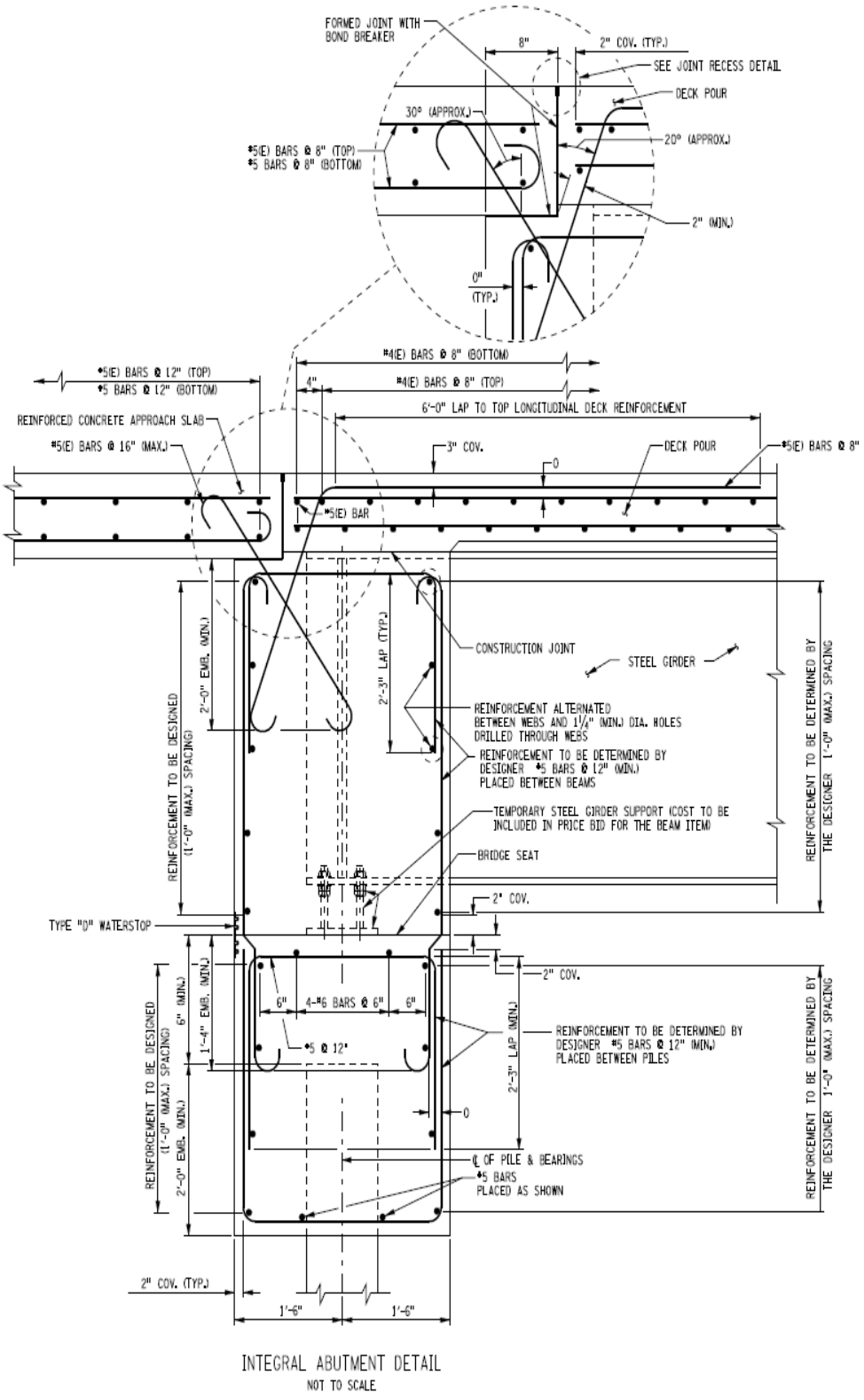

INTEGRAL ABUTMENT DETAIL
NOT TO SCALE

Figure 1-3 Typical IAB detail from New York DOT

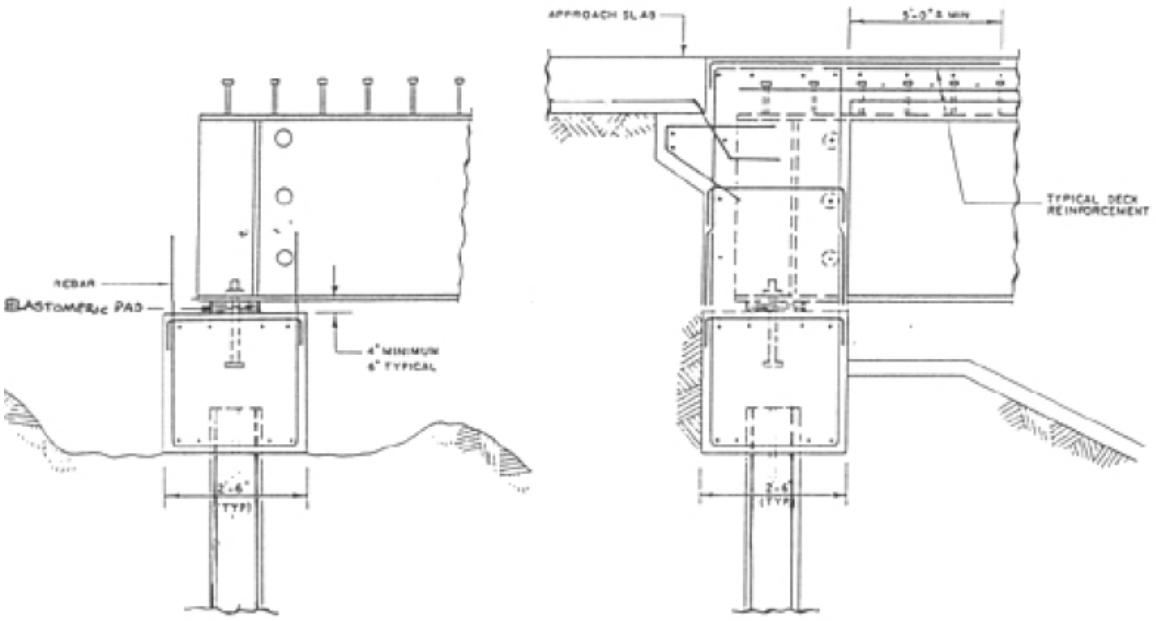

Figure 1-4 Integral abutment detail with elastomeric pad bolted between the pile cap and girder (Wasserman and Walker 1996)

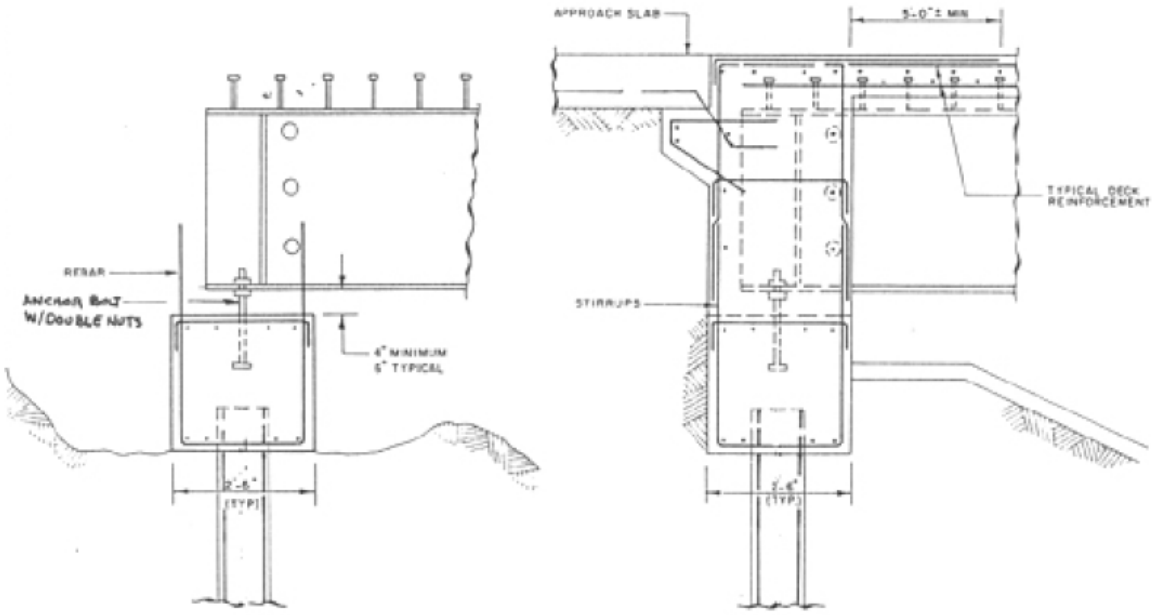

Figure 1-5 Integral abutment detail with projecting anchor bolts connecting the pile cap and girder (Wasserman and Walker 1996)

Chapter 2 LOCAL AND GLOBAL COMPUTATIONAL MODELS

Local and global computational models were developed to investigate the response characteristics of integral abutment bridges. A 3D nonlinear finite element model of the girder-abutment connection was developed using the computer program ADINA (2008). The analysis of the connection provided realistic interaction parameters between the steel girder, deck and abutment. Springs representing the nonlinear connection flexibility was then established and implemented in global 3D finite element models of integral abutment bridges. Modal analyses were used to demonstrate the effects of girder-abutment connection flexibility, abutment-soil interaction, and soil-pile interaction on the structural dynamics of integral abutment bridges.

2.1 THREE-SPAN INTEGRAL ABUTMENT BRIDGE

The three-span steel-girder bridge investigated in this study was based on the example bridge presented by Wasserman and Walker (1996). The superstructure is composed of four composite steel plate girders spaced at 11.75 ft for a total deck width of 44 ft including the overhangs. The span lengths are 105 ft, 216 ft, and 105 ft for a total length of 426 ft. The reinforced concrete deck is 9 in. thick. The piers are single column with a diameter of 60 in. and a clear height of 25 ft. The cap beams are 75 in. deep and 85 in. wide. The cross-frame spacing at end spans is 24 ft, and at main span is 22 ft. The intermediate cross-frames are composed of L5x5x5/8 while the support cross-frames are composed of 2L5x5x5/8. The basic geometry of the bridge is shown in Figure 2-1. The detail at the integral abutment is shown in Figure 2-2.

A local 3D finite element model of the girder, deck, and abutment was developed. The analysis of this model provided a set of spring properties (three translation and three rotation stiffnesses) defining the connection flexibility. These springs were then used in global 3D models to investigate the effect of connection flexibility on the overall bridge dynamic response. In addition, the effects of abutment-soil and soil-pile interactions on bridge dynamic response were also investigated.

2.2 FINITE ELEMENT (FE) MODEL AND ANALYSIS OF GIRDER-ABUTMENT CONNECTION

A detailed continuum model of the steel girder, deck, and abutment was created using the general purpose computer program ADINA. The flexibility of the girder-abutment connection detail was determined in terms of six (three translational and three rotational) nonlinear springs lumped at the abutment face.

The schematic elevation and plan view of the integral abutment is shown in Figure 2-2 and Figure 2-3, respectively. The detailed 3D finite element model developed for the girder-abutment connection is shown in Figure 2-4 through Figure 2-7. The ADINA 20-

node 3D solid element was used to model the concrete deck, concrete abutment, steel girder, and web stiffener. Nonlinearity at the interface regions (i.e. deck-to-abutment and embedded steel girder-to–abutment interface) was modeled with plastic compression-only truss elements shown in Figure 2-8. Two models were developed: (1) "fixed" model where the interface is rigid linear elastic and (2) "flexible" model where the interface is nonlinear. The two models were developed to determine the nonlinear stiffness properties of the connection. The "fixed" model assumes that the connection of the embedded girder and abutment is rigid. The "flexible" model has nonlinear compression-only springs at every point of contact of steel girder with the concrete material. A total of twelve monotonic loading cases were conducted. Displacements and rotations were applied at the centroid of the composite section 27 ft from the abutment. This is the assumed location of inflection point at the end spans as shown in Figure 2-2. The flexibility of the cantilevered part of superstructure was then eliminated by subtracting the action-deformation of the "flexible" model from that of the "fixed" model. It should be noted that there are two sources of flexibility in the model: (1) the cantilevered part which is composed of the composite girder and deck, and (2) the girder-abutment connection. The resulting action-deformation relations define the stiffness properties of the spring elements representing the nonlinear connection flexibility.

The following assumptions were made in the development of FE model:

1. The interface between the concrete deck and the abutment was located at the intersection of every node between the elements of the deck and the abutment. It is assumed that there was no concrete crushing and no tension resistance at this interface. It was observed in the preliminary analysis that plastic formation in the embedded steel girder occured earlier than any concrete crushing, therefore concrete crushing need not be considered in the analysis. Since during an earthquake the gap can open and close, it was also assumed that no shear resistance occurred at this interface. The interface of the concrete deck and the abutment was defined with plastic material. Nonlinear truss (compression-only) elements were used at common nodes of the deck and abutment.
2. The interface between the embedded steel girder and the abutment was defined with plastic material. It was assumed that no concrete crushing, no tension, and no shear resistance occurred at the interface. This interface was defined at the location of every node of the embedded steel girder and abutment elements. Nonlinear truss (compression-only) elements were located at common nodes of steel girder and abutment.
3. Fixed boundaries were used between the soil and the abutment because the results of this analysis will be used in a global model that includes the flexibilities of piles and soil.
4. The steel girder was modeled with linear elastic material properties. The stresses in the steel girder elements were monitored, and the first yield of each element was reported. The number of girder elements that reached the yielding stress

was monitored and reported as the deformation increased. This provides information on the sequence of yielding in the girder.

5. The maximum compressive strength of concrete was assumed to be 4 ksi with a modulus of elasticity of 3,600 ksi. The modulus of elasticity of steel equal to 29,000 ksi with a yield stress of 50 ksi. Although the steel girder was modeled as elastic, the yield stress was needed to monitor the sequence of yielding in the elements of the steel girder. It was assumed that the contribution of the deck reinforcement to the overall response can be neglected.

2.2.1 Summary of the Analysis Results

The force-displacement and moment-rotation relations obtained from the analyses of girder-abutment connection are presented in this section. The unsymmetrical action-deformation curves obtained in some cases are due to the interaction of the concrete deck and abutment. Figure 2-9 illustrates how the action-deformation curves will be used in the global 3D model.

The Von Mises stresses in the embedded steel girder were monitored and were used to identify the sequence of yielding. The propagation of yielding was monitored by identifying the percentage of girder elements that exceeded the yield stress (Figure 2-10 to Figure 2-15). The percentage of yielded elements was used as an indicator of the distribution of plasticity in the steel girder.

The action-deformation relations of the equivalent spring in the embedded region are summarized in Figure 2-16 to Figure 2-21. In these figures, the dotted line represents the action-deformation of the entire system which includes the cantilevered girder and deck. The solid line represents the action-deformation of the embedded region only. As stated previously, this was obtained by subtracting the flexibilities of the flexible model from that of the fixed model. The deformation at first yield and the deformation at which 20% of the steel girder has yielded are identified in the figures. The stiffnesses at first yield are summarized in Table 2-1. The Von Mises stress distributions at the first yield of the embedded steel girder are shown in Figure 2-22 to Figure 2-33. These stresses are averaged at the centroid of each element.

2.3 STRUCTURAL DYNAMICS CHARACTERISTICS OF INTEGRAL ABUTMENT BRIDGES

Detailed 3D models were developed to investigate the structural dynamics characteristics of integral abutment bridges. Several boundary conditions were identified and used to establish the effects of girder-abutment connection, abutment-soil interaction, and soil-pile interaction on the modal response. The generic model of the three-span integral abutment bridge used in the analyses is shown in Figure 2-34.

2.3.1 Modeling of Deck, Girders, Cap Beams, and Columns

In steel bridges, the modeling approach for the superstructure can have significant effect on the component (local) response. Generally, three approaches can be used to model the superstructure: (a) stick model where the entire superstructure is modeled as a single beam element with equivalent section properties, (b) grillage model where the superstructure is modeled using a plane grid of beam elements, and (c) finite element model where the deck is modeled as shell elements, and the girder can be either a shell element or beam element. In (b) and (c), the rotational inertia is automatically included in the model because the mass is distributed transversely to the nodes. This allows for a better characterization of mode shapes and better distribution of seismic forces. In (a), the rotational inertia needs to be calculated and assigned manually to the nodes of the superstructure. Although the global response from these modeling techniques can be about the same, the local responses can be significantly different.

Extensive studies on modeling of curved steel bridges currently being conducted at UNR (in which the authors are among the investigators) show that the stick model could result to unreasonable local forces. Representing the steel superstructure as a single frame element along the longitudinal direction produces an incorrect distribution of forces and an erroneous load path, especially in the transverse direction. Based on these observations, finite element modeling was selected for the integral abutment study. The nonlinear spring properties established in Section 2.2 was used at each girder-abutment connection so each girder must be modeled. The deck slab was modeled as shell elements while the girders, cross-frames, cap beams, and columns were modeled as beam elements (Figure 2-34). The shell elements were located at the center of gravity of the deck slab. The cap beams were defined with gross section properties while effective section properties were assigned to the columns. The steel piles as well as the abutment were also modeled as beam elements. Figure 2-34 and Figure 2-35 show the details of the bridge model. The computer program SAP2000 (Computers and Structures, Inc., 2008) was used in modeling the bridge.

2.3.2 Model of Girder-Abutment Connection

Under earthquake loading, the maximum negative moments in an integral abutment bridge is at the support locations, i.e. at abutments and bents. Therefore, the joint between the R/C deck and the abutment stem is expected to crack. This cracked R/C connection cannot transfer the seismic forces from the superstructure to the abutment if not properly designed and detailed. Thus, the force transfer at that location will be through the steel girder-abutment connection. Therefore, it was assumed in the computational model that the R/C deck is not rigidly connected to the abutment. This issue is further discussed in the pushover analysis of integral abutment bridges in Section 3.1.

The girder-abutment connection was represented by nonlinear translational and rotational springs. The stiffness properties of these springs were obtained from the

finite-element component analysis of a girder-abutment connection as presented in Section 2.2. The effective stiffnesses calculated at first yield of the steel girder were used in the modal analyses, shown in Table 2-1. For degrees-of-freedom (DOF) where the backbone curve is asymmetric (e.g. U1, U2 and R3 in Table 2-1), the lower values of K_{pos} and K_{neg} were used in modal analysis.

2.3.3 Model of Abutment Soil Passive Resistance

The participating mass of the soil behind the abutment was not considered in the analytical investigation. Without the complete information on embankment size and soil properties, it is very difficult to determine the effective embankment soil. Also, without shake table experiments with reasonable scale to determine the effective participating soil mass, the computational models will have limited capabilities and may produce results that vary by more than several folds. Thus, the current state-of-the-art of modeling the effect of soil behind the abutment is to consider the soil stiffness only. This approach is used by the California Department of Transportation (Caltrans).

The stiffness property of the soil behind the abutment was obtained from Caltrans' Seismic Design Criteria (SDC, Caltrans 2006) assuming a uniform soil passive pressure distribution along the abutment. The initial abutment stiffness is given by

$$K_{abut} = 20\frac{kip/in}{ft} w\left(\frac{h}{5.5}\right) \tag{2-1}$$

where, *w* is the abutment width and *h* is the abutment height. The initial stiffness of *20 kip/in/ft* was assumed based on the results of large-scale abutment testing at University of California, Davis (UC Davis). This stiffness is scaled by the ratio *(h/5.5)* because the height of the abutment tested at UC Davis was 5.5 ft. The maximum soil passive pressure that can be developed behind the abutment is 5.0 ksf. Thus, the total static passive force is given by

$$P = A_e\left(5.0ksf\right)\left(\frac{h}{5.5}\right) \tag{2-2}$$

where, A_e is the effective abutment area. Similar to initial stiffness, the maximum soil passive force was also scaled by *(h/5.5)*. As shown in Figure 2-34 and Figure 2-35, the soil resistance was distributed to the four girders. The stiffness properties of the soil springs connected to the exterior and interior girders are shown in Figure 2-36. The difference between the soil properties at exterior and interior girder is due to difference in their tributary areas. The ultimate soil displacement in Figure 2-36 is 12.9 in., 10% of the abutment height, which is the code recommended displacement for cohesive soils.

For modal analysis, only one-half of the initial abutment stiffness was assigned to the springs at each end of the longitudinal direction of the bridge. This is because the soil springs are compression only springs. In the transverse direction, it was assumed that

the contribution of the wingwall and the soil resistance behind it is negligible since the connection between the wingwall and the abutment are not normally designed to take any significant seismic forces.

2.3.4 Model of Soil-Pile Interaction

The soil-pile properties used in this study were of Wasserman and Walker (1996). Each abutment of the example bridge is supported on seven HP10x42 steel piles. In the analytical model, beam elements with lengths equal to 12.4 ft were used to represent these piles. The 12.4-ft length was based on the location of zero moment in the pile measured from the pile head. The soil-pile interaction was represented by nonlinear springs with translational stiffness properties in the longitudinal and transverse directions. These springs are located at 0 ft, 5 ft, and 10 ft below the pile head. Figure 2-37 shows the *p-y* curves that define these springs and the properties of soil profile at abutments. In modal analysis, the elastic stiffnesses used are 24 kip/in, 105 kip/in, and 144.55 kip/in for springs located at 0 ft, 5 ft, and 10 ft, respectively. Due to lack of data, it was assumed that the *p-y* curves in the transverse direction are the same as those in the longitudinal direction. However, this was revisited in the design example in Chapter 5, and the *p-y* spring properties and spacing were re-evaluated.

2.3.5 Bridge Dynamic Properties

Modal analyses were performed to investigate the effect of girder-abutment connection flexibility, abutment-soil interaction, and soil-pile interaction on the global system behavior. For this purpose, a total of six different cases isolating the effect of girder-abutment connection flexibility, abutment-soil interaction, and soil-pile interaction, were identified and considered as listed in Table 2-2. In this table, “rigid” means that the component has a very large stiffness, “free” means the component has zero stiffness, and “flexible” means the actual (realistic) component stiffness values were used. It should be noted that for Case 6, steel piles are modeled such that they are in strong axis bending with respect to the longitudinal direction of the bridge. Also, as explained before, the stiffness of the girder-abutment springs used in the analysis is the effective stiffness at first yield of steel girder while the initial stiffness was used for the abutment-soil and soil-pile springs.

The mode shapes of the significant modes of Cases 1 through 6 are shown in Figure 2-38 through Figure 2-43, respectively. The modal participating mass ratios for each mode in each case are summarized in Table 2-3 through Table 2-8. Modal participating mass ratio shows the relative importance of a particular mode in the calculation of total response quantities. The sum of the modal participating mass ratios will indicate if the requested number of modes adequately captures the overall response when analyses based on modal properties (e.g. multi-mode spectral analyses) are used.

Comparison of Cases 1 and 2 showed that the addition of the girder-abutment connection flexibility in the global model not only increased the vibration periods but

also changed the mode shapes. For example, Mode 1 in Case 1 is rotation of the superstructure about the bridge longitudinal axis while Mode 1 in Case 2 is coupled superstructure rotation and transverse translation. In Mode 4, the mode shape changes from superstructure rotation in Case 1 to in-plane rotation of the deck in Case 2. The significant increase (40%) in vibration was observed in the main transverse translational mode which is Mode 3. The same observations are also true when Cases 3 and 4 are compared but with larger increase in vibration periods due to change in abutment boundary condition. The vibration period of Mode 3 increased by 46%.

Therefore, the common assumption that the girder-abutment connection is rigid in integral abutment bridges may not be always correct. The comparisons clearly show that the typical girder embedment length is insufficient to create a rigid connection and can have a significant contribution to the flexibility of the entire bridge system. This flexibility of the connection is directly related to the embedment length of the girder into the abutment. A short embedment length may be quite flexible while a long embedment length may be essentially rigid. As such, a procedure for calculating the required girder embedment length to consider the connection as rigid was developed and is discussed in Section 2.4.

The most significant change in bridge dynamic properties is due to soil-pile interaction. In Case 5 where the soil-pile interaction was assumed rigid, the main transverse translational mode is Mode 3. But when the realistic stiffness of soil-pile interaction was used in Case 6, the main transverse translational mode became Mode 1. In addition, the vibration period of this mode increases by about 100%, from 0.552 sec to 1.071 sec. Although the main longitudinal translational mode (Mode 5) occurs at a small period when the soil-pile interaction was considered, it takes place at a significantly longer period compared to cases where the soil-pile interaction is assumed rigid. The period of the longitudinal mode in Cases 1 to 5 ranges from 0.084 sec to 0.098 sec.

2.4 PROPOSED EQUATION FOR CALCULATION OF GIRDER EMBEDMENT LENGTH

Section 2.3.5 showed that the typical girder-abutment connection is not rigid and, in fact, adds flexibility to the entire bridge. Sufficient embedment length is required to achieve a rigid connection between the girder and abutment. The embedment length is usually determined based standard details developed by US DOTs and bridge design offices. No specific guidelines were found in the literature for the proper design of this connection and under which condition it can be assumed as rigid. The finite element analysis of a typical girder-abutment connection detail with embedment length of 24 in. shows that such detail can be flexible and increases the vibration period of the bridge.

The embedment length of steel girders into the abutment can be calculated based on the mechanism proposed by Shama et al. (2002a). This assumes a simplified stress mechanism and was developed for steel embedded into concrete. The resistance to external moment *M* is developed due to the couple created by bearing stresses on the

concrete as shown in Figure 2-44. The concrete stress block force C_m can be evaluated as:

$$C_m = 0.5\alpha\beta f_c^{'} b_f l_{emb} \tag{2-3}$$

where, α is a factor applied to f'_c; β is a factor for the depth of stress block; f'_c is the concrete compressive strength; b_f is the flange width of the steel section (girder flange width in this case); and l_{emb} is the embedment length of the steel section into the concrete. The couple lever arm is:

$$jd = l_{emb}(1 - 0.5\beta) \tag{2-4}$$

Assuming $\beta = 1$, jd can be taken as $0.5l_{emb}$. The moment capacity of the connection is then

$$M_c = \phi C_m jd \tag{2-5}$$

where, ϕ is the strength reduction factor and is equal to *0.9*. By substituting Eqn. 2-5, Eqn. 2-7 can be rewritten as:

$$M_c = 0.25\phi\alpha\beta f_c^{'} b_f l_{emb}^2 \tag{2-6}$$

To maintain integrity of the connection, the $M_c \geq M$ criteria must be satisfied. Thus, the equation for embedment length is given by:

$$l_{emb} \geq 2\sqrt{\frac{M}{\phi\alpha\beta f_c^{'} b_f}} \tag{2-7}$$

For a maximum concrete strain ε_{cu} of *0.003*, the stress block factors α and β can both be taken as equal to *0.85*. Applying the ϕ factor, Eqn. 2-9 can be further simplified as:

$$l_{emb} \geq 2.5\sqrt{\frac{M}{f_c^{'} b_f}} \tag{2-8}$$

It should be noted that sufficient confinement reinforcement should be provided in addition to the embedment length recommended above. If the calculated embedment length is large and impractical, it is recommended that the width of the girder flanges embedded into the abutment structure be increased. The girder-to-abutment connection may be considered as a rigid connection with the proper embedment length and connection detail.

For the integral abutment bridge described in Section 2.1, the required embedment length is 60 in. If this length is impractical, the flanges of the girder can be widened to shorten the embedment length. For example, the required embedment length for a 30

in. flange is 45 in. The design example in Chapter 5 discusses in detail the calculation of girder embedment length.

2.5 CONCLUSIONS

A finite element model of a typical girder-abutment connection was developed to establish stiffness properties of nonlinear springs representing the connection flexibility. These nonlinear springs, along with springs that define the abutment-soil and soil-pile interactions, were then used in global 3D bridge models to determine the effect of connection flexibility, abutment-soil and soil-pile interaction on the bridge structural dynamics. It is shown that the connection flexibility increases the vibration period of the main transverse translation mode by up to 50%. This investigation has shown that the typical girder embedment length may not be sufficient to ensure rigid connection, therefore can have a significant contribution to the flexibility of the entire bridge system. A short embedment length can be quite flexible while a long embedment length can be essentially rigid. As such, a procedure for calculating the required minimum girder embedment length to achieve a rigid connection was developed. The main longitudinal translation mode is unaffected by the connection flexibility because the response is dominated by the abutment-soil interaction. It should be noted that the main longitudinal translation mode occurs at a relatively small period due to high stiffness of the abutment-soil interaction. The most significant change in global system dynamics is due to the soil-pile interaction. Up to a 100% increase in the vibration period of the main transverse translation mode was observed.

Table 2-1 Effective Stiffnesses at First Yield of Girder-Abutment Connection

DOF	Unit	Description	K_{pos}	K_{neg}	K_{mod}
U1	kip/in	vertical action	496	219	219
U2	kip/in	longitudinal action	13,465	20,068	13,465
U3	kip/in	transverse action	181	181	181
R1	kip-in/rad	rotation about vertical axis	1.08E+08	1.08E+08	1.08E+08
R2	kip-in/rad	rotation about longitudinal axis	1.94E+06	1.94E+06	1.94E+06
R3	kip-in/rad	rotation about transverse axis	1.68E+08	3.14E+08	1.68E+08

Note: K_{pos} = effective stiffness at positive region of backbone curve at first yield
K_{neg} = effective stiffness at negative region of backbone curve at first yield
K_{mod} = effective stiffness used for modal analysis

Table 2-2 Cases Investigated

Cases	Abutment-Soil Interaction	Girder-Abutment Connection	Soil-Pile Interaction
1	rigid	rigid	rigid
2	rigid	flexible	rigid
3	free	rigid	rigid
4	free	flexible	rigid
5	flexible	flexible	rigid
6	flexible	flexible	flexible

Table 2-3 Case 1 Modal Participating Mass Ratios

Mode	Period	UX	UY	UZ	RX	RY	RZ
No	Sec	%	%	%	%	%	%
1	0.623	0.0	0.2	0.0	3.3	0.0	0.1
2	0.582	0.0	0.0	25.3	0.0	18.8	0.0
3	0.378	0.0	65.8	0.0	69.5	0.0	49.8
4	0.284	0.0	0.0	0.0	0.0	0.0	0.9
5	0.234	0.0	8.6	0.0	0.2	0.0	6.5
6	0.214	0.2	0.0	0.0	0.0	0.1	0.0
7	0.188	0.0	0.0	0.0	0.0	0.0	1.0
8	0.170	0.0	0.0	0.0	0.0	0.0	11.4
9	0.145	0.0	0.0	28.7	0.0	21.3	0.0
10	0.138	0.1	0.0	0.0	0.0	14.1	0.0
11	0.134	0.0	0.1	0.0	0.8	0.0	0.1
12	0.110	0.0	0.0	0.0	0.0	0.0	0.1
13	0.107	0.0	0.0	20.8	0.0	15.4	0.0
14	0.098	0.0	8.1	0.0	8.7	0.0	6.2
15	0.085	75.3	0.0	0.0	0.0	2.5	0.0
16	0.085	0.0	2.4	0.0	1.9	0.0	1.8
17	0.073	2.1	0.0	0.0	0.0	1.3	0.0
18	0.071	0.0	0.0	0.1	0.0	0.0	0.0
19	0.069	0.0	0.0	0.0	0.0	0.0	0.0
20	0.065	0.0	0.0	0.0	0.0	0.0	0.0
21	0.065	0.0	0.0	3.9	0.0	2.9	0.0
22	0.064	0.2	0.0	0.0	0.0	0.0	0.0
23	0.063	1.4	0.0	0.0	0.0	0.0	0.0
24	0.062	0.0	0.0	0.7	0.0	0.5	0.0
25	0.061	1.0	0.0	0.0	0.0	0.0	0.0
26	0.059	0.0	0.0	0.0	0.0	0.0	2.7
27	0.058	3.2	0.0	0.0	0.0	0.3	0.0
28	0.056	0.0	0.0	0.2	0.0	0.2	0.0
29	0.055	0.0	0.1	0.0	0.9	0.0	0.1
30	0.053	0.0	0.0	0.0	0.0	0.0	0.8
Sum		83.4	85.4	79.7	85.4	77.3	81.5

Table 2-4 Case 2 Modal Participating Mass Ratios

Mode	Period	UX	UY	UZ	RX	RY	RZ
No	Sec	%	%	%	%	%	%
1	0.667	0.0	12.9	0.0	32.3	0.0	9.8
2	0.599	0.0	0.0	21.1	0.0	15.7	0.0
3	0.530	0.0	71.5	0.0	62.0	0.0	54.2
4	0.335	0.0	0.0	0.0	0.0	0.0	15.4
5	0.280	0.0	0.0	0.0	0.0	0.0	6.9
6	0.250	0.0	9.5	0.0	0.1	0.0	7.2
7	0.238	0.1	0.0	0.0	0.0	3.9	0.0
8	0.216	0.0	0.0	0.0	0.0	0.0	0.4
9	0.207	0.0	0.0	41.3	0.0	30.7	0.0
10	0.183	0.0	0.0	0.0	0.0	14.2	0.0
11	0.173	0.0	4.1	0.0	4.5	0.0	3.1
12	0.164	0.0	0.0	0.0	0.0	0.0	0.0
13	0.136	0.0	0.0	0.0	0.0	0.0	0.0
14	0.110	0.0	0.0	10.1	0.0	7.5	0.0
15	0.101	0.0	0.0	0.0	0.0	0.0	1.0
16	0.100	0.0	0.0	0.0	0.0	0.0	0.0
17	0.093	3.5	0.0	0.0	0.0	0.0	0.0
18	0.092	0.0	0.0	7.1	0.0	5.2	0.0
19	0.084	72.1	0.0	0.0	0.0	2.2	0.0
20	0.082	0.0	0.0	0.0	0.0	0.0	0.0
21	0.078	0.0	0.0	0.0	0.1	0.0	0.0
22	0.073	2.8	0.0	0.0	0.0	1.5	0.0
23	0.070	0.0	0.0	0.0	0.0	0.0	0.0
24	0.069	0.0	0.0	0.0	0.0	0.0	0.0
25	0.068	0.0	0.1	0.0	0.0	0.0	0.1
26	0.064	0.0	0.0	0.0	0.0	0.0	0.0
27	0.063	0.0	0.0	0.8	0.0	0.6	0.0
28	0.062	0.0	0.0	0.0	0.0	0.0	0.0
29	0.062	0.0	0.0	0.0	0.0	0.0	0.0
30	0.059	4.9	0.0	0.0	0.0	0.5	0.0
Sum		83.5	98.1	80.5	99.0	82.0	98.1

Table 2-5 Case 3 Modal Participating Mass Ratios

Mode	Period	UX	UY	UZ	RX	RY	RZ
No	Sec	%	%	%	%	%	%
1	0.623	0.0	0.2	0.0	3.3	0.0	0.1
2	0.582	0.0	0.0	25.3	0.0	18.8	0.0
3	0.378	0.0	65.8	0.0	69.5	0.0	49.8
4	0.284	0.0	0.0	0.0	0.0	0.0	0.9
5	0.234	0.0	8.6	0.0	0.2	0.0	6.5
6	0.214	0.2	0.0	0.0	0.0	0.1	0.0
7	0.188	0.0	0.0	0.0	0.0	0.0	1.0
8	0.170	0.0	0.0	0.0	0.0	0.0	11.4
9	0.145	0.0	0.0	28.7	0.0	21.3	0.0
10	0.138	0.1	0.0	0.0	0.0	14.1	0.0
11	0.134	0.0	0.1	0.0	0.8	0.0	0.1
12	0.110	0.0	0.0	0.0	0.0	0.0	0.1
13	0.107	0.0	0.0	20.8	0.0	15.4	0.0
14	0.098	0.0	8.1	0.0	8.7	0.0	6.2
15	0.085	75.3	0.0	0.0	0.0	2.5	0.0
16	0.085	0.0	2.4	0.0	1.9	0.0	1.8
17	0.073	2.1	0.0	0.0	0.0	1.3	0.0
18	0.071	0.0	0.0	0.1	0.0	0.0	0.0
19	0.069	0.0	0.0	0.0	0.0	0.0	0.0
20	0.065	0.0	0.0	0.0	0.0	0.0	0.0
21	0.065	0.0	0.0	3.9	0.0	2.9	0.0
22	0.064	0.2	0.0	0.0	0.0	0.0	0.0
23	0.063	1.4	0.0	0.0	0.0	0.0	0.0
24	0.062	0.0	0.0	0.7	0.0	0.5	0.0
25	0.061	1.0	0.0	0.0	0.0	0.0	0.0
26	0.059	0.0	0.0	0.0	0.0	0.0	2.7
27	0.058	3.2	0.0	0.0	0.0	0.3	0.0
28	0.056	0.0	0.0	0.2	0.0	0.2	0.0
29	0.055	0.0	0.1	0.0	0.9	0.0	0.1
30	0.053	0.0	0.0	0.0	0.0	0.0	0.8
Sum		83.4	85.4	79.7	85.4	77.3	81.5

Table 2-6 Case 4 Modal Participating Mass Ratios

Mode	Period	UX	UY	UZ	RX	RY	RZ
No	Sec	%	%	%	%	%	%
1	0.691	0.0	24.4	0.0	47.4	0.0	18.5
2	0.599	0.0	0.0	21.1	0.0	15.7	0.0
3	0.552	0.0	59.1	0.0	45.5	0.0	44.8
4	0.335	0.0	0.0	0.0	0.0	0.0	15.4
5	0.280	0.0	0.0	0.0	0.0	0.0	6.8
6	0.250	0.0	9.1	0.0	0.1	0.0	6.9
7	0.238	0.1	0.0	0.0	0.0	3.9	0.0
8	0.216	0.0	0.0	0.0	0.0	0.0	0.4
9	0.207	0.0	0.0	41.3	0.0	30.7	0.0
10	0.183	0.0	0.0	0.0	0.0	14.2	0.0
11	0.177	0.0	5.5	0.0	5.8	0.0	4.1
12	0.165	0.0	0.0	0.0	0.0	0.0	0.0
13	0.136	0.0	0.0	0.0	0.0	0.0	0.0
14	0.110	0.0	0.0	10.1	0.0	7.5	0.0
15	0.106	0.0	0.0	0.0	0.0	0.0	1.1
16	0.100	0.0	0.0	0.0	0.0	0.0	0.0
17	0.098	79.5	0.0	0.0	0.0	1.5	0.0
18	0.093	0.0	0.0	7.1	0.0	5.3	0.0
19	0.092	9.8	0.0	0.0	0.0	0.7	0.0
20	0.082	0.0	0.0	0.0	0.0	0.0	0.0
21	0.079	0.0	0.0	0.0	0.1	0.0	0.0
22	0.073	0.6	0.0	0.0	0.0	1.8	0.0
23	0.071	0.0	0.0	0.0	0.0	0.0	0.0
24	0.070	0.0	0.2	0.0	0.0	0.0	0.1
25	0.069	0.0	0.0	0.0	0.0	0.0	0.0
26	0.064	0.0	0.0	0.0	0.0	0.0	0.0
27	0.063	0.0	0.0	0.8	0.0	0.6	0.0
28	0.062	0.0	0.0	0.0	0.0	0.0	0.0
29	0.062	0.0	0.0	0.0	0.0	0.0	0.0
30	0.061	1.0	0.0	0.0	0.0	0.4	0.0
Sum		91.1	98.1	80.4	99.0	82.2	98.1

Table 2-7 Case 5 Modal Participating Mass Ratios

Mode	Period	UX	UY	UZ	RX	RY	RZ
No	Sec	%	%	%	%	%	%
1	0.691	0.0	24.2	0.0	47.2	0.0	18.4
2	0.599	0.0	0.0	21.1	0.0	15.7	0.0
3	0.552	0.0	59.2	0.0	45.7	0.0	44.9
4	0.335	0.0	0.0	0.0	0.0	0.0	15.4
5	0.280	0.0	0.0	0.0	0.0	0.0	6.8
6	0.250	0.0	9.1	0.0	0.1	0.0	6.9
7	0.238	0.1	0.0	0.0	0.0	3.9	0.0
8	0.216	0.0	0.0	0.0	0.0	0.0	0.4
9	0.207	0.0	0.0	41.3	0.0	30.7	0.0
10	0.183	0.0	0.0	0.0	0.0	14.2	0.0
11	0.177	0.0	5.5	0.0	5.8	0.0	4.1
12	0.165	0.0	0.0	0.0	0.0	0.0	0.0
13	0.136	0.0	0.0	0.0	0.0	0.0	0.0
14	0.110	0.0	0.0	10.1	0.0	7.5	0.0
15	0.106	0.0	0.0	0.0	0.0	0.0	1.1
16	0.100	0.0	0.0	0.0	0.0	0.0	0.0
17	0.098	78.8	0.0	0.0	0.0	1.5	0.0
18	0.093	0.0	0.0	7.1	0.0	5.3	0.0
19	0.092	10.4	0.0	0.0	0.0	0.7	0.0
20	0.082	0.0	0.0	0.0	0.0	0.0	0.0
21	0.079	0.0	0.0	0.0	0.1	0.0	0.0
22	0.073	0.6	0.0	0.0	0.0	1.8	0.0
23	0.071	0.0	0.0	0.0	0.0	0.0	0.0
24	0.070	0.0	0.2	0.0	0.0	0.0	0.1
25	0.069	0.0	0.0	0.0	0.0	0.0	0.0
26	0.064	0.0	0.0	0.0	0.0	0.0	0.0
27	0.063	0.0	0.0	0.8	0.0	0.6	0.0
28	0.062	0.0	0.0	0.0	0.0	0.0	0.0
29	0.062	0.0	0.0	0.0	0.0	0.0	0.0
30	0.061	1.0	0.0	0.0	0.0	0.4	0.0
Sum		91.1	98.1	80.4	99.0	82.2	98.1

Table 2-8 Case 6 Modal Participating Mass Ratios

Mode	Period	UX	UY	UZ	RX	RY	RZ
No	Sec	%]	%]	%]	%]	%]	%]
1	1.071	0.0	66.6	0.0	87.3	0.0	57.1
2	0.615	0.0	0.0	19.0	0.0	14.1	0.0
3	0.595	0.0	18.7	0.0	6.5	0.0	17.7
4	0.527	0.0	1.1	0.0	1.0	0.0	13.0
5	0.350	95.6	0.0	0.0	0.0	1.3	0.0
6	0.285	0.0	0.0	0.0	0.0	0.0	3.1
7	0.263	0.0	6.8	0.0	2.9	0.0	3.0
8	0.254	1.1	0.0	0.0	0.0	6.6	0.0
9	0.251	0.0	4.3	0.0	0.3	0.0	3.6
10	0.224	0.0	0.0	43.4	0.0	32.2	0.0
11	0.219	0.0	0.0	0.0	0.0	0.0	0.1
12	0.186	0.0	0.0	0.0	0.0	12.0	0.0
13	0.168	0.0	0.6	0.0	0.9	0.0	0.5
14	0.146	0.0	0.0	0.0	0.0	0.0	0.0
15	0.131	0.0	0.0	0.0	0.0	0.0	0.1
16	0.110	0.0	0.0	9.3	0.0	6.9	0.0
17	0.102	0.0	0.0	0.0	0.1	0.0	0.0
18	0.097	0.0	0.0	0.0	0.0	0.0	0.0
19	0.097	0.0	0.0	5.9	0.0	4.4	0.0
20	0.086	0.0	0.0	0.0	0.0	0.0	0.0
21	0.083	0.0	0.0	0.0	0.0	0.0	0.0
22	0.081	0.0	0.0	0.0	0.0	0.0	0.0
23	0.074	0.0	0.1	0.0	0.0	0.0	0.0
24	0.073	0.0	0.0	0.0	0.0	2.2	0.0
25	0.069	0.0	0.0	0.0	0.0	0.0	0.0
26	0.065	0.2	0.0	0.0	0.0	0.1	0.0
27	0.064	0.8	0.0	0.0	0.0	0.3	0.0
28	0.063	0.0	0.0	1.6	0.0	1.2	0.0
29	0.062	0.0	0.0	0.0	0.0	0.0	0.0
30	0.062	0.0	0.0	0.0	0.0	0.0	0.0
Sum		97.8	98.1	79.2	99.0	81.2	98.2

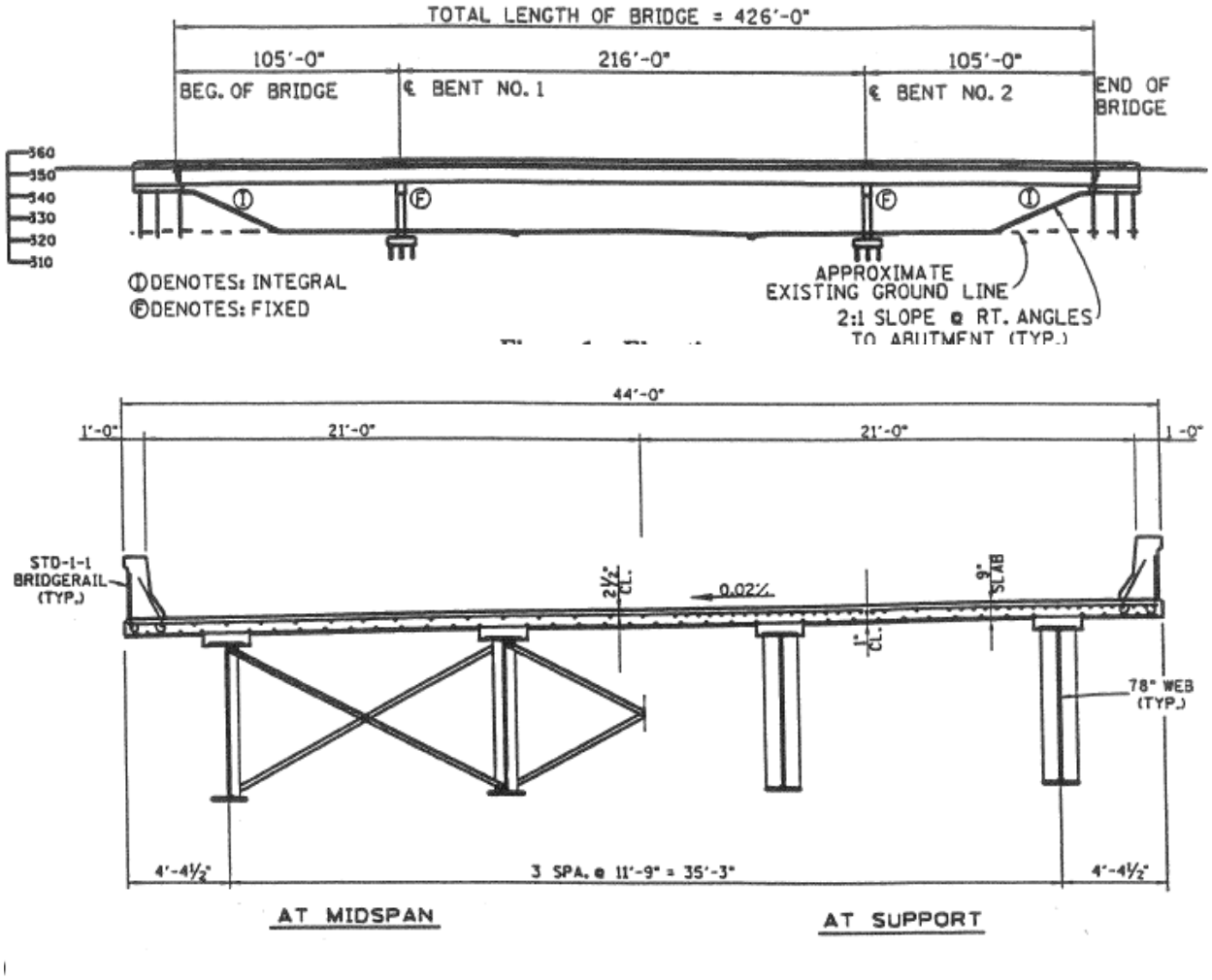

Figure 2-1 Elevation and cross-sectional view of the bridge (Wasserman and Walker 1996)

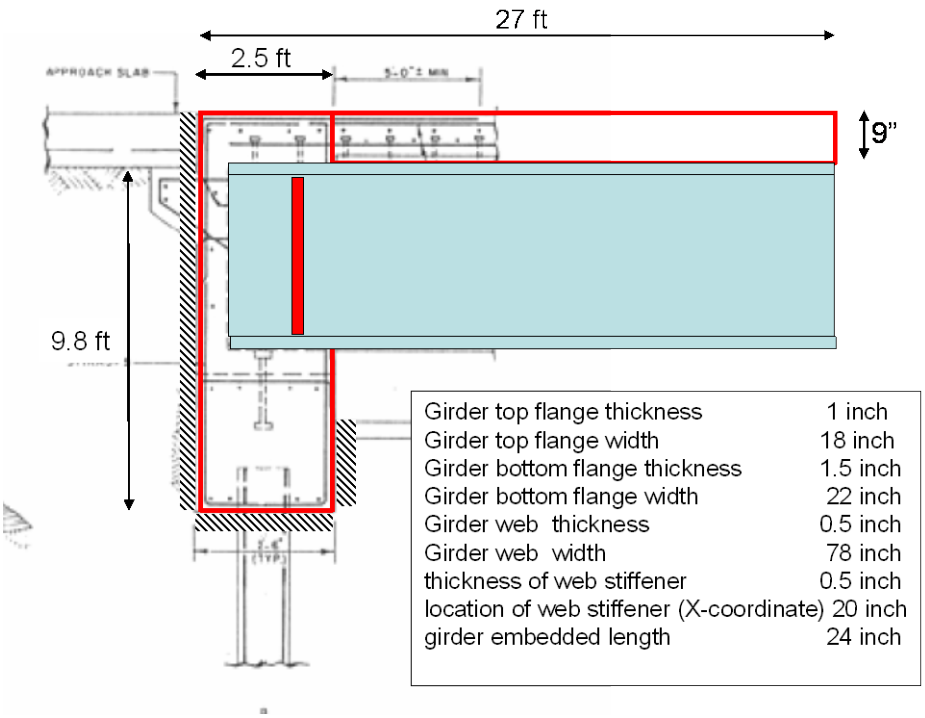

Figure 2-2 Elevation at the integral abutment considered for the FE model

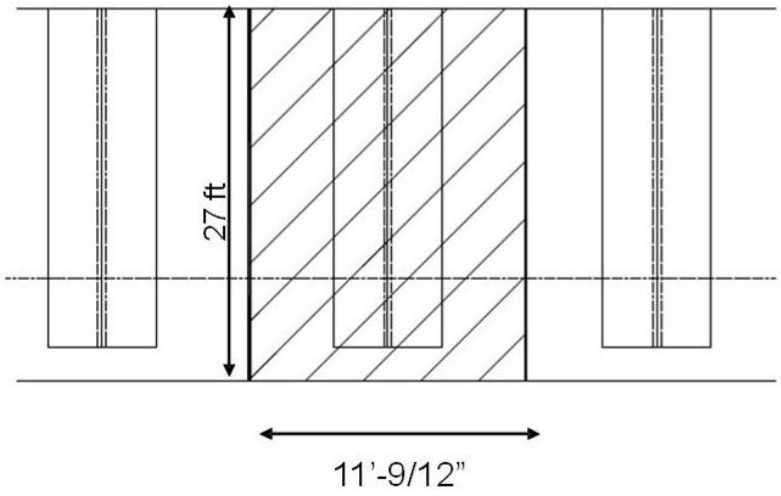

Figure 2-3 Plan view at the integral abutment considered in the FE model

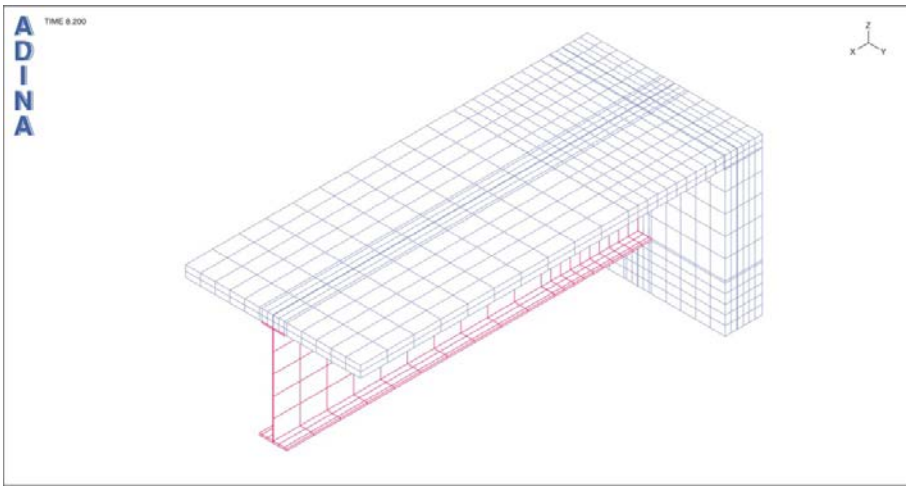

Figure 2-4 Isometric View of the FE Model from Top

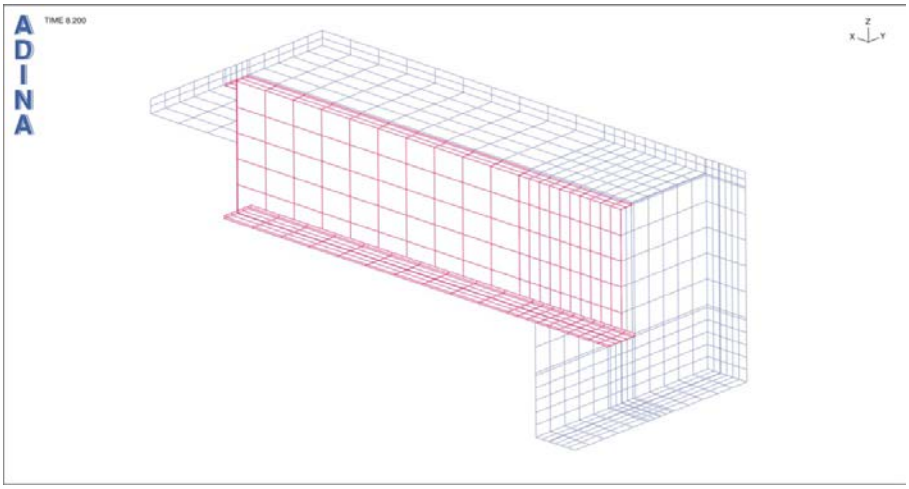

Figure 2-5 Isometric View of the FE Model from Bottom

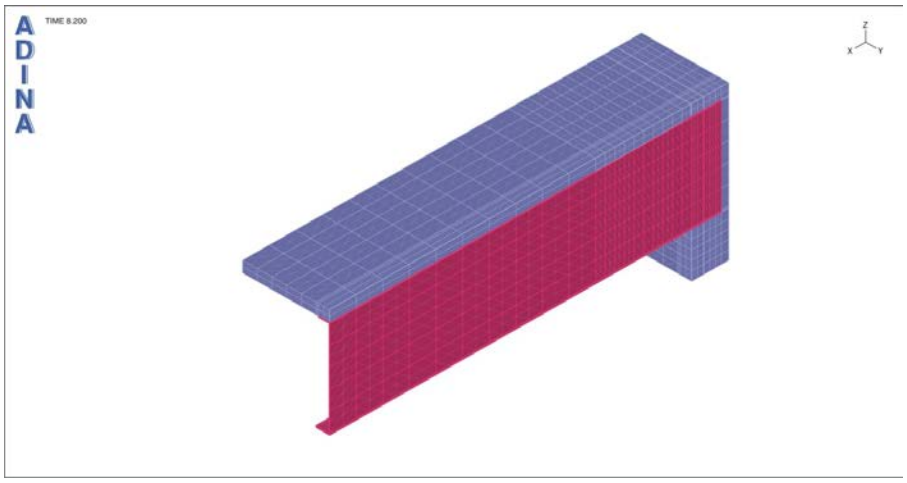

Figure 2-6 Section through the Web Showing the Embedment

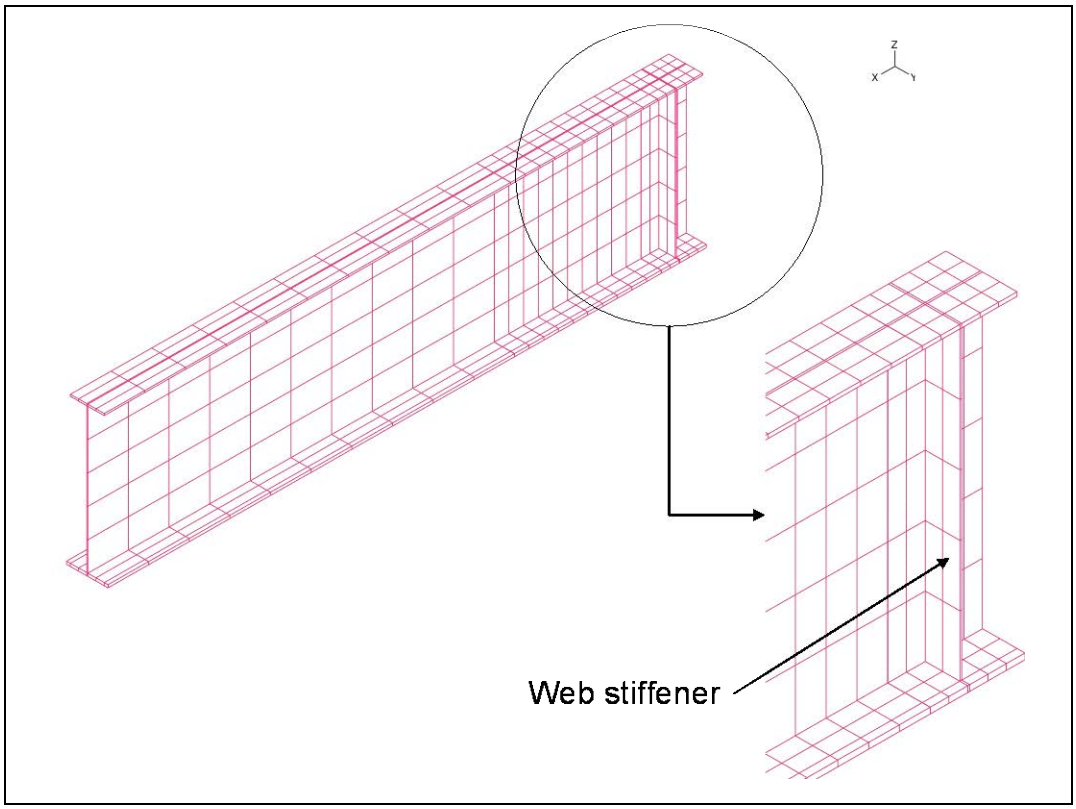

Figure 2-7 Girder and the Web Stiffener

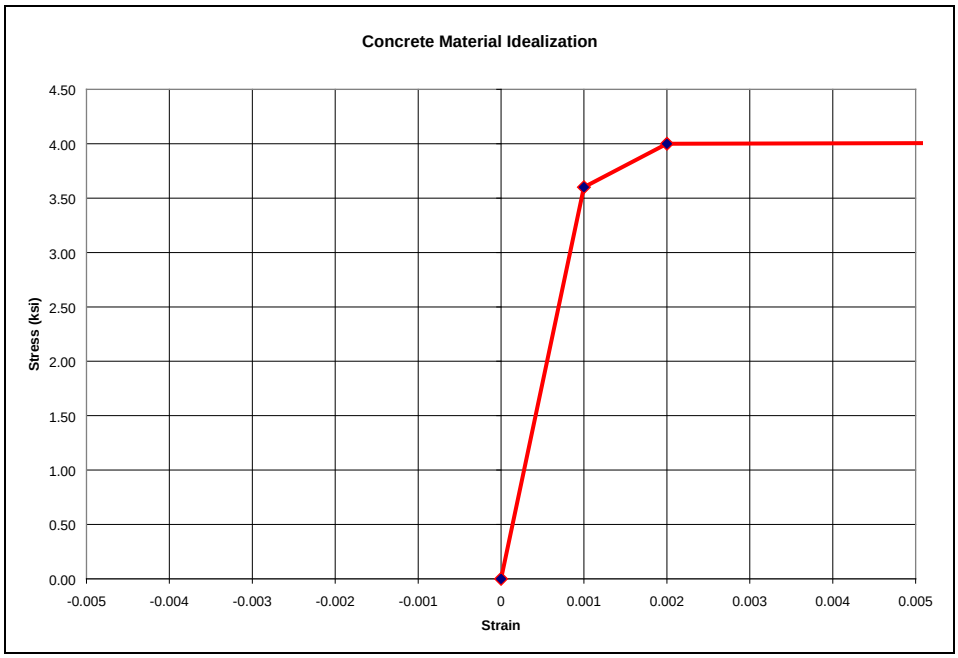

Figure 2-8 Idealized Concrete Material

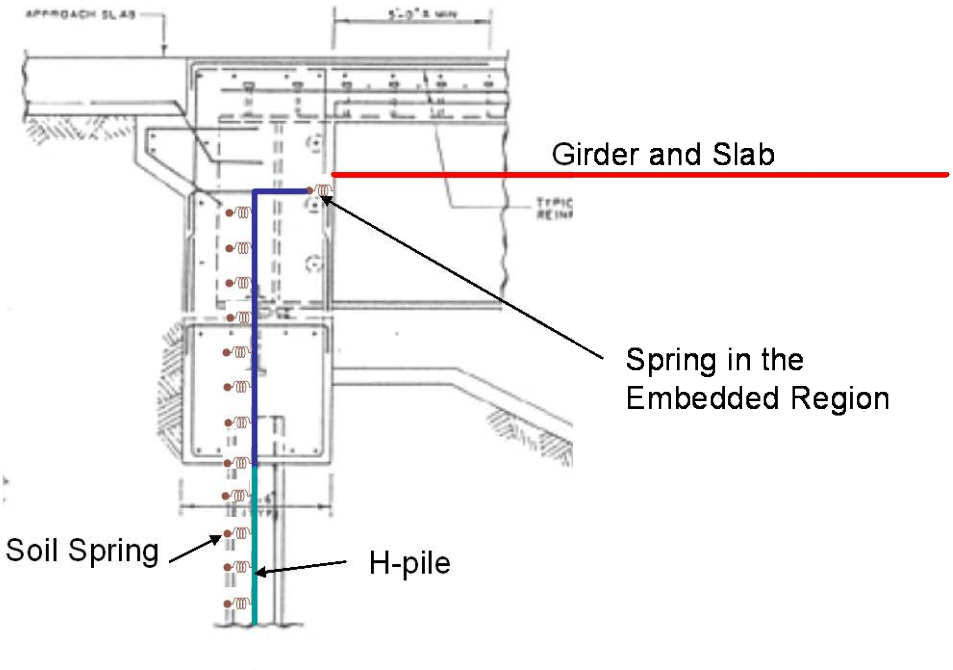

Figure 2-9 Elements of a global model

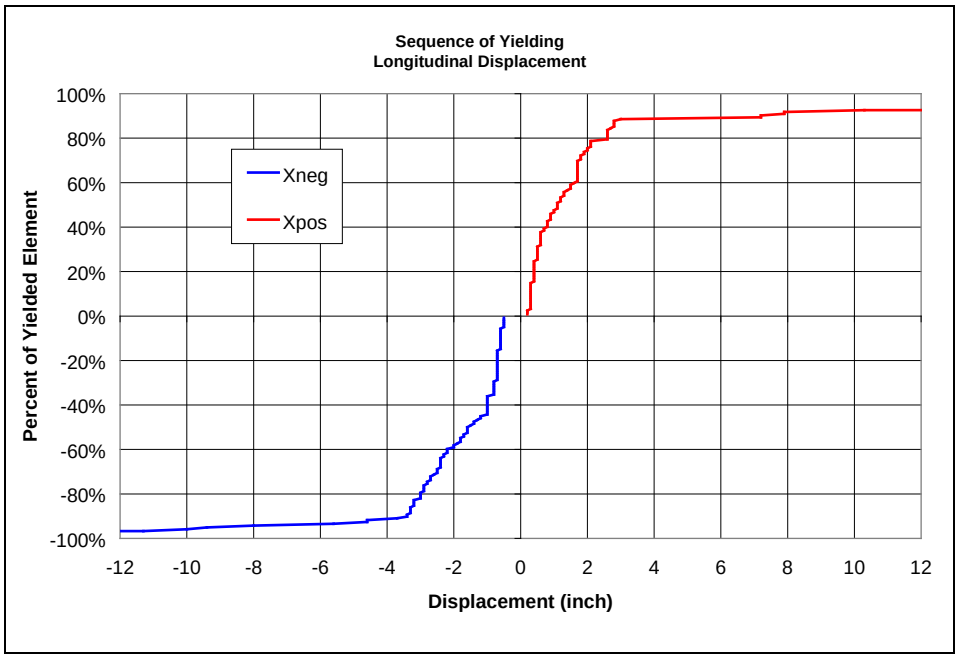

Figure 2-10 Sequence of Yielding of the Embedded Steel Girder - Longitudinal

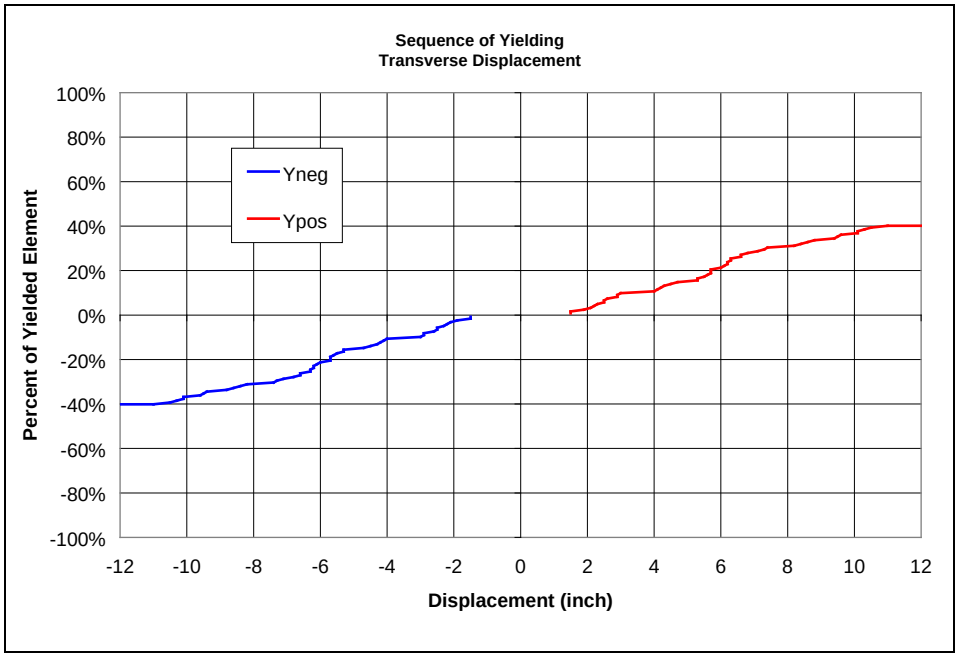

Figure 2-11 Sequence of Yielding of the Embedded Steel Girder - Transverse

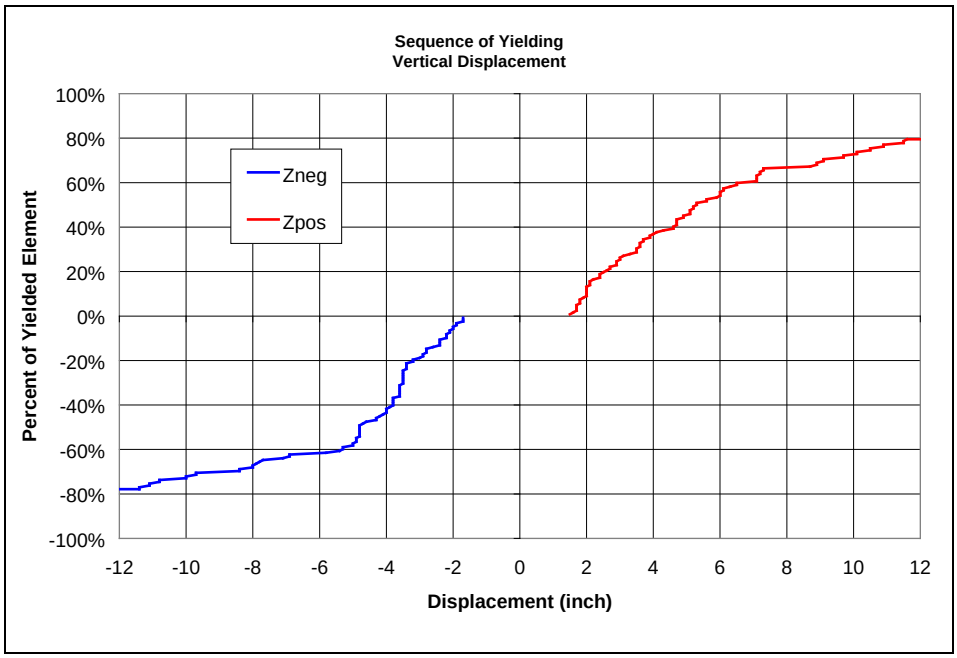

Figure 2-12 Sequence of Yielding of the Embedded Steel Girder - Vertical

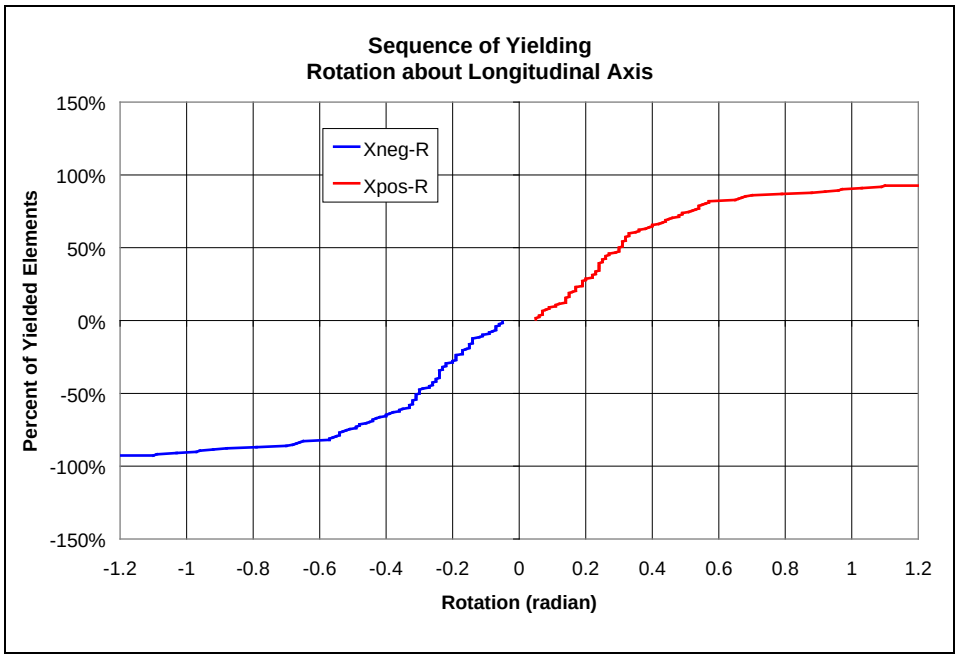

Figure 2-13 Sequence of Yielding of the Embedded Steel Girder – Rotation about Longitudinal Axis

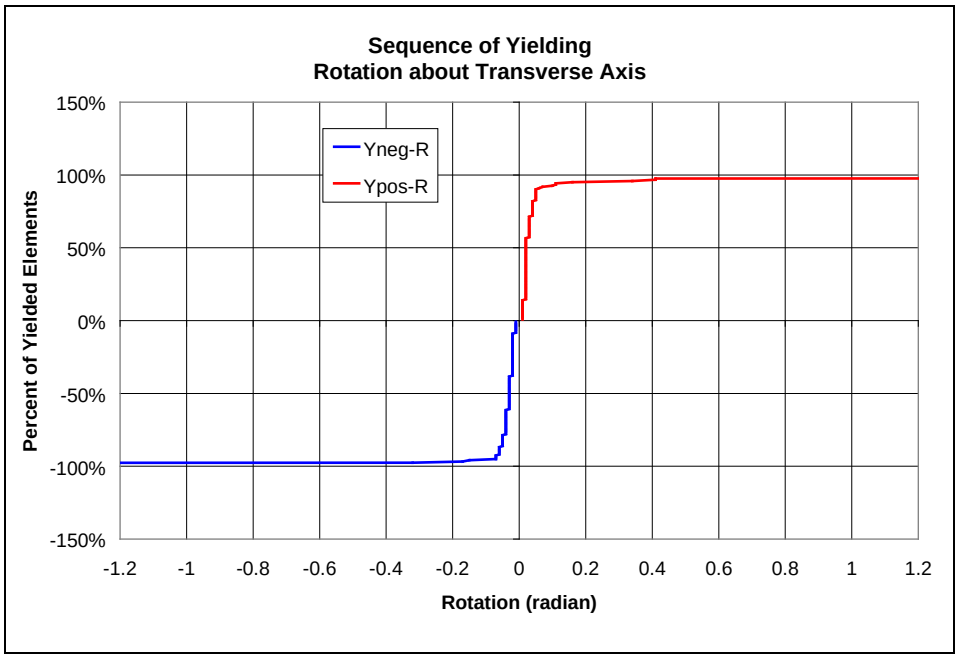

Figure 2-14 Sequence of Yielding of the Embedded Steel Girder – Rotation about Transverse Axis

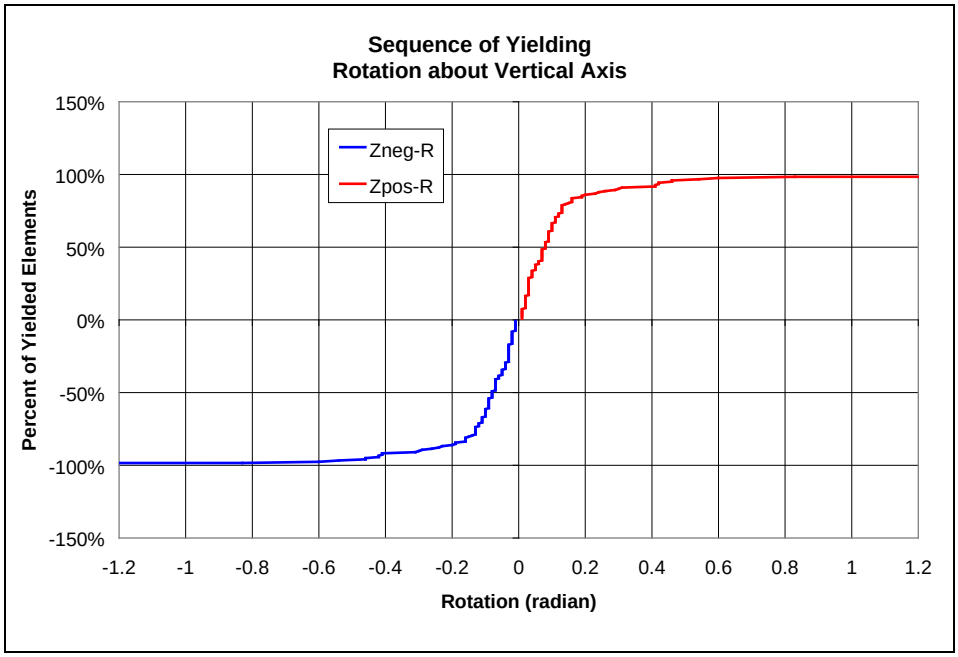

Figure 2-15 Sequence of Yielding of the Embedded Steel Girder – Rotation about Vertical Axis

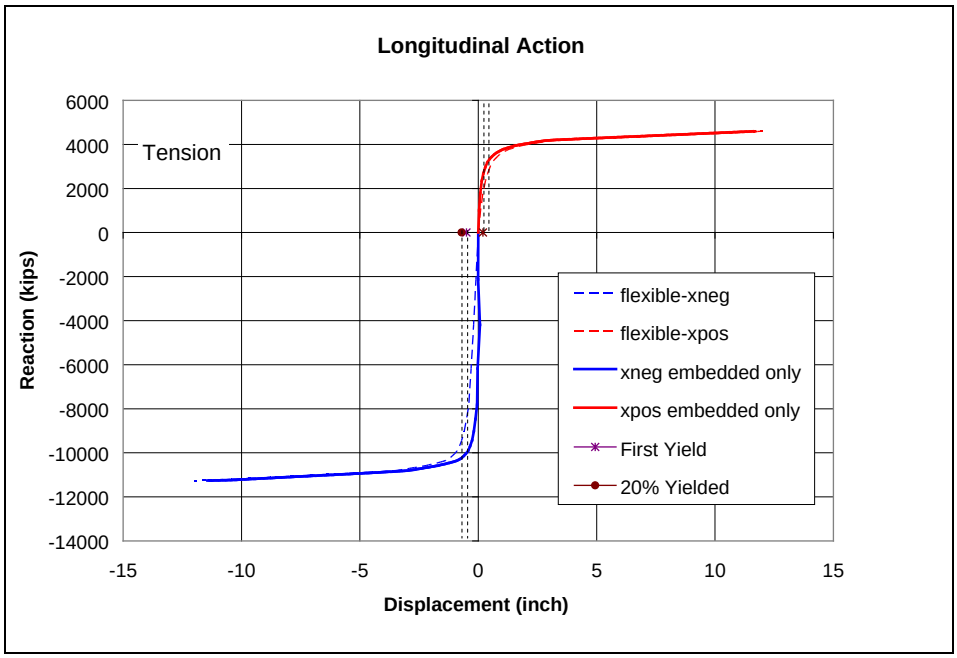

Figure 2-16 Force-Displacement Relation in the Longitudinal Direction

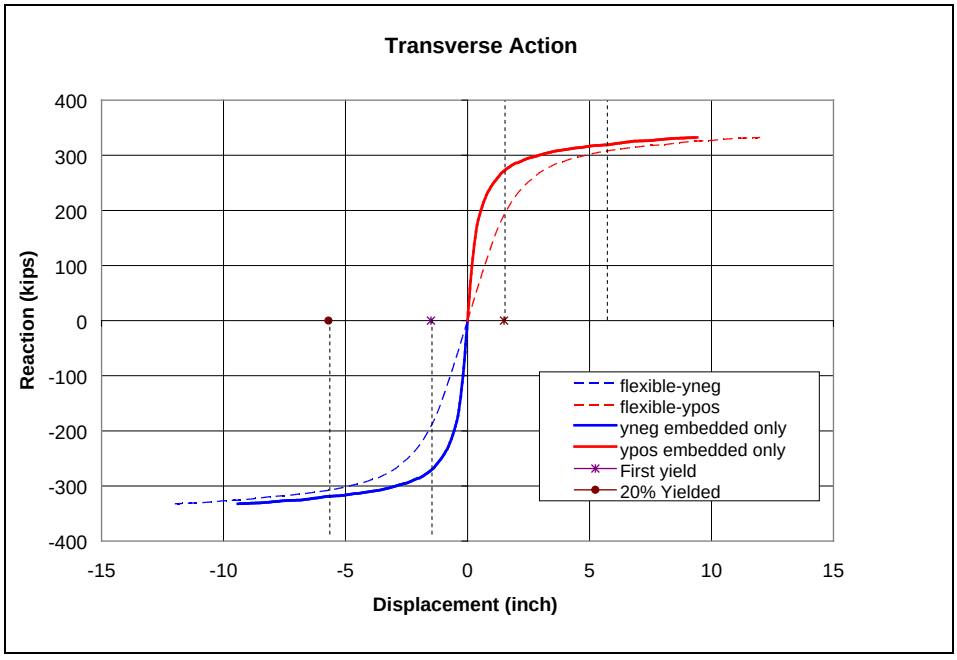

Figure 2-17 Force-Displacement Relation in the Transverse Direction

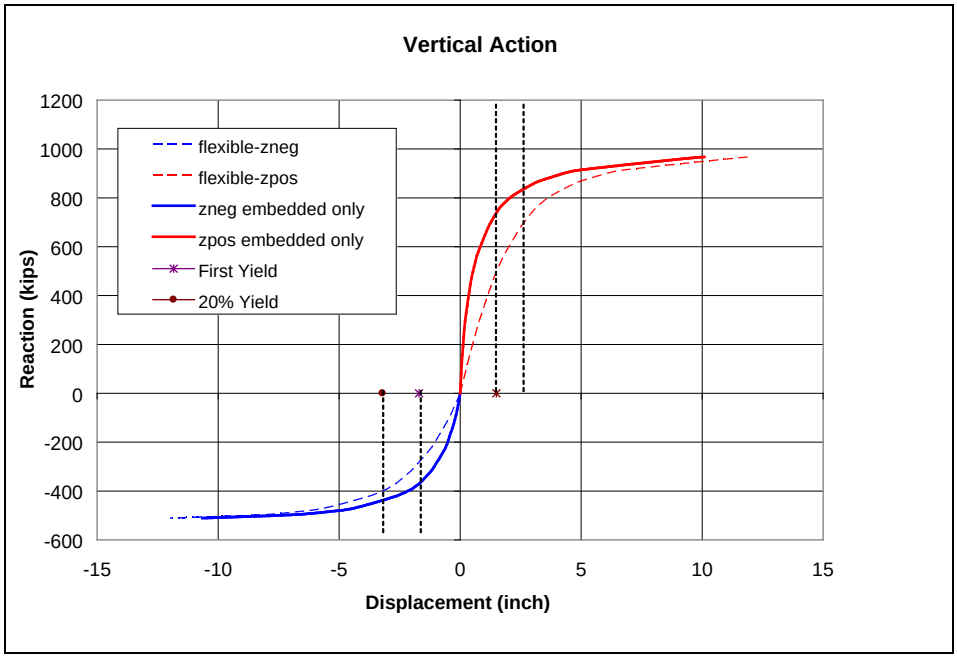

Figure 2-18 Force-Displacement Relation in the Vertical Direction

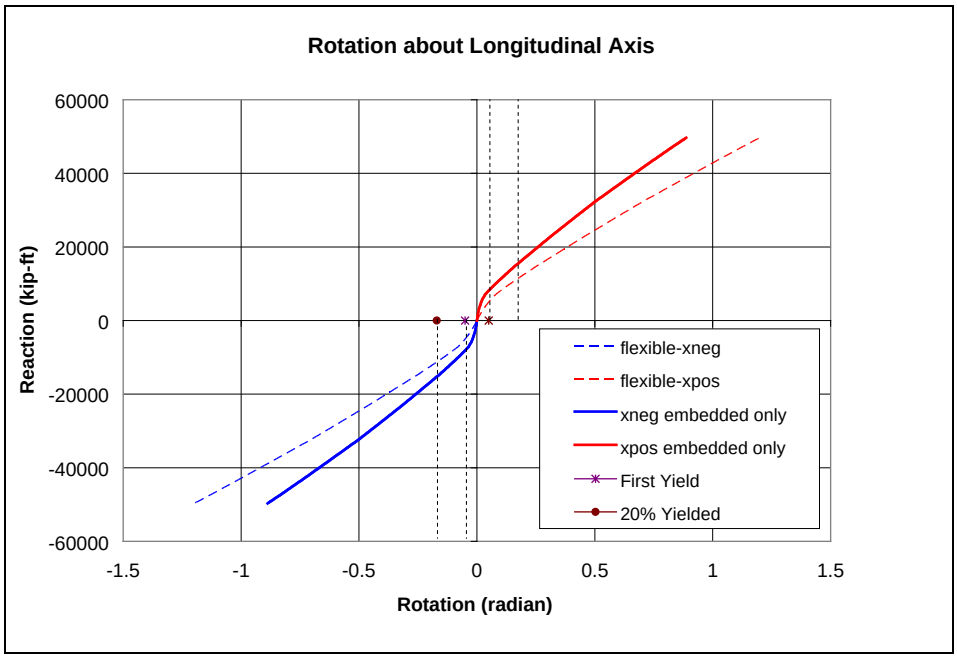

Figure 2-19 Moment-Rotation Relation – Rotation about Longitudinal Axis

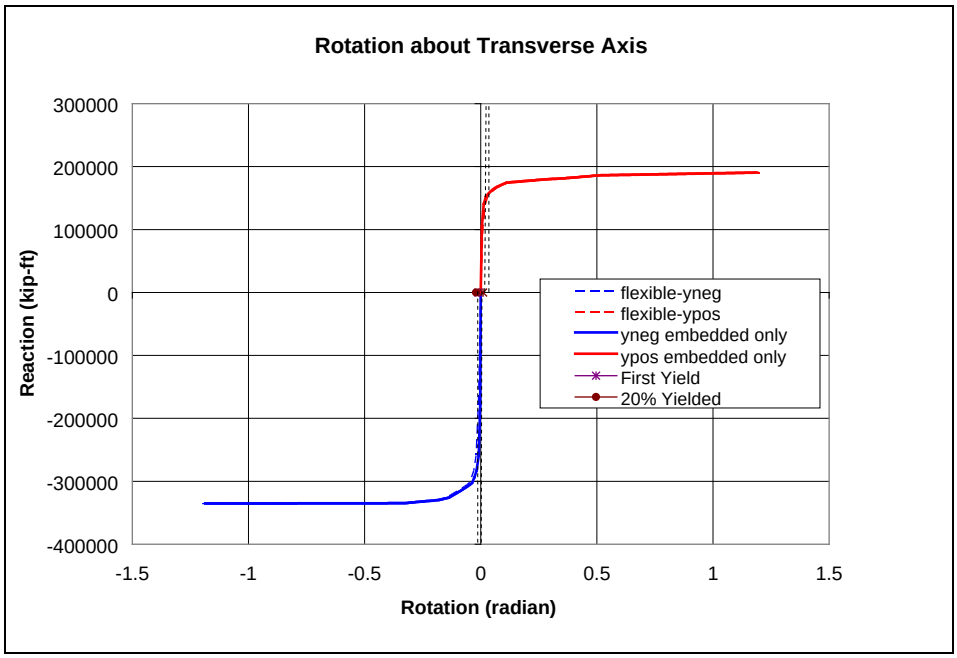

Figure 2-20 Moment-Rotation Relation – Rotation about Transverse Axis

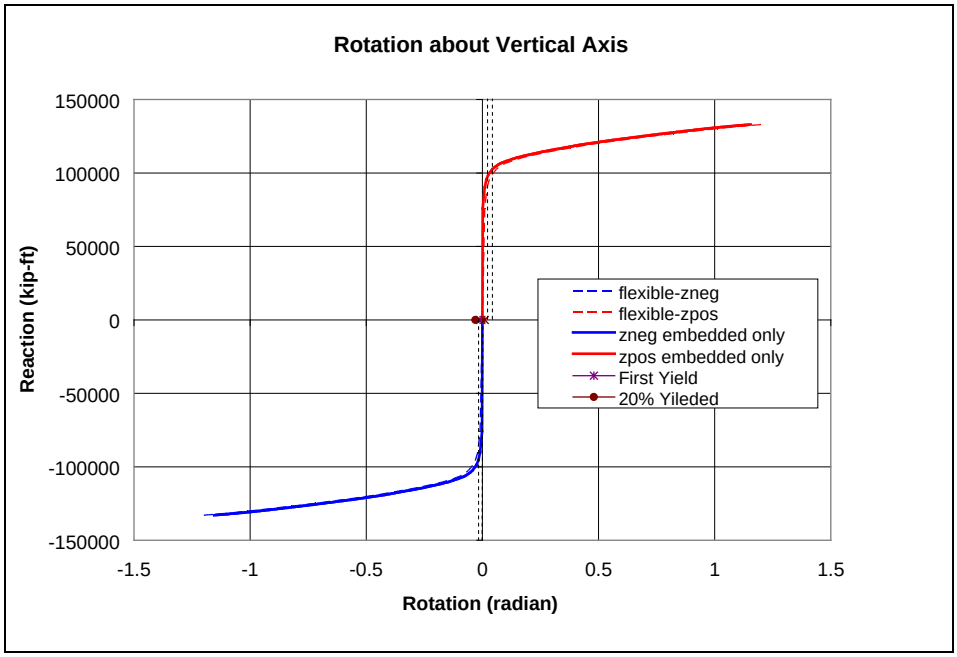

Figure 2-21 Moment-Rotation Relation – Rotation about Vertical Axis

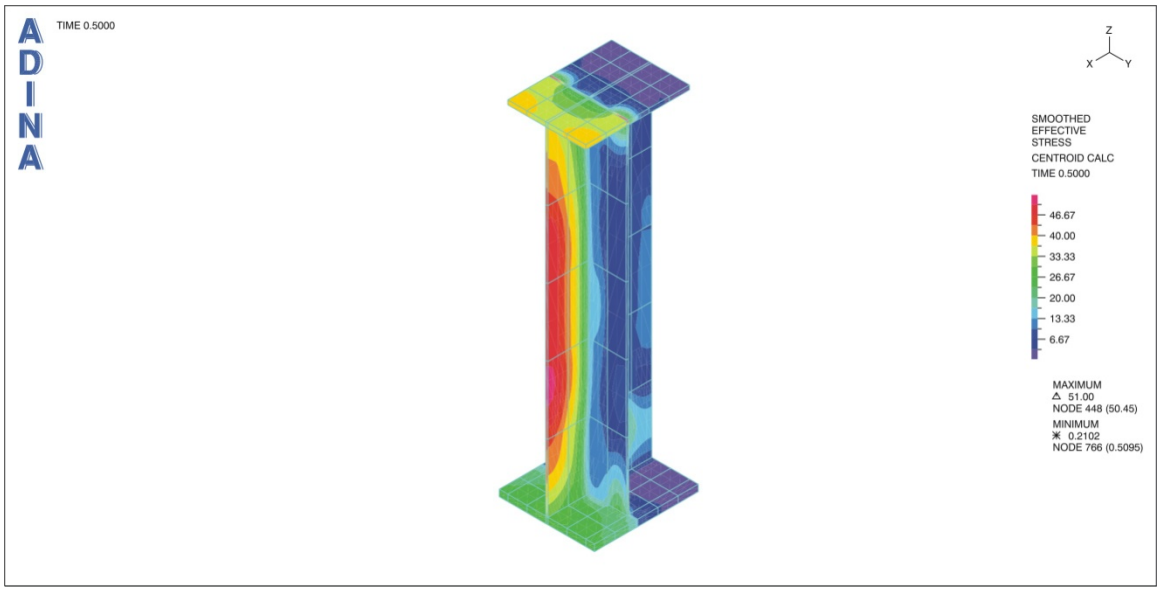

Figure 2-22 Von Mises Stresses in the Embedded Steel Girder – Negative Longitudinal Displacement (Xneg) – At First Yield of Embedded Steel Girder

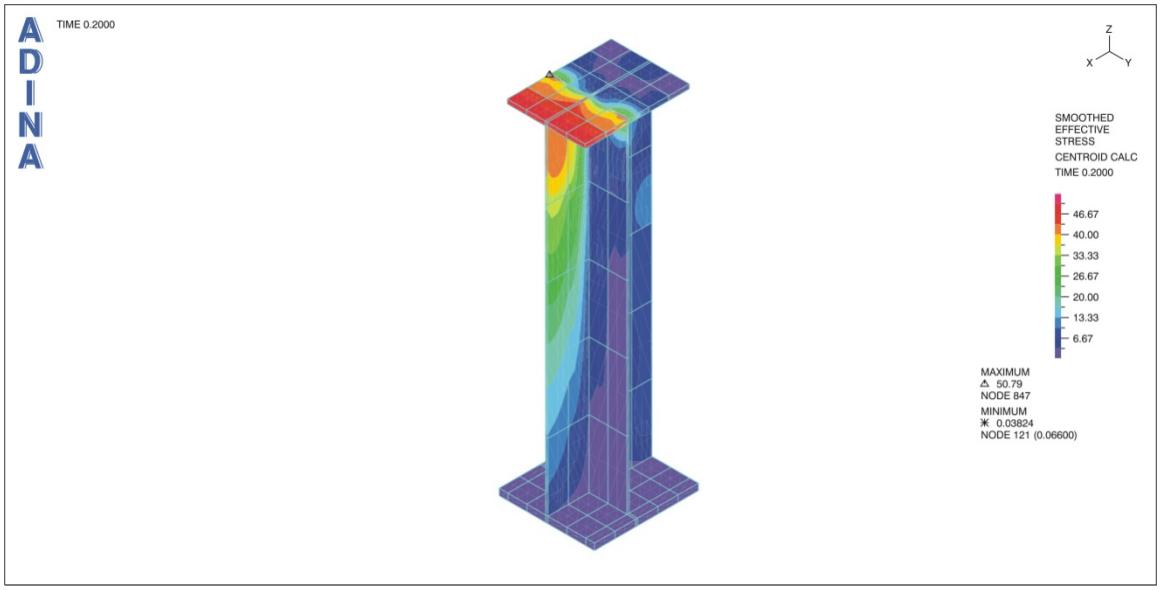

Figure 2-23 Von Mises Stresses in the Embedded Steel Girder – Positive Longitudinal Displacement (Xpos) – At First Yield of Embedded Steel Girder

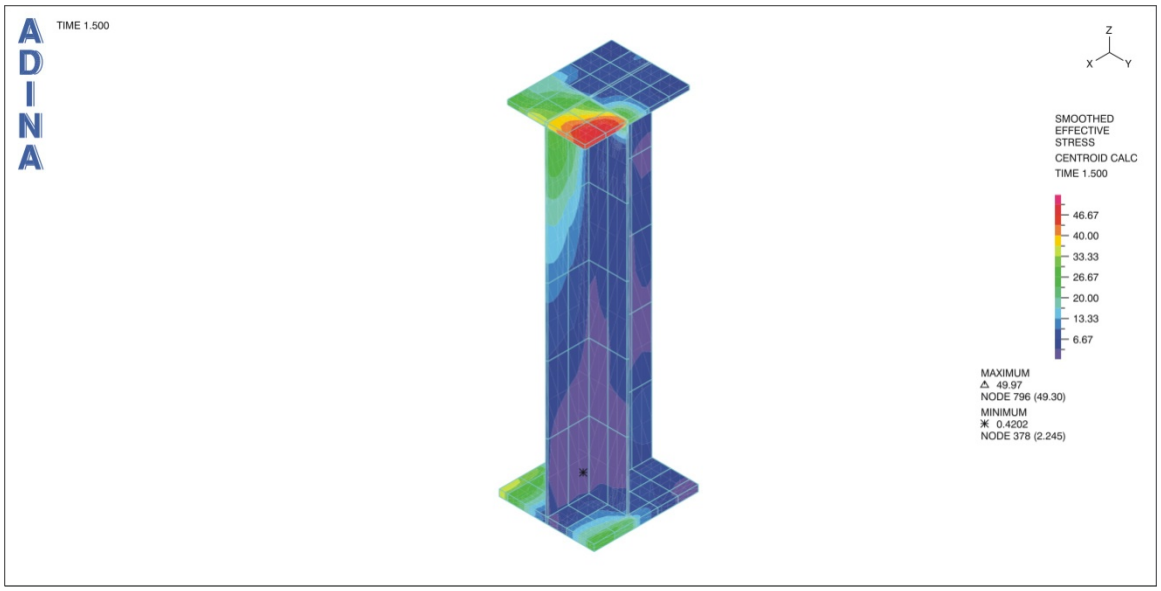

Figure 2-24 Von Mises Stresses in the Embedded Steel Girder – Negative Transverse Displacement (Yneg) – At First Yield of Embedded Steel Girder

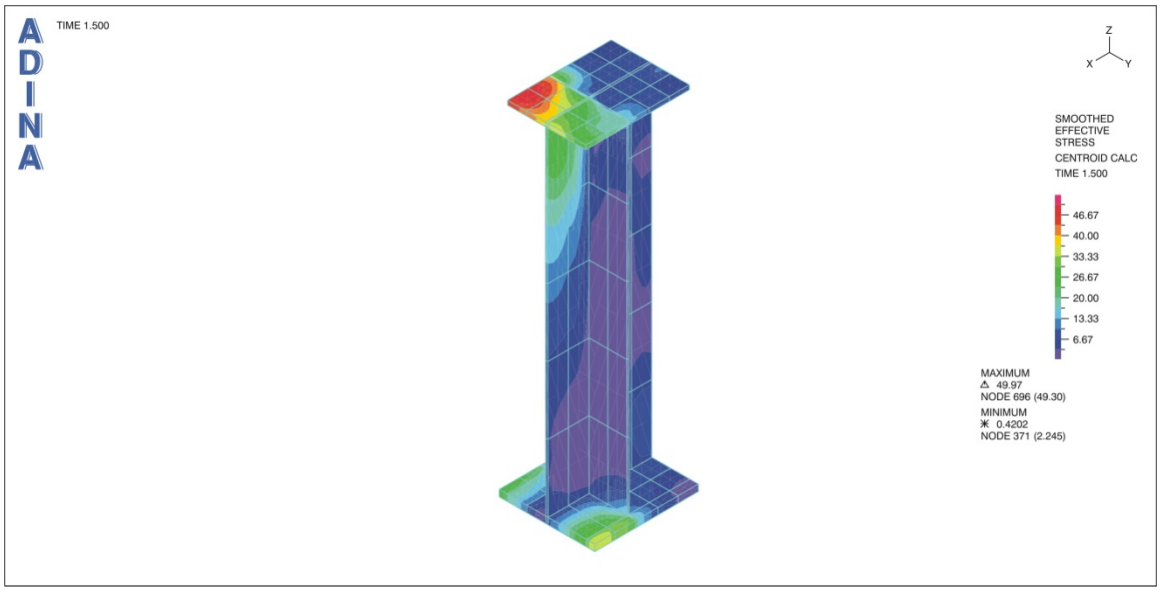

Figure 2-25 Von Mises Stresses in the Embedded Steel Girder – Positive Transverse Displacement (Ypos) – At First Yield of Embedded Steel Girder

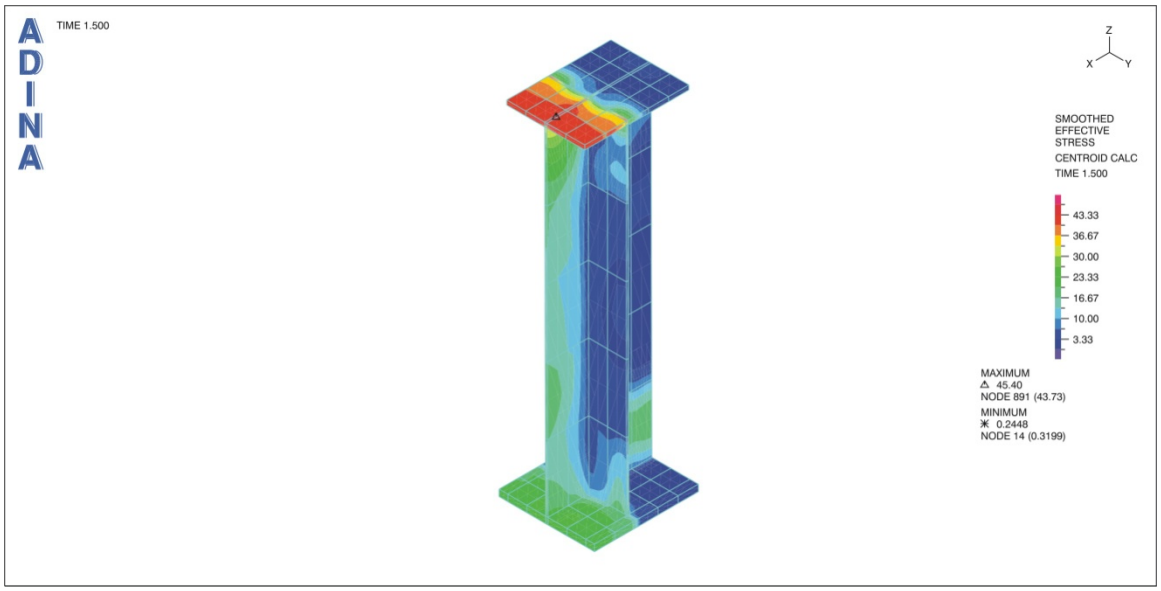

Figure 2-26 Von Mises Stresses in the Embedded Steel Girder – Negative Vertical Displacement (Zneg) – At First Yield of Embedded Steel Girder

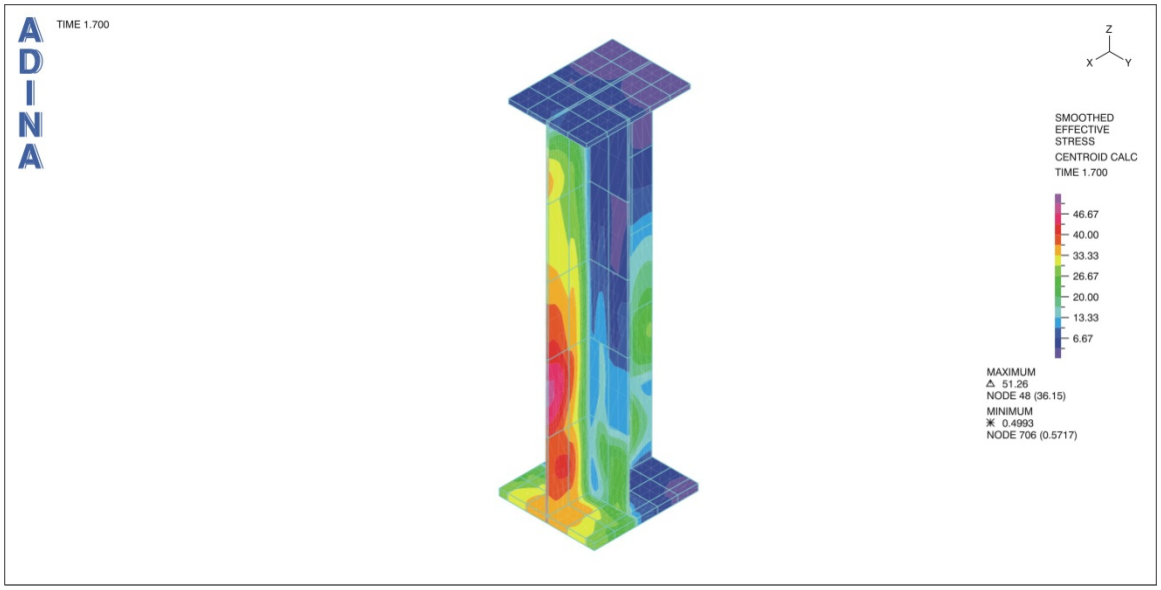

Figure 2-27 Von Mises Stresses in the Embedded Steel Girder – Positive Vertical Displacement (Zpos) – At First Yield of Embedded Steel Girder

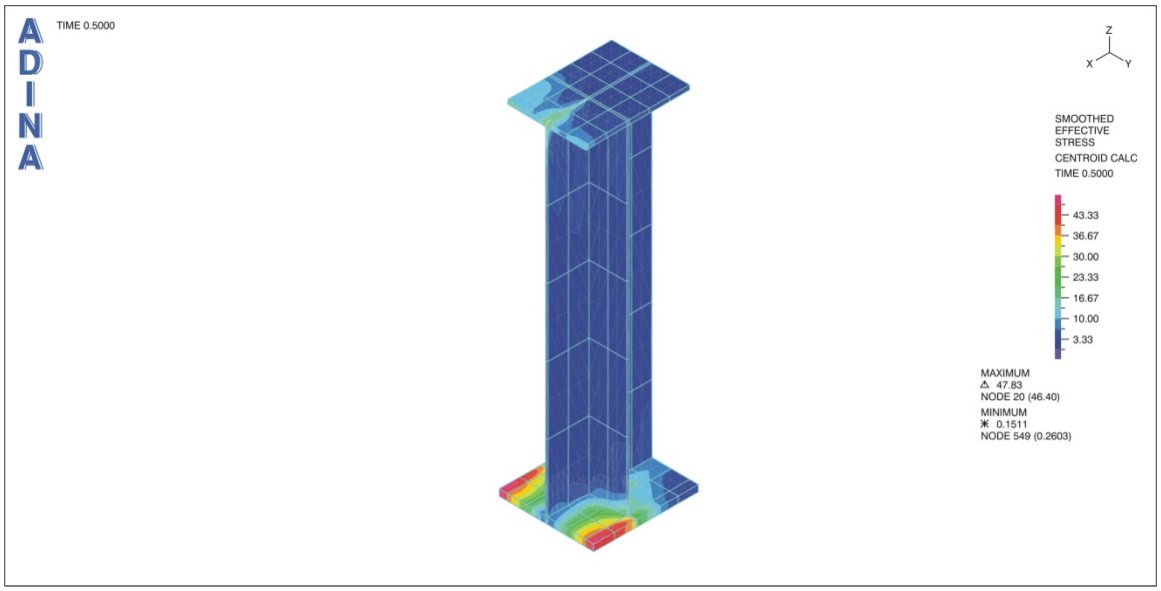

Figure 2-28 Von Mises Stresses in the Embedded Steel Girder – Negative Rotation about the Longitudinal Axis (Xneg-R) – At First Yield of Embedded Steel Girder

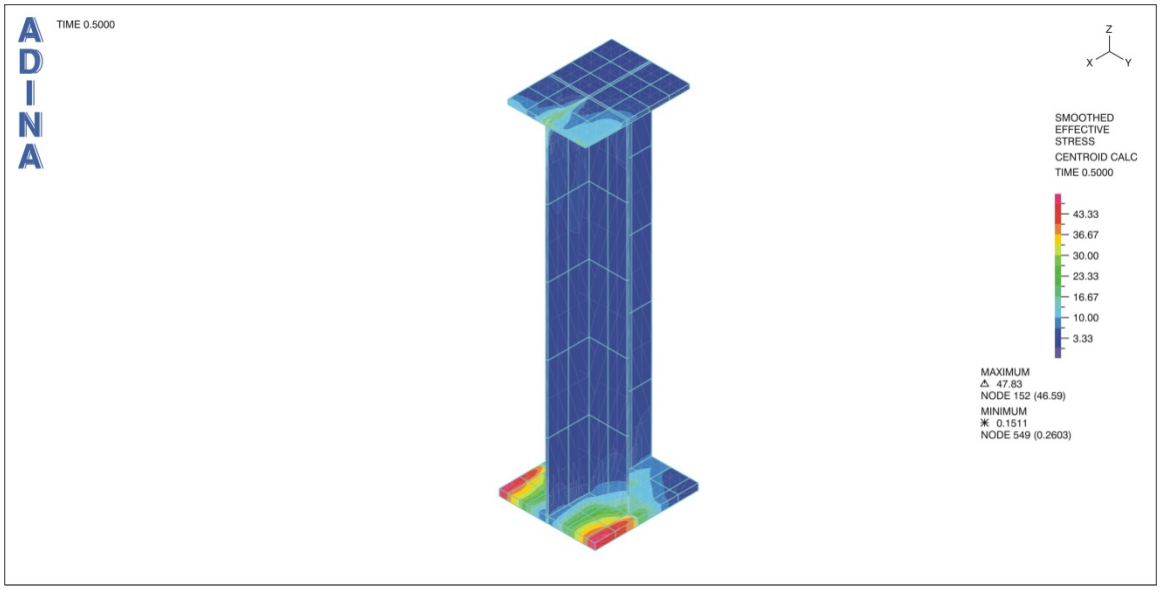

Figure 2-29 Von Mises Stresses in the Embedded Steel Girder – Positive Rotation about the Longitudinal Axis (Xpos-R) – At First Yield of Embedded Steel Girder

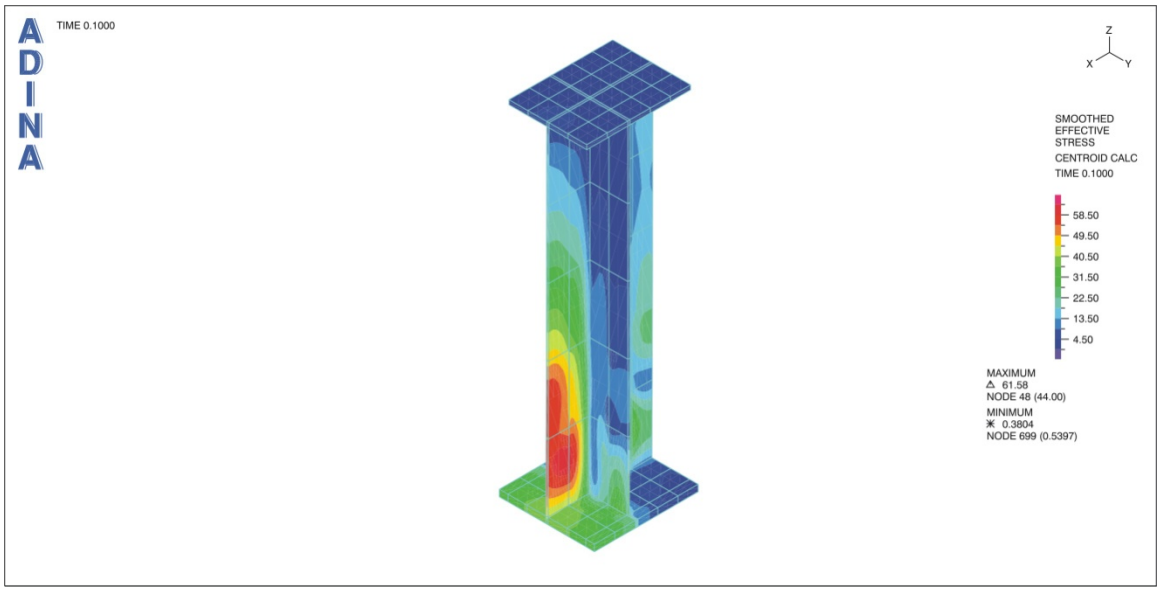

Figure 2-30 Von Mises Stresses in the Embedded Steel Girder – Negative Rotation about the Transverse Axis (Yneg-R) – At First Yield of Embedded Steel Girder

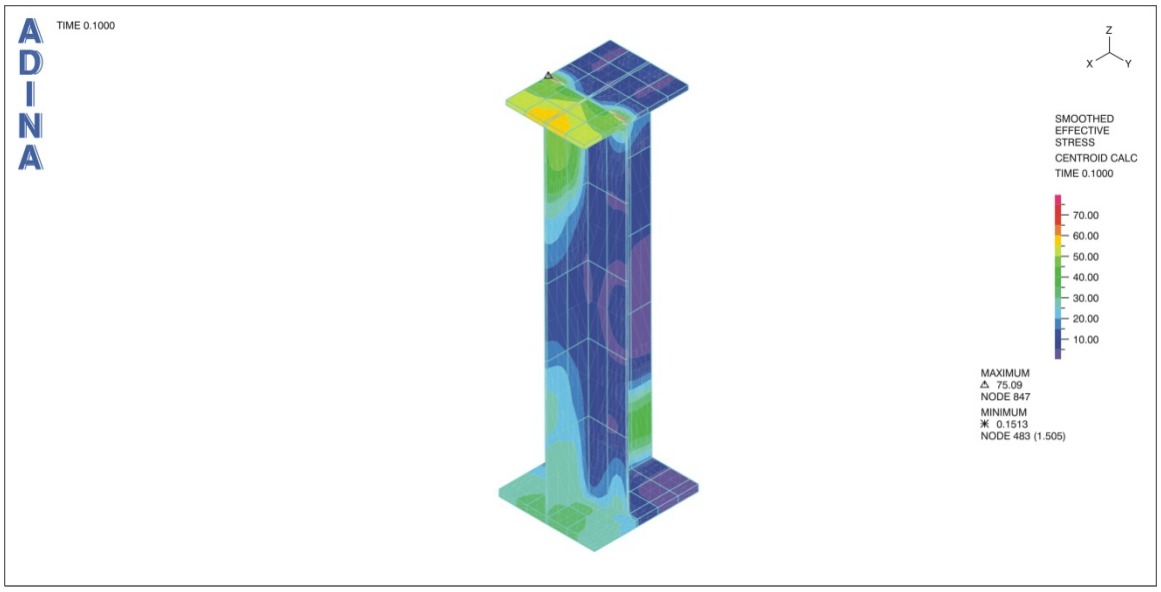

Figure 2-31 Von Mises Stresses in the Embedded Steel Girder – Positive Rotation about Transverse Axis (Ypos-R) – At First Yield of Embedded Steel Girder

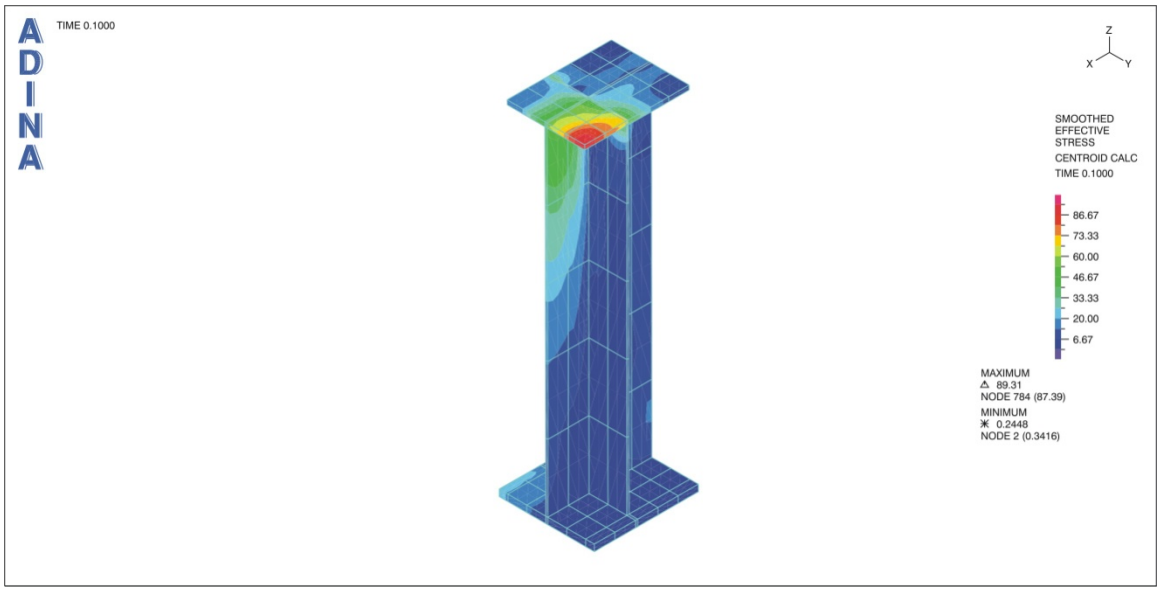

Figure 2-32 Von Mises Stresses in the Embedded Steel Girder – Negative Rotation about Vertical Axis (Zneg-R) – At First Yield of Embedded Steel Girder

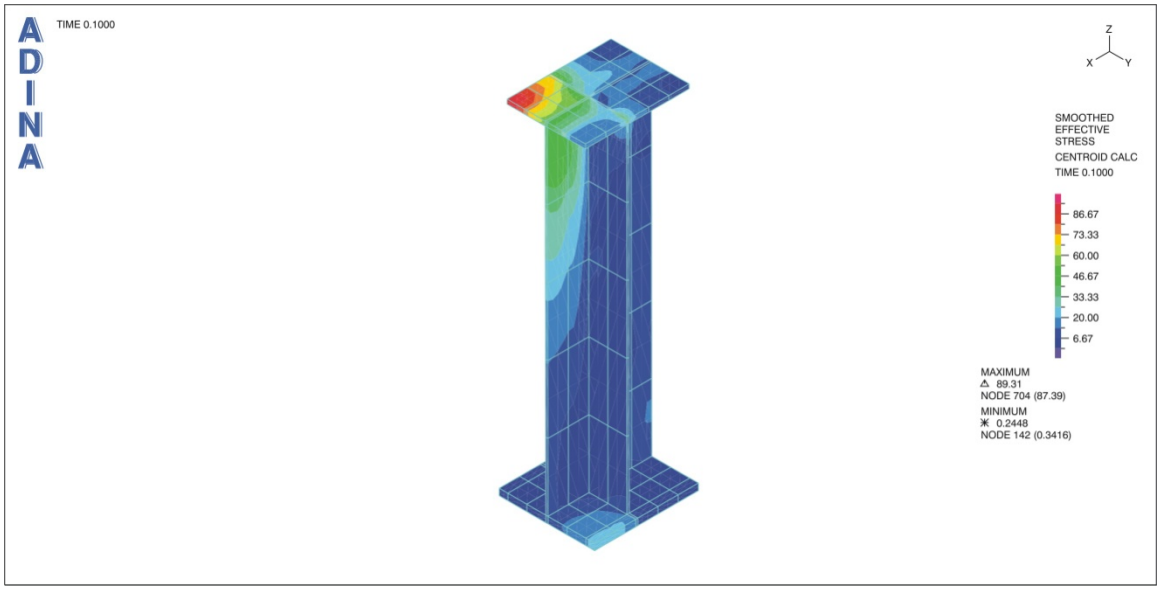

Figure 2-33 Von Mises Stresses in the Embedded Steel Girder – Positive Rotation about Vertical Axis (Zpos-R) – At First Yield of Embedded Steel Girder

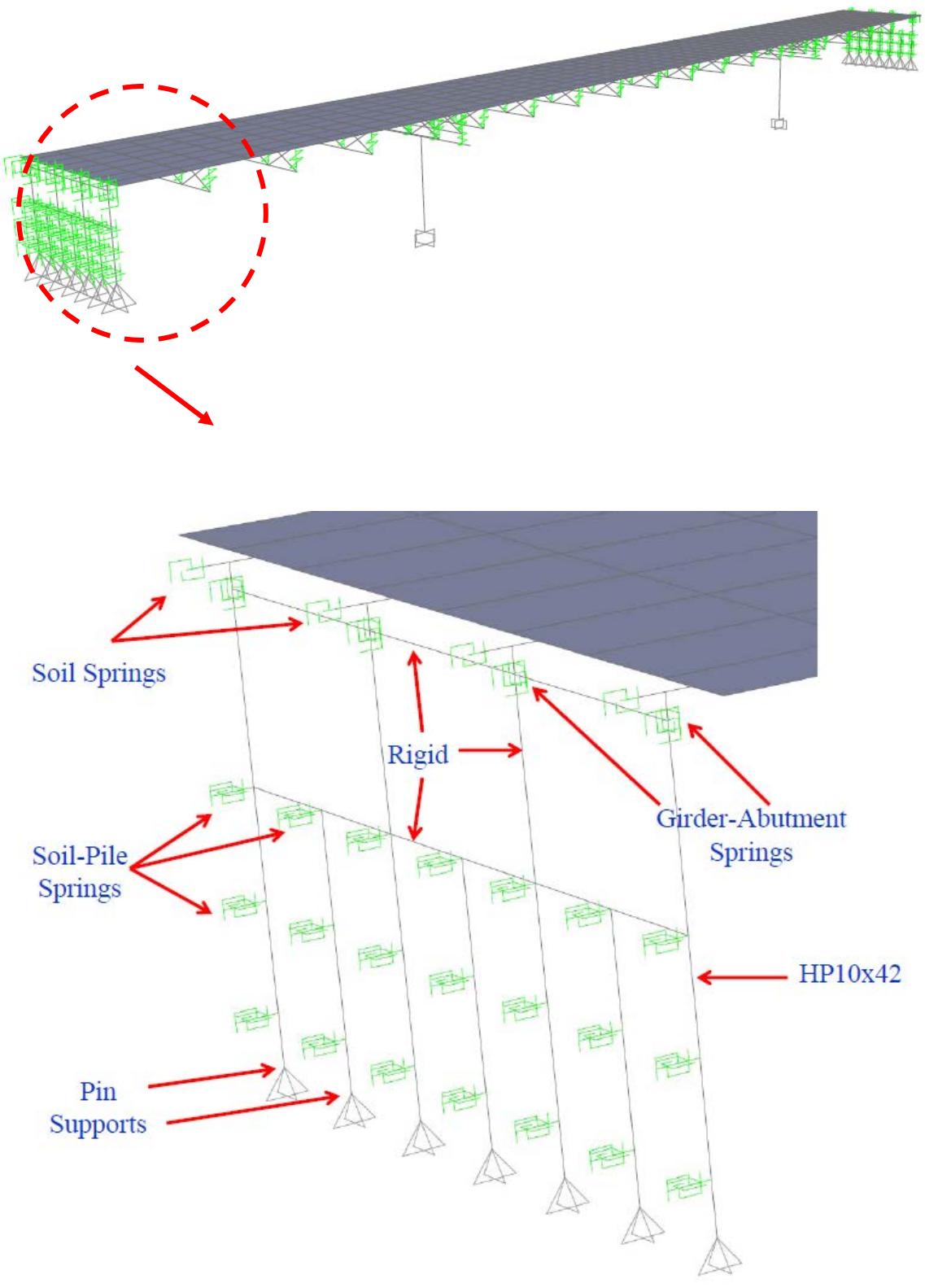

Figure 2-34 3D view of bridge model

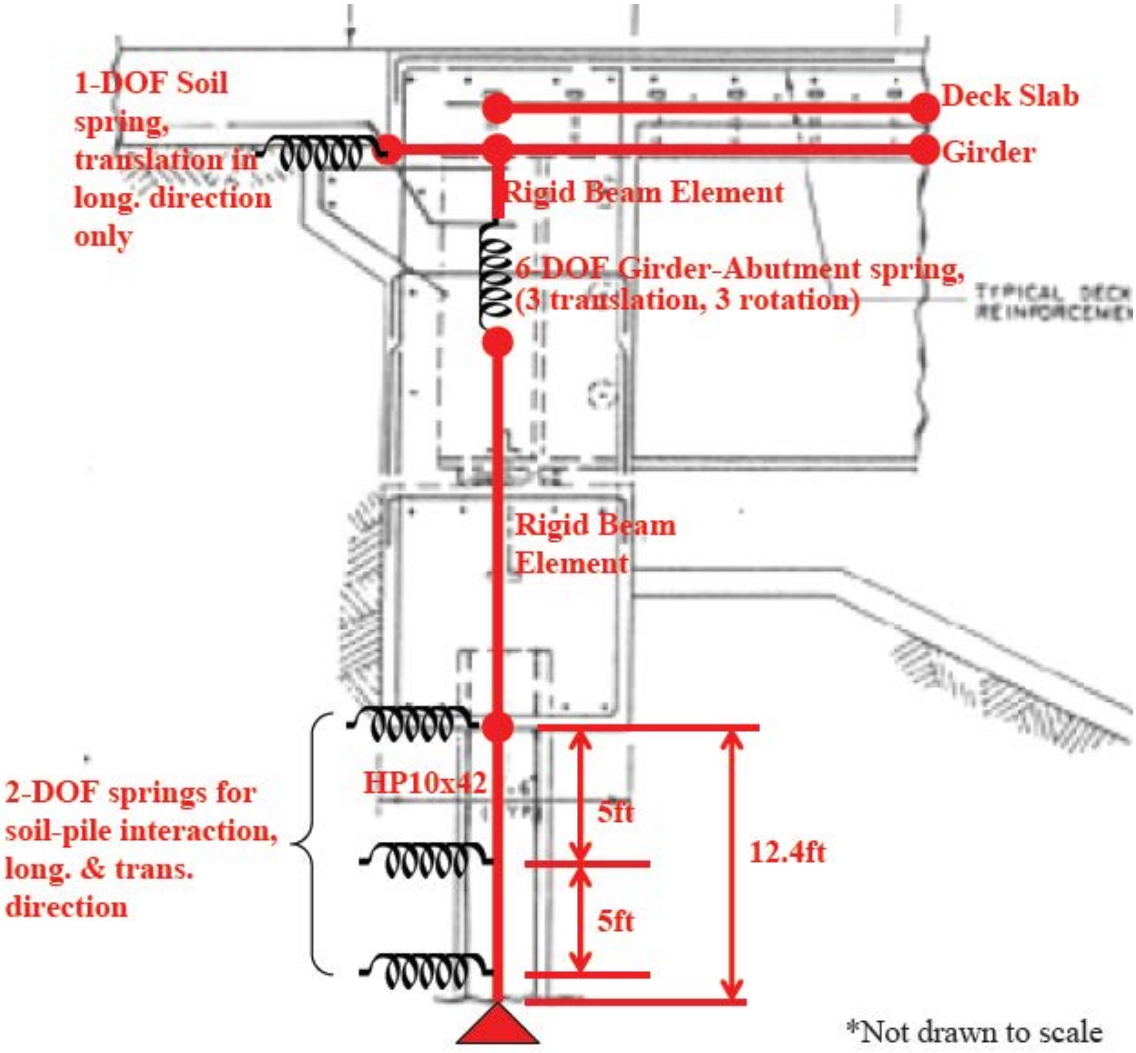

Figure 2-35 Abutment model at each girder

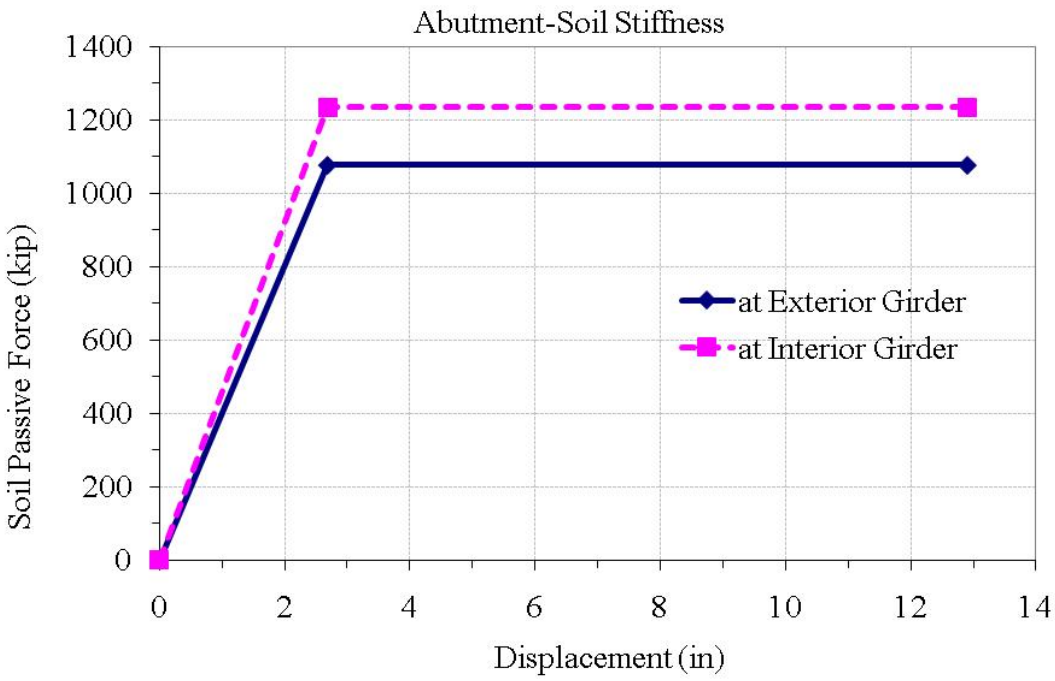

Figure 2-36 Soil Passive Force – Displacement at Exterior and Interior Girder

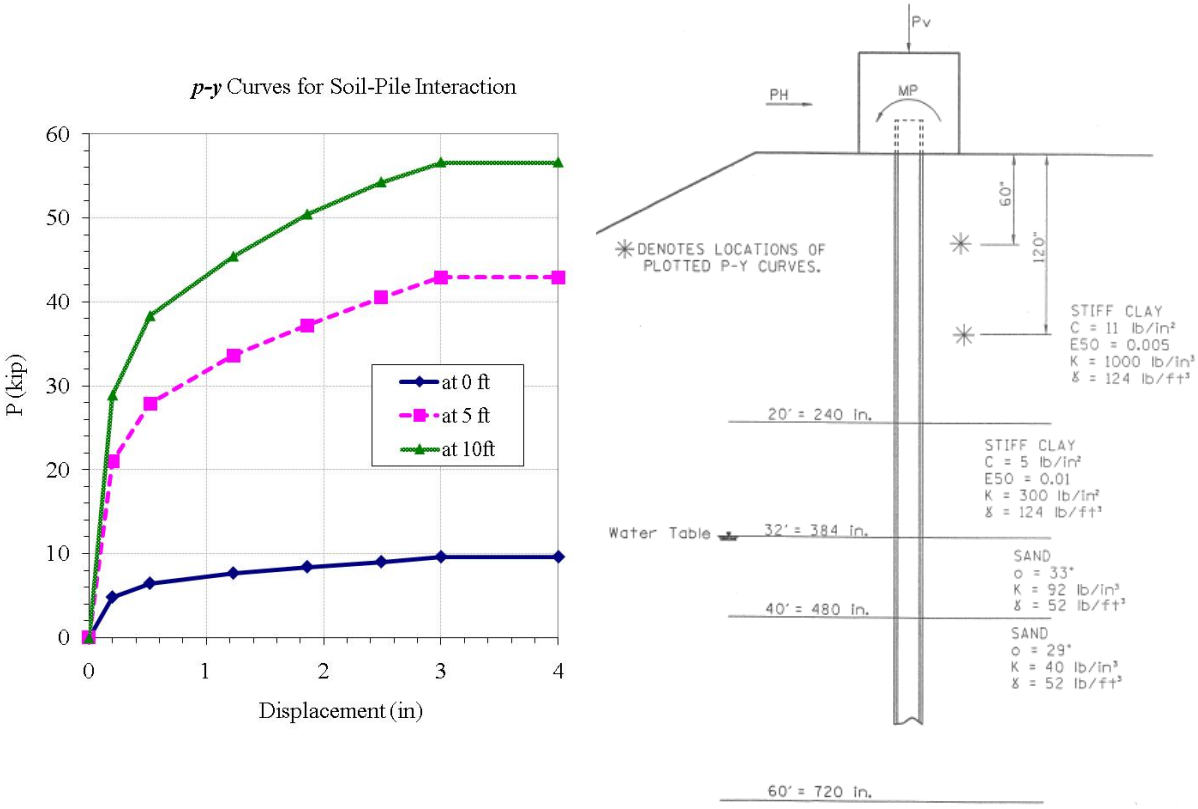

Figure 2-37 *p-y* Curves for Soil-Pile Interaction

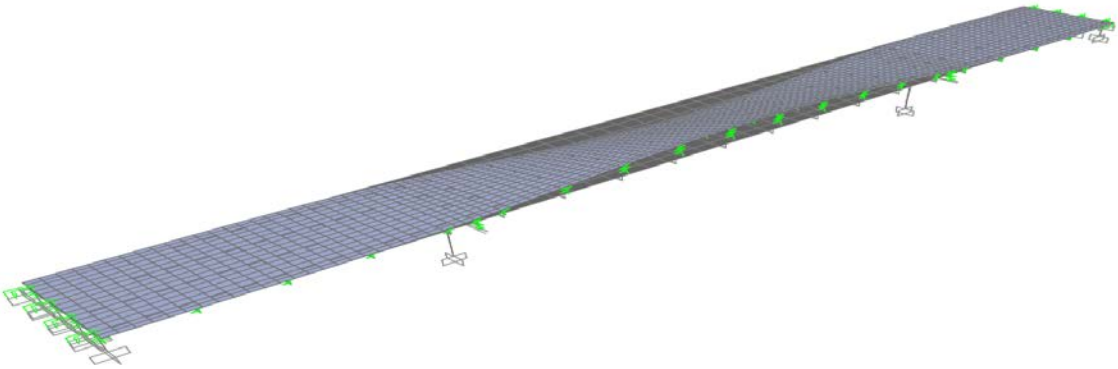

T1 = 0.623 sec

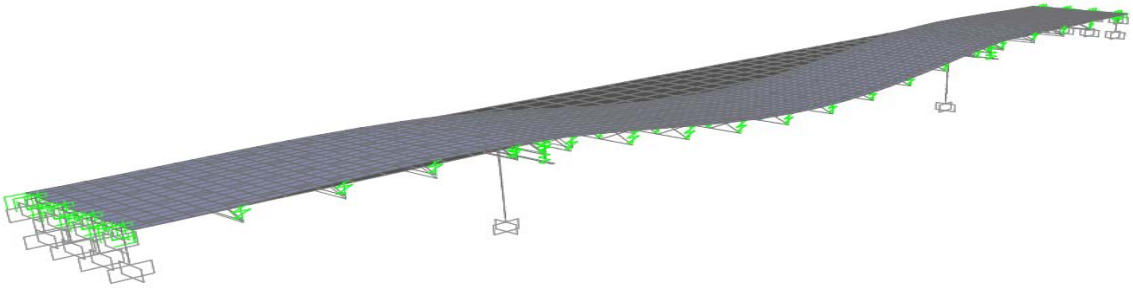

T2 = 0.582 sec

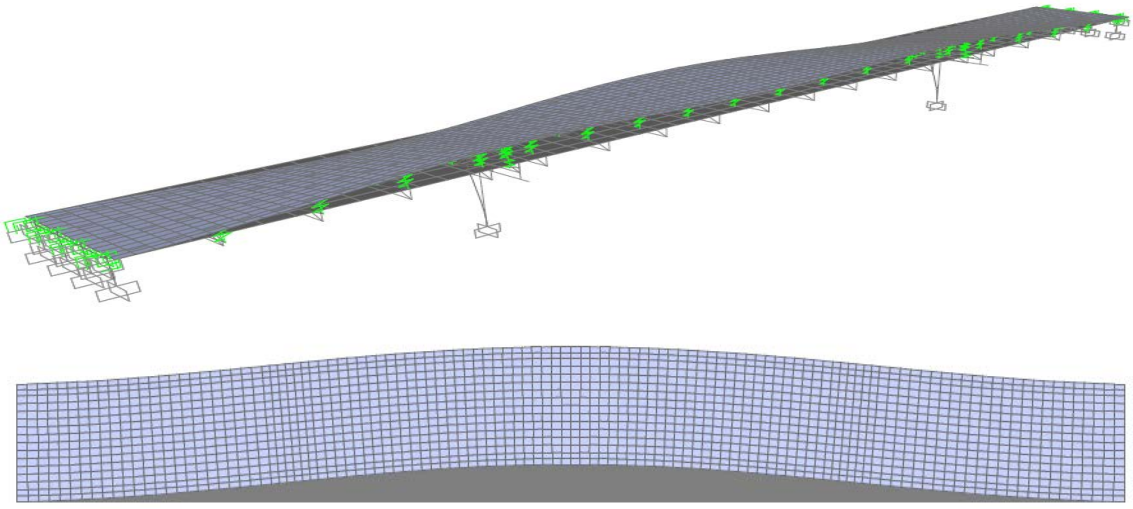

T3 = 0.378 sec

Figure 2-38a Mode Shapes of Case 1 (Modes 1, 2, and 3)

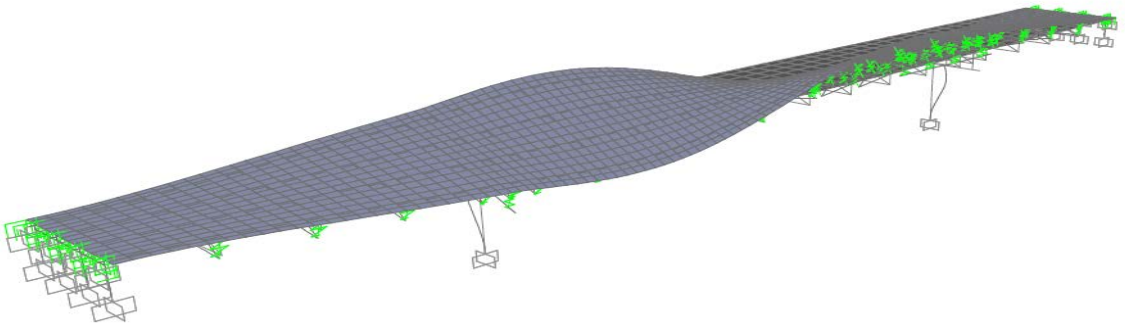

T4 = 0.284 sec

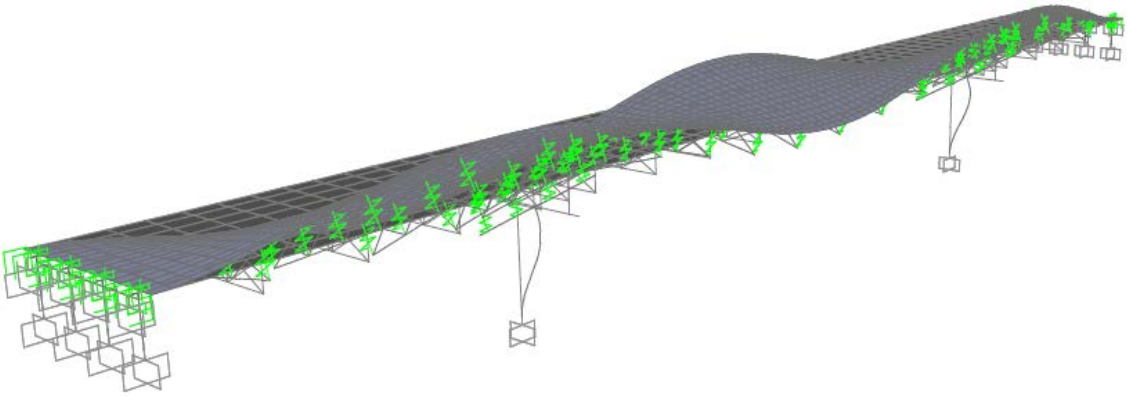

T5 = 0.234 sec

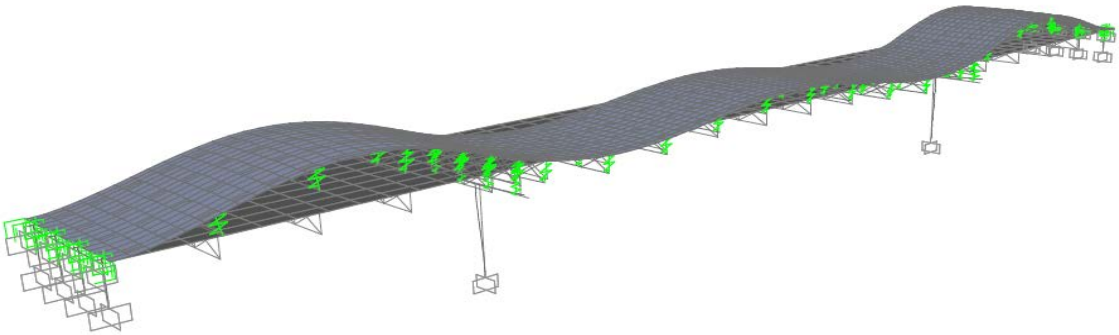

T9 = 0.145 sec

Figure 2-38b Mode Shapes of Case 1 (Modes 4, 5, and 9)

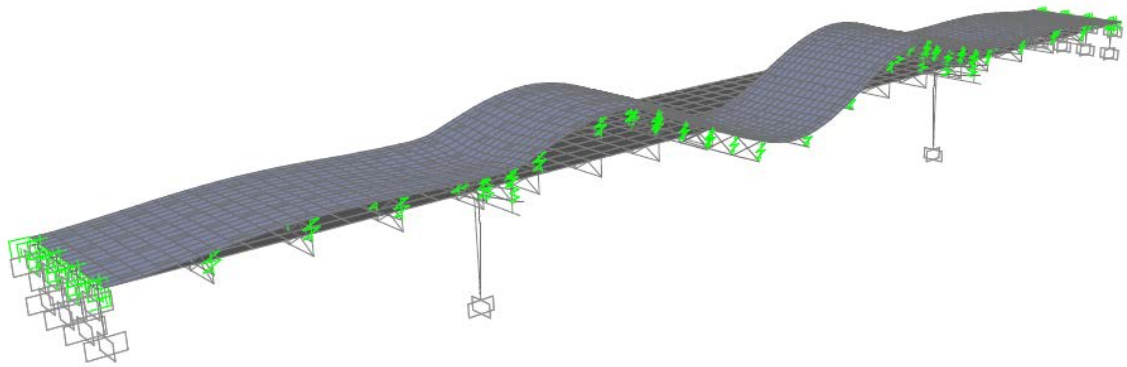

T13 = 0.107 sec

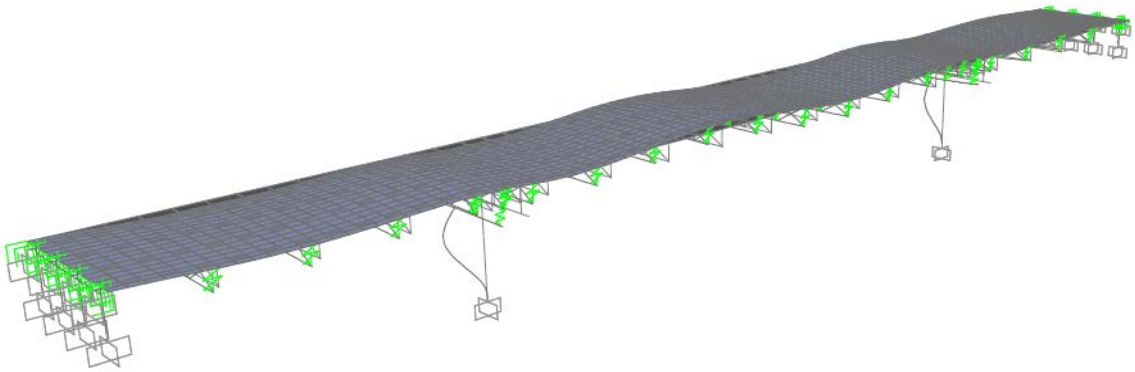

T15 = 0.085 sec

Figure 2-38 Mode shapes of Case 1

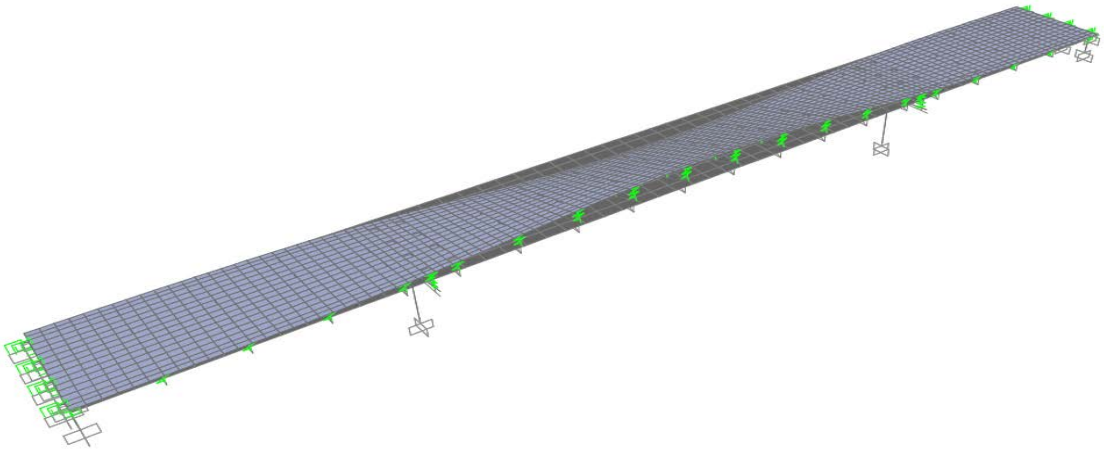

T1 = 0.667 sec

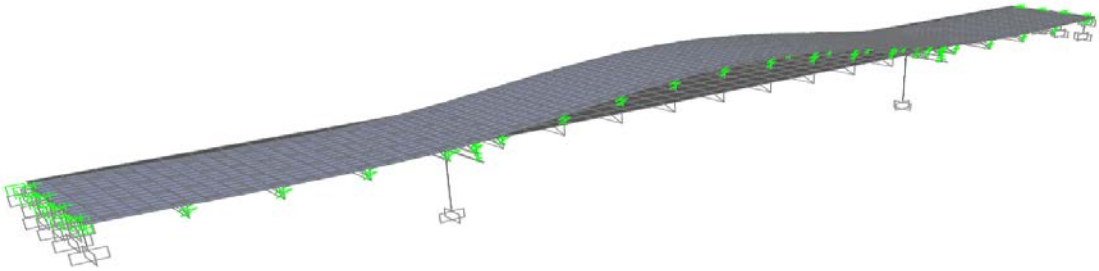

T2 = 0.599 sec

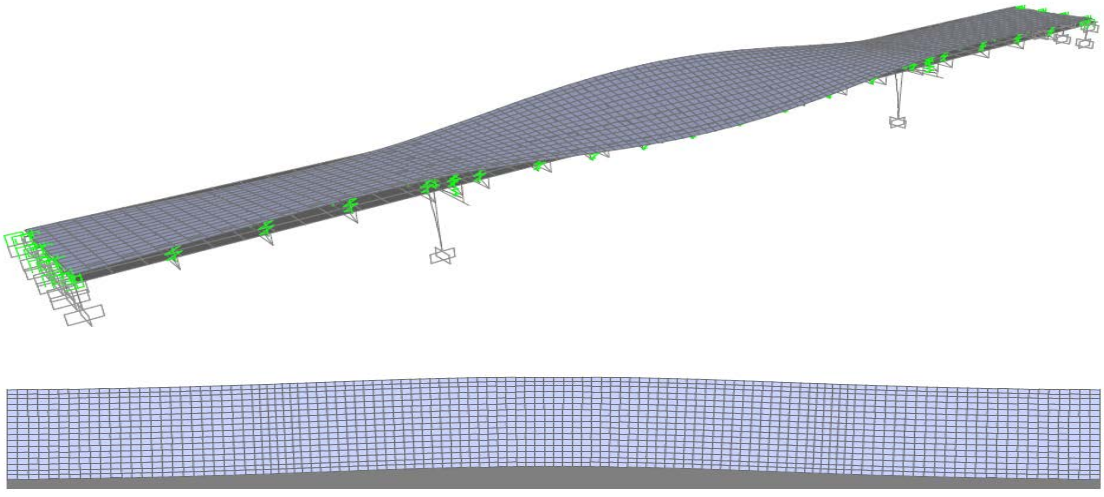

T3 = 0.530 sec

Figure 2-39a Mode Shapes of Case 2 (Modes 1, 2, and 3)

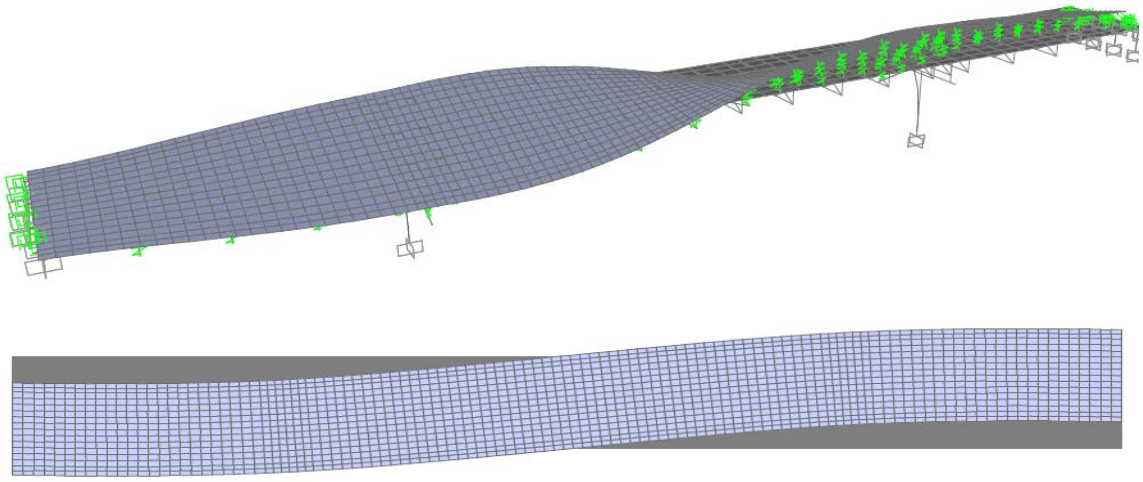

T4 = 0.335 sec

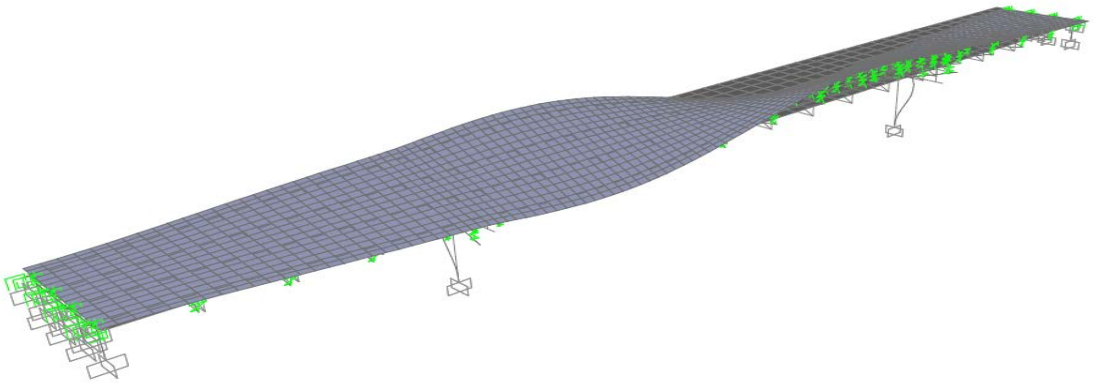

T5 = 0.280 sec

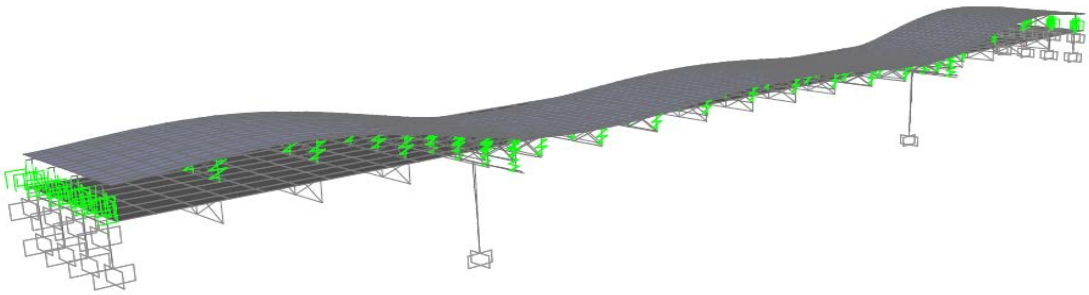

T9 = 0.207 sec

Figure 2-39b Mode Shapes of Case 2 (Modes 4, 5, and 9)

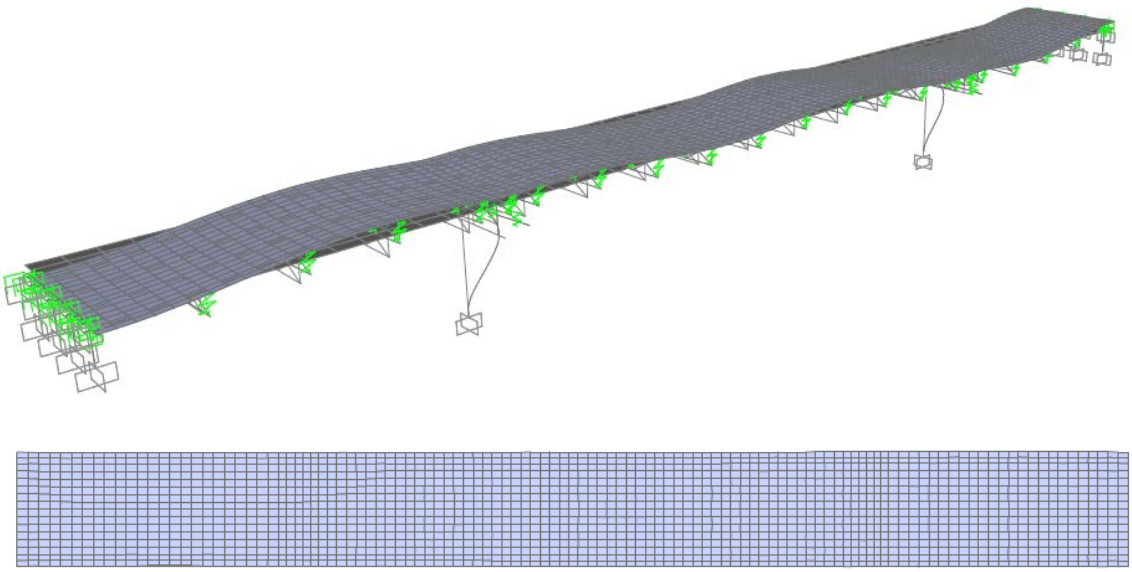

T19 = 0.084 sec

Figure 2-39 Mode shapes of Case 2

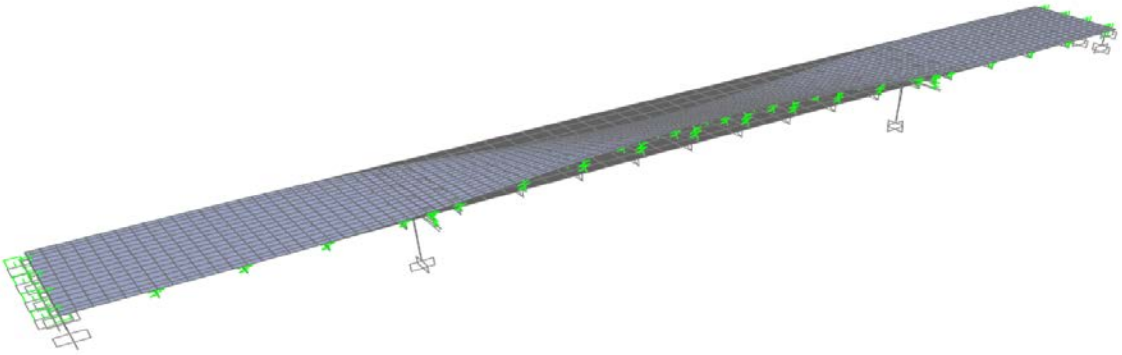

T1 = 0.623 sec

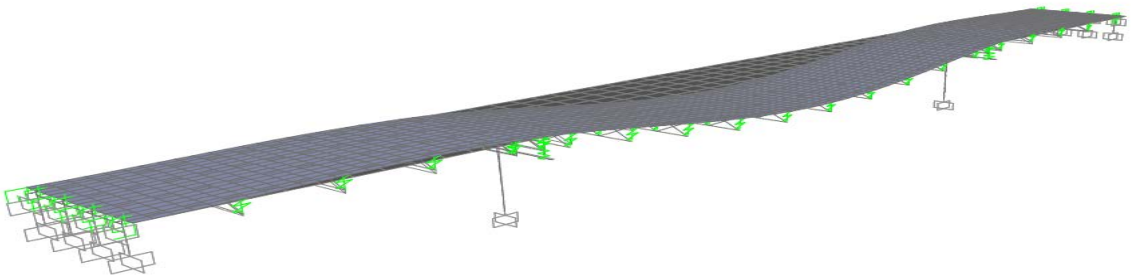

T2 = 0.582 sec

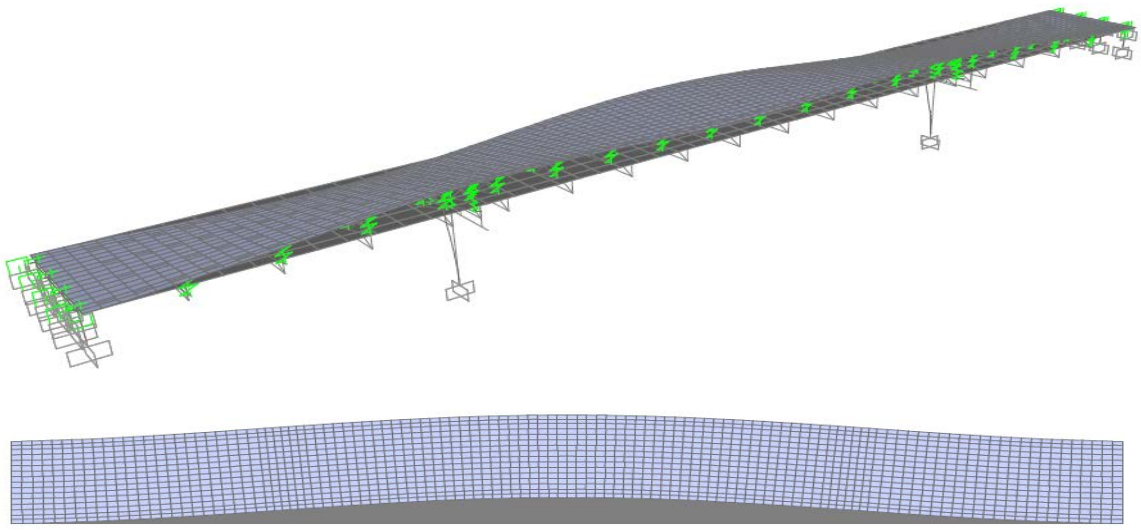

T3 = 0.378 sec

Figure 2-40a Mode Shapes of Case 3 (Modes 1, 2, and 3)

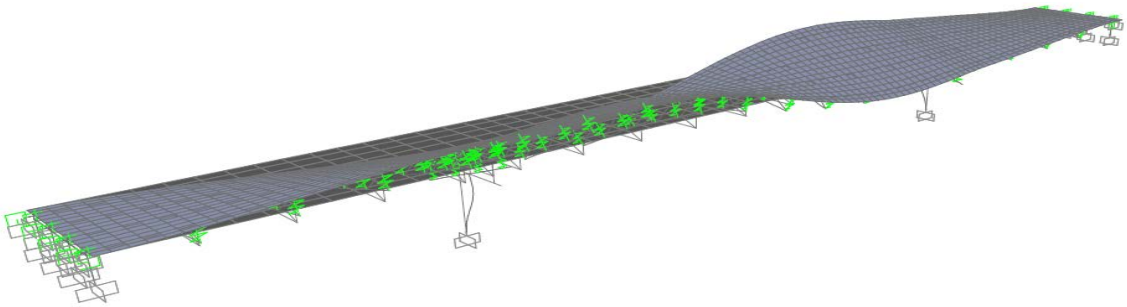

T4 = 0.284 sec

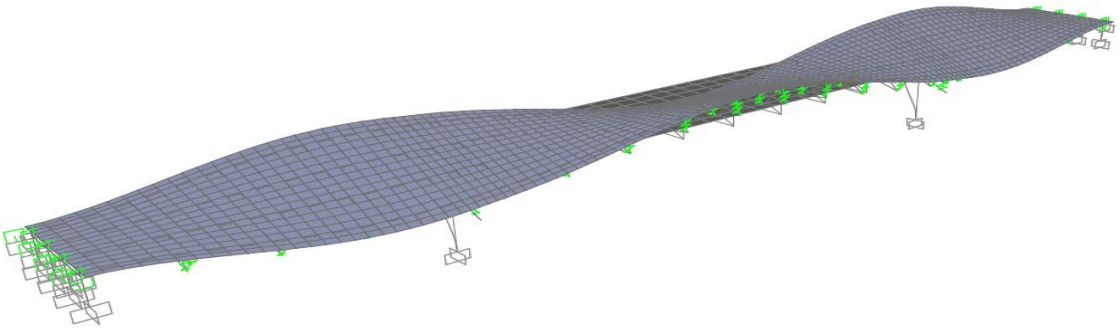

T5 = 0.234 sec

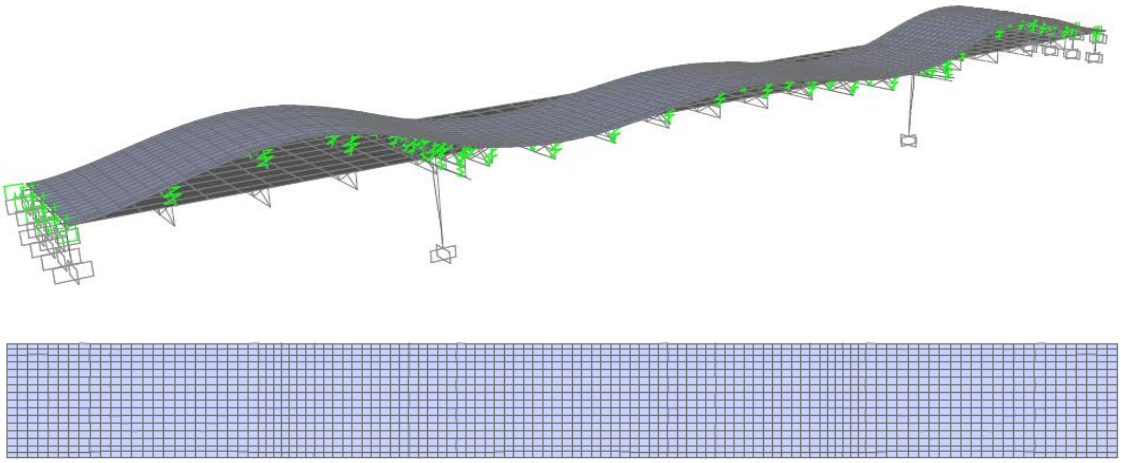

T9 = 0.145 sec

Figure 2-40b Mode Shapes of Case 3 (Modes 4, 5, and 9)

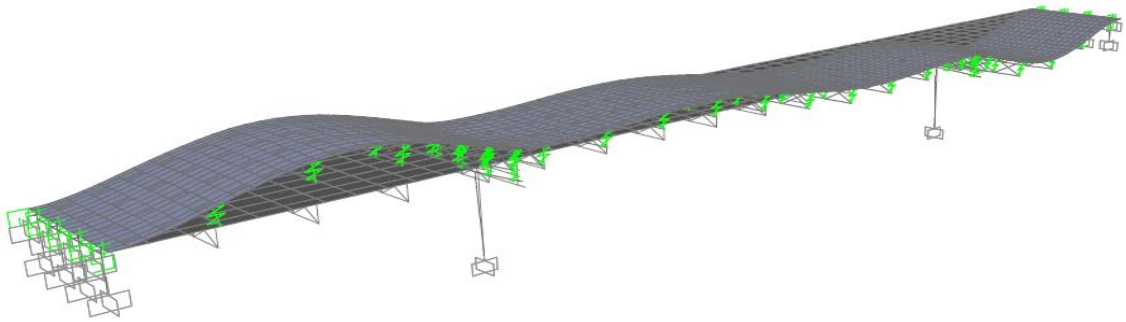

T10 = 0.138 sec

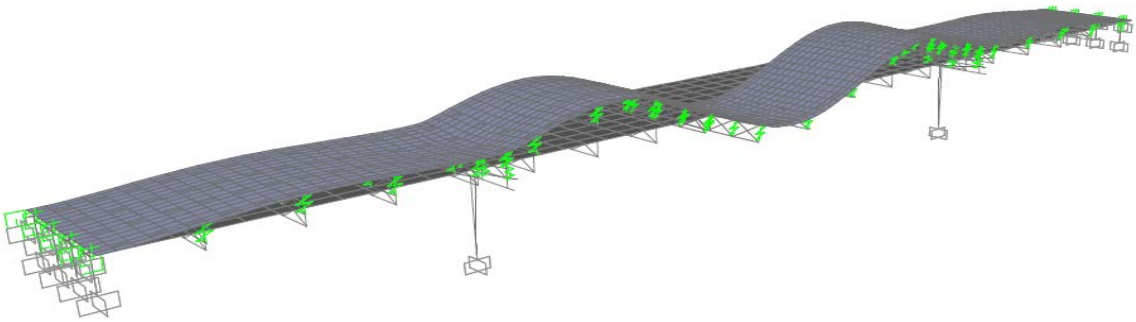

T13 = 0.107 sec

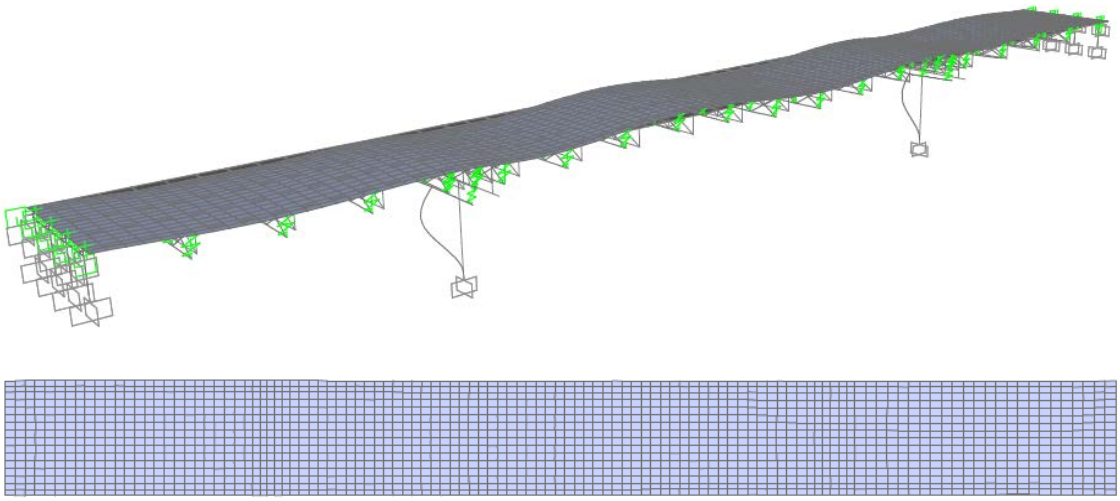

T15 = 0.085 sec

Figure 2-40 Mode shapes of Case 3

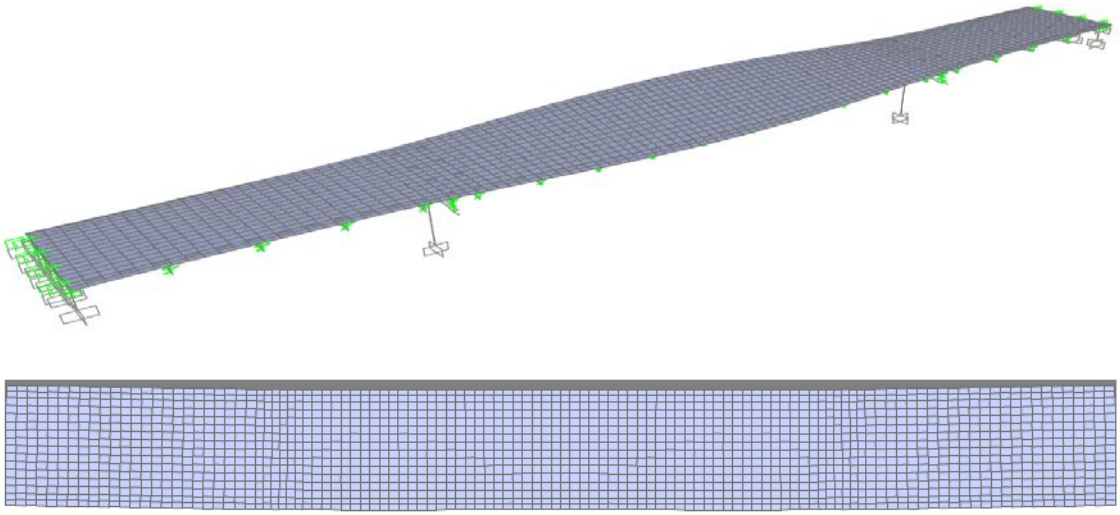

T1 = 0.691 sec

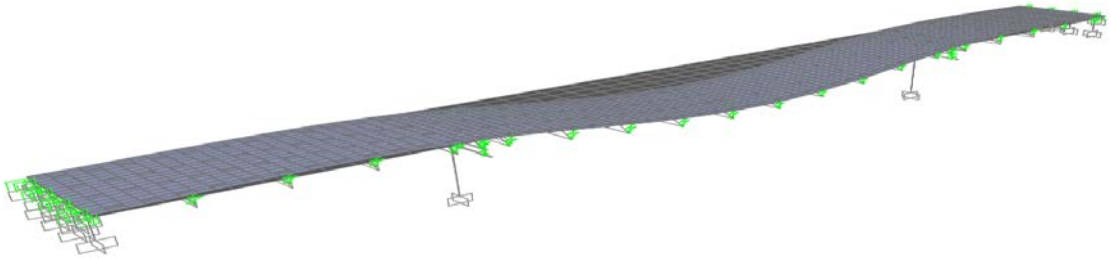

T2 = 0.599 sec

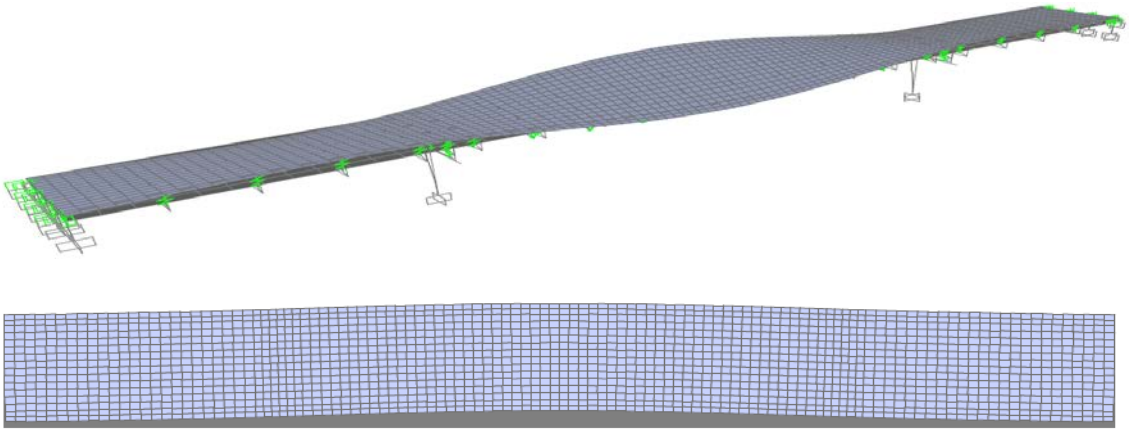

T3 = 0.552 sec

Figure 2-41a Mode Shapes of Case 4 (Modes 1, 2, and 3)

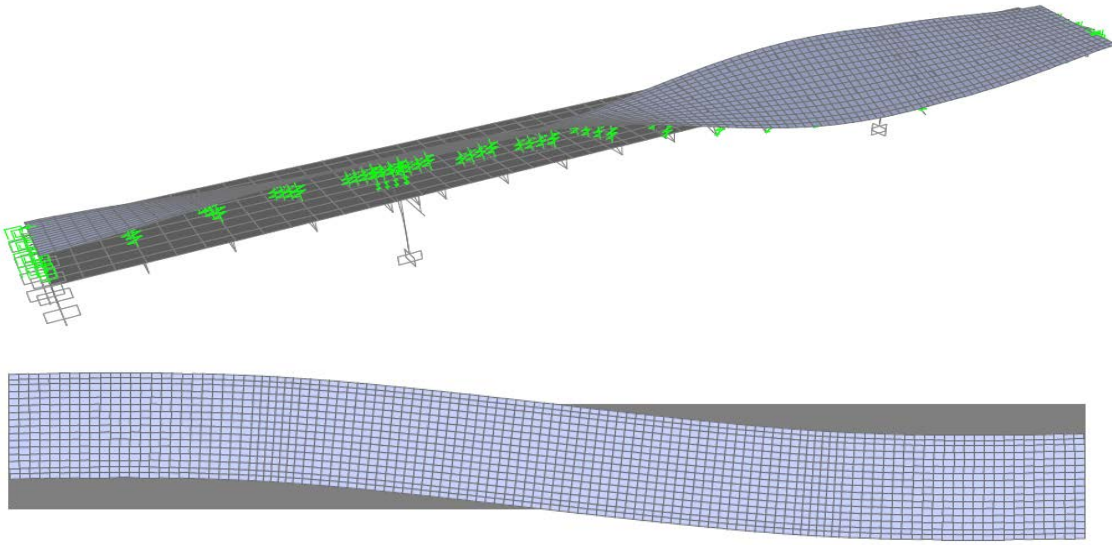

T4 = 0.335 sec

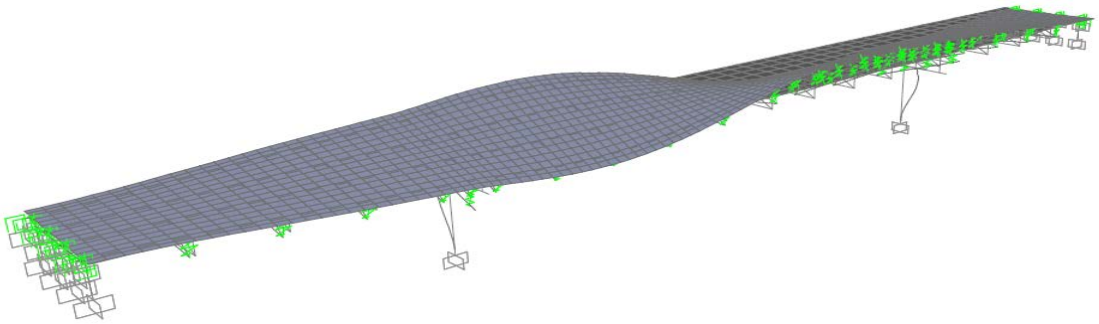

T5 = 0.280 sec

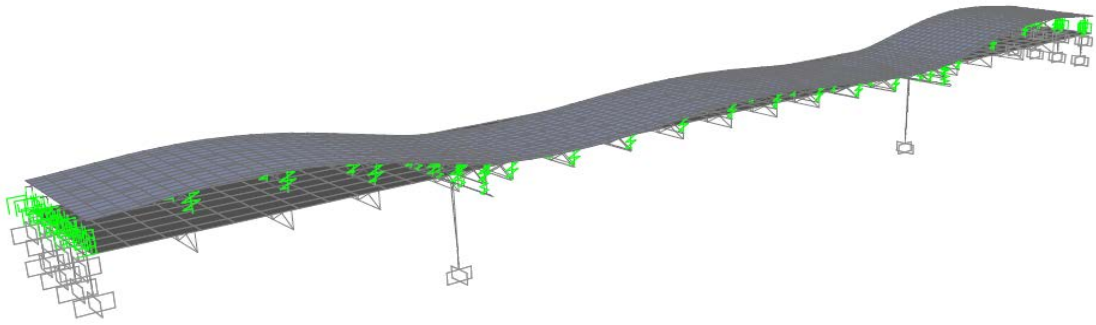

T9 = 0.207 sec

Figure 2-41b Mode Shapes of Case 4 (Modes 4, 5 and 9)

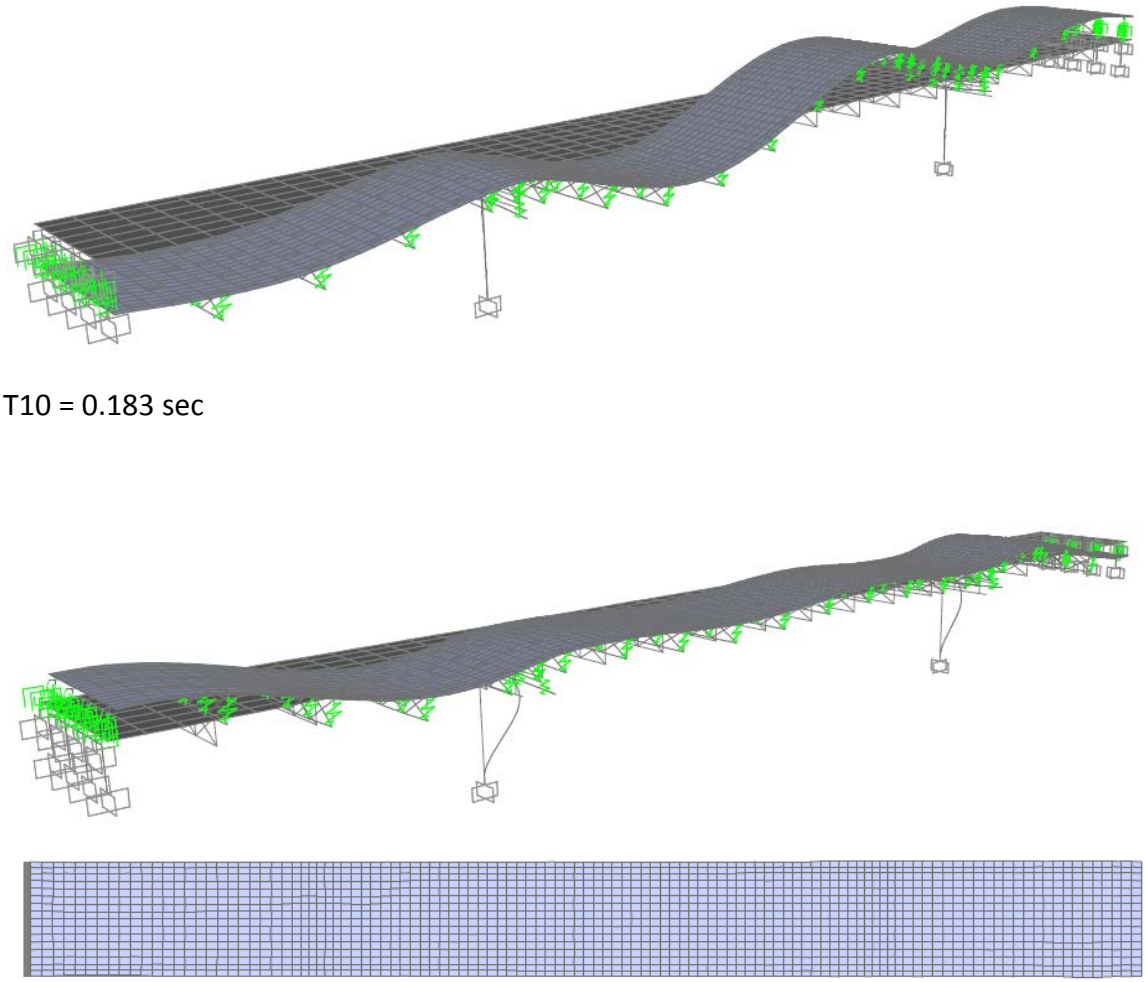

T10 = 0.183 sec

T17 = 0.098 sec

Figure 2-41 Mode shapes of Case 4

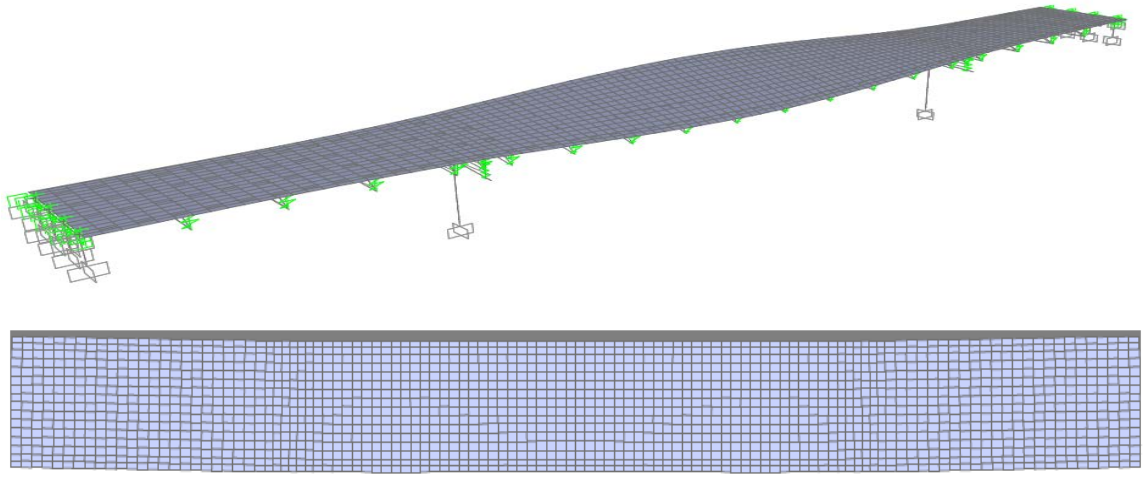

T1 = 0.691 sec

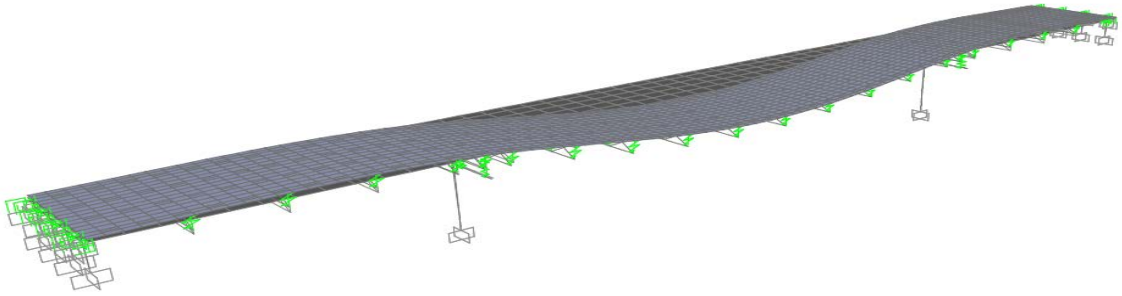

T2 = 0.599 sec

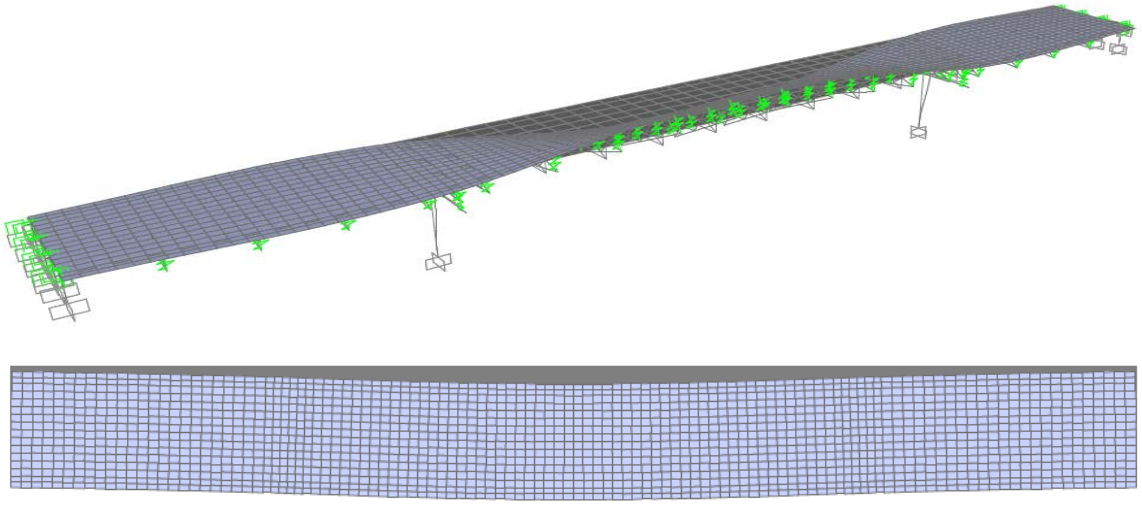

T3 = 0.552 sec

Figure 2-42a Mode Shapes of Case 5 (Modes 1, 2, and 3)

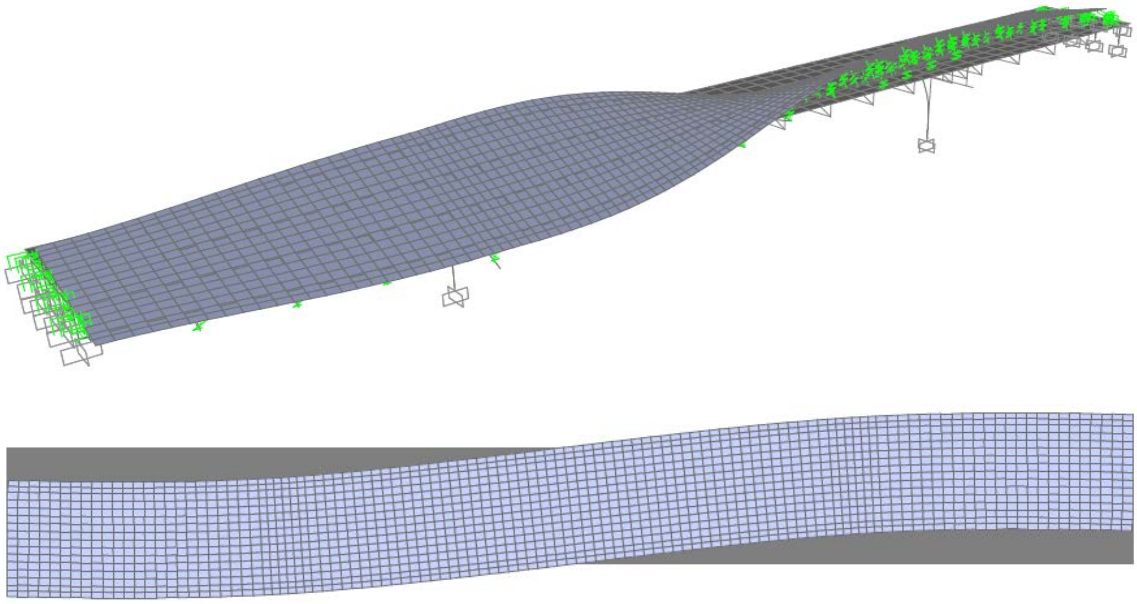

T4 = 0.335 sec

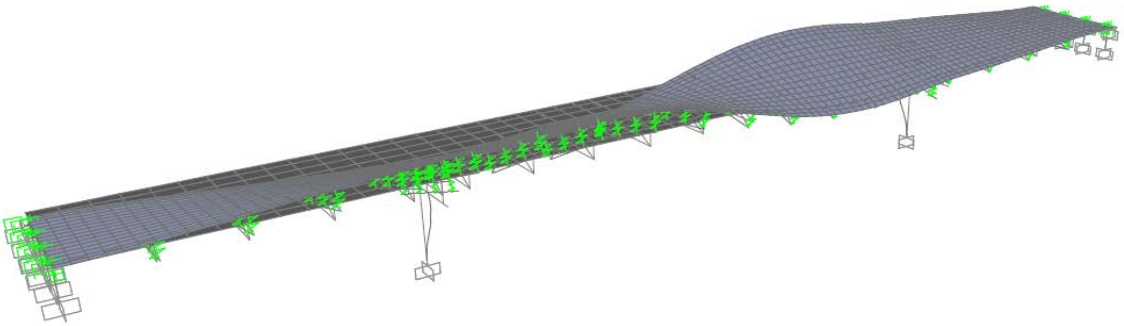

T5 = 0.280 sec

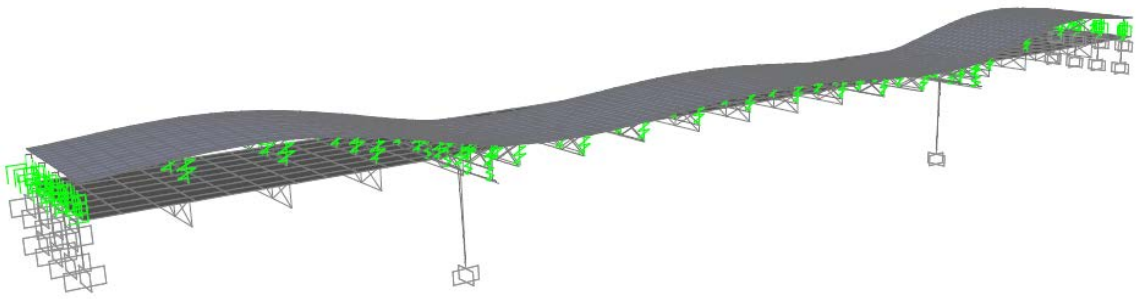

T9 = 0.207 sec

Figure 2-42b Mode Shapes of Case 5 (Modes 4, 5, and 9)

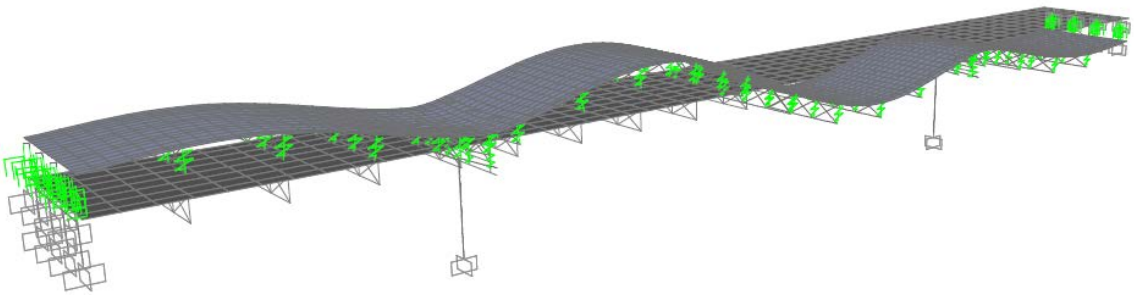

T10 = 0.183 sec

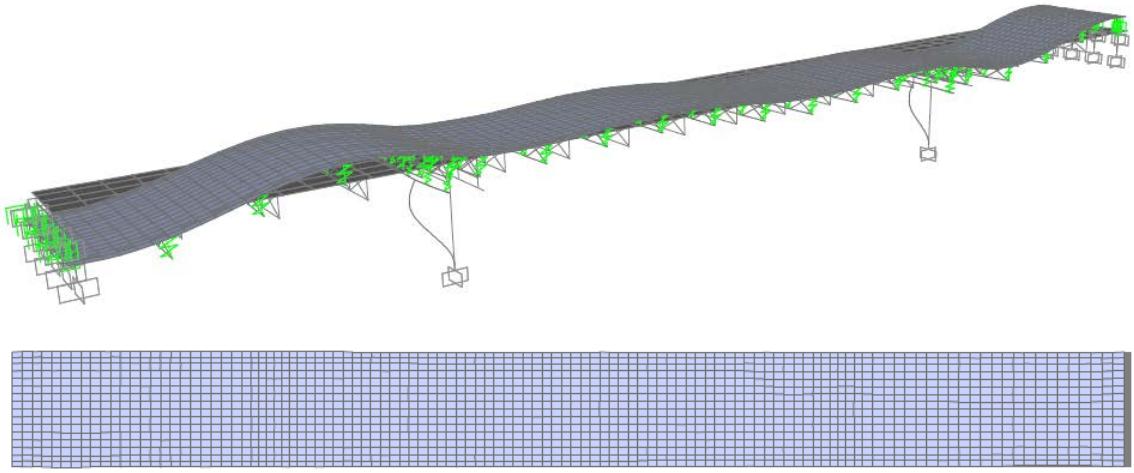

T17 = 0.098 sec

Figure 2-42 Mode shapes of Case 5

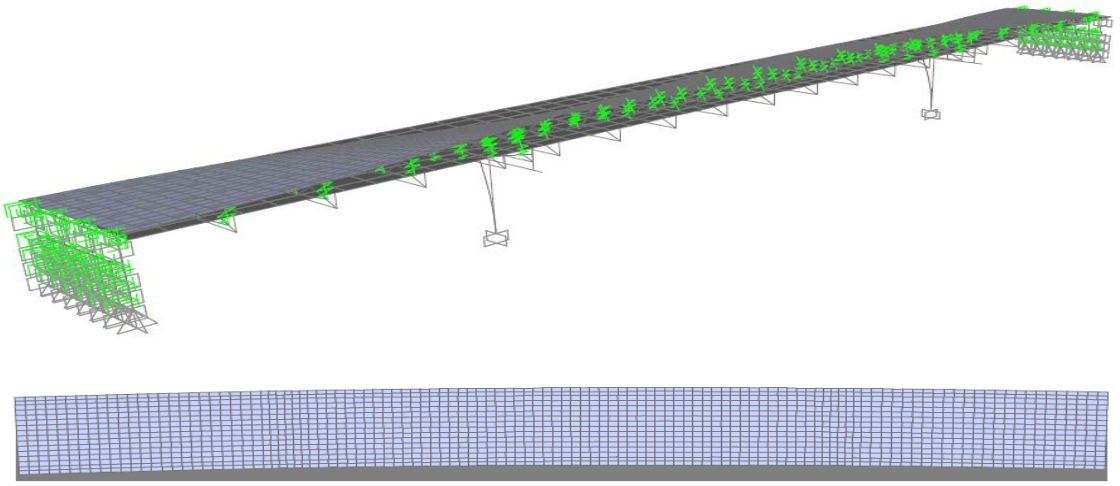

T1 = 1.071 sec

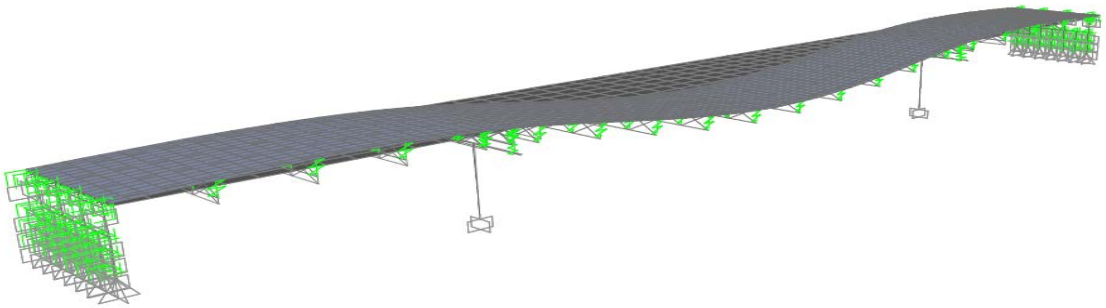

T2 = 0.615 sec

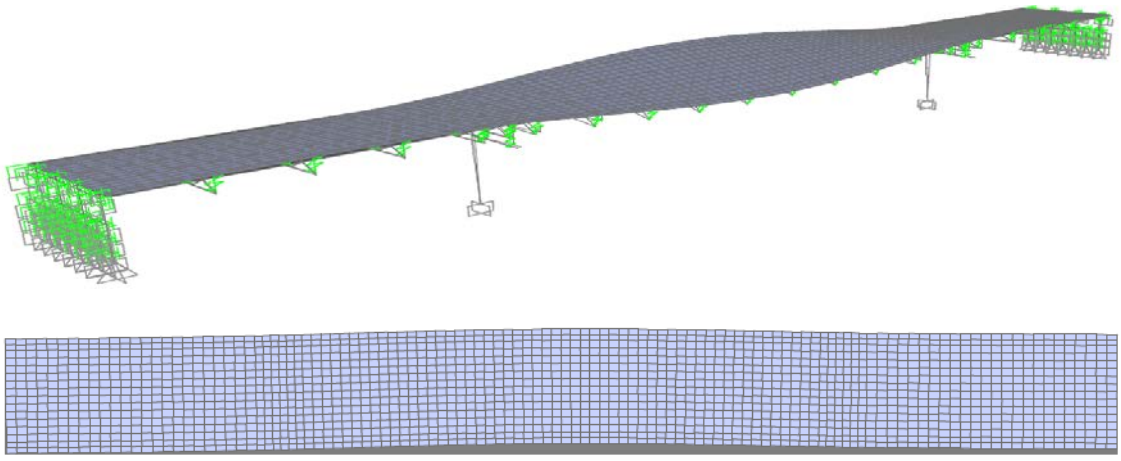

T3 = 0.595 sec

Figure 2-43a Mode Shapes of Case 6 (Modes 1, 2, 3)

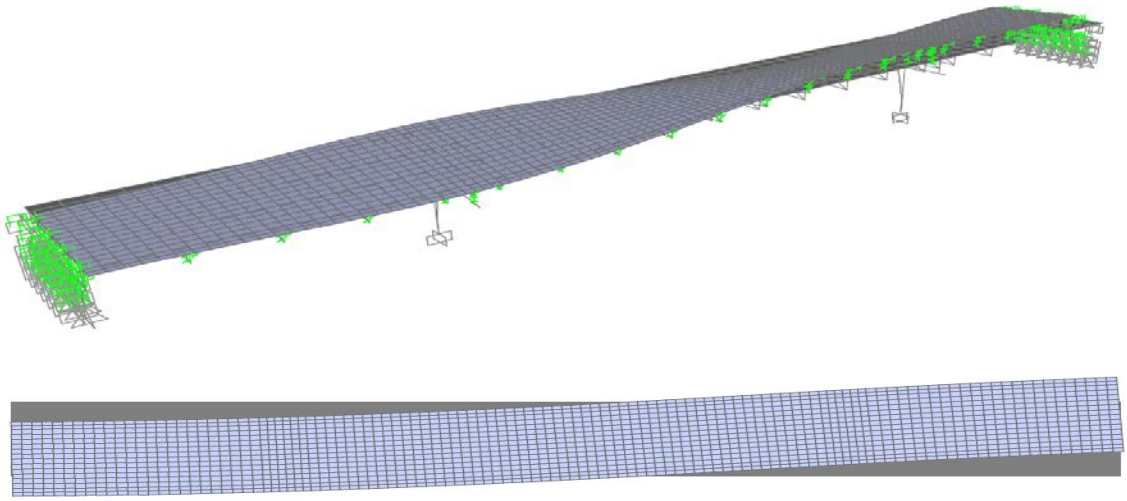

T4 = 0.527 sec

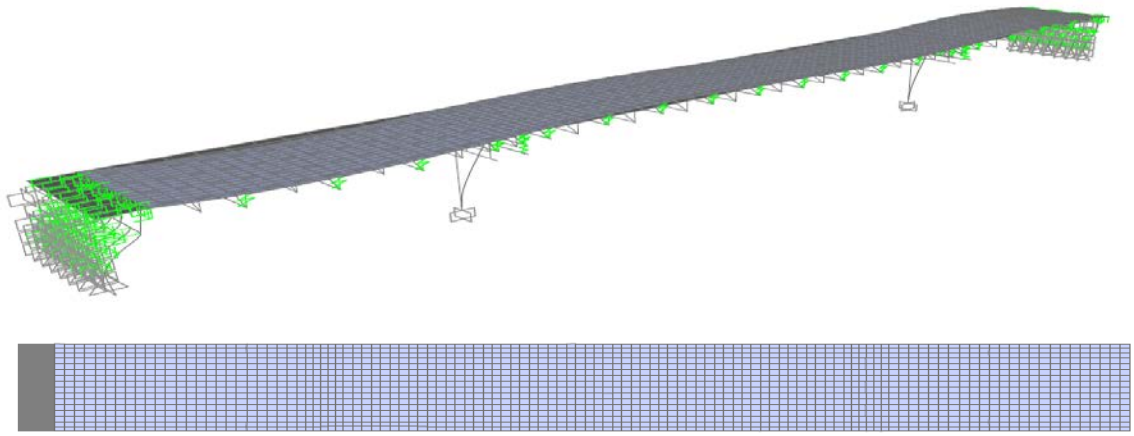

T5 = 0.350 sec

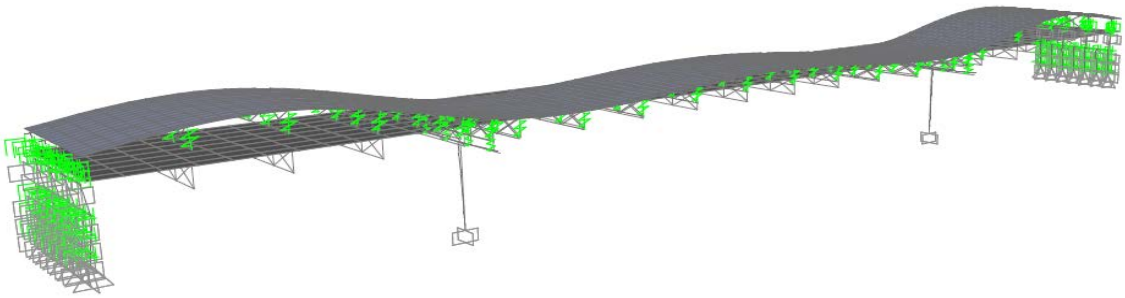

T10 = 0.224 sec

Figure 2-43 Mode Shapes of Case 6

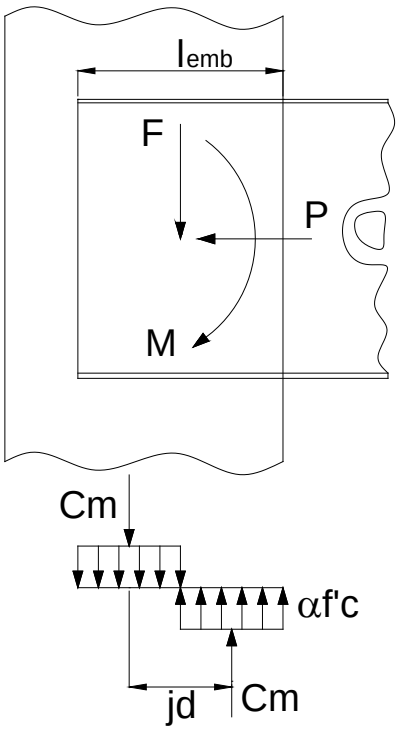

Figure 2-44 Elevation of girder-abutment connection showing the simplified mechanism used for calculating the embedment length

Chapter 3 SEISMIC LOAD PATH IN STRAIGHT AND SKEW INTEGRAL ABUTMENT BRIDGES

Pushover analyses were performed to establish the seismic load path in the longitudinal and transverse directions for straight and skew integral abutment bridges. The mathematical models established in Chapter 2 were used for this purpose. The cases investigated consist of one- and three-span integral abutment bridges. Skew is introduced only in the one-span bridge. The geometry of three-span bridge is the same as discussed in Chapter 2.

3.1 NONLINEAR PUSHOVER ANALYSES OF 3-SPAN STRAIGHT BRIDGE

Nonlinear pushover analyses were performed on the three-span straight bridge that was modeled and presented in Chapter 2. The primary purpose of the various pushover analyses was to understand the seismic load path and sequence of damage formation, in particular to the supporting piles. Simple distribution patterns of forces, such as a uniform distribution and/or elastic mode-proportional distribution, are usually used in pushover analysis. These force distribution patterns are typically appropriate and accurate for simple structures. However, for complex structures, such force distribution may not provide accurate prediction of the capacity of the bridge and its components. Based on the stated objectives of this study, it was appropriate to use pushover analysis procedure with force distributions that are proportional to the dominant mode shapes.

The bridge investigated here corresponds to Case 6 in Chapter 2 where the girder-abutment connection flexibility, abutment-soil interaction, and soil-pile interaction were included in the model. In addition, plastic hinges were assigned at the top of the piles where the moment is expected to be the largest. These plastic hinges were defined by PMM (axial – biaxial moment) interaction that is based on FEMA 356 (FEMA, 2000) equations. For HP10x42 pile, the expected bending strength about the strong axis is 2,608 kip-in at zero axial load, and the corresponding yield rotation is 0.0106 radians. In the weak axis, the expected bending strength at zero axial load is 1,177 kip-in, and the yield rotation is 0.0141 radians. These values were calculated using the following equations:

$$M_{CE} = 1.18ZF_{ye}\left(1 - P/P_{ye}\right) \le ZF_{ye} \tag{3-1}$$

$$\theta_y = \frac{ZF_{ye}L_C}{6EI_C}\left(1 - \frac{P}{P_{ye}}\right) \tag{3-2}$$

where Z is the plastic modulus, F_{ye} is the expected yield strength, P_{ye} is the expected axial yield strength given by

$$P_{ye} = A_g F_{ye} \tag{3-3},$$

L_C is the length, E is the modulus of elasticity, I_C is the moment of inertia, and A_g is the gross area of the pile. Figure 3-1 shows the moment-rotation curve from FEMA 356.

For HP10x42 pile with axial load to compression strength ratio less than *0.2*, the plastic rotation θ_p is $4.0\theta_y$. At axial load to compression strength ratio of larger than *0.*2 but smaller than *0.5*, the plastic rotation θ_p is $1.0\theta_y$. The strain-hardening slope in Figure 3-1 is 3% of the elastic slope. Point B in the figure represents the initiation of yielding in the pile, Point C is at the ultimate strength of the pile, and Point E represents pile failure.

The bridge was subjected to pushover forces in the longitudinal and transverse directions that are proportional to the mode shapes of Modes 5 and 1, respectively. Mode 5 is the dominant translational mode in the longitudinal direction while Mode 1 is the dominant translational mode in the transverse direction. The pushover analyses were displacement controlled and the deck displacement that was monitored is at the center of the bridge. The base shear versus deck displacements in the longitudinal and transverse directions are shown in Figure 3-2 and Figure 3-4, respectively. Three stages were monitored in these analyses to capture pile yielding, ultimate strength, and failure which correspond to points B, C and D or E (Figure 3-1). Stage 1 is defined as when one or more piles reached first yield (point B); Stage 2 is defined as when one or more piles reached the ultimate strength (point C); and Stage 3 is defined as when one or more piles reached failure (either point D or E).

3.1.1 Pushover Analysis Results in the Longitudinal Direction

Table 3-1 summarizes the base shears, deck displacements, pile displacements, and pile forces at different stages of pile damage under Mode 5 pushover. The pushover curve is shown in Figure 3-2. Piles started to yield (Stage 1) at a base shear of 3,709 kips, and Stage 2 was reached at 6,450 kips. These were largely due to abutment-soil resistance, which is 72% of the total base shear. The contribution of soil-pile resistance to total base shear is only 10% at Stage 1 and 7% at Stage 2. The bent columns contribution to the total base shear is even smaller, 4% at Stage 1 and 7% at Stage 2. The pile displacement at Stage 1 was 1.84 in. (1.23% drift) and 7.2 in. (4.83%) at Stage 2. This is equivalent to a displacement ductility ratio of 3.9. Ductility ratio is defined here as the ratio of ultimate displacement to yield displacement. Note that as mentioned above, the plastic rotation is equal to $4.0\theta_y$ when the axial load to compression strength ratio is less than 0.2.

As stated in Section 2.3.2, the deck-abutment joint was assumed as non-rigid connection due to the cracking of the R/C deck as a result of the large negative moment moments at the abutments. The results of the pushover analysis show that the maximum negative moment occurs at the abutments as shown in Figure 3-3. This figure shows the vertical moment (M_x) of an interior girder along the bridge length. As the shown in the figure, the maximum negative moment occurs at Abutment 4 and is equal to 5,843 kip-ft. The cracking moment of an interior girder with an R/C is equal to 3,600 kip-ft. Therefore, the cracked R/C deck cannot transfer the seismic forces from the superstructure to the abutment stem, and thus the assumption that the R/C deck is not rigidly connected to the abutment is adequate.

3.1.2 Pushover Analysis Results in the Transverse Direction

Under Mode 1 push, Stage 1 occurred at 513 kips base shear which is about 86% smaller compared to that in Mode 5 push. This is because Mode 1 push is in the transverse direction where the lateral forces are resisted only by the soil-pile interaction. Also, the weak axis of the piles is oriented in the transverse direction so the piles would yield at a much lower base shear. As a result, Stage 1 occurred at 1.12 in. pile displacement which is equivalent to 0.75% drift. Stage 2 was reached at 2.28 in. pile displacement which is equivalent to 1.53% drift. The shear forces in the bent columns were still small (6% at Stage 1 and 11% at Stage 2) compared to abutment shears. Figure 3-5 shows the lateral bending moment diagram (M_y) of an interior girder along the bridge length.

3.2 SINGLE-SPAN BRIDGES WITH AND WITHOUT SKEW

Detailed global 3D models of single-span bridges with integral abutments were developed to investigate the effect of skew. These bridges consist of abutments that are (a) without skew which is called straight bridge, (b) 45-degree skew, and (c) 60-degree skew as shown in Figure 3-6 through Figure 3-9. Single span bridges were selected for this part of the study to isolate the potential effects of skew on the response characteristics of the integral abutment bridges. The superstructures are composed of steel girders and concrete deck with cross-section properties that are the same as those in the three-span bridges except that the bridges here are single spans only. The span length is 216 ft. In the skew bridges, the intermediate cross-frames are oriented perpendicular to the girders. The girder-abutment connection is represented by nonlinear springs with stiffness properties similar to those in the three-span bridges.

In the skew bridges, the strong axis of the piles is oriented parallel to the direction of the abutment or skew (Figure 3-6). The soil-pile interaction (*p-y* curves) stiffness properties are the same as those used for the three-span bridge. Each pile is 12.4 ft long measured from the top of the pile to the location of inflection point. The abutment soil properties are also the same as those used in three-span bridge models, but are stiffer because of larger tributary areas in skew abutments. The springs representing the abutment-soil interaction are oriented perpendicular to the abutment.

3.2.1 Structural Dynamic Characteristics

In the straight bridge, the first mode has a period of 0.81 sec and is translation in the vertical direction as tabulated in Table 3-2 and illustrated in Figure 3-10. The second mode is the dominant translational mode in the transverse direction with a period of 0.52 sec. The dominant translational mode in the longitudinal direction is the fifth mode with a period of 0.28 sec. The sixth mode is also a longitudinal translation mode but with smaller mass participation compared to that in Mode 5. Mode 3 is the torsional mode about the bridge's longitudinal axis. Mode 4 is the torsional mode about the vertical axis of the bridge.

In the 45-degree skew bridge, the first mode is translation in the vertical direction. The period of this mode is 0.77 sec (Table 3-3 and Figure 3-11) which is 5% smaller than that in the straight

bridge. This is attributed to smaller superstructure effective length which in turn made the superstructure stiffer vertically. The dominant translational modes are Modes 2 and 4 but are coupled longitudinal and transverse translations because of skew. Mode 2 is a translational mode parallel to the skew with a period of 0.52 sec. As indicated by the mode shape (Figure 3-11), there is no contribution from the abutment-soil passive resistance in this mode. Note that the abutment soil springs are oriented perpendicular to the abutments, thus they will not be engaged when the bridge translates parallel to the skew angle. Mode 4 has a period of 0.301 sec and has a larger participation factor in the longitudinal translational component in comparison to Mode 2. The abutment-soil resistance has some contribution to this mode. Mode 3 is rotation about the bridge's longitudinal axis, similar to that in straight bridge but with a period that is 11% smaller due to shorter superstructure effective length.

In the 60-degree skew bridge, the first mode is also translation in the vertical direction but with period that is 13% smaller in comparison to the 45-degree skew bridge and 17% smaller in comparison to the straight bridge. Again, the period was further shortened due to further decrease in the effective length of the bridge. The modal properties for this bridge are summarized in Table 3-4 and mode shapes are illustrated in Figure 3-12. The dominant translational modes are again Modes 2 and 4 which are coupled longitudinal and transverse translations. Comparisons of the 45-degree and 60-degree skew bridges show that the periods at these modes are about the same. However, the mass participation ratios show significant difference. In the 45-degree skew bridge, Mode 2 has more transverse component than longitudinal, while Mode 4 has more longitudinal component than transverse (Table 3-3). The opposite is true in the 60-degree skew bridge; Mode 2 has more longitudinal component, and Mode 4 has more transverse component. This difference is attributed to the change in the bridge dynamic properties due to change in the skew angle. Thus, the bridge dynamic response could change significantly as the skew angle increases.

3.2.2 Nonlinear Pushover Analyses

Single-mode pushover analyses were performed on the straight, 45-degree, and 60-degree skew bridges. Three stages were monitored in these analyses to capture the pile yielding, ultimate strength, and failure which correspond to points B, C and D or E in Figure 3-1. Stage 1 is when one or more piles reached first yield (point B); Stage 2 is when one or more piles reached the ultimate strength (point C); and Stage 3 is when one or more piles reached failure (point D or E). The corresponding base shears, deck displacement, pile displacements, and pile forces were obtained and reported at these stages. Pushover curves were plotted to show the variation of base shears versus the deck displacement. The deck displacement at the center of the bridge or the center of gravity of the deck was monitored. The pushover curves associated with coupled modes of vibration were plotted for both the x- and y-directions; x- and y-directions correspond to the longitudinal and transverse directions, respectively.

3.2.2.1 Straight Bridge

Pushover analyses were performed using the dominant modes, Modes 5 and 2. Mode 5 is the dominant translational mode in the longitudinal direction while Mode 2 is the dominant

translational mode in the transverse direction. Table 3-5 and Figure 3-13 summarize the results of pushover analyses of this bridge. Similar to the observation in the three-span bridge, the response in the longitudinal pushover (Mode 5 pushover) is dominated by the abutment-soil passive resistance. 90% of the total base shear is coming from the abutment-soil passive resistance. Under Mode 5 pushover, Stage 1 occurred at a base shear of 3,645 kips and 2.08 in deck displacement. The pile drift was 1.29% which is about equal to the drift observed at Stage 1 of Mode 5 pushover of the three-span bridge (Table 3-1). At Stage 2, the pile drift was 2.09% which is equivalent to ductility ratio of 1.62. This is smaller than the ductility ratio observed in the three-span bridge because of larger axial load.

Under Mode 2 pushover analysis, the total base shear was 459 kips at Stage 1 and 529 kips at Stage 2. The pile drift at Stage 1 was 0.78%, and at Stage 2 it was 1.51%; these are about the same as that in the three-span bridge. Good correlation was observed because the columns in the 3-span bridge were taking only a small percentage of the total base shear which means that the response is dominated by the piles and soil-pile interaction.

3.2.2.2 45-degree Skew Bridge

Pushover analyses were performed using the dominant modes, Modes 2 and 4. The results are summarized in Table 3-6, and pushover curves are shown in Figure 3-14 and Figure 3-15 for Mode 2 and Mode 4, respectively. Under Mode 2 pushover, the resultant base shears at Stages 1 and 2 were 452 kips and 527 kips, respectively. Note that these are about the same as the base shears under the transverse push (Mode 2 push) of the 1-span straight bridge. This is because Mode 2 is translation parallel to the direction of skew angle as discussed in Section 3.2.1. Thus, the base shears are due to the soil-pile resistance, and there is little or no contribution from the abutment-soil passive resistance. Accordingly, the pile drifts and ductility ratios are about the same as those in the transverse push of the 1-span straight bridge.

Under Mode 4 pushover, the resultant base shears at Stages 1 and 2 were 1,066 kips and 1,314 kips, respectively. These are about 150% larger than the base shears under Mode 2 push because Mode 4 has larger participation factors in the longitudinal component. The increased participation factor in longitudinal direction increased the contribution of abutment-soil passive resistance to total response. However, the pile drifts under Modes 2 and 4 pushover analyses are about the same.

3.2.2.3 60-degree Skew Bridge

The pushover analyses of the 60-degree skew bridge were also carried out using Modes 2 and 4 which are the dominant translational modes. The results of the pushover analyses are summarized in Table 3-7, and pushover curves are shown in Figure 3-16 and Figure 3-17 for Mode 2 and Mode 4, respectively. The base shears under Mode 2 pushover are about the same as those in Mode 2 pushover of the 45-degree skew bridge and transverse pushover (also Mode 2) of the straight bridge. This is because Mode 2 is also translation parallel to the direction of skew or parallel to the weak axis of the piles. The same observation is also true for the pile displacements and forces.

Under Mode 4 pushover, the base shears, although smaller, are about the same as those in Mode 4 pushover of the 45-degree skew bridge, particularly at Stages 1 and 2. However, the pile drifts are about 45% to 70% larger. This could be due to change in the dynamic properties associated with change in skew angle. These values are actually about the same as the pile drifts under Mode 5 pushover (longitudinal push shown in Table 3-5) of the straight bridge.

3.3 CONCLUSIONS

The seismic load paths in the longitudinal and transverse directions of a three-span integral abutment bridge were determined using pushover analysis for the dominant translational modes. In the longitudinal direction, a large percentage (72%) of the seismic force was resisted by the abutment-soil passive resistance. In the transverse direction, the overall response was governed by the soil-pile interaction. About 40% of the transverse seismic force was resisted by the soil-pile interaction for each abutment. This shows that the columns in integral abutment bridges were subjected to low seismic forces, thus limiting their damage during seismic events.

A limited investigation on the effect of skew was conducted on a single-span bridge with integral abutments to determine the effect of skew on the dynamic properties and seismic load path. Three models were developed: a) no skew, b) 45-degree skew, and c) 60-degree skew. The results of the analyses showed that the variation of the skew angle caused significant changes in the bridge dynamic characteristics in terms of periods and mode shapes. It was also shown that the translational modes in the skew bridge are highly coupled between the longitudinal and the transverse translations.

Table 3-1 3-Span Straight Bridge - Summary of Modal Pushover Results (Modes 5 and 1)

A. Mode 5 Push (Longitudinal Direction)

	Step	Base Shear (kip)										
		Total			Abutment 1		Bent 2		Bent 3		Abutment 4	
		X	Y	Resultant	X	Y	X	Y	X	Y	X	Y
1	20	3709	0	3709	363	0	159	0	150	0	3037	0
2	73	6450	0	6450	446	0	479	0	464	0	5061	0
3												

	Step	Δ_{DECK} (in)		Most Stressed Piles	Δ_{PILE} (in)			Pile Drift (%)	M_{PILE} (kip-in)			P_{PILE} (kip)
		X	Y		X	Y	Resultant		M3	M2	Resultant	
1	20	1.96	0	1-7	1.84	0	1.84	1.23	2608	0	2608	-43
2	73	7.32	0	1-7	7.2	0	7.2	4.83	2913	0	2913	-46
3												

B. Mode 1 Push (Transverse Direction)

	Step	Base Shear (kip)										
		Total			Abutment 1		Bent 2		Bent 3		Abutment 4	
		X	Y	Resultant	X	Y	X	Y	X	Y	X	Y
1	21	0	513	513	61	223	0	33	0	33	-61	223
2	34	0	672	672	74	264	0	72	0	72	-74	264
3												

	Step	Δ_{DECK} (in)		Most Stressed Piles	Δ_{PILE} (in)			Pile Drift (%)	M_{PILE} (kip-in)			P_{PILE} (kip)
		X	Y		X	Y	Resultant		M3	M2	Resultant	
1	21	0	2.1	1, 8	0.16	1.11	1.12	0.75	321	1129	1174	26
2	34	0	3.36	7, 14	0.16	2.27	2.28	1.53	190	1196	1211	-134
3												

Notes:
Stage 1 = one or more piles reached first yield (B)
Stage 2 = one or more piles reached ultimate strength (C)
Stage 3 = one or more piles failed (D or E)
M3 = moment at pile strong axis (local axis)
M2 = moment at pile weak axis (local axis)
Δ_{DECK} = deck displacement at center of bridge
Δ_{PILE} = deflection at top of most stressed pile
M_{PILE} = moment at top of most stressed pile
P_{PILE} = axial load at most stressed pile, (+) is tension and (-) is compression
X = global x-axis
Y = global y-axis

Table 3-2 Straight Bridge: Mass participating ratios

Mode	Period	UX	UY	UZ	RX	RY	RZ
No	Sec	Unitless	Unitless	Unitless	Unitless	Unitless	Unitless
1	0.805	0.000	0.000	0.645	0.000	0.407	0.000
2	0.520	0.000	0.963	0.000	0.814	0.000	0.652
3	0.415	0.000	0.019	0.000	0.139	0.000	0.013
4	0.331	0.000	0.000	0.000	0.000	0.000	0.319
5	0.282	0.764	0.000	0.000	0.000	0.008	0.000
6	0.226	0.219	0.000	0.000	0.000	0.172	0.000
7	0.167	0.000	0.000	0.000	0.000	0.000	0.000
8	0.121	0.000	0.008	0.000	0.000	0.000	0.005
9	0.115	0.000	0.000	0.093	0.000	0.058	0.000
10	0.094	0.000	0.000	0.000	0.016	0.000	0.000
11	0.071	0.001	0.000	0.000	0.000	0.046	0.000
12	0.068	0.000	0.000	0.000	0.000	0.000	0.000

Table 3-3 45-degree Skew Bridge: Mass participating ratios

Mode	Period	UX	UY	UZ	RX	RY	RZ
No	Sec	Unitless	Unitless	Unitless	Unitless	Unitless	Unitless
1	0.772	0.000	0.000	0.584	0.000	0.359	0.005
2	0.519	0.407	0.569	0.000	0.508	0.031	0.373
3	0.373	0.004	0.000	0.000	0.051	0.010	0.000
4	0.301	0.442	0.280	0.000	0.278	0.001	0.185
5	0.229	0.000	0.000	0.005	0.000	0.004	0.336
6	0.211	0.107	0.088	0.000	0.092	0.125	0.050
7	0.154	0.000	0.000	0.001	0.000	0.001	0.000
8	0.120	0.020	0.044	0.000	0.018	0.002	0.028
9	0.111	0.000	0.000	0.091	0.000	0.055	0.004
10	0.091	0.000	0.000	0.000	0.017	0.004	0.000
11	0.070	0.001	0.001	0.000	0.001	0.048	0.001
12	0.068	0.000	0.000	0.000	0.000	0.000	0.000

Table 3-4 60-degree Skew Bridge: Mass participating ratios

Mode	**Period**	**UX**	**UY**	**UZ**	**RX**	**RY**	**RZ**
No	Sec	Unitless	Unitless	Unitless	Unitless	Unitless	Unitless
1	0.671	0.000	0.000	0.516	0.000	0.302	0.006
2	0.533	0.693	0.286	0.000	0.263	0.049	0.178
3	0.335	0.026	0.050	0.000	0.182	0.017	0.031
4	0.297	0.197	0.414	0.000	0.304	0.003	0.258
5	0.198	0.000	0.000	0.004	0.000	0.002	0.333
6	0.191	0.049	0.126	0.000	0.135	0.087	0.079
7	0.147	0.000	0.000	0.004	0.000	0.002	0.010
8	0.122	0.018	0.088	0.000	0.052	0.001	0.055
9	0.105	0.000	0.000	0.085	0.000	0.050	0.012
10	0.094	0.000	0.002	0.000	0.015	0.007	0.001
11	0.071	0.000	0.000	0.006	0.000	0.003	0.002
12	0.070	0.001	0.003	0.000	0.003	0.047	0.002

Table 3-5 1-Span Straight Bridge: Modal Pushover Analyses (Modes 5 & 2)

A. Mode 5 Push (Longitudinal Direction)

Stage	Step	Base Shear (kip)							Δ_{DECK} (in)	
		Total			Abutment 1		Abutment 2			
		X	Y	Resultant	X	Y	X	Y	X	Y
1	21	3645	0	3645	3279	0	365	0	2.08	0
2	32	5072	0	5072	4671	0	400	0	3.22	0
3										

Stage	Step	Most Stressed Piles	Δ_{PILE} (in)			Pile Drift (%)	M_{PILE} (kip-in)			P_{PILE} (kip)
			X	Y	Resultant		M3	M2	Resultant	
1	21	7-14	1.92	0	1.92	1.29	2608	0	2608	-167
2	32	7-14	3.11	0	3.11	2.09	2674	0	2674	-185
3										

B. Mode 2 Push (Transverse Direction)

Stage	Step	Base Shear (kip)							Δ_{DECK} (in)	
		Total			Abutment 1		Abutment 2			
		X	Y	Resultant	X	Y	X	Y	X	Y
1	14	0	459	459	14	229	-14	229	0	1.35
2	25	0	529	529	17	264	-17	264	0	2.47
3										

Stage	Step	Most Stressed Piles	Δ_{PILE} (in)			Pile Drift (%)	M_{PILE} (kip-in)			P_{PILE} (kip)
			X	Y	Resultant		M3	M2	Resultant	
1	14	1-14	0	1.16	1.16	0.78	17	1170	1170	-167
2	25	1-3,8-10	0	2.25	2.25	1.51	0	1207	1207	-173
3										

Notes:
Stage 1 = one or more piles reached first yield (B)
Stage 2 = one or more piles reached ultimate strength (C)
Stage 3 = one or more piles failed (D or E)
M3 = moment at pile strong axis (local axis)
M2 = moment at pile weak axis (local axis)
Δ_{DECK} = deck displacement at center of bridge
Δ_{PILE} = deflection at top of most stressed pile
M_{PILE} = moment at top of most stressed pile
P_{PILE} = axial load at most stressed pile, (+) is tension and (-) is compression
X = global x-axis
Y = global y-axis

Table 3-6 1-Span 45-degree Skew Bridge: Modal Pushover Analyses (Modes 2 & 4)

A. Mode 2 Push (Longitudinal & Transverse Push)

Stage	Step	Base Shear (kip)							Δ_{DECK} (in)	
		Total			Abutment 1		Abutment 2			
		X	Y	Resultant	X	Y	X	Y	X	Y
1	8	292	345	452	139	176	153	170	0.78	0.93
2	16	340	403	527	165	205	175	198	1.54	1.73
3										

Stage	Step	Most Stressed Piles	Δ_{PILE} (in)			Pile Drift (%)	M_{PILE} (kip-in)			P_{PILE} (kip)
			X	Y	Resultant		M3	M2	Resultant	
1	8	8-14	0.81	0.81	1.15	0.77	89	1168	1171	-141
2	16	1,2,12-14	1.53	1.64	2.24	1.51	7	1212	1212	-156
3										

B. Mode 4 Push (Longitudinal & Transverse Push)

Stage	Step	Base Shear (kip)							Δ_{DECK} (in)	
		Total			Abutment 1		Abutment 2			
		X	Y	Resultant	X	Y	X	Y	X	Y
1	10	834	664	1066	684	374	150	289	0.98	0.73
2	17	1028	819	1314	838	474	190	344	1.78	0.91
3	62	1225	975	1566	1101	620	124	356	6.45	1.96

Stage	Step	Most Stressed Piles	Δ_{PILE} (in)			Pile Drift (%)	M_{PILE} (kip-in)			P_{PILE} (kip)
			X	Y	Resultant		M3	M2	Resultant	
1	10	1	1.07	0.42	1.15	0.77	837	1103	1385	-203
2	17	1,2,8	1.99	1.03	2.24	1.50	964	1124	1481	-206
3	62	13	5.46	8.77	10.33	6.93	400	66	405	-144

Notes:
Stage 1 = one or more piles reached first yield (B)
Stage 2 = one or more piles reached ultimate strength (C)
Stage 3 = one or more piles failed (D or E)
M3 = moment at pile strong axis (local axis)
M2 = moment at pile weak axis (local axis)
Δ_{DECK} = deck displacement at center of bridge
Δ_{PILE} = deflection at top of most stressed pile
M_{PILE} = moment at top of most stressed pile
P_{PILE} = axial load at most stressed pile, (+) is tension and (-) is compression
X = global x-axis
Y = global y-axis

Table 3-7 1-Span 60-degree Skew Bridge: Modal Pushover Analyses (Modes 2 & 4)

A. Mode 2 Push (Longitudinal & Transverse Push)

Stage	Step	Base Shear (kip)							Δ_{DECK} (in)	
		Total			Abutment 1		Abutment 2			
		X	Y	Resultant	X	Y	X	Y	X	Y
1	11	387	251	461	190	129	197	122	1.02	0.68
2	18	436	283	520	215	145	221	138	1.8	1.14
3										

Stage	Step	Most Stressed Piles	Δ_{PILE} (in)			Pile Drift (%)	M_{PILE} (kip-in)			P_{PILE} (kip)
			X	Y	Resultant		M3	M2	Resultant	
1	11	1-14	1.02	0.64	1.20	0.81	76	1174	1176	-230
2	18	1,2,13,14	1.8	1.1	2.11	1.42	13	1212	1212	-226
3										

A. Mode 4 Push (Longitudinal & Transverse Push)

Stage	Step	Base Shear (kip)							Δ_{DECK} (in)	
		Total			Abutment 1		Abutment 2			
		X	Y	Resultant	X	Y	X	Y	X	Y
1	25	594	869	1053	522	531	72	338	0.74	1.18
2	36	713	1044	1264	636	649	78	395	1.15	1.7
3	76	783	1146	1388	745	753	38	393	2.46	3.49

Stage	Step	Most Stressed Piles	Δ_{PILE} (in)			Pile Drift (%)	M_{PILE} (kip-in)			P_{PILE} (kip)
			X	Y	Resultant		M3	M2	Resultant	
1	25	8	0.67	1.82	1.94	1.30	2424	424	2461	-75
2	36	9,10	1.08	3.03	3.22	2.16	2436	426	2473	-103
3	76	9	2.8	8.73	9.17	6.15	420	74	426	-86

Notes:
Stage 1 = one or more piles reached first yield (B)
Stage 2 = one or more piles reached ultimate strength (C)
Stage 3 = one or more piles failed (D or E)
M3 = moment at pile strong axis (local axis)
M2 = moment at pile weak axis (local axis)
Δ_{DECK} = deck displacement at center of bridge
Δ_{PILE} = deflection at top of most stressed pile
M_{PILE} = moment at top of most stressed pile
P_{PILE} = axial load at most stressed pile, (+) is tension and (-) is compression
X = global x-axis
Y = global y-axis

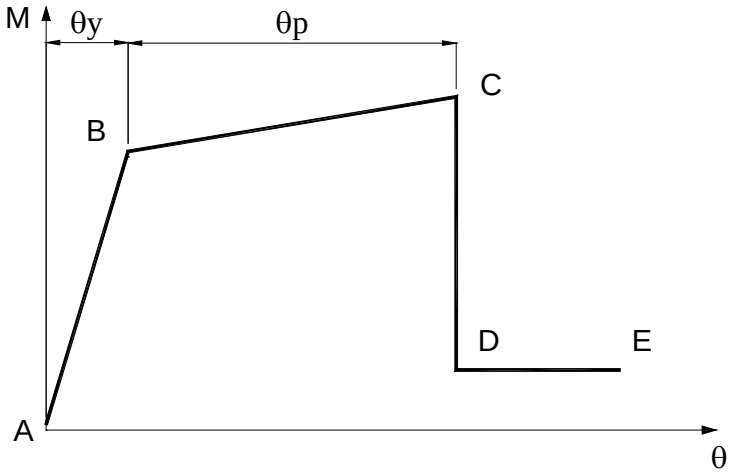

Figure 3-1 Moment-rotation curve for piles

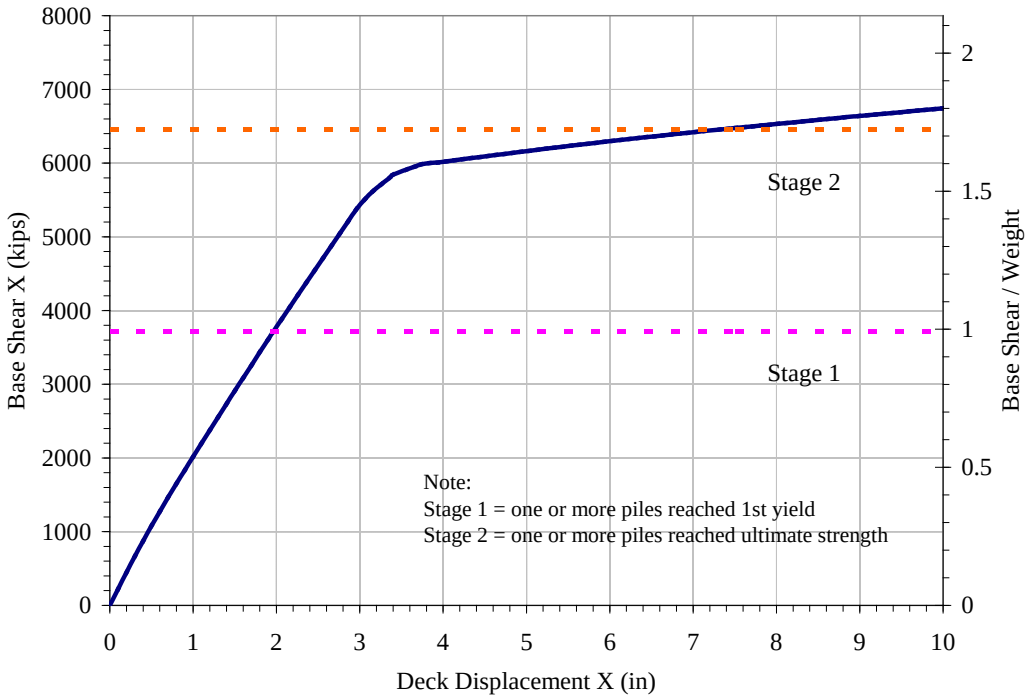

Figure 3-2 3-Span Straight Bridge Pushover Curve under Mode 5 Push (Longitudinal Direction)

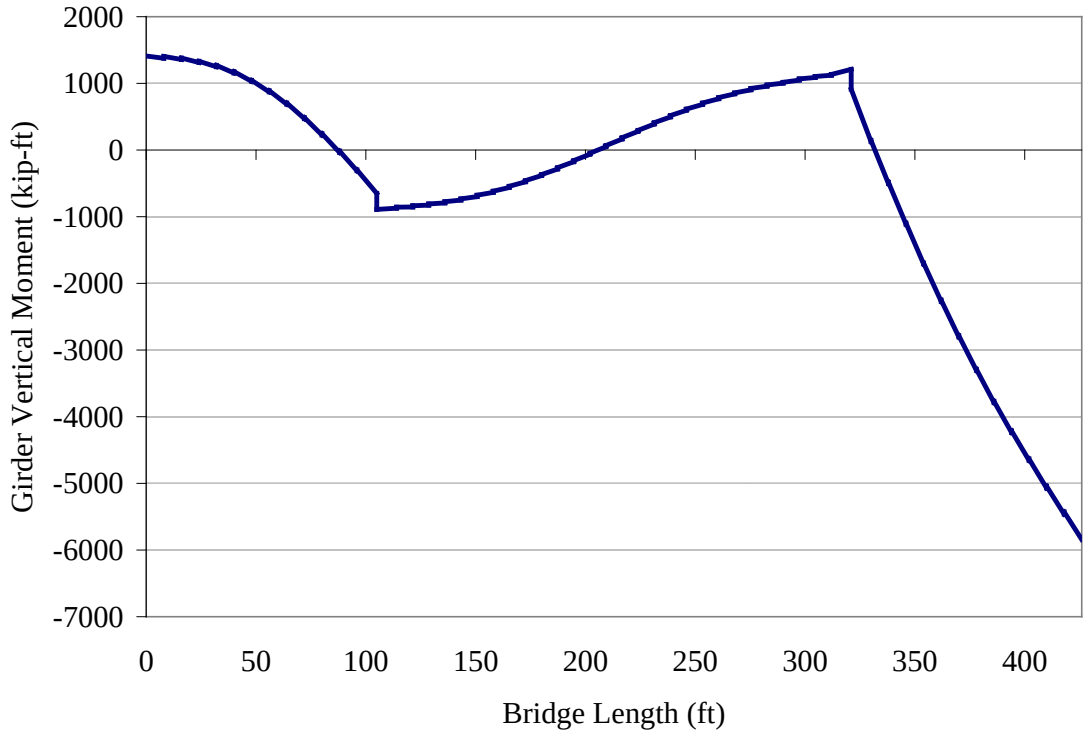

Figure 3-3 Bending Moment (vertical) Diagram of an Interior Girder under Mode 5 Push

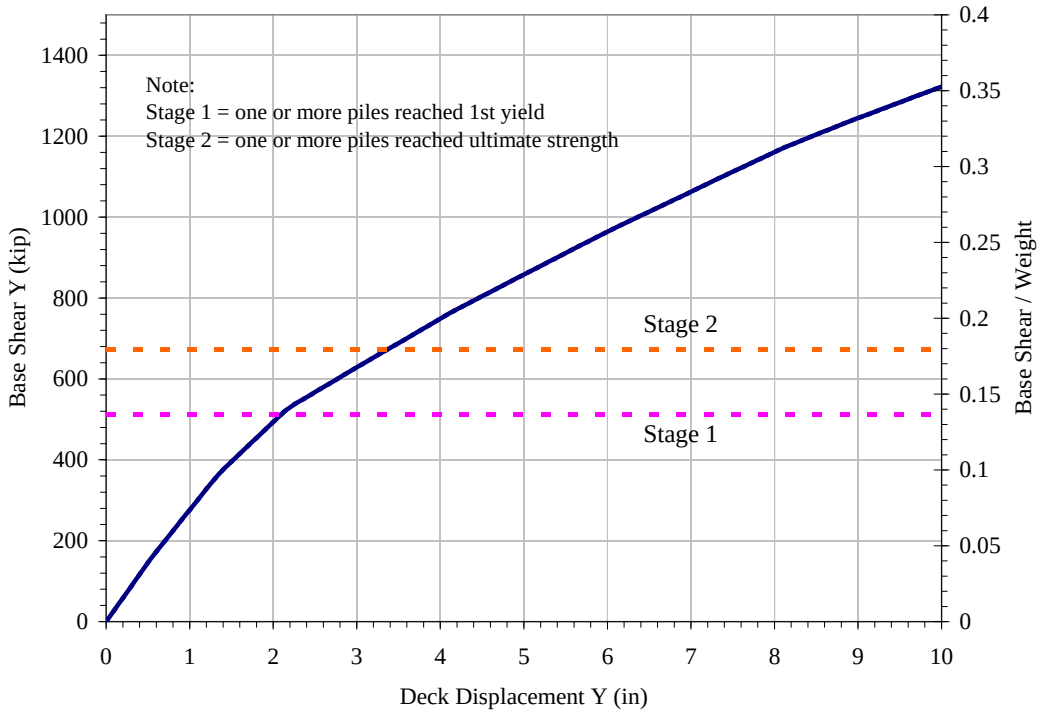

Figure 3-4 3-Span Straight Bridge Mode 1 Push (Transverse Direction)

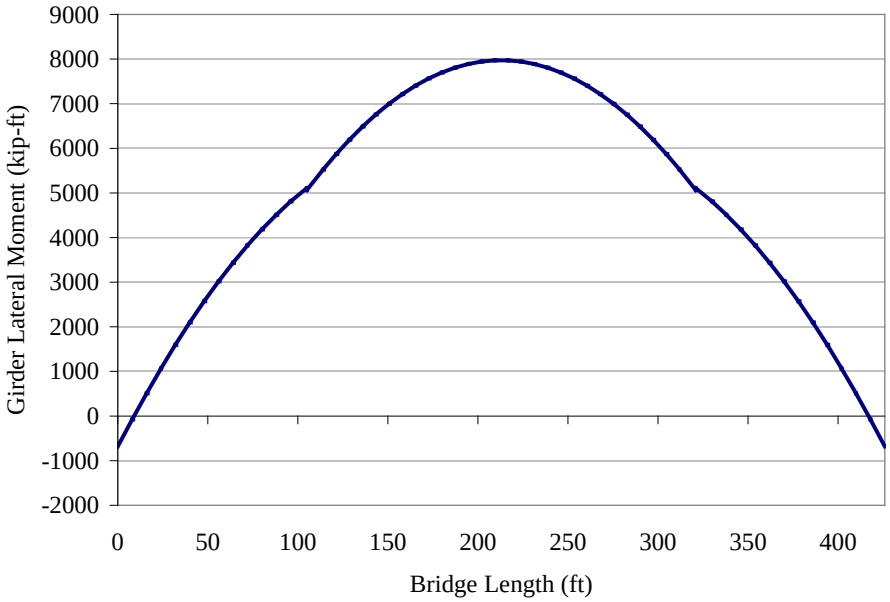

Figure 3-5 Bending Moment (lateral) Diagram of an Interior Girder under Mode 1 Push

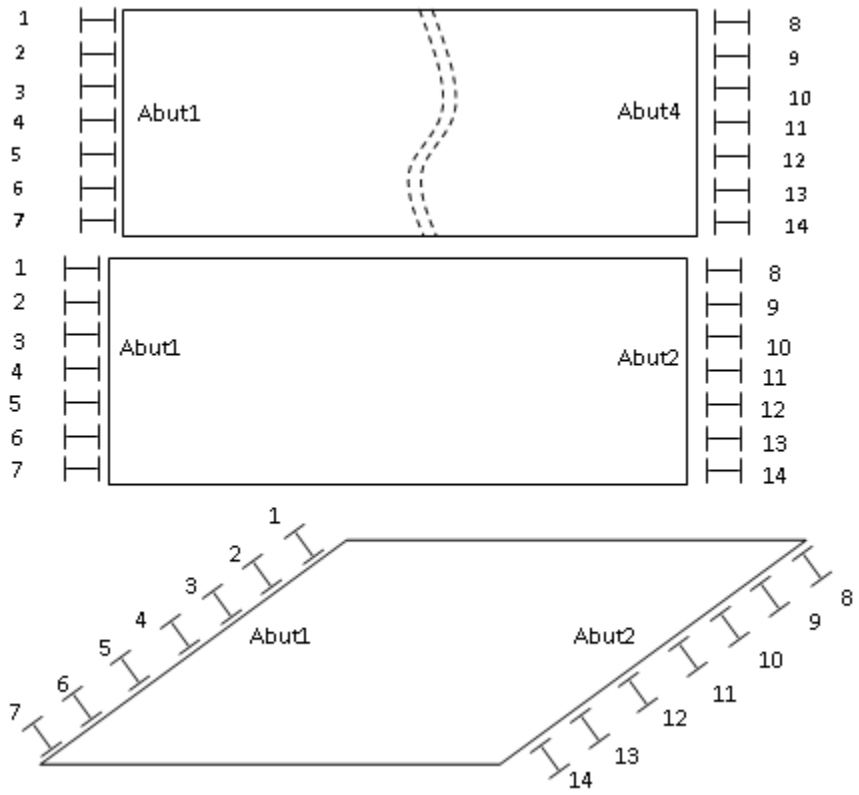

Figure 3-6 Pile numbering referred to in the tables for straight and skewed bridges

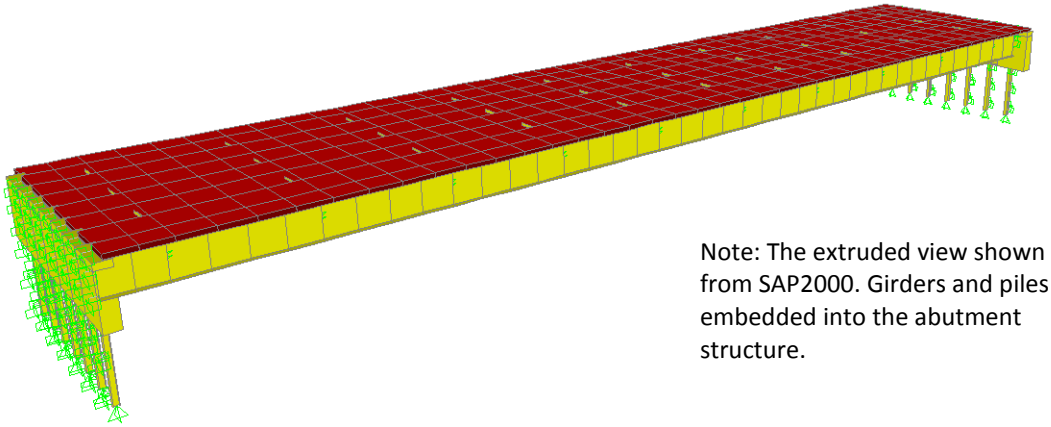

Note: The extruded view shown is from SAP2000. Girders and piles are embedded into the abutment structure.

Figure 3-7 3D view of Single-span Straight Bridge

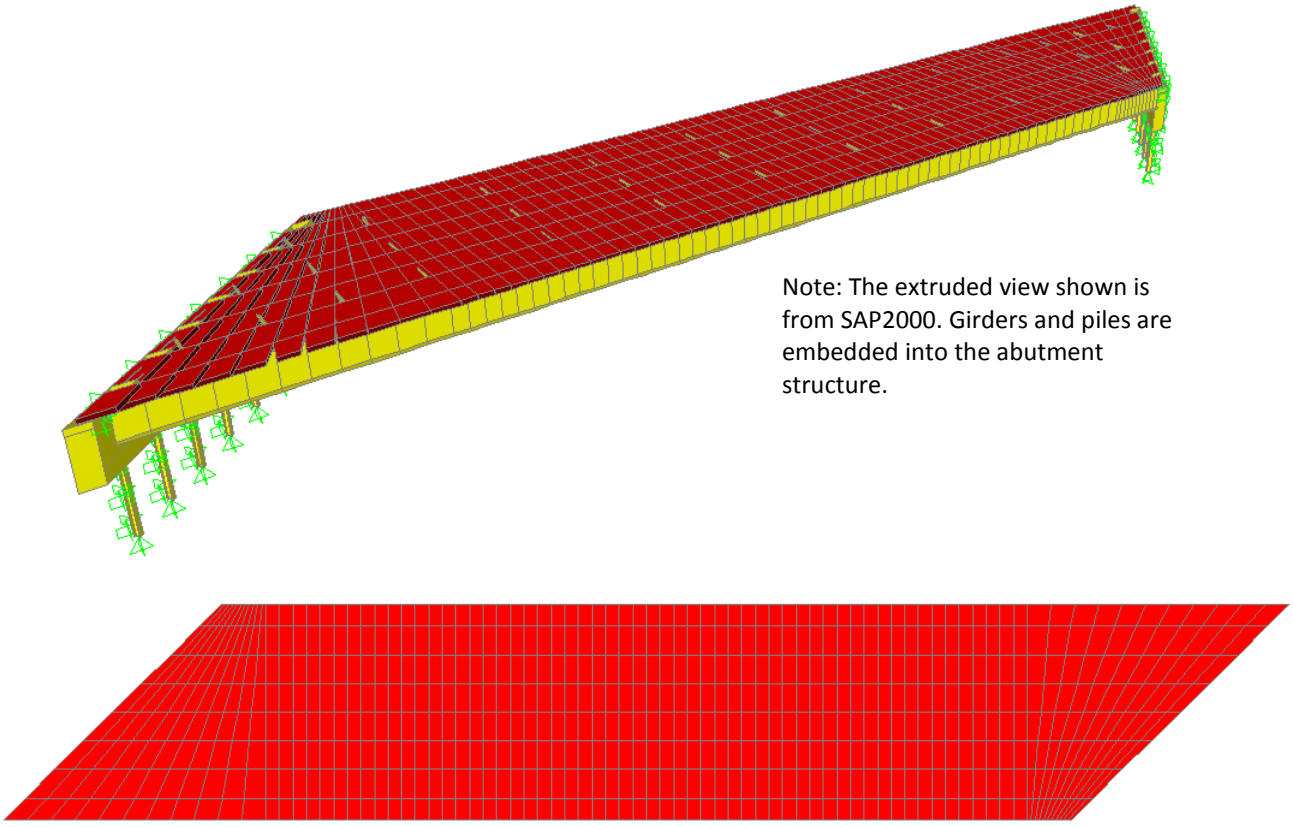

Note: The extruded view shown is from SAP2000. Girders and piles are embedded into the abutment structure.

Figure 3-8 3D view and plan view of 45-degree Skew Bridge

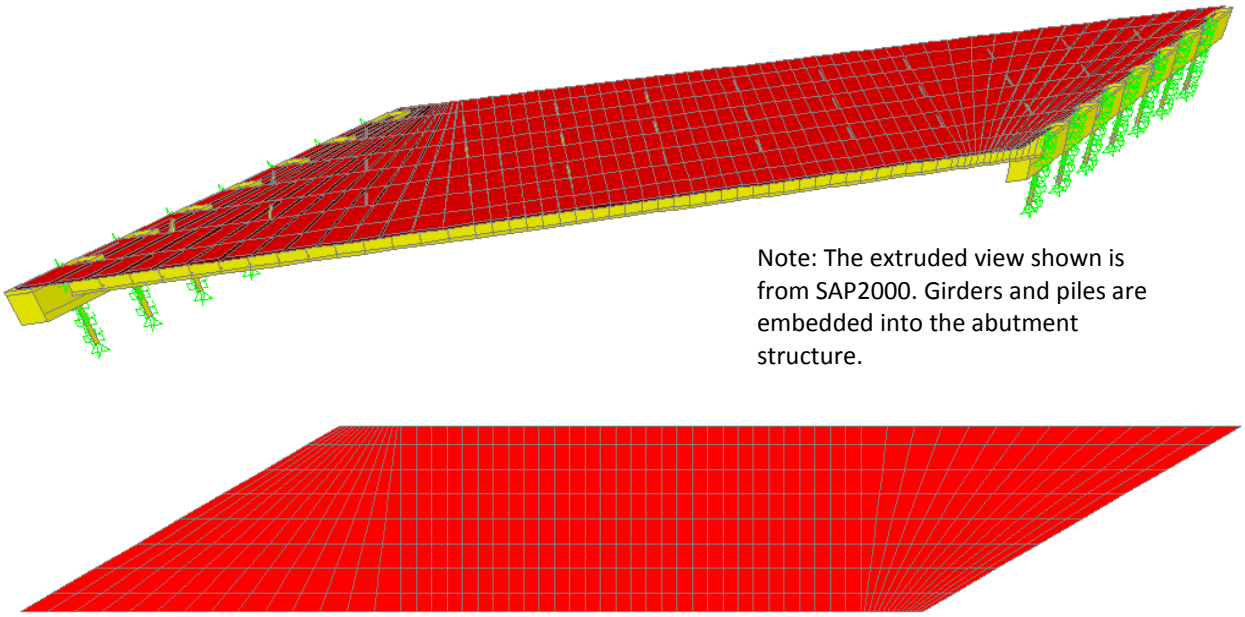

Note: The extruded view shown is from SAP2000. Girders and piles are embedded into the abutment structure.

Figure 3-9 3D view and plan view of 60-degree Skew Bridge

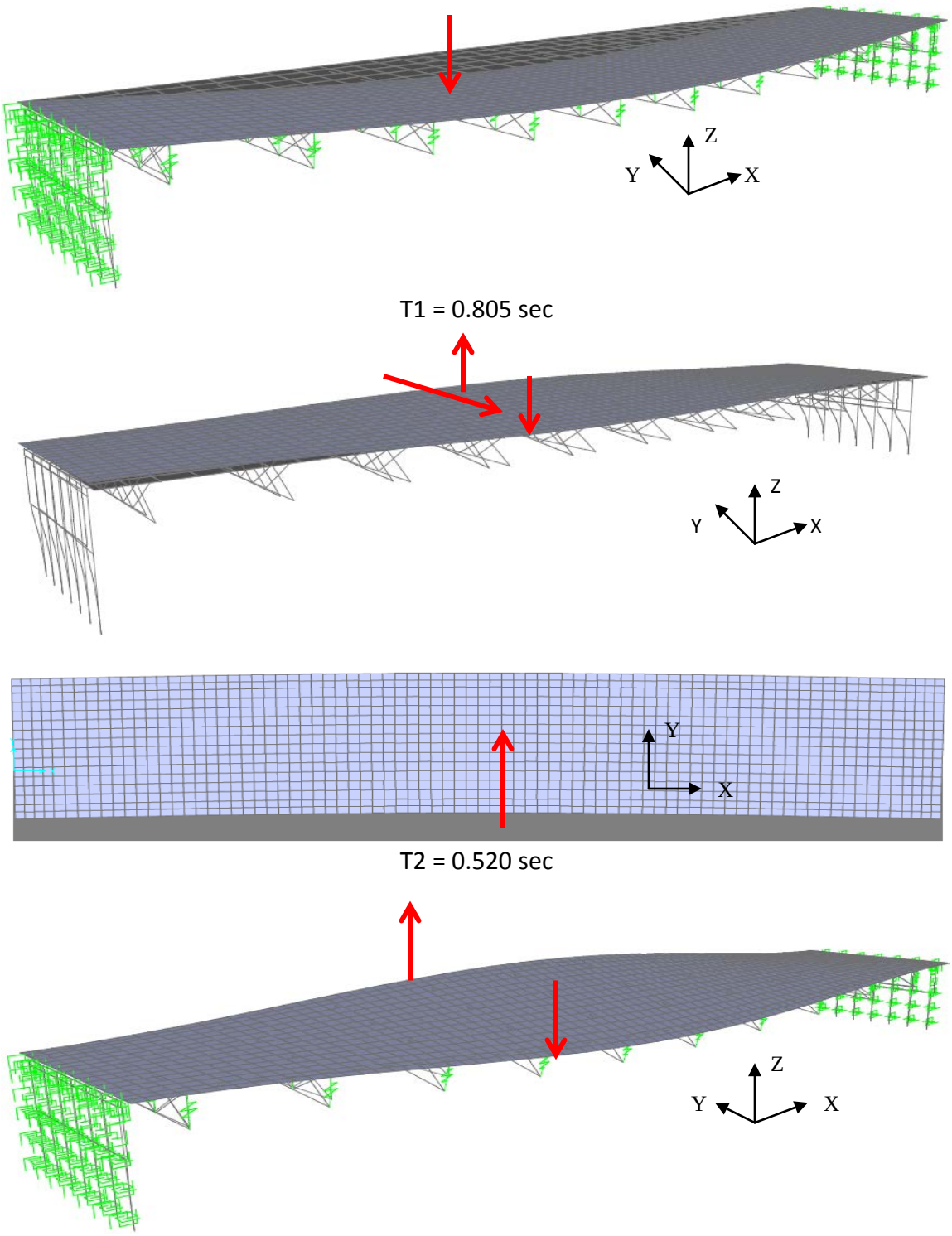

Figure 3-10a Mode shapes of the Straight Bridge (Modes 1, 2, and 3)

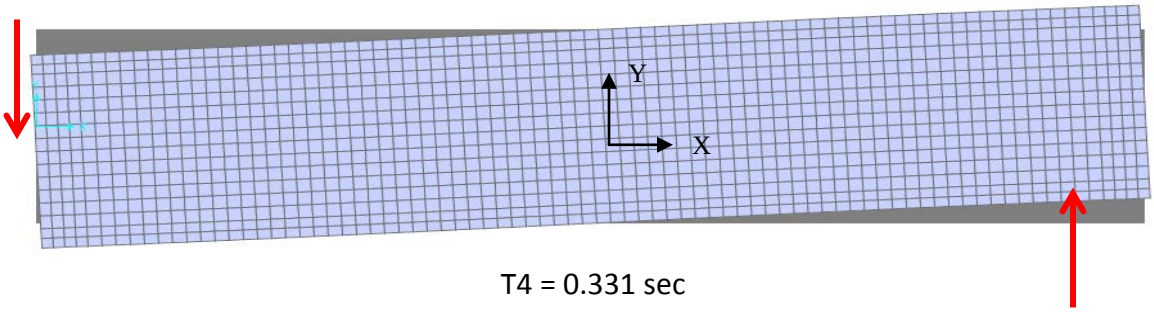

T4 = 0.331 sec

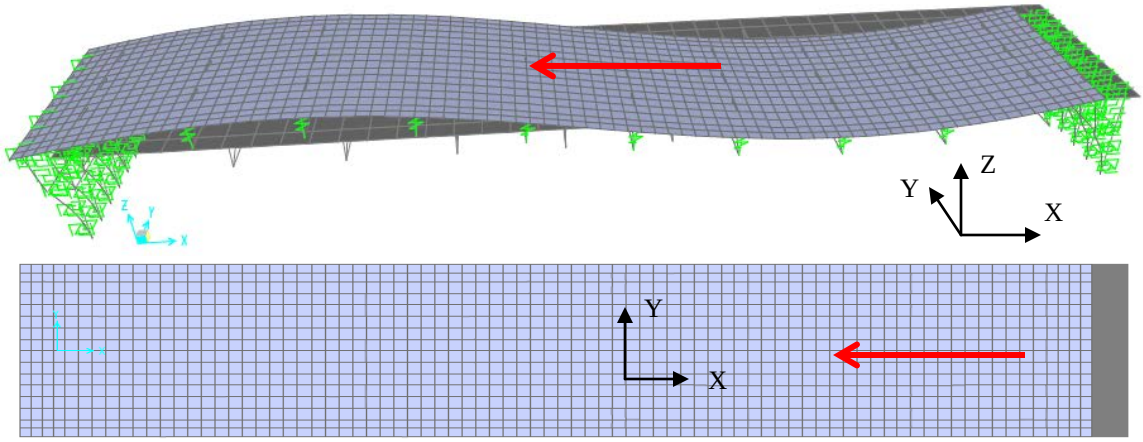

T5 = 0.282 sec

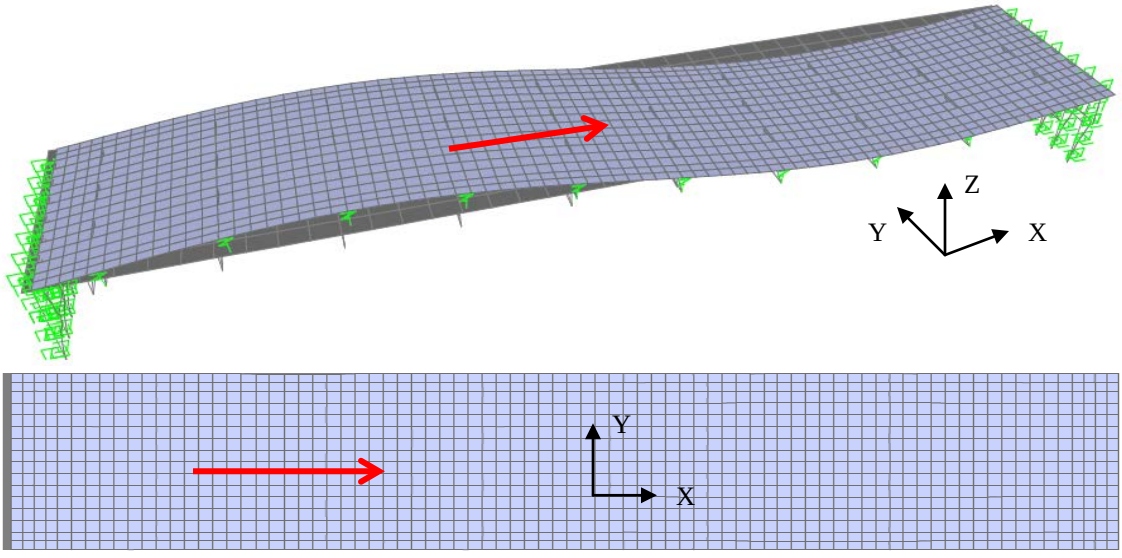

T6 = 0.226 sec

Figure 3-10 Mode shapes of the Straight Bridge

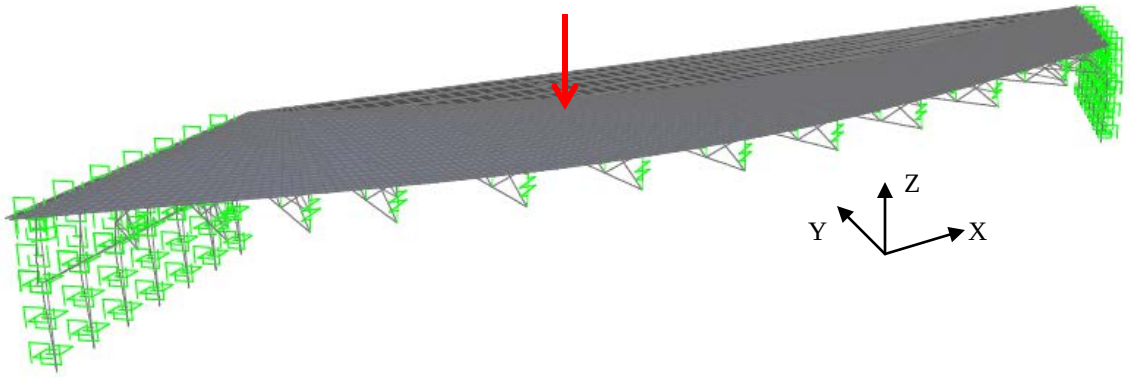

T1 = 0.772 sec

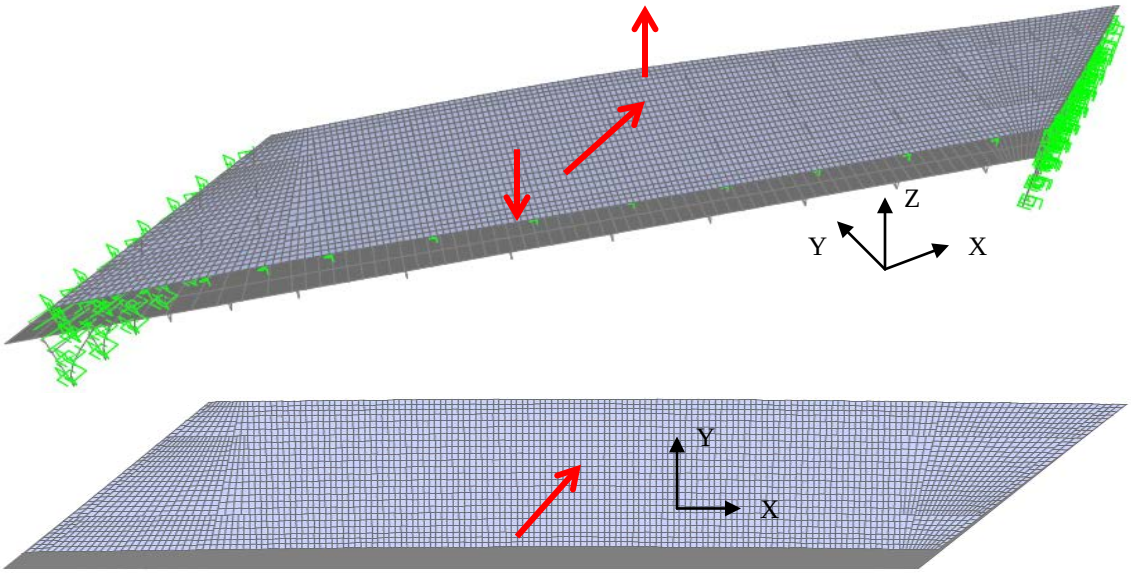

T2 = 0.519 sec

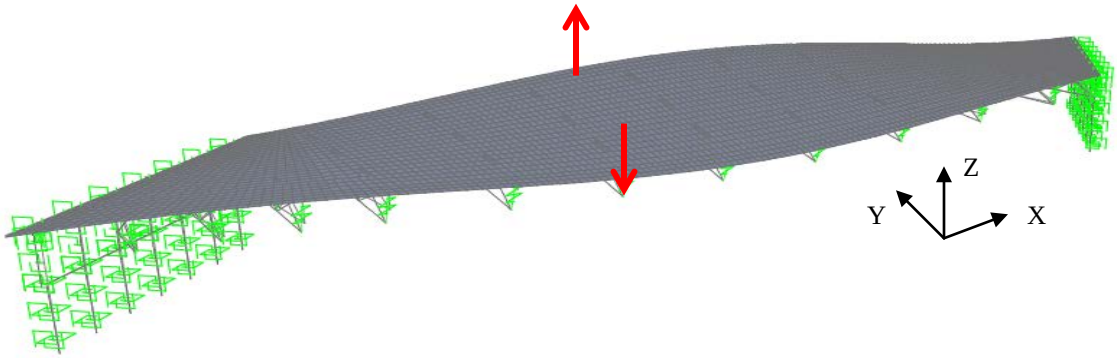

T3 = 0.373 sec

Figure 3-11a Mode shapes of the 45-degree skew bridge (Modes 1, 2, and 3)

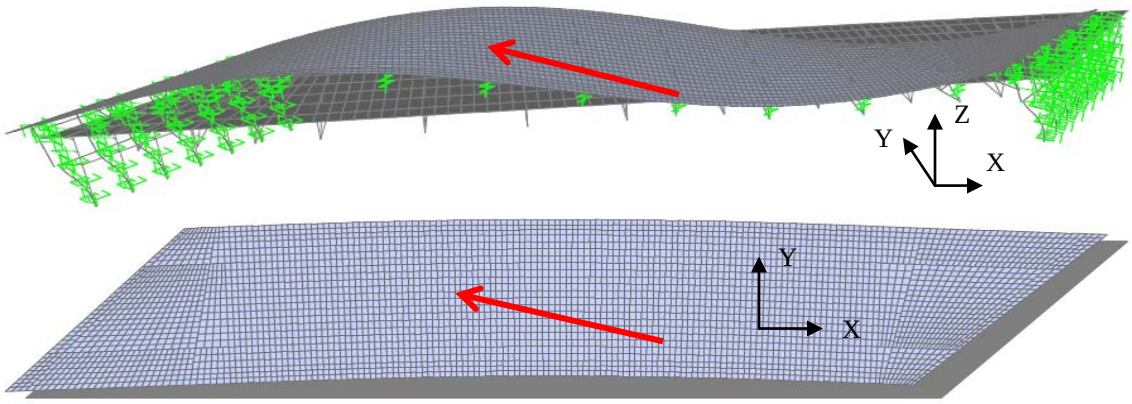

T4 = 0.301 sec

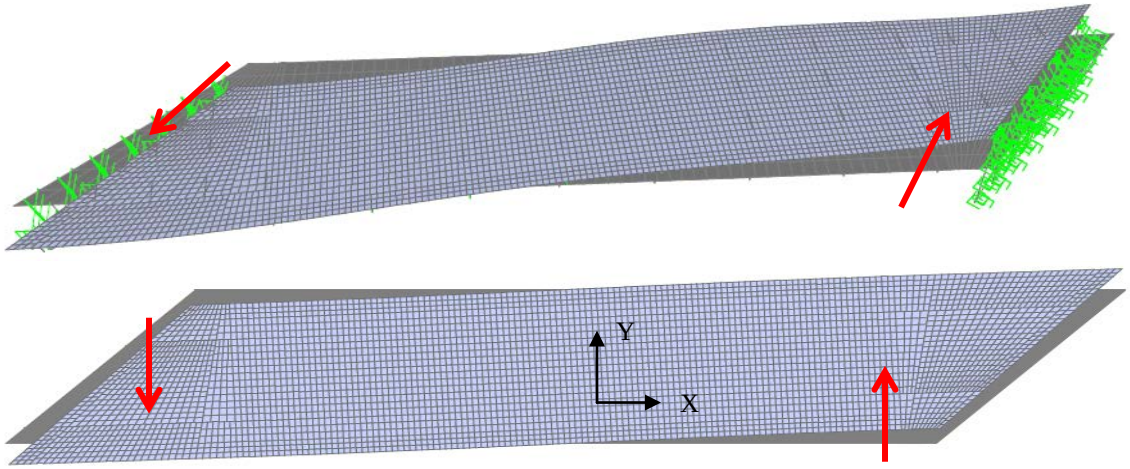

T5 = 0.229 sec

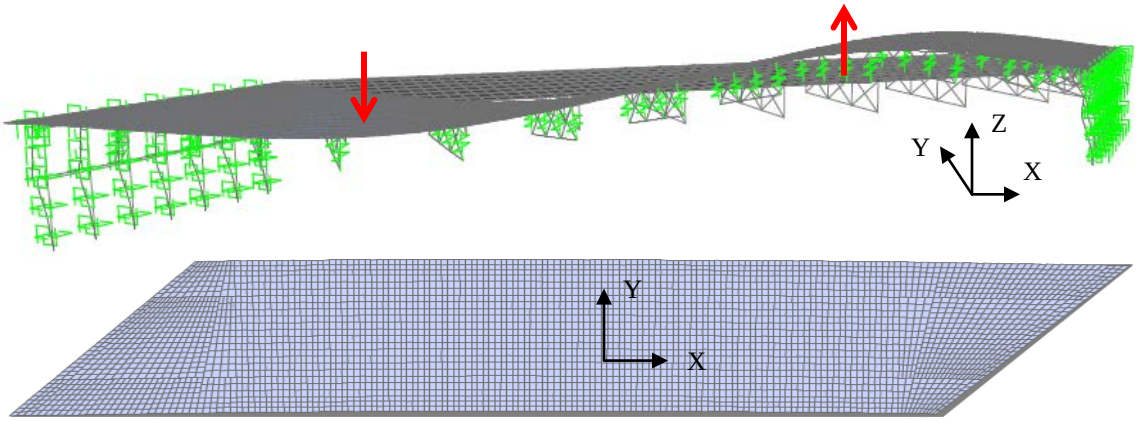

T6 = 0.211 sec

Figure 3-11 Mode shapes of the 45-degree Skew Bridge

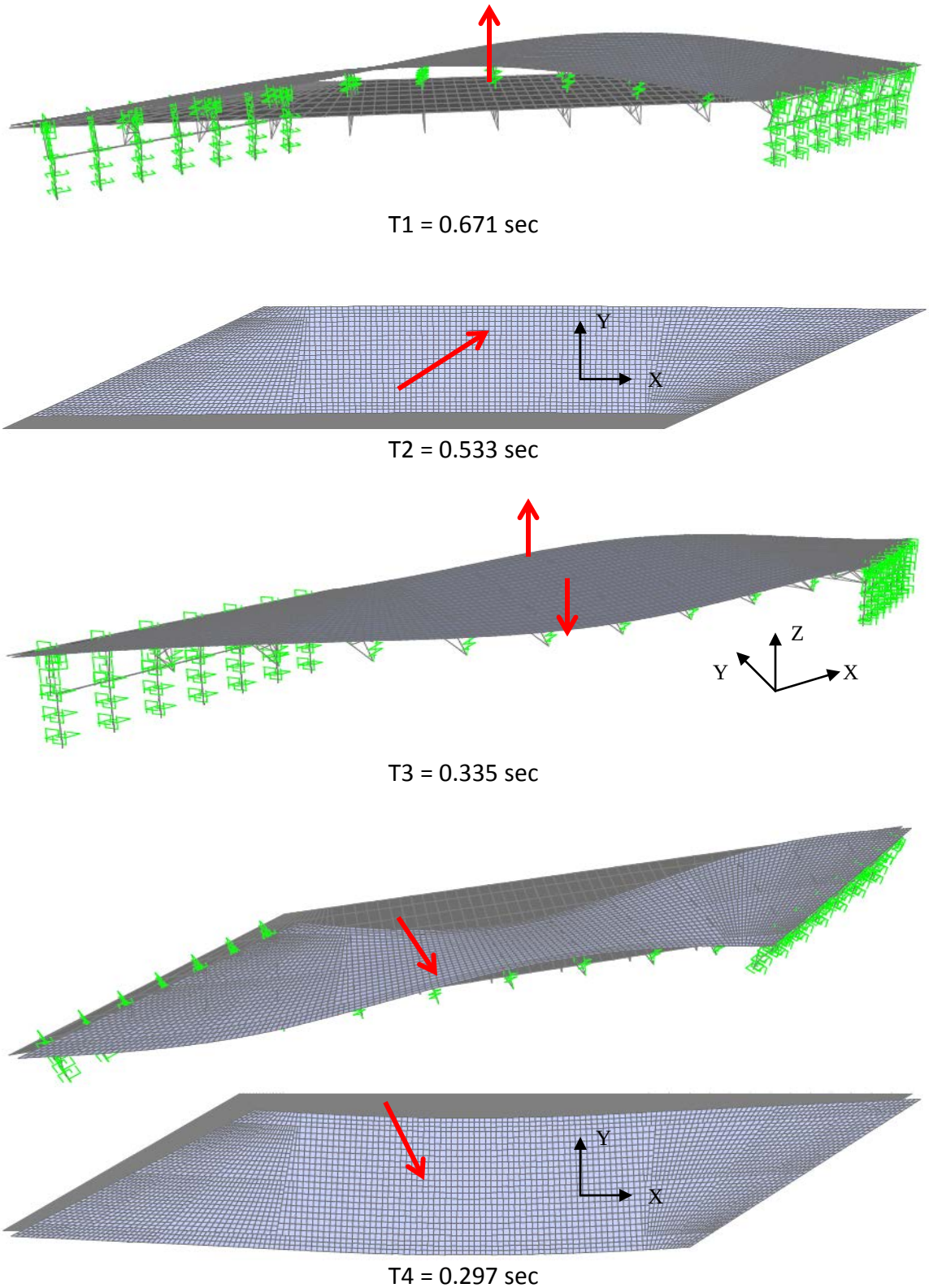

Figure 3-12a Mode shapes of the 60-degree skew bridge (Modes 1, 2, 3, and 4)

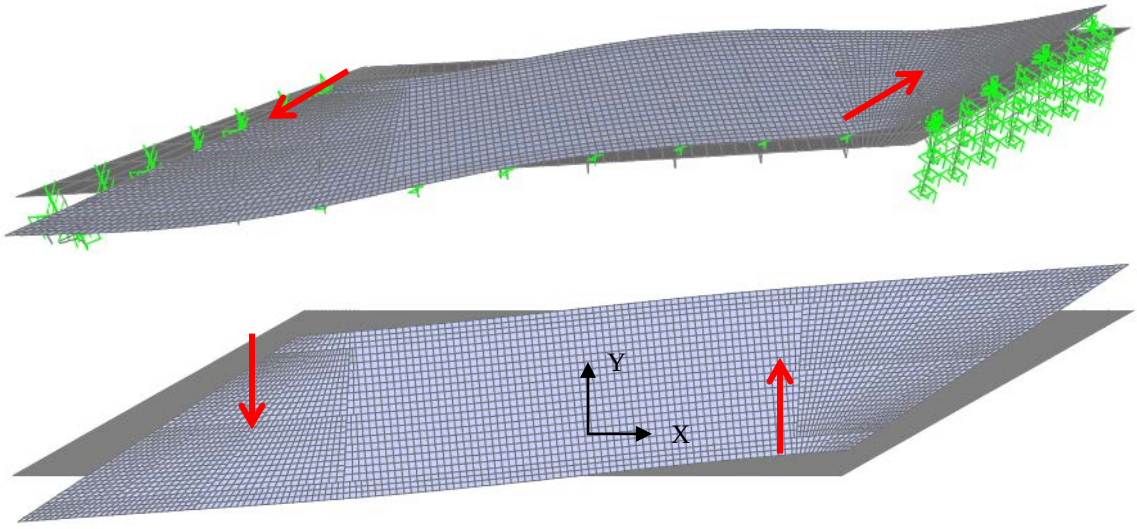

T5 = 0.198 sec

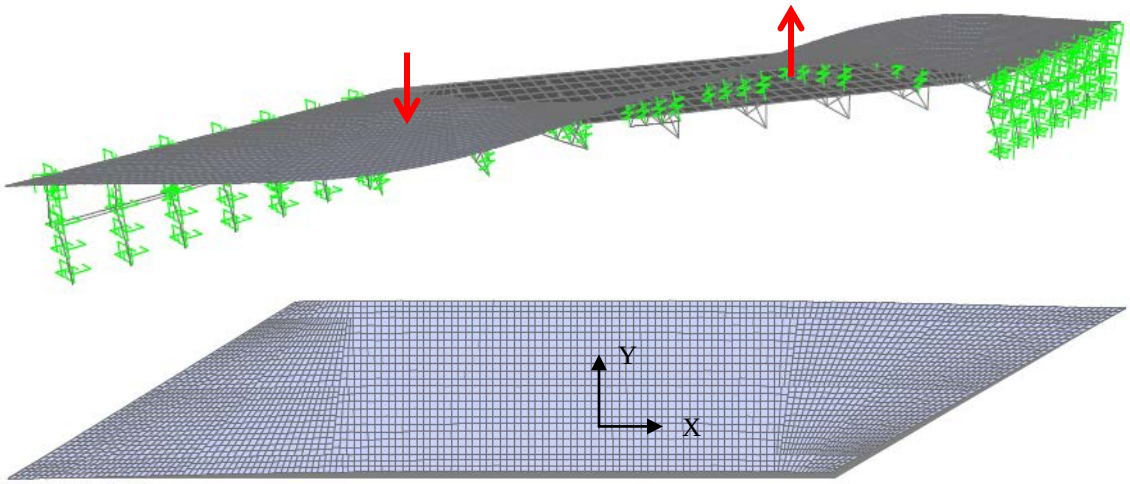

T6 = 0.191 sec

Figure 3-12 Mode shapes of the 60-degree Skew Bridge

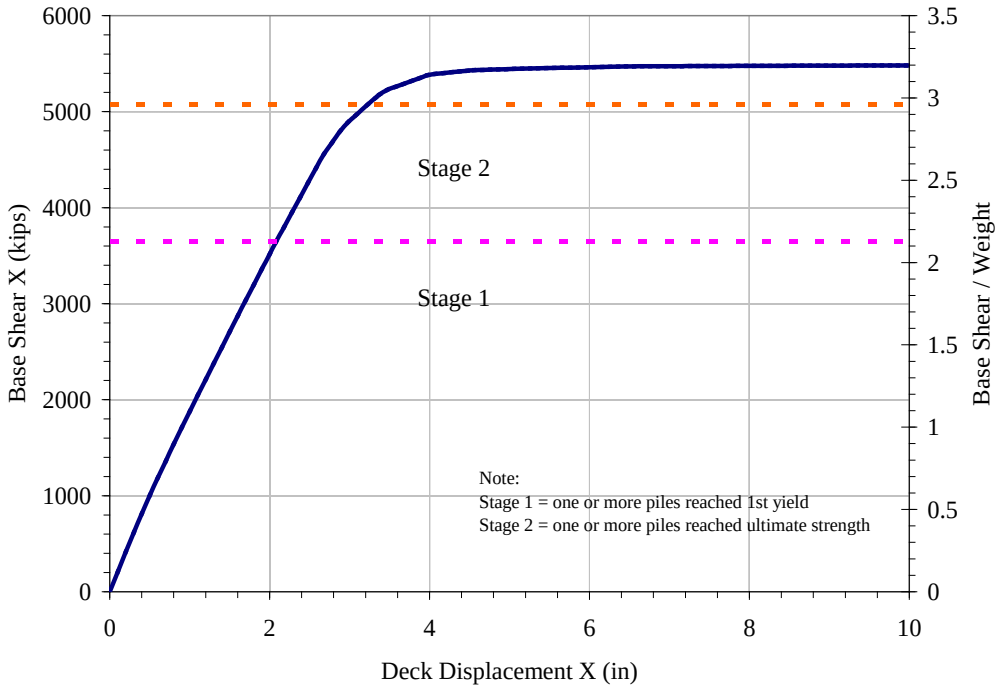

(a) Mode 5 Pushover Curve (push in longitudinal direction)

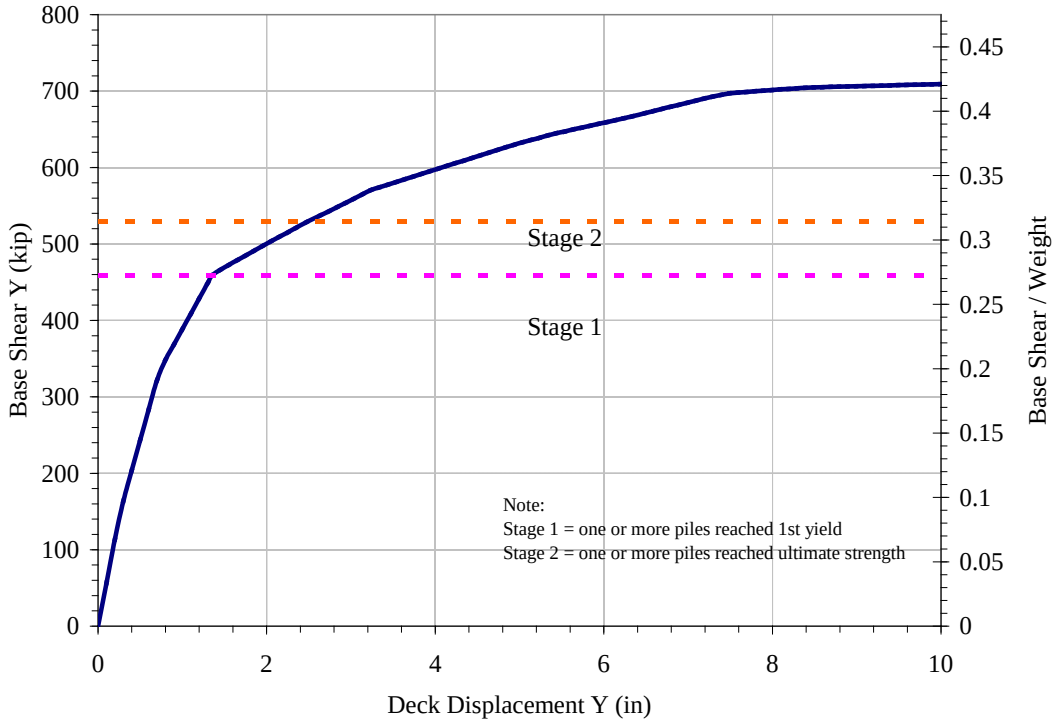

(b) Mode 2 Pushover Curve (push in transverse direction)

Figure 3-13 1-Span Straight Bridges: Pushover Curves

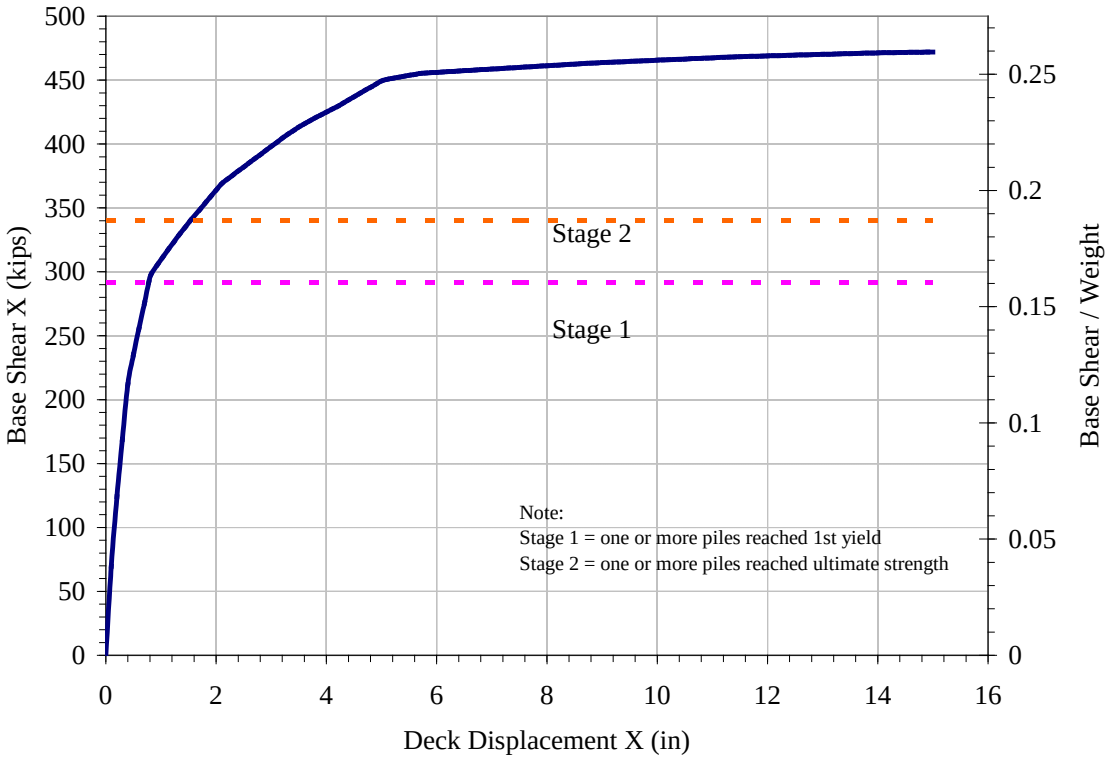

(a) Base Shear vs Deck Displacement: X-direction

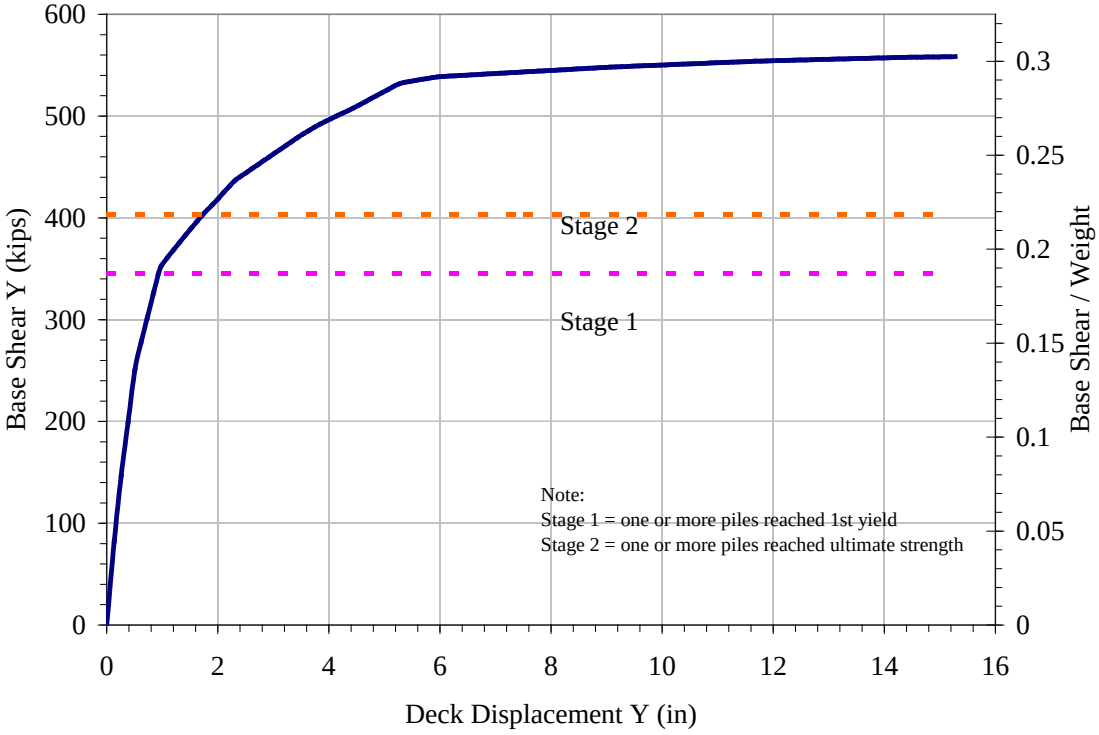

(b) Base Shear vs Deck Displacement: Y-direction

Figure 3-14 45-degree Skew Bridge: Mode 2 Pushover Curves

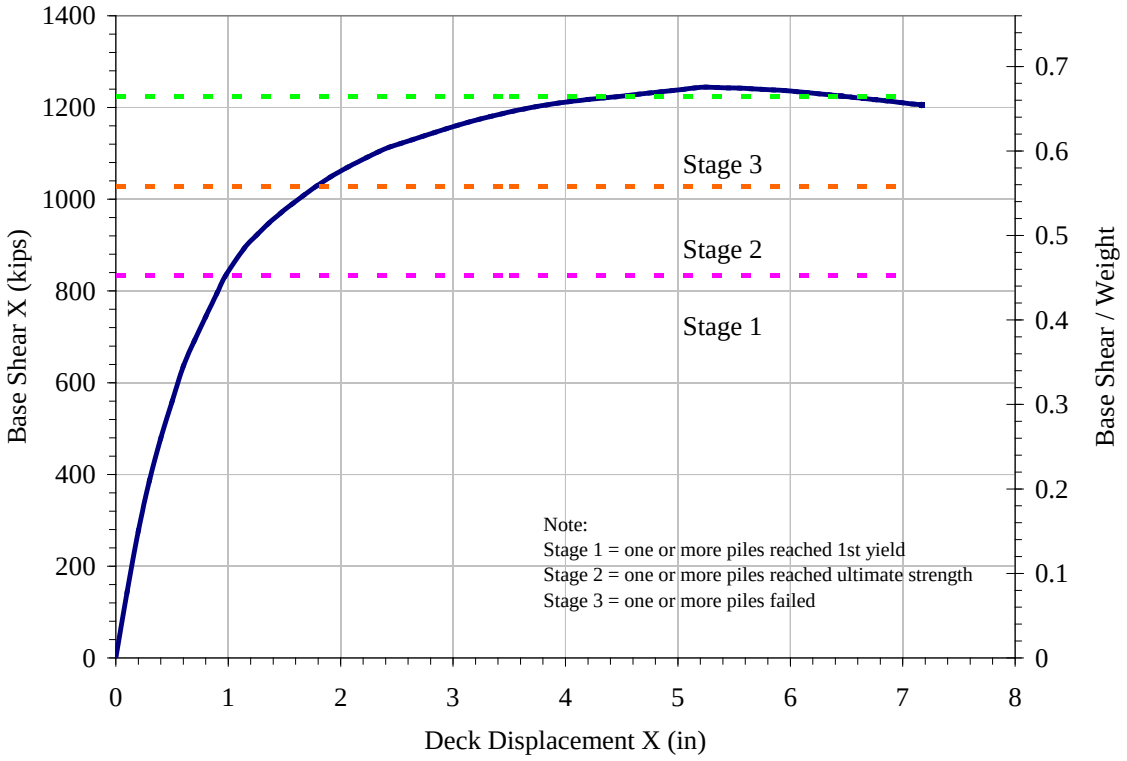

(a) Base Shear vs Deck Displacement: X-direction

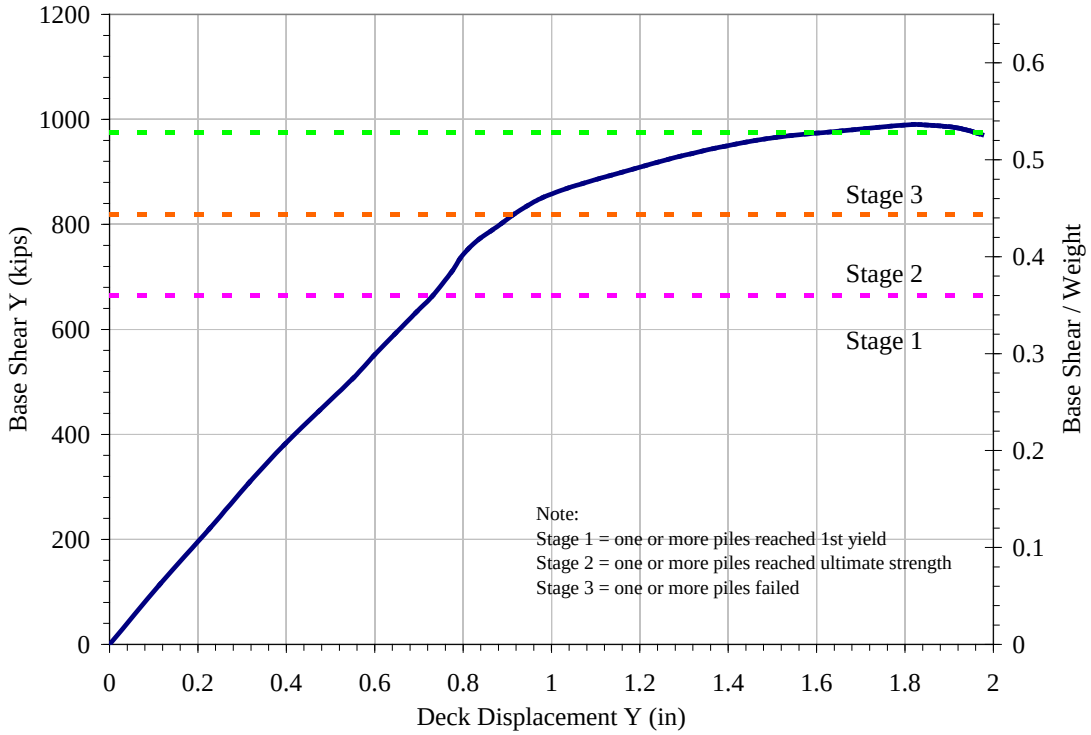

(b) Base Shear vs Deck Displacement: Y-direction

Figure 3-15 45-degree Skew Bridge: Mode 4 Pushover Curves

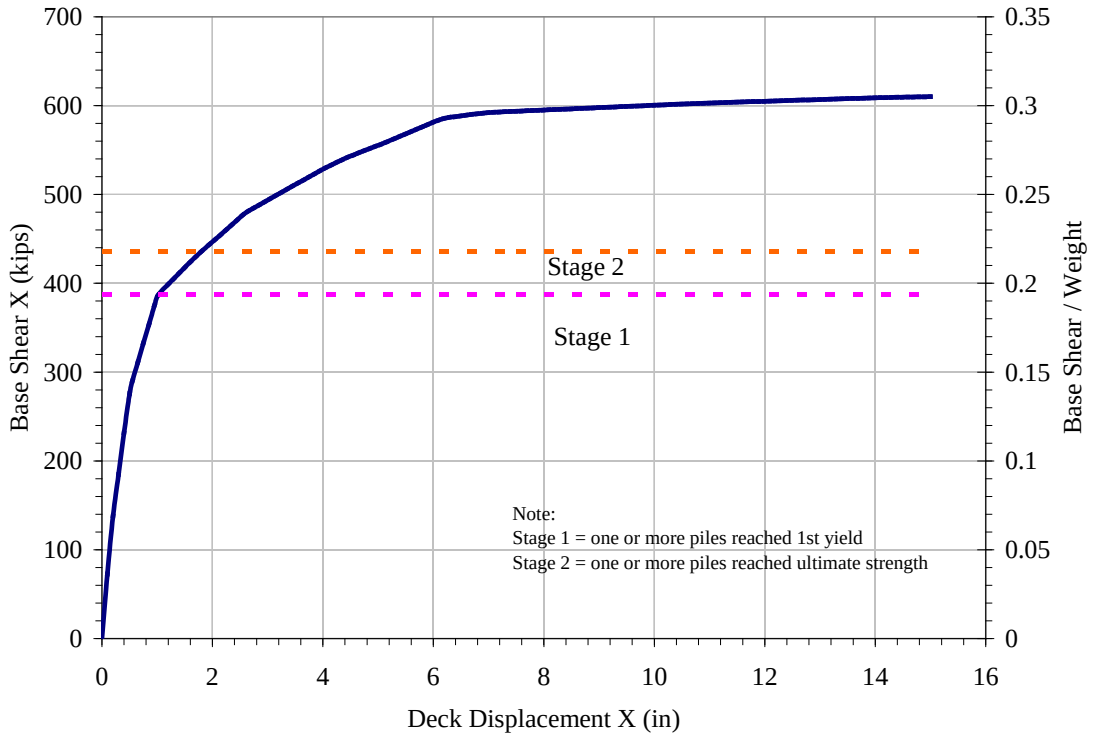

(a) Base Shear vs Deck Displacement: X-direction

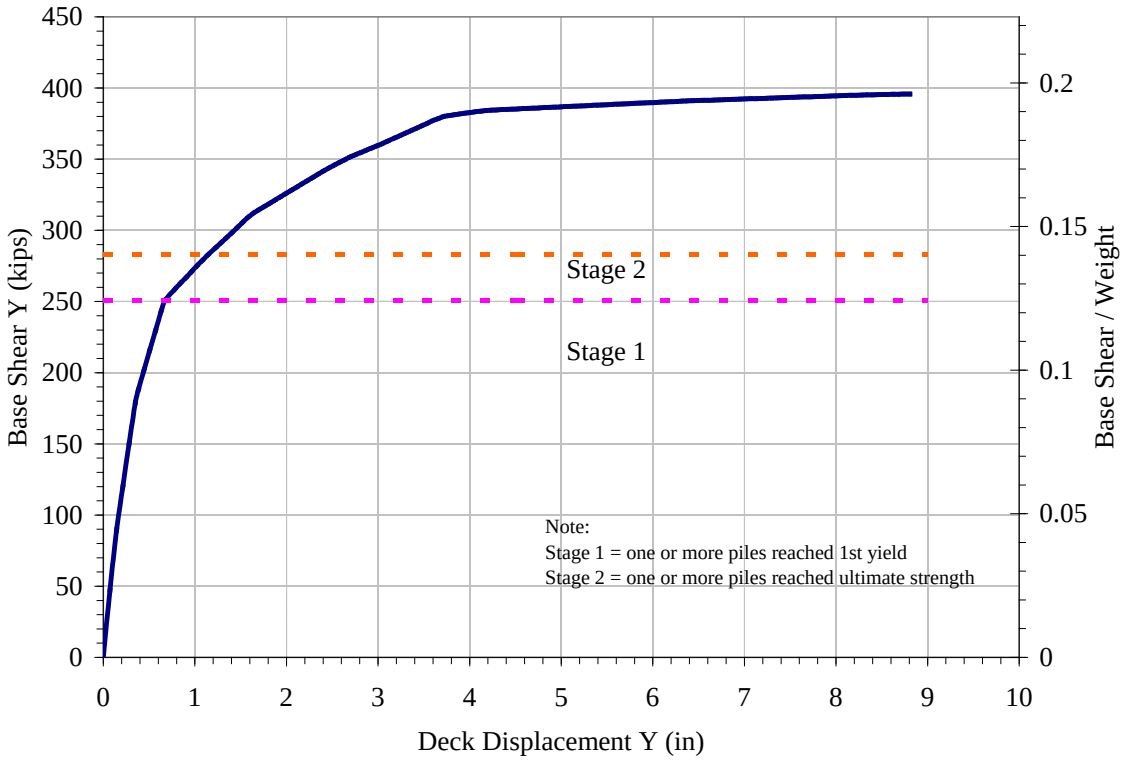

(b) Base Shear vs Deck Displacement: Y-direction

Figure 3-16 60-degree Skew Bridge: Mode 2 Pushover Curves

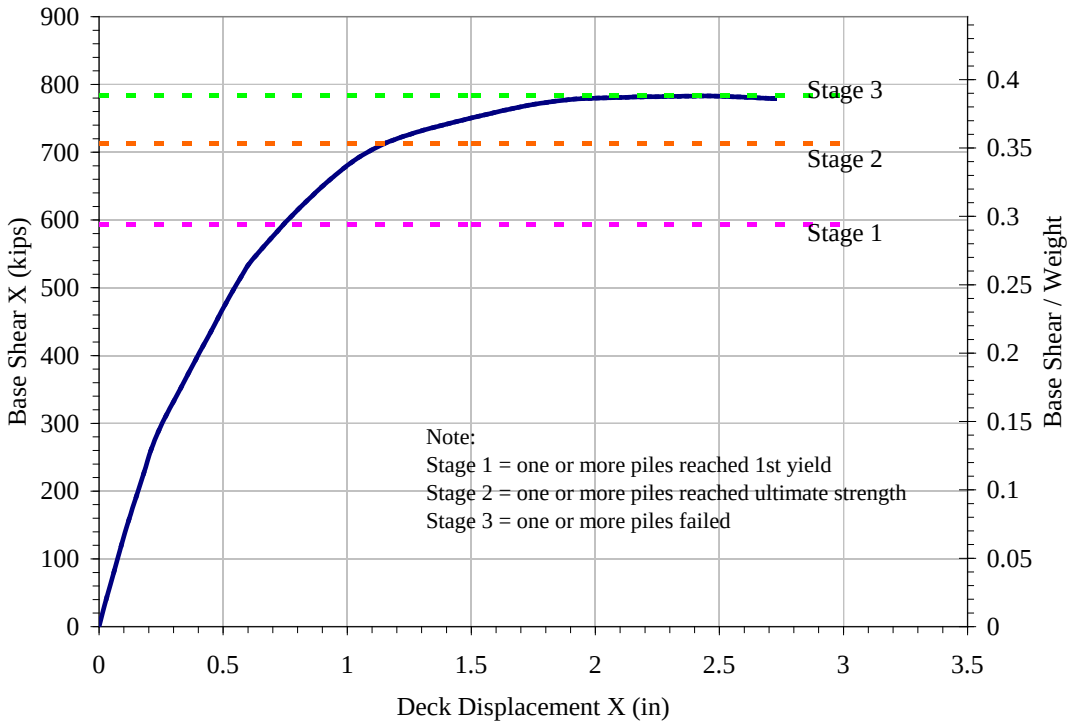

(a) Base Shear vs Deck Displacement: X-direction

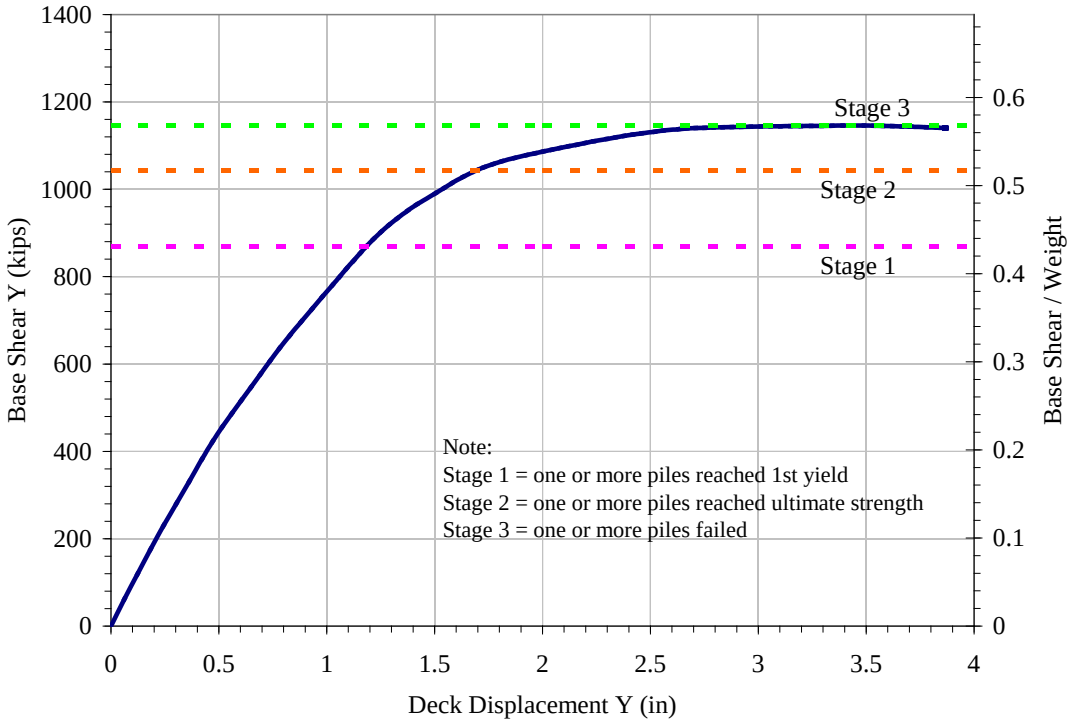

(b) Base Shear vs Deck Displacement: Y-direction

Figure 3-17 60-degree Skew Bridge: Mode 4 Pushover Curves

Chapter 4 SEISMIC RESPONSE OF STEEL BRIDGES WITH INTEGRAL ABUTMENT

The effectiveness of steel bridges with integral abutments in seismic zones is investigated in this chapter. The seismic responses of integral abutment bridges were compared to that of seat-type abutment bridges. A preliminary procedure was developed to design the bridges used in the nonlinear time history analyses. It was assumed that these bridges are located in a high seismic zone. The input motions were artificially generated using SIMQKE (Gasparini and Vanmarcke 1976) and were scaled to match an AASHTO response spectrum.

4.1 PRELIMINARY DESIGN PROCEDURE

A preliminary design procedure was developed based on the findings of earlier tasks and subsequent analyses. In integral abutment bridges, the yielding of the piles will limit the seismic forces on the components along the load path. Most of the seismic forces are attracted to the abutments because of high stiffness of integral abutments compared to bents. This, in turn, increases the force demand on the piles. The preliminary design procedure is a displacement-based approach where inelasticity is in the piles as well as in the columns.

The following is the iterative step-by-step seismic design procedure used in this study.

Step 1: Select the pile section, number, and pile length.

Based on dead load analysis, the pile section, number, and length are selected. The pile capacity should also be checked against the axial loads coming from live loads and seismic loads. These loads could be significant compared to dead loads.

Step 2: Perform soil-pile (*p*-*y*) analysis to obtain the *p*-*y* springs along the length of the piles.

This analysis will establish the nonlinear soil springs along the length of the pile. Also, the inflection point along the length of the pile will be determined.

Step 3: Develop bridge finite element model.

It is recommended to use shell elements for the deck and beam elements for other components such as girders, cross-frames, bent caps, columns, and piles as discussed in Chapter 2.

The pile length that can be included in the model can be up to the location of the inflection point determined in Step 2 such that pin support can be assigned to the bottom of the pile.

The *p*-*y* springs represented by nonlinear link elements are assigned along the length of the pile.

A P-M-M (axial load-biaxial moment interaction) is assigned to the top of the pile to account the inelasticity in the pile.

The passive resistance of the soil behind the abutment backwall is represented by a series of gap and nonlinear link elements. The nonlinear link element represents the passive resistance exerted by the soil behind the abutment backwall. The gap link element is provided to ensure that the nonlinear link element will be under compression only.

At the columns, fiber hinges can be assigned to the top and bottom plastic hinge locations. For linear modal and static analyses, modification factors for moment of inertia and torsional constant are used based on section analysis.

Step 4: Perform response spectrum analysis then determine the seismic displacement demand (Δ_d).

A sufficient number of modes should be used in the response spectrum analysis. To determine the number of modes needed, the cumulative sum of modal mass participation ratios up to the *n*th mode should be close or equal to 1.0.

Step 5: Perform modal pushover analysis to determine displacement capacity.

Pushover analysis should be performed for the dominant longitudinal and transverse modes. In cases where not all of the piles yield at the same time, yield displacement capacity (Δ_y) may be defined as the displacement when one or more piles have reached the yielding stage. In the same manner, ultimate displacement capacity (Δ_u) may be defined as the displacement when one or more piles have reached the ultimate point.

Step 6: Compare the pile displacements from Steps 4 and 5 (Δ_d vs Δ_u). If Δ_u is smaller than Δ_d, change the pile section or increase the number of piles and repeat Steps 2 to 5.

Step 7: The columns are designed according to AASHTO LRFD Specifications where the seismic demand is reduced by the response modification factor. The R-factor for columns is equal to 3.0.

4.2 DESIGN EXAMPLES

Three steel girder bridges were used to illustrate the design procedure described above:

1. Three-span steel girder bridge with integral abutments where pile strong axis is oriented parallel to abutment axis (3SIAB-PSA).
2. Three-span steel girder bridge with integral abutments where pile strong axis is oriented perpendicular to abutment axis (3SIAB-PWA).
3. Three-span steel girder bridge with seat-type abutments (3SSAB).

Examples 1 and 2 were used to investigate the effect of pile orientation on the overall seismic behavior of integral abutment bridges. This investigation will also shed light on what should be the preferred pile orientation, especially in locations of high seismicity. Example 3 was developed to compare the seismic behavior of a bridge with seat-type abutments to that of a bridge with integral abutments.

The geometry and components of these bridges were taken from the example by Wasserman and Walker (1996) as described in Chapter 2. Thus the soil-pile and abutment-soil stiffness properties are the same as previously discussed. The columns, however, were modified to reflect the seismic design as discussed below.

Figure 4-1 shows the AASHTO design spectrum that is used for seismic analysis. This spectrum is for a location with high seismicity in Claremont, California. The first 30 modes of the above design examples were considered sufficient for use in the response spectrum analysis according to the cumulative sum of mass participating ratios. The Complete Quadratic Combination (CQC) of modal responses was used in the analysis. Response spectrum analysis was performed in the longitudinal and transverse directions. The seismic displacements and forces used in the design were based on the directional combination prescribed by AASHTO LRFD Specifications (i.e. maximum of either (100%X + 30%Y) or (30%X + 100%Y)).

4.2.1 Seismic Design of Three-Span Integral Abutment Bridge with Pile Strong Axis Parallel to Abutment Axis (3SIAB-PSA)

Step 1: The total reaction at the abutments from dead load analysis is 300 kips. If seven piles are to be placed on each abutment, the axial dead load on each pile is 43 kips. An HP10x42 pile with an unbraced length of 12.4 ft would have axial load capacity in compression of 423 kips. That is, the demand-capacity ratio for each pile under dead load is only 10% which seems small, but it does not include the axial loads coming from live and seismic loads which may be significant compared to dead load. Thus, a single row of seven HP10x42 piles is deemed sufficient at each abutment.

Step 2: The properties of the *p-y* soil springs that will be used in the analysis are the same as those described in Chapter 2 because the pile section and number of piles are the same.

Step 3: Figure 4-2 shows the finite element model of the bridge. The pile strong axis is oriented parallel to abutment axis. Also, included in this model is the flexibility of the girder-abutment connection discussed in Chapter 2.

Step 4: The design spectrum shown in Figure 4-1 was used in the response spectrum analysis. The response spectrum analysis was performed in the longitudinal and transverse directions, and the directional combination discussed above was used to determine the seismic demands. The seismic demands were then combined with dead loads to determine the design loads.

For the piles, the seismic displacement demands, Δ_d, are:

$(\Delta_d)_{longitudinal}$ = 2.42 in

$(\Delta_d)_{transverse}$ = 2.59 in

Step 5: The pushover analyses were based on force distributions proportional to the dominant modes of vibration (modal pushover analysis). Table 4-1 shows the mass participation ratios of the first 12 modes for 3SIAB-PSA. The dominant mode of vibration in the longitudinal direction is the 5th mode, thus it will be used in determining the pile displacement capacity in the longitudinal direction. The dominant mode of vibration in the transverse direction is the 1st mode. The 2nd and 7th modes are also transverse modes but the associated mass participation ratios are small compared to that in the 1st mode. Thus, the 1st mode would be used in evaluating the capacity of the piles in the transverse direction.

Since all piles do not reach yielding at the same time in the transverse direction, the yield displacement capacity is defined as the displacement when one or more piles reached yielding. Similarly, the ultimate displacement capacity is defined as the displacement when one or more piles reached ultimate strength. These capacities will be obtained from the pushover analysis of the bridge.

From the pushover analyses and based on the definition of yield and ultimate capacities, the yield and ultimate displacements are:

Longitudinal Direction:	Δ_y = 1.82 in	Δ_u = 7.08 in
Transverse Direction:	Δ_y = 1.11 in	Δ_u = 2.67 in

Step 6: Comparison with the demand displacements from response spectrum analysis shows that there is a significant reserve displacement capacity in the longitudinal direction but not in the transverse direction.

As noted above, the pile capacities are defined as when one or more piles reached yielding or ultimate point. In this preliminary design procedure, this definition can be overly conservative compared to when the capacity is defined as the displacement when all piles have reached the ultimate strength. If the capacity is defined as such, the ultimate displacement capacity in the transverse direction would be 6.53 in.

Another factor that should be considered is the selection of modes used for the transverse pushover. It can be argued that 2nd and 7th modes should be also included in the pushover analysis because the mass participation ratios from these modes in the transverse direction are 23% and 11%, respectively. However, for the sake of simplicity, only the 1st mode was used in evaluating the pile capacity in the transverse direction. If there are two or more modes with mass participation ratios that are about equal, then it would be logical to perform the pushover analysis in a number of modes.

Step 7: The column design was based on the combined dead and seismic forces. The seismic forces were obtained from response spectrum analysis and then divided by the response modification factor, R-factor, equal to 3.0. The column design loads are:

Dead: P_{DL} = 1,570 kips
M_{DL} = 292 kip-ft

Earthquake / (R = 3): P_{EQ} = 159 kips
M_{EQ} = 2,830 kip-ft

Therefore, the combined design loads (dead + earthquake) are:
P = 1,729 kips
M = 3,122 kip-ft

The columns are 5 ft in diameter with 5 ksi concrete. The longitudinal steel ratio is 1% while the transverse steel ratio is 0.56%. Section analysis was performed using the computer program Xtract (2008). The shear capacity was evaluated using the provisions of NCHRP 12-49 Guidelines for Seismic Design of Highway Bridges. The design capacities are:

P/f'_cA_g = 12%
$V_{capacity}$ = 653 kips
$M_{plastic}$ = 6,320 kip-ft

The plastic moment, $M_{plastic}$, was based on the idealized elastic-plastic representation of moment-curvature curve. In the finite element model, however, the actual moment-curvature was used because column inelasticity was represented by fiber hinges.

4.2.2 Seismic Design of Three-Span Integral Abutment Bridge with Pile Strong Axis Perpendicular to Abutment Axis (3SIAB-PWA)

This section describes the second example bridge with the pile strong axis oriented perpendicular to the abutment axis. A survey of bridge construction practices showed that there is no definite consensus on how the pile strong axis should be positioned relative to the abutment. Some states prefer the pile strong axis parallel to abutment wall while other states prefer the opposite. Comparison of the response of 3SIAB-PWA and 3SIAB-PSA would give an insight on the effect of pile orientation on the seismic behavior of integral abutment bridges.

Step 1: The pile section and number of piles is the same as those for 3SIAB-PSA.

Step 2: The *p-y* soil springs used are the same as those in 3SIAB-PSA.

Step 3: Figure 4-3 shows the finite element model of 3SIAB-PWA.

Step 4: The pile design displacements from seismic analysis are:

$(\Delta_d)_{longitudinal}$ = 2.59 in
$(\Delta_d)_{transverse}$ = 2.10 in

The displacement in the longitudinal direction is about the same as that in 3SIAB-PSA because the response is dominated by the abutment-soil response. The displacement in the transverse direction is smaller than that in 3SIAB-PSA because of the pile axis orientation.

Step 5: Table 4-2 shows the modal mass participation ratios for the first 12 modes. Similar to 3SIAB-PSA, the dominant longitudinal and transverse modes are the 5th and 1st modes, respectively. From the pushover analyses and based on the definition of yield and ultimate capacities, the yield and ultimate displacements are:

Longitudinal Direction:	Δ_y = 1.16 in	Δ_u = 6.50 in
Transverse Direction:	Δ_y = 1.70 in	Δ_u = 3.27 in

Larger displacement capacity is apparent in the transverse direction compared to that in 3SIAB-PSA because of the orientation of pile strong axis.

Step 7: The column seismic forces are approximately the same as for 3SIAB-PSA therefore the same column properties were used in this design example.

4.2.3 Seismic Design of Three-Span Seat Abutment Bridge (3SSAB)

A design example with seat-type abutments was developed to compare its behavior to that of integral abutment bridges (3SIAB-PSA and 3SIAB-PWA). The geometry and bridge components are the same as those used for the integral abutment bridges except the size of columns. A larger column is needed due to larger seismic forces, especially in the transverse direction where only the columns are providing the resistance. The shear keys that restrain the transverse direction are designed to fail at a low level of lateral force to protect the piles supporting the abutment seat from damage. In the longitudinal direction, most of the seismic forces are resisted by the soil passive resistance behind the abutment backwall. This is because the soil behind the abutment backwall is engaged once the joint gap at the end of the bridge is closed. Figure 4-4 shows the finite element model of the 3-span bridge with seat abutments (3SSAB). Table 4-3 shows the mass participation ratios of the first 12 modes. Similar to the integral abutment bridges, the 5th and 1st modes are the dominant longitudinal and transverse modes, respectively. The 3SSAB bridge is more flexible in the transverse direction because the abutments are free to translate in this direction. The 2nd mode is a torsional mode in the plane of the bridge.

The column design procedure is the same as that illustrated in integral abutment bridges. The column design forces are:

Dead: P_{DL} = 1,603 kips

M_{DL} = 575 kip-ft

Earthquake / (R = 3): P_{EQ} = 29 kips
M_{EQ} = 7,890 kip-ft

Therefore, the combined design loads (dead + earthquake) are:
P = 1,632 kips
M = 8,465 kip-ft

The columns are 6 ft in diameter with 5 ksi concrete. The longitudinal steel ratio is 1.1% while the transverse steel ratio is 0.5%. Section analysis was performed using the computer program Xtract (2008). The shear capacity was evaluated using the provisions of NCHRP 12-49 Guidelines for Seismic Design of Highway Bridges. The design capacities are:

P/f'_cA_g = 8%
$V_{capacity}$ = 852 kips
$M_{plastic}$ = 10,490 kip-ft

4.3 NONLINEAR TIME HISTORY ANALYSIS OF DESIGN EXAMPLES

Nonlinear time history analyses were performed to compare the seismic performance of the design examples. Three artificially generated ground motions that approximately match the design spectrum were used in these analyses. Figure 4-5 shows the comparison of the design spectrum and response spectrum of the generated ground motions. Combinations (Sets A, B, and C) of these ground motions were used in the time history analyses as shown in Table 4-4. Each ground motion in these combinations was scaled such that the vector sum of the response spectrum of the applied ground motions in the longitudinal and transverse directions approximately matched that of the design spectrum as shown in Figure 4-6.

The results of the nonlinear time history analyses performed on the design examples are discussed below. The comparison of 3SIAB-PSA and 3SIAB-PWA is discussed in Section 4.4. The comparison of response of integral abutment bridges and seat-supported bridges is discussed in Section 4.5.

4.3.1 3SIAB-PSA

Table 4-5 shows the summary of results of the time history analysis for 3SIAB-PSA. Under Set A ground motions, none of piles failed (i.e. the ultimate capacity was not exceeded). The abutment displacements (which are about the same as pile displacements) were 2.31 in. and 2.12 in. in the longitudinal and transverse direction, respectively. These are close to the design displacements described in Section 4.2.1. Yielding was observed in the columns which were expected since an R-factor of 3 was used in the design.

Under Set B ground motions, pile displacements were larger, but no pile failure was observed. The maximum transverse displacement at Abutment 1 was 4.36 in. This displacement is more

than the “capacity” of 2.59 in. from the pushover analysis but, again, this capacity is defined as when one or more piles reached the ultimate displacement. If the capacity was defined as when all piles reached ultimate, then the displacement capacity in the transverse direction would be 6.53 in. which is larger than the maximum displacement under Set B ground motions.

Under Set C ground motions, all piles exceeded ultimate capacity as indicated by large displacements in the transverse direction. Once the piles failed, the forces were shed to the columns which eventually led to column failure as observed in the analysis.

4.3.2 3SIAB-PWA

Table 4-6 shows the summary of results from the nonlinear time history analyses. Under Set A ground motions, none of the piles failed. The maximum displacements are 2.37 in. and 1.86 in. in the longitudinal and transverse directions, respectively. These are about the same as the design displacements shown in Section 4.2.2.

Under Sets B and C ground motions, all piles exceeded the ultimate capacity and large displacements were observed due to failure of the piles and columns. Once the piles failed, the seismic loads were shed to the columns which eventually led to the column failure.

The performance under Sets B and C ground motions indicate a deficiency in the preliminary design procedure because there should be no pile failures under ground motions equivalent to the design spectrum. A factor needs to be introduced such that there is no pile failure during earthquakes that are smaller or equivalent to the design earthquake. In addition, it also indicates that the characteristics of input motion affect the seismic performance of the bridge.

4.3.3 3SSAB

Table 4-7 shows the summary of the nonlinear time history analyses of 3SSAB. The average displacements from the three sets of ground motions were 4.37 in. and 9.24 in. in the longitudinal and transverse directions, respectively. In the longitudinal direction, most of the seismic forces are resisted by the abutment-soil passive resistance and only 13% of the total seismic force is resisted by the bent column. In the transverse direction, all the seismic forces are resisted by the bent columns. Thus, significant yielding was observed in the columns.

4.4 COMPARISON OF RESPONSE OF 3SIAB-PSA AND 3SIAB-PWA

Figure 4-7, Figure 4-8, and Figure 4-9 show the comparison of maximum base shears, displacements, and column moments from the nonlinear time history analyses of 3SIAB-PSA, 3SIA-PWA, and 3SSAB.

Comparison of base shears and displacements show that 3SIAB-PSA performed better than 3SIAB-PWA. It is to note that the components of 3SIAB-PSA and 3SIAB-PWA are the same (e.g. size and number piles, and size of columns) except the orientation of piles. The difference in between the two integral abutment bridges is more pronounced in the transverse response.

The transverse base shears and displacements in 3SIAB-PWA are larger than that in 3SIAB-PSA. Moreover, pile failures are observed in 3SIAB-PWA under Sets B and C ground motions. Thus, better seismic performance is achieved when the pile strong axis is oriented parallel to the abutment axis. Because of the pile axis orientation, the abutments in 3SIAB-PWA are stiffer in the transverse direction than in 3SIAB-PSA. This, in turn, increased the seismic demand at the abutments of 3SIAB-PWA which eventually led to pile failure. In the longitudinal direction, the effect of pile axis orientation has little effect on the bridge performance because most of the seismic forces are resisted by the abutment-soil passive resistance.

4.5 COMPARISON OF RESPONSE OF INTEGRAL ABUTMENT BRIDGES AND SEAT-TYPE ABUTMENT BRIDGES

In bridges with seat-type abutments, the load path in the longitudinal direction is from the superstructure to the soil behind the abutment. The abutment-soil passive resistance is mobilized once the joint gap between the superstructure and abutment wall is closed. Due to high stiffness of the abutment-soil compared to the columns, most of the seismic forces are resisted by the abutment-soil passive resistance. The abutment backwall is typically designed to shear-off at a lower level of earthquake to protect the piles below.

In the transverse direction, the ends of the bridge are assumed to be unrestrained because the wingwalls are also designed to shear-off at a lower level of earthquake to protect the piles. As such, the seismic forces are resisted at the piers only. Thus, in bridges with seat-type abutments, the column stiffness and ductility are more important in the transverse direction than in the longitudinal direction.

On the other hand, in bridges with integral abutments, the forces that go to the abutments in the longitudinal direction are shared by the abutment-soil resistance, piles, and soil-pile interaction. A significant percentage of these forces are resisted by the abutment-soil resistance. In the transverse direction, the forces that go to the abutments are taken by the piles and soil-pile interaction only. Thus, in integral abutment bridges, pile stiffness and ductility are more important in the transverse direction than in the longitudinal direction.

Large longitudinal displacements were observed in 3SSAB compared to integral abutment bridges, as shown in Figure 4-8. Because of large displacements, unseating of the bridge at abutments is likely in seat-type abutments. In the transverse direction, the 3SSAB displacements at abutments are also larger than that in integral abutment bridges. The significant difference between seat-type and integral abutments is in the column forces, as shown in Figure 4-9. The column moments in integral abutment bridges are less than half of the column moments in seat-type abutment bridges. This means that bridge collapse due to column failure is unlikely to happen in integral abutment bridges because the seismic forces are resisted at the abutments.

4.6 CONCLUSIONS

The effectiveness of steel bridges with integral abutments in high seismic zones was investigated in this chapter. Three global 3D models of three-span bridges were developed: (a) integral abutment bridge with pile strong axis parallel to abutment axis (3SIAB-PSA), (b) integral abutment bridge with pile strong axis perpendicular to abutment axis (3SIAB-PWA), and (c) simply supported or seat-type bridge. A preliminary procedure was outlined to design these bridges. This was to ensure adequate pile and column sizes although the bridge geometry was the same as those bridges described in Chapter 2. Comparison of the responses of the first two bridges provided insight on how the pile orientation affects the seismic behavior of integral abutment bridges. Comparison of the responses of the integral abutment bridges and simply supported bridge provided insight on the effectiveness of integral abutment bridges in high seismic zones. Nonlinear time history analyses were performed using a suite of artificially generated ground motions that approximate an AASHTO design spectrum in a high seismic zone. Each bridge was subjected to three sets (Sets A, B, and C) of ground motions.

The following observations and conclusions were made based on the comparison of the responses of 3SIAB-PSA and 3SIAB-PWA:

- The 3SIAB-PSA performed better than 3SIAB-PWA in terms of the nonlinear response of piles. Thus, the pile strong axis should be oriented parallel to the abutment axis in seismic zones.

- Due to the pile axis orientation, the abutments in 3SIAB-PWA were stiffer in the transverse direction than those in 3SIAB-PSA. This increased the seismic demands at the abutments of 3SIAB-PWA.

- The pile axis orientation was insignificant in the longitudinal direction because this response was dominated by the abutment-soil interaction.

The following observations and conclusions were made based on the comparison of the responses of the integral abutment bridges (3SIAB-PSA and 3SIAB-PWA) and the seat-type abutment bridge (3SSAB):

- The seismic performances of the integral abutment bridges were better than the seat-type abutment bridge in terms of overall displacements and column forces.

- Large displacements were observed in 3SSAB in the longitudinal and transverse directions. The longitudinal displacement in 3SSAB was almost twice the displacement of the integral abutment bridges. Thus, a relatively large seat width should be provided for the seat type bridge due to these large displacements.

- In 3SSAB, all of the seismic forces in the transverse direction were resisted by the columns only. Thus, these columns will experience large inelastic activity (damage) after

an earthquake which may require their replacement or bridge removal after severe ground motions.

The preliminary design procedure is refined in Chapter 5 and is demonstrated by a design example. Procedures for evaluating the pile displacement capacity and incorporating system damping in the analysis are discussed.

Table 4-1 3SIAB-PSA Bridge – Modal Mass Participation Ratios

Mode	Period	UX	UY	UZ	RX	RY	RZ
No	Sec	Unitless	Unitless	Unitless	Unitless	Unitless	Unitless
1	0.959	0.000	0.609	0.000	0.811	0.000	0.441
2	0.609	0.000	0.234	0.000	0.089	0.000	0.170
3	0.607	0.000	0.000	0.195	0.000	0.139	0.000
4	0.452	0.000	0.000	0.000	0.000	0.000	0.242
5	0.390	0.951	0.000	0.000	0.000	0.010	0.000
6	0.312	0.000	0.000	0.000	0.000	0.000	0.024
7	0.278	0.000	0.110	0.000	0.067	0.000	0.079
8	0.256	0.000	0.029	0.000	0.002	0.000	0.021
9	0.233	0.014	0.000	0.000	0.000	0.018	0.000
10	0.192	0.000	0.000	0.364	0.000	0.258	0.000
11	0.188	0.000	0.000	0.000	0.000	0.000	0.001
12	0.172	0.005	0.000	0.000	0.000	0.136	0.000

Table 4-2 3SIAB-PWA Bridge – Modal Participation Mass ratios

Mode	Period	UX	UY	UZ	RX	RY	RZ
No	Sec	Unitless	Unitless	Unitless	Unitless	Unitless	Unitless
1	0.926	0.000	0.579	0.000	0.785	0.000	0.420
2	0.608	0.000	0.244	0.000	0.096	0.000	0.177
3	0.608	0.000	0.000	0.194	0.000	0.138	0.000
4	0.411	0.000	0.000	0.000	0.000	0.000	0.235
5	0.400	0.957	0.000	0.000	0.000	0.012	0.000
6	0.312	0.000	0.000	0.000	0.000	0.000	0.029
7	0.261	0.000	0.158	0.000	0.053	0.000	0.115
8	0.254	0.000	0.001	0.000	0.036	0.000	0.001
9	0.234	0.010	0.000	0.000	0.000	0.019	0.000
10	0.193	0.000	0.000	0.365	0.000	0.259	0.000
11	0.188	0.000	0.000	0.000	0.000	0.000	0.001
12	0.173	0.003	0.000	0.000	0.000	0.133	0.000

Table 4-3 3SSAB Modal Participation Mass Ratios

Mode	**Period**	**UX**	**UY**	**UZ**	**RX**	**RY**	**RZ**
No	Sec	Unitless	Unitless	Unitless	Unitless	Unitless	Unitless
1	1.739	0.000	0.744	0.000	0.930	0.000	0.563
2	1.532	0.000	0.000	0.000	0.000	0.000	0.215
3	0.609	0.000	0.000	0.209	0.000	0.156	0.000
4	0.571	0.000	0.150	0.000	0.043	0.000	0.113
5	0.492	0.964	0.000	0.000	0.000	0.019	0.000
6	0.346	0.000	0.000	0.000	0.000	0.000	0.000
7	0.251	0.000	0.000	0.000	0.000	0.000	0.019
8	0.236	0.000	0.000	0.000	0.000	0.020	0.000
9	0.208	0.000	0.080	0.000	0.000	0.000	0.061
10	0.194	0.000	0.000	0.384	0.000	0.287	0.000
11	0.183	0.000	0.000	0.000	0.000	0.000	0.004
12	0.172	0.000	0.000	0.000	0.000	0.139	0.000

Table 4-4 Combinations of Generated Ground Motions in the Time History Analyses (X- and Y-directions correspond to longitudinal and transverse directions, respectively)

Combination	Direction	Input Motion
Set A	X	AASHTO1
	Y	AASHTO3
Set B	X	AASHTO2
	Y	AASHTO1
Set C	X	AASHTO3
	Y	AASHTO2

Table 4-5 Summary of Results of Nonlinear Time History Analysis of 3SIAB-PSA

A) Base Shears

EQ	Base Shears (kip)									
	Total		Abut 1		Bent 2		Bent 3		Abut 4	
	X	Y	X	Y	X	Y	X	Y	X	Y
Set A	4195	1087	3554	255	189	368	224	362	3512	257
Set B	4629	1242	3897	270	237	370	231	352	3896	265
Set C	3624	1077	2745	265	165	342	181	348	3200	254
Average	4149	1135	3399	263	197	360	212	354	3536	259

B) Displacements

EQ	Deck Displacement (in)			Abut1 Displacement (in)			Abut4 Displacement (in)		
	X	Y	Z	X	Y	Z	X	Y	Z
Set A	2.27	3.65	4.09	2.31	2.12	0.003	2.34	2.07	0.003
Set B	2.53	3.97	4.94	2.58	4.36	3.44	2.59	2.28	0.003
Set C	2.26	13.36	3.98	2.14	6.68	9.48	2.11	18.71	3.27
Average	2.35	6.99	4.34	2.34	4.39	4.31	2.35	7.69	1.09

Notes: X = longitudinal direction, Y = transverse direction, Z = vertical direction

C) Column Moments and Rotations (at base of column)

EQ	Bent 2				Bent 3			
	Moment (kip-ft)		Rotation (rad)		Moment (kip-ft)		Rotation (rad)	
	X*	Y*	X*	Y*	X*	Y*	X*	Y*
Set A	3311	4055	0.001	0.002	3636	4101	0.002	0.002
Set B	3862	5127	0.002	0.003	3763	4582	0.002	0.003
Set C	2765	5983	0.003	0.009	2936	5877	0.004	0.013
Average	3313	5055	0.002	0.005	3445	4853	0.003	0.006

Notes: X* = longitudinal moment and rotation (moment and rotation about y-axis)

Y* = transverse moment and rotation (moment and rotation about x-axis)

Table 4-6 Summary of Results of Nonlinear Time History Analyses of 3SIAB-PWA

A) Base Shears

EQ	Base Shears (kip)									
	Total		Abut 1		Bent 2		Bent 3		Abut 4	
	X	Y	X	Y	X	Y	X	Y	X	Y
Set A	4178	1243	3634	357	195	389	219	381	3546	349
Set B	4474	951	3851	312	231	371	226	554	4439	302
Set C	3825	1211	3232	356	190	374	198	380	3429	333
Average	4159	1135	3572	342	205	378	214	438	3805	328

B) Displacements

EQ	Deck Displ (in)			Abut1 Displ (in)			Abut4 Displ (in)		
	X	Y	Z	X	Y	Z	X	Y	Z
Set A	2.35	3.47	4.11	2.37	1.86	0.003	2.42	1.83	0.03
Set B	-	-	-	-	-	-	-	-	-
Set C	2.46	15.02	5.14	2.5	11.02	10.55	2.61	14.74	6.81
Average	2.41	9.25	4.63	2.44	6.44	5.28	2.52	8.29	3.42

Notes: Very large displacements were observed under Set B ground motions due to bridge collapse and are not included in the table.

X = longitudinal direction, Y = transverse direction, Z = vertical direction

C) Column Moments and Rotations (at base of column)

EQ	Bent 2				Bent 3			
	Moment (kip-ft)		Rotation (rad)		Moment (kip-ft)		Rotation (rad)	
	X*	Y*	X*	Y*	X*	Y*	X*	Y*
Set A	3387	4067	0.002	0.002	3537	4048	0.002	0.002
Set B	3817	3951	0.024	1.783	4036	6708	0.028	1.766
Set C	3160	6128	0.003	0.011	3244	3843	0.002	0.002
Average	3455	4715	0.010	0.599	3606	4866	0.011	0.590

Notes: X* = longitudinal moment and rotation (moment and rotation about y-axis)

Y* = transverse moment and rotation (moment and rotation about x-axis)

Table 4-7 Summary of Results of Nonlinear Time History Analyses of 3SSAB

A) Base Shears

EQ	Base Shears (kip)									
	Total		Abut 1		Bent 2		Bent 3		Abut 4	
	X	Y	X	Y	X	Y	X	Y	X	Y
Set A	2222	982	1480	0	296	494	327	493	1663	0
Set B	2428	824	1864	0	321	412	299	419	1648	0
Set C	3025	955	2321	0	389	477	395	485	2326	0
Average	2558	920	1888	0	335	461	340	466	1879	0

B) Displacements

EQ	Deck Displ (in)			Abut1 Displ (in)			Abut4 Displ (in)		
	X	Y	Z	X	Y	Z	X	Y	Z
Set A	3.48	7.98	3.95	3.51	8.5	0	3.38	8.56	0
Set B	3.68	8.94	4.01	3.57	10.01	0	3.72	9.99	0
Set C	6	8.68	4.03	6.03	9.22	0	5.86	9.17	0
Average	4.39	8.53	4.00	4.37	9.24	0.00	4.32	9.24	0.00

Notes: X = longitudinal direction, Y = transverse direction, Z = vertical direction

C) Column Moments and Rotations (at base of column)

EQ	Bent 2				Bent 3			
	Moment (kip-ft)		Rotation (rad)		Moment (kip-ft)		Rotation (rad)	
	X*	Y*	X*	Y*	X*	Y*	X*	Y*
Set A	7745	9216	0.003	0.009	8253	9234	0.004	0.009
Set B	7918	9953	0.004	0.011	7734	9842	0.004	0.011
Set C	9732	9430	0.007	0.012	9424	9608	0.009	0.012
Average	8465	9533	0.005	0.011	8470	9561	0.006	0.011

Notes: X* = longitudinal moment and rotation (moment and rotation about y-axis)

Y* = transverse moment and rotation (moment and rotation about x-axis)

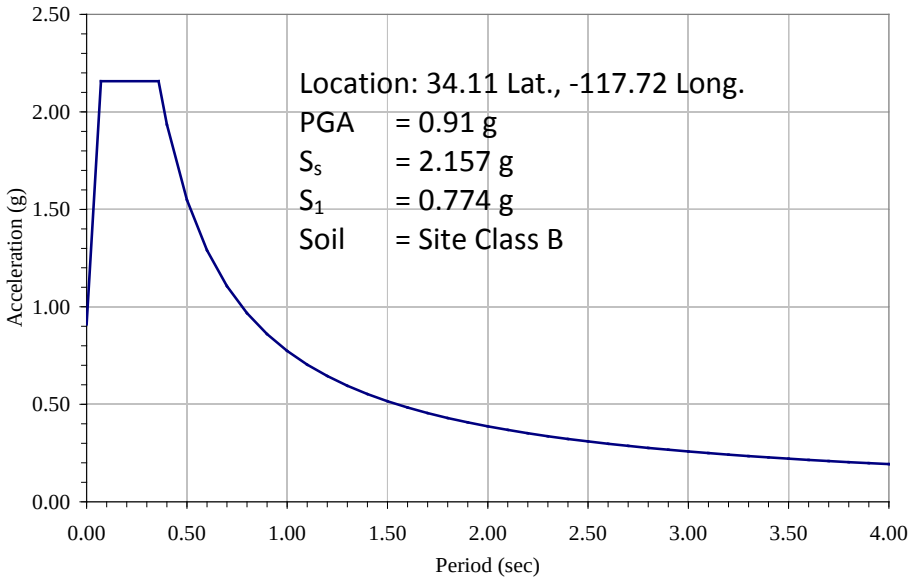

Figure 4-1 AASHTO Design Spectrum

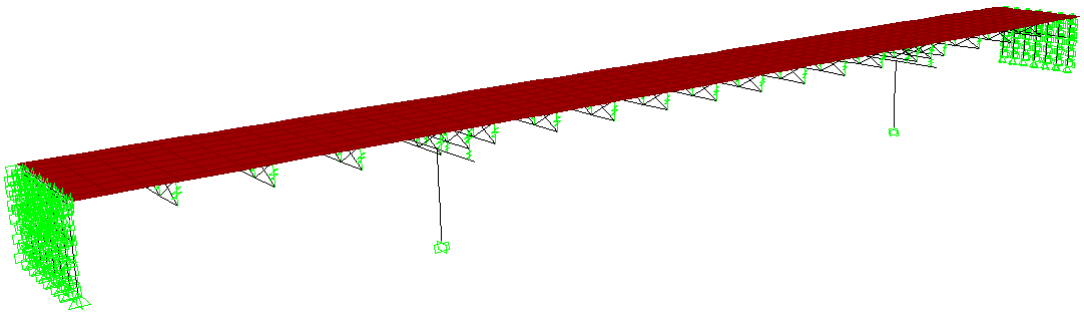

(a) 3-D finite element of the bridge

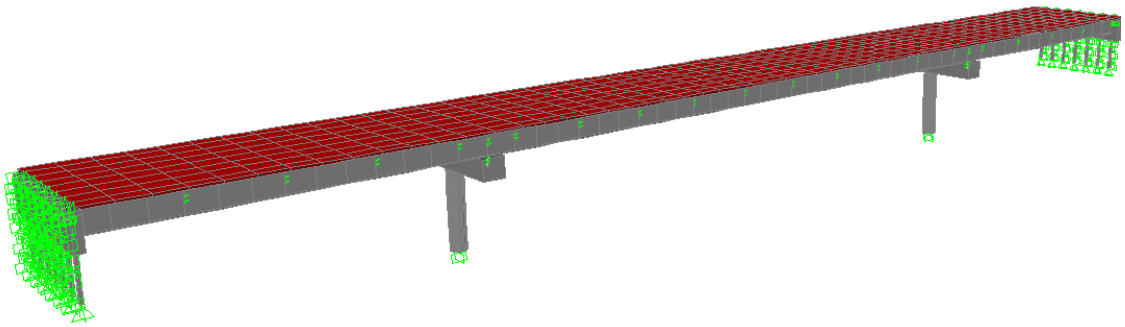

(b) Extruded view of the bridge

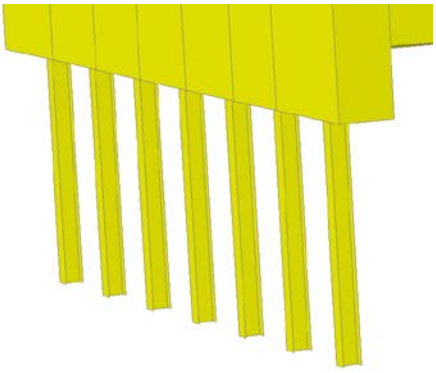

(c) Pile strong axis is parallel to abutment axis (*p-y* springs and soil-abutment springs are not shown)

Figure 4-2 Integral abutment bridge with pile strong axis parallel to abutment axis (3SIAB-PSA).

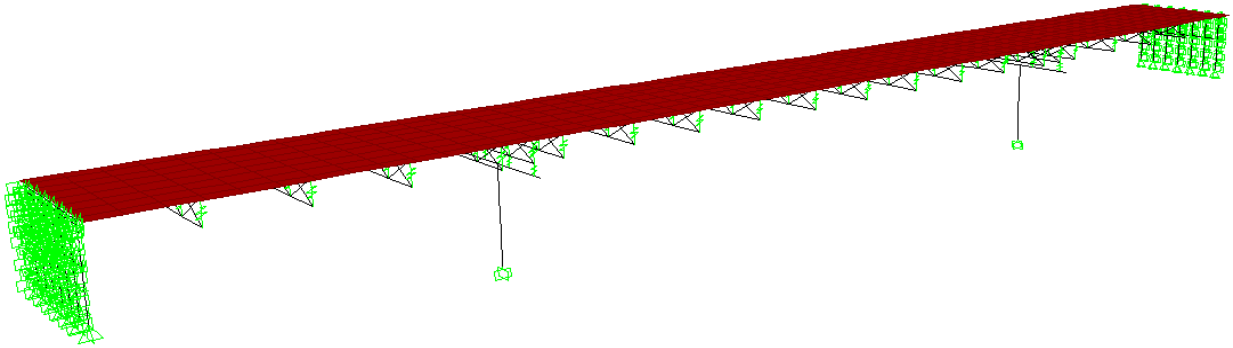

(a) 3-D finite element of the bridge

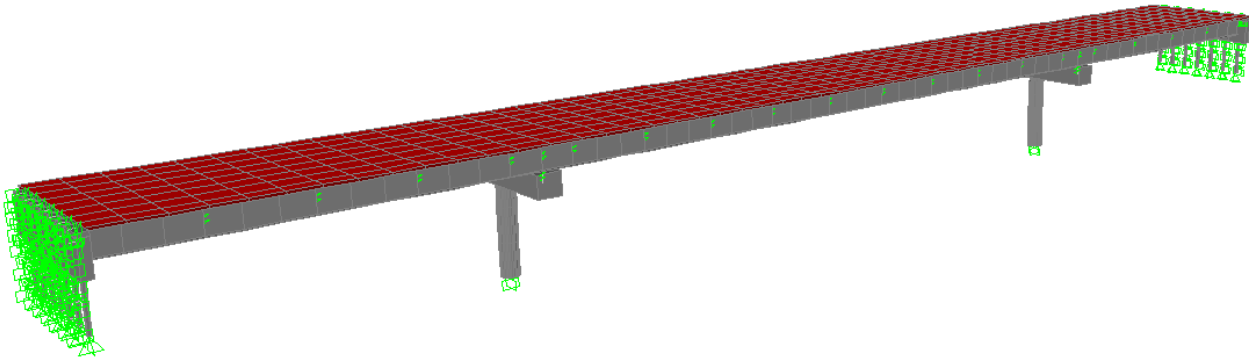

(b) Extruded view of the bridge

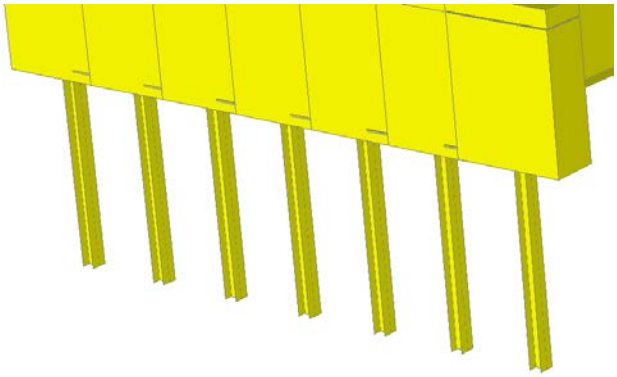

(c) Pile strong axis is perpendicular to abutment axis (*p-y* and soil-abutment springs not shown)

Figure 4-3 Integral abutment bridge with pile strong axis perpendicular to abutment axis.

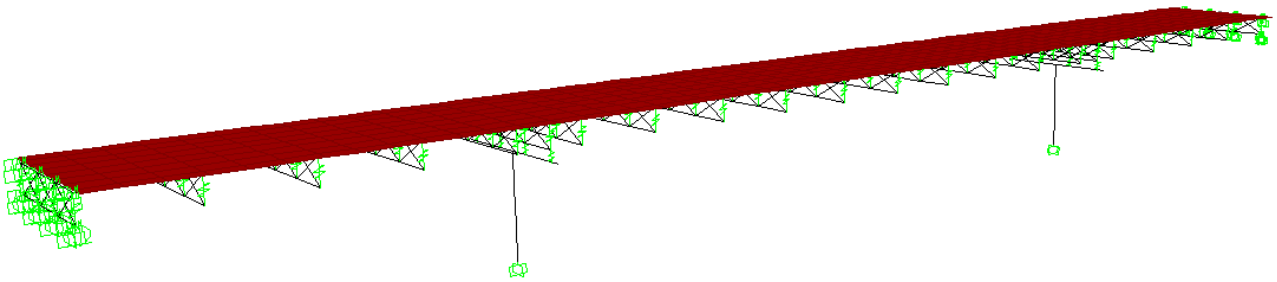

(a) 3-D finite element of the bridge

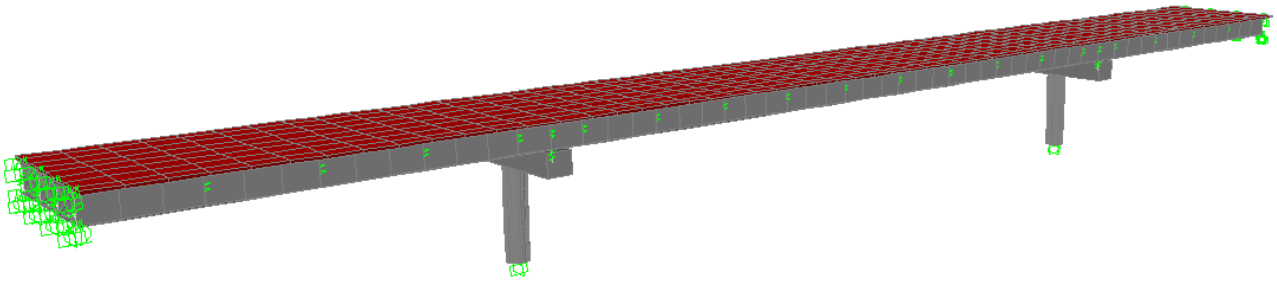

(b) Extruded view of the bridge

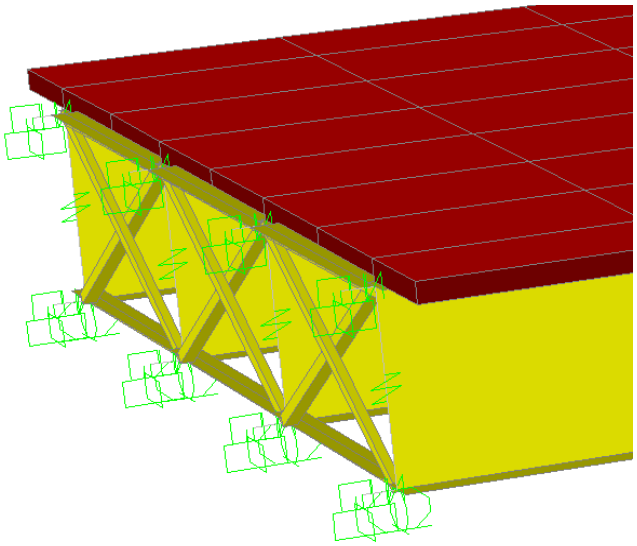

(c) Detail at abutment

Figure 4-4 Seat-type abutment bridge.

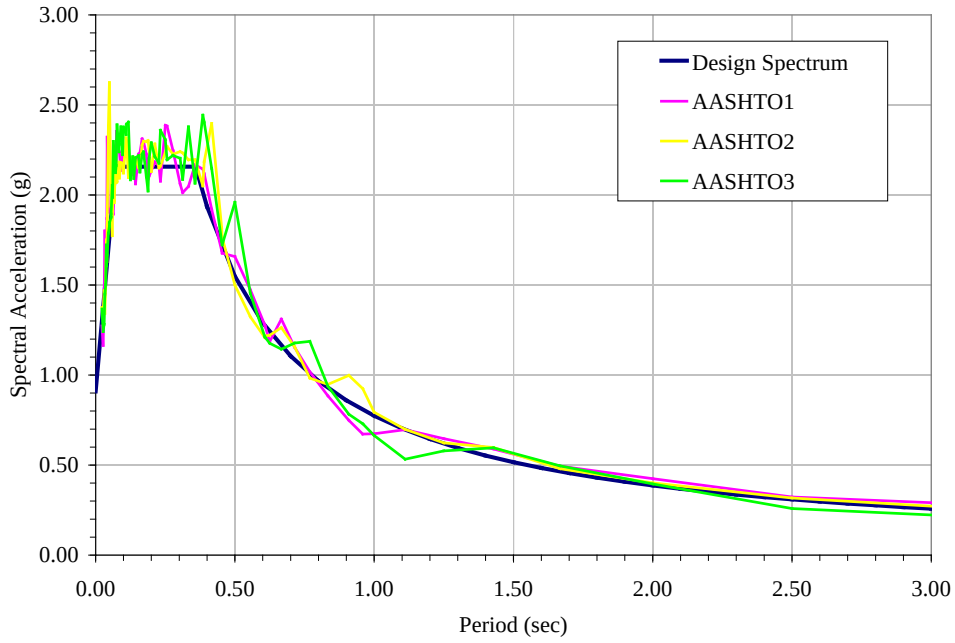

Figure 4-5 Design Spectrum and Response Spectrum of Generated Ground Motions

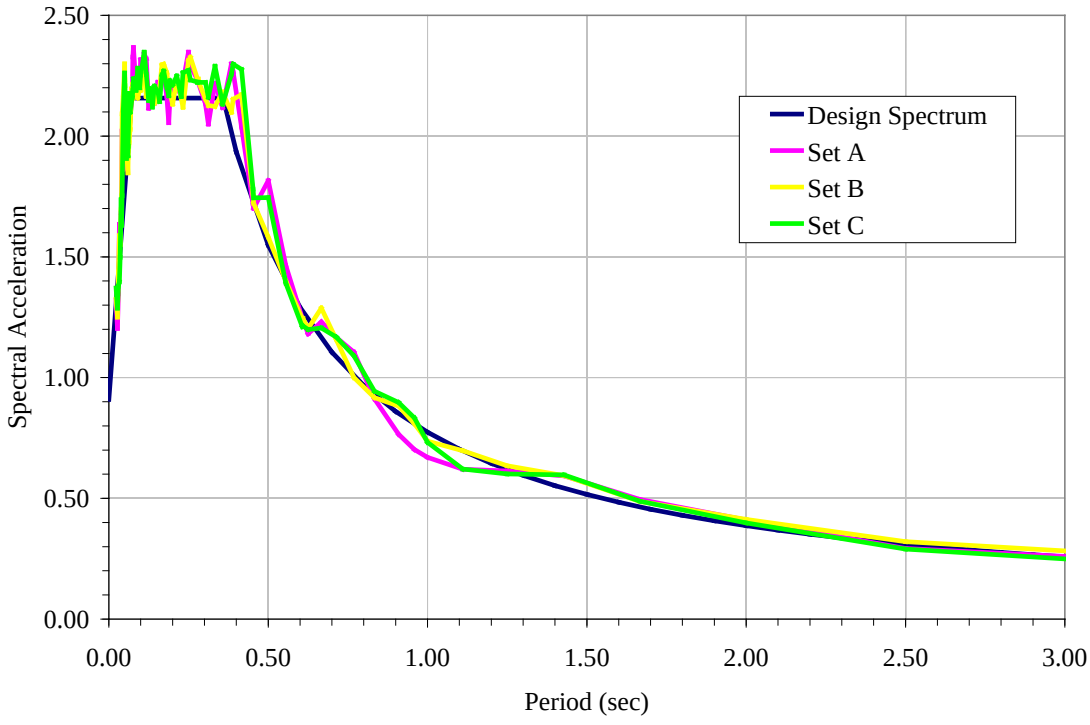

Figure 4-6 Design Spectrum and Vector Sum of Response Spectrum of Input Motions

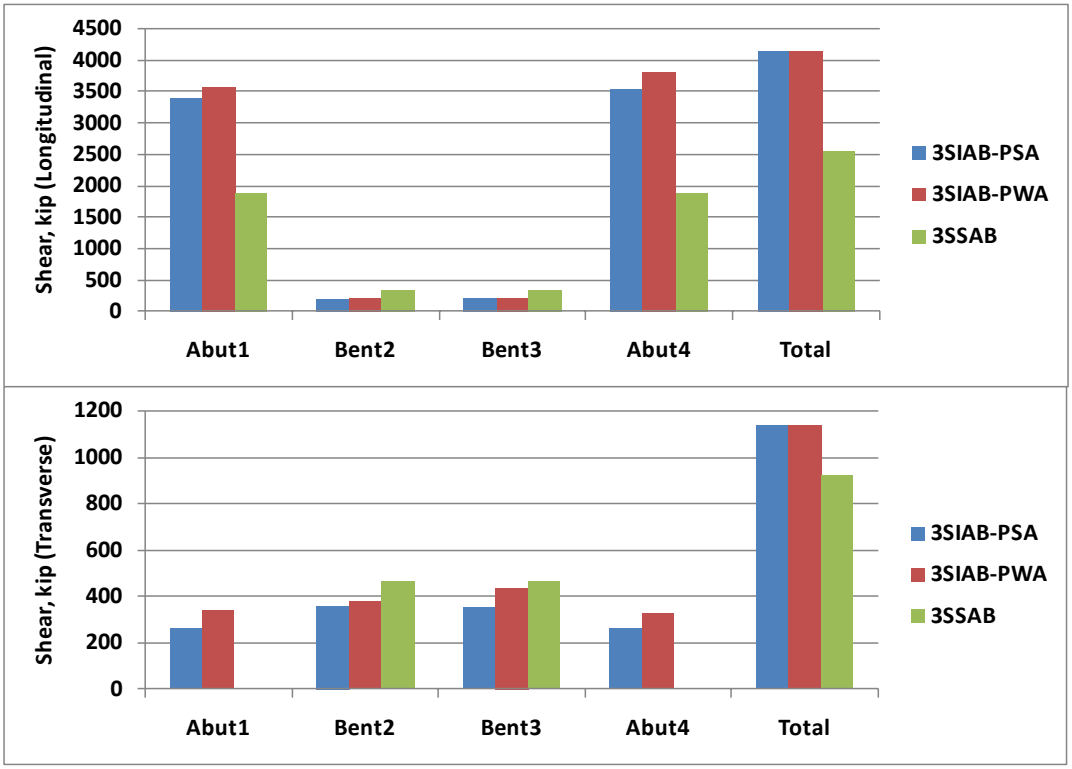

Figure 4-7 Comparison of average maximum shear

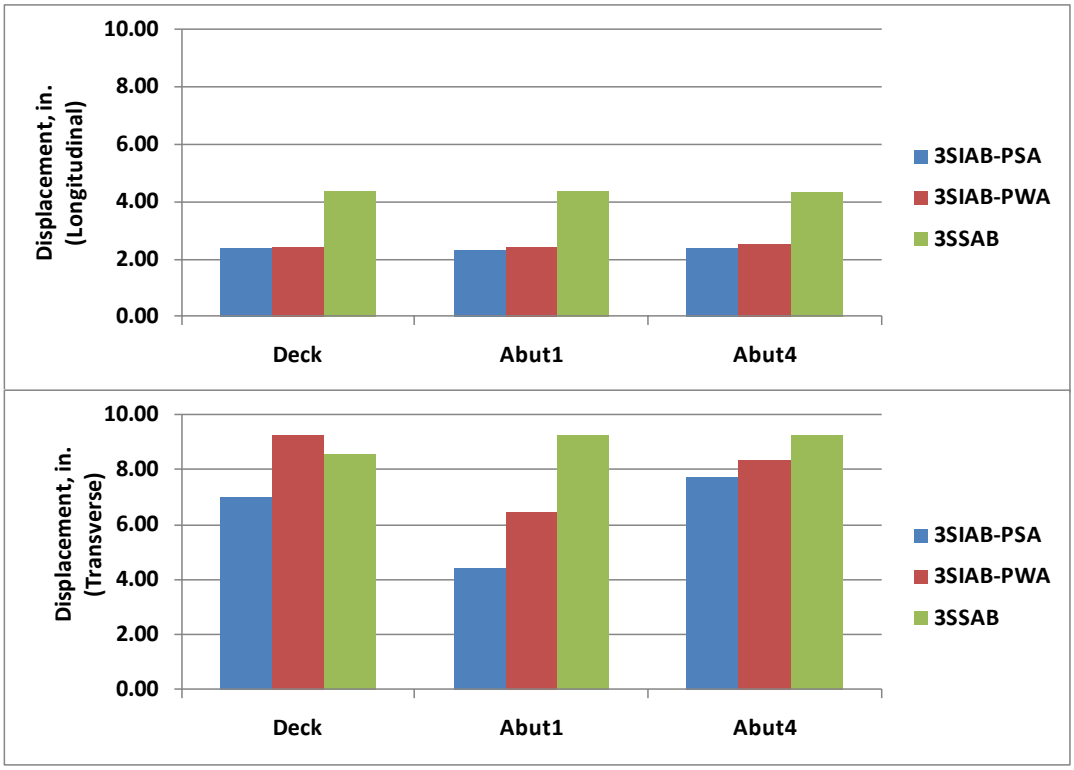

Figure 4-8 Comparison of average maximum displacement

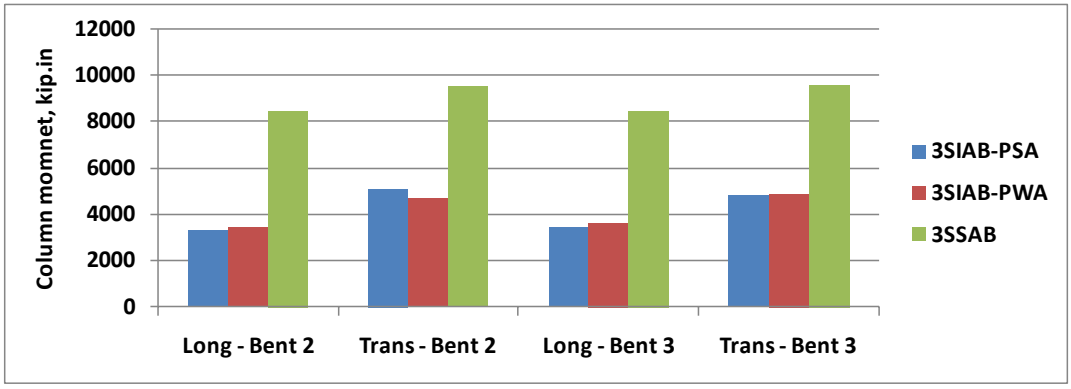

Figure 4-9 Comparison of average maximum column moment

Chapter 5 PROPOSED SEISMIC DESIGN GUIDELINES FOR STEEL BRIDGES WITH INTEGRAL ABUTMENTS

The design guidelines for the girder-abutment connection, pile displacement capacity, and pile-abutment connection are summarized in this chapter. These guidelines were based on the analytical investigations as well as available experimental research. A procedure for incorporating damping in the system due to yielding of the components along the load path is also discussed. Flowcharts illustrating of the design procedure are shown in Figure 5-1 through Figure 5-4 and discussed in the following sections. A design example is provided illustrating the application of the recommended design guidelines.

5.1 GIRDER-ABUTMENT CONNECTION

Sufficient embedment length is required to achieve a rigid connection between the girder and abutment. The development of equation to calculate the embedment length is presented in Chapter 2. The mechanism assumes a simplified stress distribution and was actually developed for steel pile embedment into a concrete cap beam or abutment. The resistance to external moment *M* is developed due to the couple created by concrete bearing stresses. The simplified equation is:

$$l_{emb} \geq 2.5\sqrt{\frac{M}{f_c' b_f}} \tag{5-1}$$

It should be noted that sufficient confinement reinforcement should be provided in addition to the embedment length recommended above. If the calculated embedment length is large and impractical, it is recommended that the width of the girder flanges embedded into the abutment structure be increased. The girder-to-abutment connection can be considered as rigid connection with the proper embedment length and connection detail.

5.2 BEHAVIOR OF PILES

Experimental investigations on the cyclic behavior of piles indicate that they can sustain large ductility. Cyclic testing on steel piles conducted by Astaneh-Asl and Ravat (1998) showed that a maximum displacement of 16 in. relative to the point of inflection (at a depth of 20 ft below the pile cap) can be reached. A plastic rotation of 8% was recommended for design purposes. Experimental testing conducted by Shama et al. (2002a; 2002b) showed that sufficient pile-to-abutment embedment length should be provided for a ductile behavior. However, it should be noted that these tests were conducted on steel piles only and without the presence of soil. The confinement provided by soil tends to increase the ductility in the pile and thus increase its displacement capacity. Tests conducted by Burdette et al. (2003) on HP10x42 piles driven into undisturbed clay showed that large displacements can be imposed without breaking the piles, but the maximum sustainable displacement is limited by the pile-to-abutment connection.

Burdette et al. were able to induce displacements in excess of 12 in. without completely breaking the piles out of the concrete abutment.

Therefore, to be able to sustain large displacements similar to those observed in major seismic events, the pile-to-abutment connection should be able to develop the full plastic moment of the pile without loss of integrity. The equation described in Section 5.1 is also applicable for calculating the required embedment length of piles into the abutment structure. The moment in Eqn. 5-1 is the plastic moment capacity of the pile about the strong axis multiplied by an overstrength factor of 1.2.

Under seismic loads, the piles in a bridge with integral abutments are designed according to displacement-based approach. A maximum pile rotation of 10% (0.10 radian) is recommended in the evaluation of the displacement capacity. This is larger than what was recommended by Astanehl-Asl and Ravat (1998) because the confinement provided by the soil tends to increase the ductility in the pile as stated above. Modal pushover analysis is preferred over the traditional pushover analysis because the loads are applied in a more realistic fashion. In modal pushover analysis, the structure is loaded according to the shape of the dominant modes.

It is recommended that the length of pile to be included in the analytical model is the length from the pile cap down to the location where moment and deflection is essentially zero. Using pile length that is from the pile cap to the inflection point tends to underestimate the pile deflections. A closer spacing of *p-y* springs is also preferred to accurately determine the locations of plastic hinge formations along the length of the pile. Finite element analysis showed that in addition to the plastic hinge just below the pile cap, plastic hinging could also occur at about the mid-length of the pile. A *p-y* spring spacing of 12 in. is recommended if possible. The use of fiber hinges to model the pile inelasticity is favored over the traditional P-M-M (axial load-biaxial moment interaction) hinge, especially when conducting static and/or dynamic nonlinear analysis (see Appendix 1). It is not necessary to assign a series of fiber hinges along the length of the piles. Fiber hinges assigned at the expected locations of plastic hinges are deemed sufficient.

5.3 DAMPING

It is commonly acknowledged that large damping occurs in a bridge with integral abutments during a seismic event. Several factors contribute to the increase in damping including the yielding of the components along the load path, i.e. the piles, columns, and soil behind the abutments. Another source of damping is the radiation damping that occurs when the abutment soils are engaged during a seismic excitation. This is particularly true in the longitudinal direction where the bridge is restrained by the abutment soil. Because of its relatively large stiffness, most of the seismic forces are attracted to the abutment soil than to the piles and columns. In fact, a survey of the damping ratios observed on a skew two-span bridge during small to moderate earthquakes indicate that, even in the transverse direction, damping can be more than twice the inherent structure damping (Goel, 1997). Goel observed up to 12% damping from the motions of an integral abutment bridge recorded during actual

earthquake events. The damping ratio is expected to be larger at higher levels of shaking where there is increased abutment participation.

The total damping ζ in a bridge with integral abutments can be expressed as the sum of the inherent structure damping and the hysteretic damping of the yielding elements which includes the abutment soil:

$$\zeta = \zeta_o + \zeta_{sys} \tag{5-2}$$

where, ζ_o is the inherent structure damping usually taken equal to 5%, and ζ_{sys} is the system damping associated with the yielding of the piles, columns, and abutment soil.

Equivalent hysteretic damping can be expressed as (Mander and Cheng, 1997):

$$\zeta_{sys} = \frac{2\eta}{\pi} \frac{(1-\alpha)\left(1-\frac{1}{\mu}\right)}{(1-\alpha+\mu\alpha)} \tag{5-3}$$

where, η is the energy absorption efficiency factor, α is the post-yield stiffness ratio, and μ is the ductility demand ratio $\Delta_{max}/\Delta_{yield}$. The factor η can be assumed to be equal to 0.3 in the absence of complete information but can be refined by further study. For elastic-plastic behavior, Eqn. 5-3 can be further simplified as:

$$\zeta_{sys} = 0.2\left(1-\frac{1}{\mu}\right) \tag{5-4}$$

It is recommended that ζ_{sys} be evaluated at the system level instead of at the component level. This can be achieved by establishing first the system capacity by pushover analysis as illustrated in the Design Example (Section 5.4). The advantage of evaluating the damping at the system level is that it takes into account all the inelasticity occurring in the bridge which would be difficult to accomplish at the component level because not all components undergo inelasticity at the same time.

5.4 DESIGN EXAMPLE

Flowcharts for the seismic design of integral abutment bridges are shown in Figure 5-1 to Figure 5-4. The application of these is illustrated in the design example below. The geometry of the example bridge is the same as the three-span bridge described in previous chapters.

For seismic design purposes, it was assumed that the bridge is located on a rock site (Site Class B) in a high seismic zone in Claremont, California. The peak ground acceleration (PGA) is 0.91 g, the 0.2 sec spectral acceleration is 2.16g, and the 1.0 sec spectral acceleration is 0.77 g. The design spectrum is shown in Figure 5-5.

Step 1: Pile Selection and Analysis

The HP10x42 pile used in the AISI document was used as the preliminary section. The computer program COM624P (Wang and Reese 1993) was used to generate the *p-y* springs along the length of the pile. The pile was analyzed in the strong and weak axis, and thereby two sets of *p-y* springs were generated at each point. It was desired to have the *p-y* springs located every 12 in. to accurately model the pile behavior and determine the possible locations of plastic hinges.

Only the length of the pile down to the location of zero moment and zero deflection was included in the model at which point it is assumed to be pin supported. It should be noted that there could be a number of locations along the length of the pile where the bending moment is zero (inflection point). The intent, however, is to model the pile up to the location where the deflection is essentially zero at which point the moment is also essentially zero.

The properties of the soil profile are summarized in Table 5-1. The plastic moment of the pile about at the strong axis (x-axis), M_{px}, is equal to 2,656.5 kip-in. With a fixed-head condition, M_{px} was reached at a deflection of 1.17 in. (Figure 5-6) and at a shear of 56.25 kips. Figure 5-7 shows the deflection and moment profile when the deflection at the top of the pile is equal to 5.0 in. It can be observed that at larger deflections, plastic hinging would occur not only at the top of pile but also at about its mid-length. Thus, a plastic hinge should be also assigned at this location.

The plastic moment about the weak axis (y-axis), M_{py}, is equal to 1,199 kip-in and was reached at a pile deflection of 0.87 in. (Figure 5-8) and at a shear of 34 kips. Figure 5-9 shows the deflection and moment profile when the deflection at the top of pile is 4.0 in.

Based on the analysis of pile at different deflections, it was decided that the total length of pile to be included in the model is 216 in. which is the location where the deflection and moment are essentially zero. Thus, *p-y* springs along the strong axis (Figure 5-10) and along the weak axis (Figure 5-11) were generated from the top of pile down to 216 in. It can be observed that the *p-y* springs are the same from a depth of 108 in. to 216 in.

A total of seven piles (1 row of seven piles) were assumed for the initial analysis. If after Step 4 it was determined that this is insufficient, the piles could be either increased in number or increased in size whichever is the most economical option.

Step 2: Bridge Modeling

The computer program SAP2000 (Computers and Structures, 2010) was used to model the bridge and its components (Figure 5-12). The deck was modeled as shell elements while the girders, cross-frames, cap beams, columns, and piles were modeled as beam elements. Link elements where used to model the *p-y* springs and the abutment soil passive resistance.

The passive resistance of the soil behind the abutment was modeled by a series of gap and nonlinear link elements since it is effective under compression only. These link elements were connected to the abutment structure at the ends of the bridge and were implemented in the longitudinal direction only. The stiffness property was obtained from the Caltrans' Seismic

Design Criteria (SDC v1.4, Caltrans 2006). It assumes a uniform soil passive pressure distribution along the abutment. The initial abutment stiffness is given by:

$$K_{abut} = 20\frac{kip-in}{ft} w\left(\frac{h}{5.5}\right) \quad (5\text{-}5)$$

where, *w* is the abutment width and *h* is the abutment height. The initial stiffness of *20 kip/in/ft* was assumed based on the large-scale abutment testing at University of California, Davis. The maximum passive pressure that can be developed behind the abutments is *5.0 ksf,* and thus, the total static passive force is given by:

$$P = A_e(5.0ksf)\left(\frac{h}{5.5}\right) \quad (5\text{-}6)$$

where, A_e is the effective abutment area. The stiffness and passive force in the equations are scaled by (*h/5.5*) because the height of the abutment that was tested was 5.5 ft. The total height of the abutment is 10.75 ft. The soil yield displacement is 2.7 in based on the initial abutment stiffness calculated using Eqn. 5-5, and the total passive force calculated using Equation 15. The ultimate displacement, assuming cohesive soil, was taken as 10% of the total abutment height which is 12.9 in.

The *p-y* springs were modeled by nonlinear link elements and were based on the force-displacement relationships shown in Figure 5-10 for the spring along the strong (x-) axis and in Figure 5-11 for the spring along the weak (y-) axis. These springs were located every 12 in. along the length of the pile.

The nonlinearity of the piles was modeled by assigning fiber hinges at particular locations along its length. The moments about the strong axis were expected to be the largest at the top of pile and at a depth of 108 in. according to pushover analysis. About the weak axis, the maximum moments were expected at the top of pile and at a depth of 84 in. Thus, fiber hinges were assigned at these three locations. As noted in the design guidelines above, it is not necessary to assign a series of fiber hinges along the pile length but at locations of maximum moments only.

The nonlinearity of the columns was also modeled using fiber hinges assigned to the expected plastic hinge locations - at the top and at the base of column. The unconfined and confined properties of the concrete section were considered in the fiber hinge models. An effective moment of inertia of 34% of the gross was used along the length of the column.

Step 3: Evaluation of Pile Displacement Capacity

First, the dynamic properties of the bridge were determined, and the main vibration modes in the longitudinal and transverse directions were identified by examining the mass participation ratios (Table 5-3). In this example, the 5th mode is the main longitudinal vibration mode, and the 1st mode is the main transverse vibration mode. Thus, modal pushover analysis will be performed in the 5th and 1st modes to determine the pile displacement capacity in the longitudinal and transverse directions, respectively. The displacement monitored in the

pushover analyses was that of the joint located on the deck at the geometric center of the bridge.

Figure 5-13 shows the total base shear under the 5th mode pushover plotted against the deck displacement in the longitudinal direction. It is shown that the overall behavior in the longitudinal direction is dominated by the response of the soil behind the abutment. The system remains essentially elastic even when the top of the piles started yielding. After the abutment soil had yielded, the pushover curve is essentially flat similar to the assumed elastic-plastic response of the abutment soil. The system yield displacement is 3.4 in. This information will be used in Step 4 in calculating the system damping.

The pile displacement capacity in the longitudinal direction was then determined by plotting the displacement at the top of pile against the rotations at the locations of the plastic hinges, as shown in Figure 5-14. Inelasticity in the piles occurred at the top and at a depth of 108 in. The displacement at a maximum pile rotation of 10% (0.10 radian) is 12.5 in.

Figure 5-15 shows the total base shear under the 1st mode pushover plotted against the deck displacement in the transverse direction. Unlike in the 5th mode pushover, a gradual decrease in stiffness can be observed as the components become inelastic. The system yield displacement is 3.8 in. and was determined using a bilinear representation of the pushover curve as shown in Figure 5-14. The post-yield stiffness ratio is 0.06. This information will be used to calculate the system damping in Step 4.

Figure 5-16 shows the pile rotation at the locations of plastic hinges plotted against the transverse displacement at the top of pile. Inelasticity in the piles occurred at the top and at a depth of 84 in. At 10% pile rotation, the corresponding displacement at the top of pile is 9.0 in.

Based on the pushover analysis, the pile displacement capacities are 12.5 in. and 9.0 in. in the longitudinal and transverse directions, respectively.

Step 4: Response Spectrum Analysis

Response spectrum analysis was used to determine the seismic demands. The design spectrum (Figure 5-5) was applied in the longitudinal and transverse directions. The demands from these loadings were then combined based on the AASHTO orthogonal combination rule. The procedure implemented here, however, was an iterative process as explained below:

- First, modal analysis is performed to determine the vibration periods and mass participation ratios. The mass participation ratios are used to determine how many modes are needed to perform the response spectrum analysis. The sum of the mass participation ratios should be at least 95% in the directions for which the earthquake is applied. In this first iteration, the initial stiffnesses of the yielding elements can be used as the effective stiffnesses.

- Response spectrum analysis is then performed by applying the design spectrum in the longitudinal and transverse directions. A damping ratio of 5% for all modes can be assumed for the first run of the analysis.
- Then, the global displacement demands are determined for the purpose of calculating the system damping (ζ_{sys}). For this purpose, the displacements should be that of the joint located on the deck at the geometric center of bridge. Note that in the pushover analysis (Step 3), it is the displacement of this joint that was monitored, thus the pushover curves are based on the displacement of this joint. The total damping calculated from this step shall be applied only to the modes where the pushover analysis was performed.
- Determine the displacement demands on the yielding elements and determine their effective stiffnesses.
- The response spectrum analysis is rerun using the total damping applied to some particular modes and the effective stiffness of each yielding element is calculated. The displacements are then determined, total damping is recalculated, and effective stiffnesses are updated. This process is repeated until convergence is obtained.

Using the procedure described above, convergence was achieved after three iterations. Table 5-3 shows the vibration periods and mass participation ratios of the first 12 modes after the last iteration. It is to note that although only 12 modes are shown in Table 5-3, a total of 30 modes were used in the response spectrum analysis, and the sum of mass participation ratios are all more than 95%.

The displacements at the center of the bridge were 3.6 in. and 7.0 in. in the longitudinal and transverse directions, respectively. Therefore, the total damping ratios in the corresponding directions are 6% and 13%, respectively. These were calculated using Eqn. 5-4 together with the pushover curves shown in Figure 5-13 (longitudinal or 5^{th} mode pushover) and Figure 5-15 (transverse or 1^{st} mode push). In the response spectrum analysis, these damping ratios were applied only to the 5^{th} and 1^{st} modes since they are calculated from such modes. All other modes were assigned 5% damping.

The displacement of the soil behind the abutment was 3.2 in. in the longitudinal direction and 7.6 in. in the transverse direction. The longitudinal displacements are smaller compared to the transverse displacements because of the restraint offered by the abutment soil. The displacement at the top of pile is 2.9 in. in the longitudinal direction and 7.5 in. in the transverse direction.

Step 5: Design of Columns

An R-factor (response modification factor) of 3.0 was used in the design of columns. The design forces under the Extreme Event load combination are: 1,610 kips axial load, 171 kips shear, and 3,320 kip-ft bending moment.

The column was 60 in. in diameter with 1% longitudinal steel ratio, 0.6% transverse steel ratio, and 5,000 psi concrete. The plastic moment capacity of the column was determined using fiber section analysis where the unconfined and confined concrete properties were taken into account. The calculated plastic moment based on the section analysis is 5,734 kip-ft which corresponds to a demand-capacity ratio of about 60%. The shear capacity of the section calculated according to the AASHTO Guide Specifications for Seismic Design was 707 kips. The plastic shear (i.e. shear corresponding to plastic moment) is 229 kips assuming a single curvature column behavior.

Step 6: Pile Embedment Length into Abutment

(5-1 was used to determine the required embedment length of the pile into the abutment structure. The moment that will be used in this equation is the plastic moment capacity of the pile about the strong axis (M_{px} *= 2,656.5 kip-in*) multiplied by an overstrength factor of 1.2. Thus, the required embedment length assuming concrete strength of 3,000 psi is:

$$l_{emb} \geq 2.5\sqrt{\frac{1.2(2656.5)}{3(10.1)}} = 26in.$$

An embedment length of 30 in. can be used. Although not discussed here, sufficient confinement reinforcement should be provided at the connection.

Step 7: Girder Embedment Length into Abutment

(5-1 was used to determine the required embedment length of the girder into the abutment structure. The moment used in this equation is the maximum of the steel girder moment based on either the longitudinal or the transverse pushover. This is the moment corresponding to 10% pile rotation where the pile displacement capacity was established. Note that the moment to be used in the design is not the moment obtained from the response spectrum analysis. The piles are the "weak links" in the system, thus the forces on the components along the load path are limited by the capacity of the piles. It is therefore logical to use the moment obtained from the pushover analysis for the girder-to-abutment connection. The maximum moment was found on the interior steel girder and is equal to 2,393 kip-ft. If larger moments are found from other load cases like gravity loads, they should be used instead of that coming from pushover analysis. The required embedment length is:

$$l_{emb} \geq 2.5\sqrt{\frac{(2{,}393x12)}{3(18)}} = 58in.$$

An embedment length of 60 in. can be used. If this length is impractical, the flanges of the embedded girders can be widened. For a 30 in. flange width, the required embedment length is 45 in. Although not discussed here, sufficient confinement reinforcement should be provided at the connection.

5.5 CONCLUSIONS

Seismic design guidelines were developed based on the analytical investigations and available experimental research. This includes the calculation of the embedment lengths, pile displacement capacity evaluation, and damping evaluation as discussed above. In addition, guidelines for analytical modeling of piles and soil-pile interaction were presented. A detailed example is presented in a step-by-step manner to illustrate the application of the recommended design guidelines.

Equations for calculating the embedment length of steel girders into the abutment to ensure the connection rigidity are presented. It was shown that a typical girder-abutment connection introduces flexibility in the system, and sufficient embedment length is required so that the rigid connection assumption is valid. These equations are also used to determine the embedment length of piles into the abutment to develop their plastic flexural capacity. The piles should have sufficient embedment length into the abutment such that plastic capacity can be developed without loss of integrity in the connection.

Pile displacement capacity corresponding to 10% radian rotation in the pile is recommended based on the available experimental research. It is noted that because of the confinement provided by the soil, the piles can sustain large ductility demand as long as the pile has sufficient embedment length into the abutment. Research has shown that large displacements can be imposed without breaking the piles, but the maximum sustainable displacement is limited by the pile-abutment connection. The typical pile embedment length may not be sufficient and could lead to premature disintegration of the connection limiting the displacement capacity.

A procedure for incorporating the system level damping that uses modal pushover response is introduced. This procedure takes into account the yielding and inelastic response of various components like abutment-soil interaction, soil-pile interaction, pile inelasticity, and column inelasticity. The system level damping is evaluated on the main longitudinal and transverse translation modes where the pushover was performed. In the earthquake analysis (i.e. response spectrum analysis), the calculated damping is applied to these modes only. A 5% structural damping is applied to the remaining modes. In the design example used to illustrate the recommended seismic design guidelines, the calculating damping ratio in the longitudinal direction is 6% and in the transverse direction the damping ratio is 13%. Damping in the transverse direction is larger due to more inelastic demand in the piles.

Table 5-1 Soil Profile

Depth (in)	Soil Type	C (lb/in^2)	ϕ (degrees)	E50	K (lb/in^3)	γ (lb/ft^3)
0 – 240	Stiff Clay	11	0	0.005	1000	124
240 – 384	Stiff Clay	5	0	0.01	300	124
384 – 480	Sand	0	33	0	92	52
480- 720	Sand	0	29	0	40	52

Table 5-2 Effective stiffness at first yield of the girder-abutment connection

DOF	**Unit**	**Description**	**K_{pos}**	**K_{neg}**
U1	kip/in	vertical action	496	219
U2	kip/in	longitudinal action	13,465	20,068
U3	kip/in	transverse action	181	181
R1	kip-in/rad	rotation about vertical axis	1.08E+08	1.08E+08
R2	kip-in/rad	rotation about longitudinal axis	1.94E+06	1.94E+06
R3	kip-in/rad	rotation about transverse axis	1.68E+08	3.14E+08

K_{pos} = effective stiffness at positive region of the backbone curve

K_{neg} = effective stiffness at negative region of the backbone curve

Table 5-3 Vibration periods and mass participation ratios

Mode	**Period**	**UX**	**UY**	**UZ**	**RX**	**RY**	**RZ**
No	Sec	Unitless	Unitless	Unitless	Unitless	Unitless	Unitless
1	1.373	0	0.750	0	0.917	0	0.541
2	0.873	0	0	0	0	0	0.255
3	0.609	0	0.163	0	0.045	0	0.117
4	0.609	0	0	0.196	0	0.139	0
5	0.439	0.965	0	0	0	0.014	0
6	0.372	0	0.012	0	0.003	0	0.009
7	0.299	0	0	0	0	0	0.018
8	0.252	0	0.054	0	0	0	0.039
9	0.236	0.005	0	0	0	0.021	0
10	0.200	0	0	0	0	0	0.001
11	0.195	0	0	0.378	0	0.268	0
12	0.174	0.002	0	0	0	0.134	0

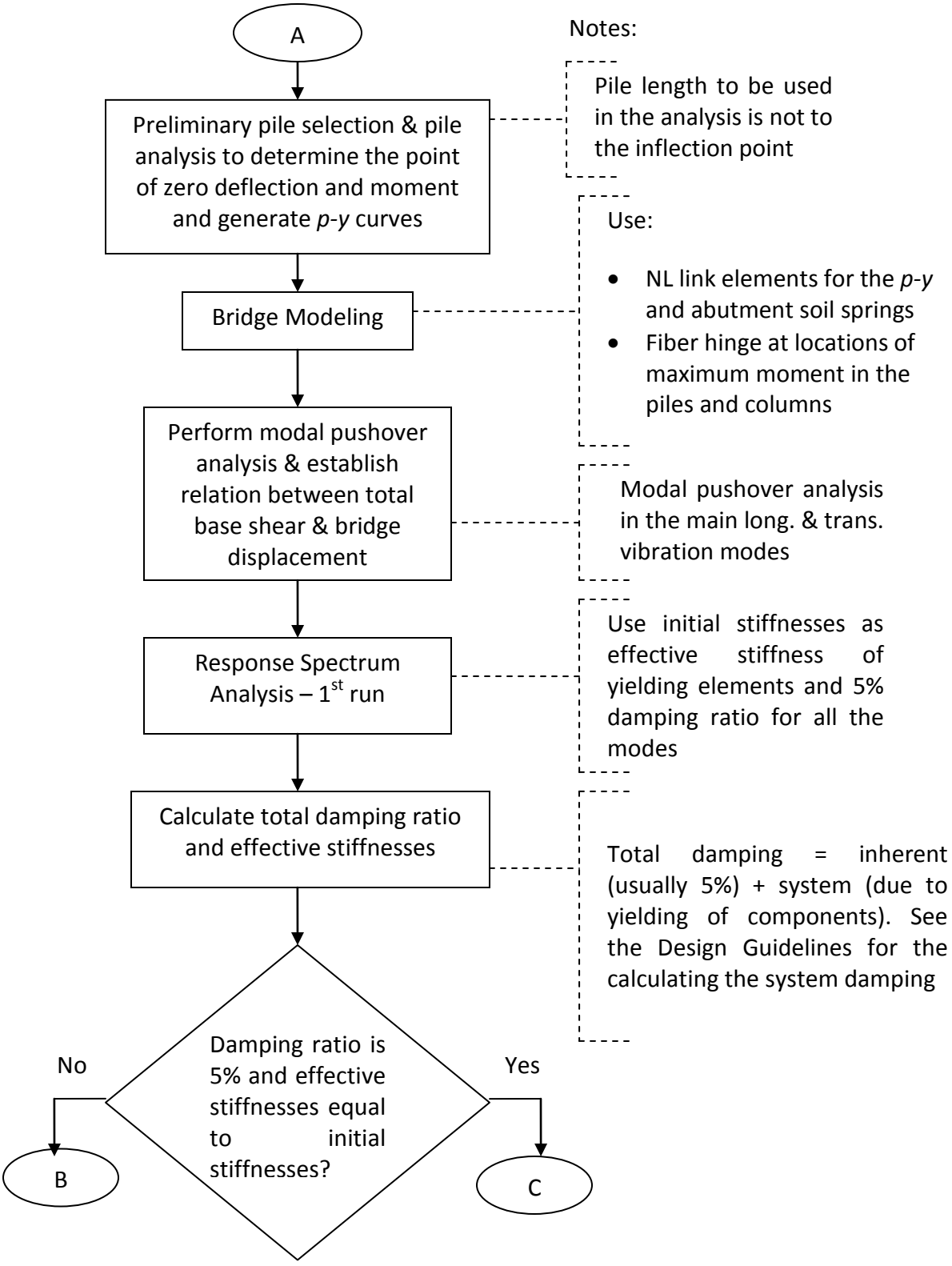

Figure 5-1 Flowchart for the seismic analysis and design of bridges with integral abutments

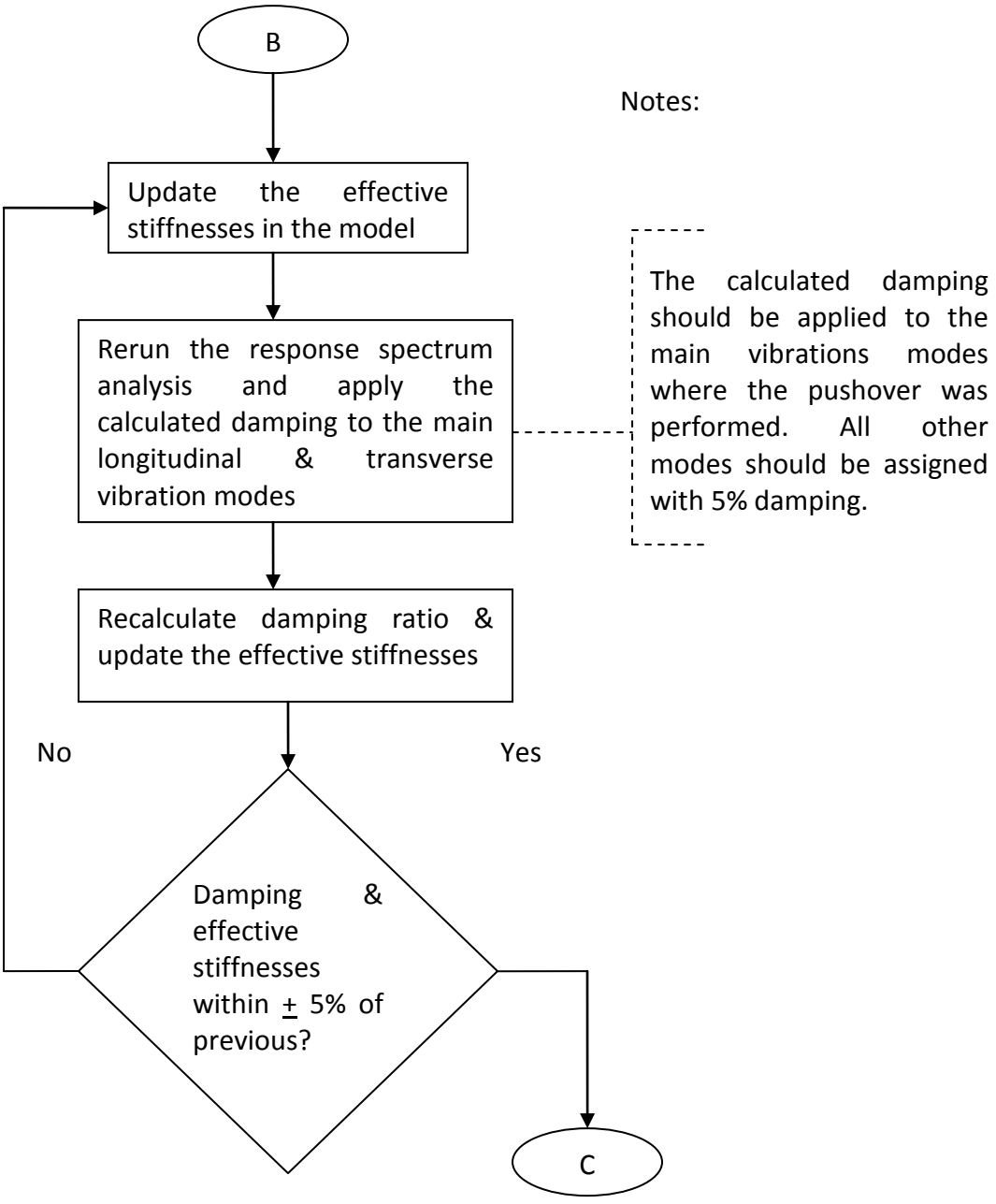

Figure 5-2 Flowchart for the iteration on damping ratio and effective stiffnesses of yielding elements

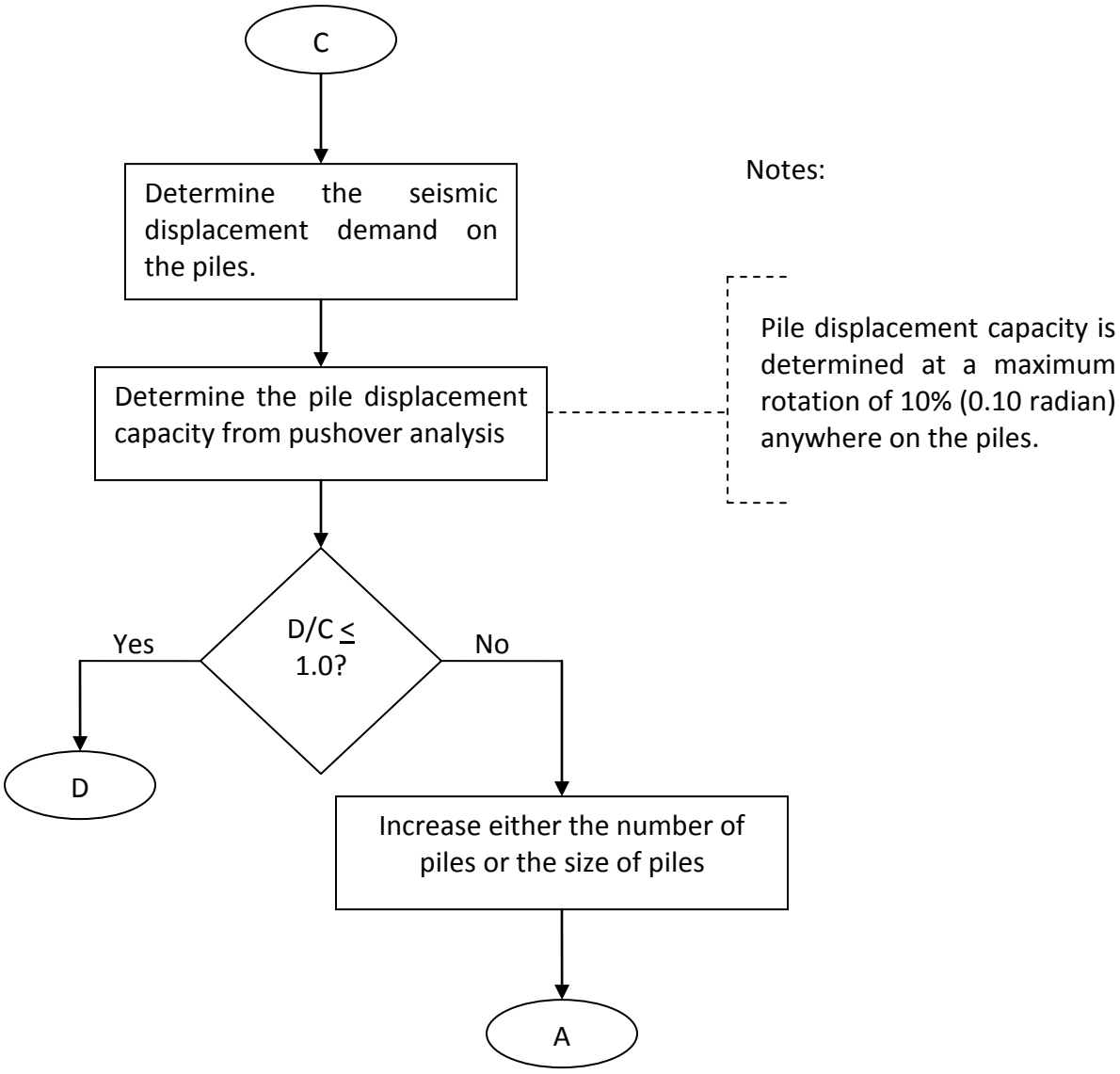

Figure 5-3 Flowchart for the determination of pile displacement demand-capacity ratio

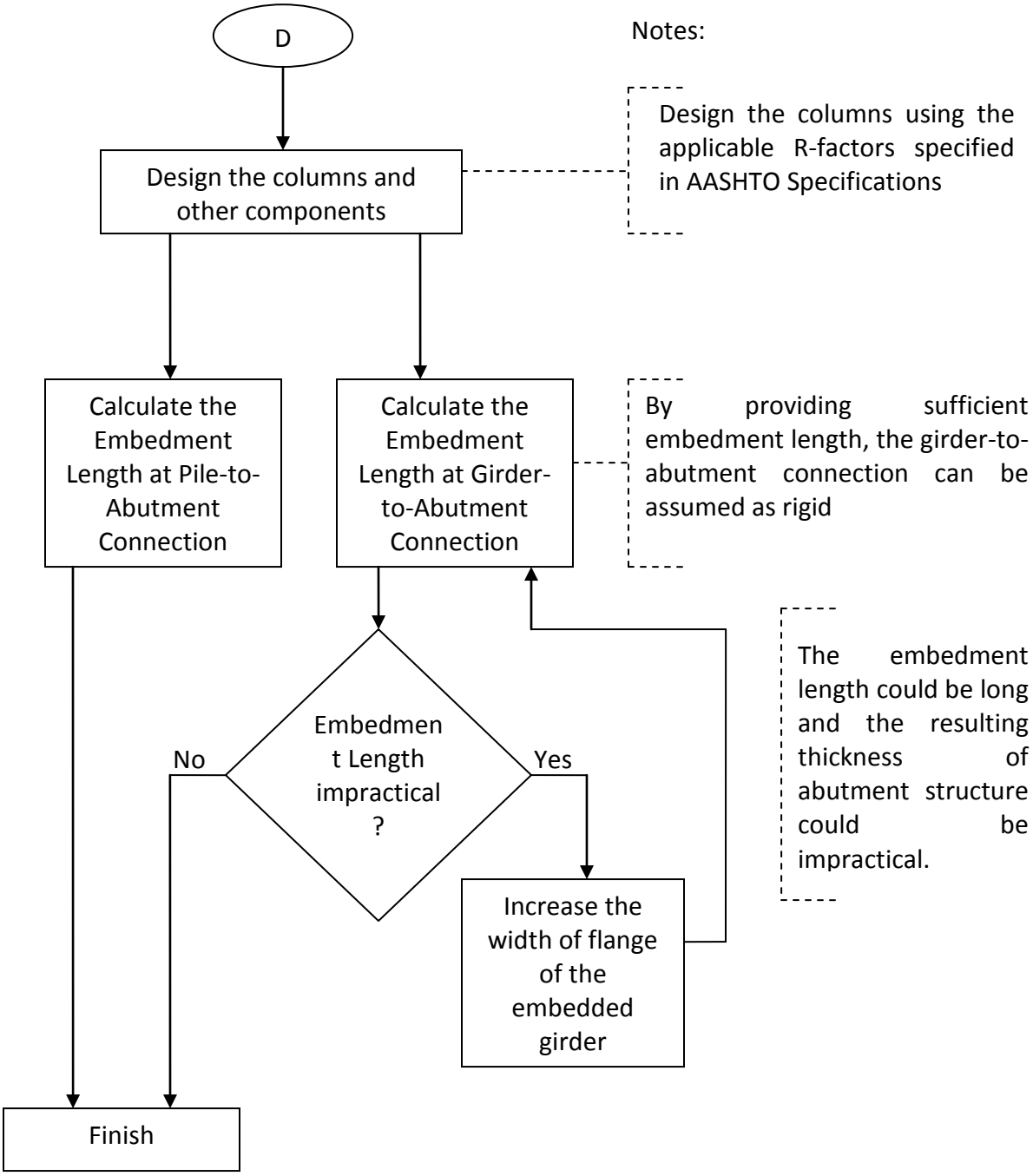

Figure 5-4 Flowchart for the determination of pile and embedment length into the abutment structure

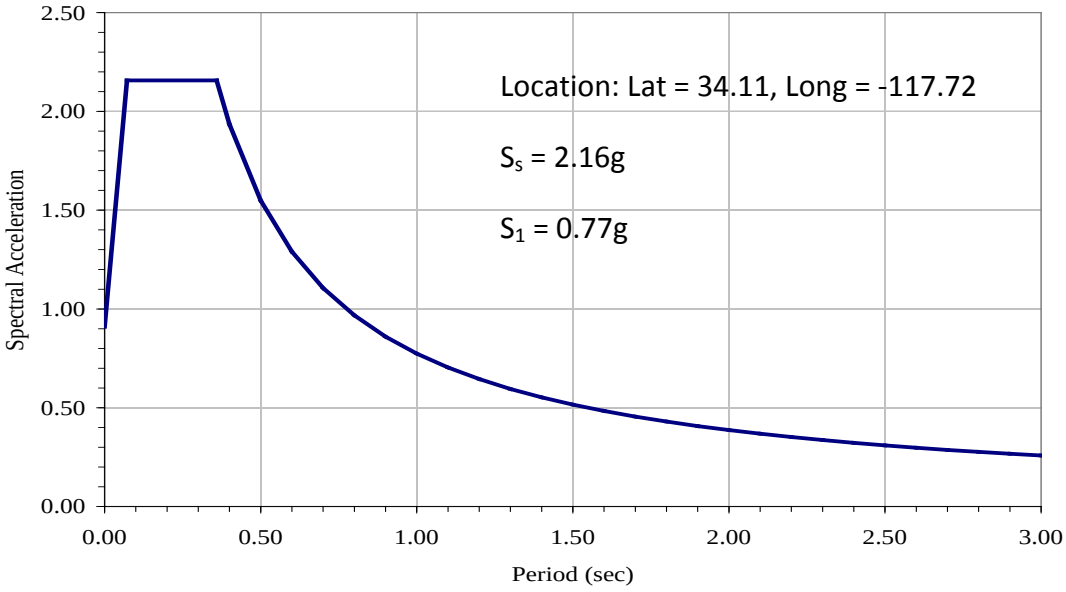

Figure 5-5 Design spectrum

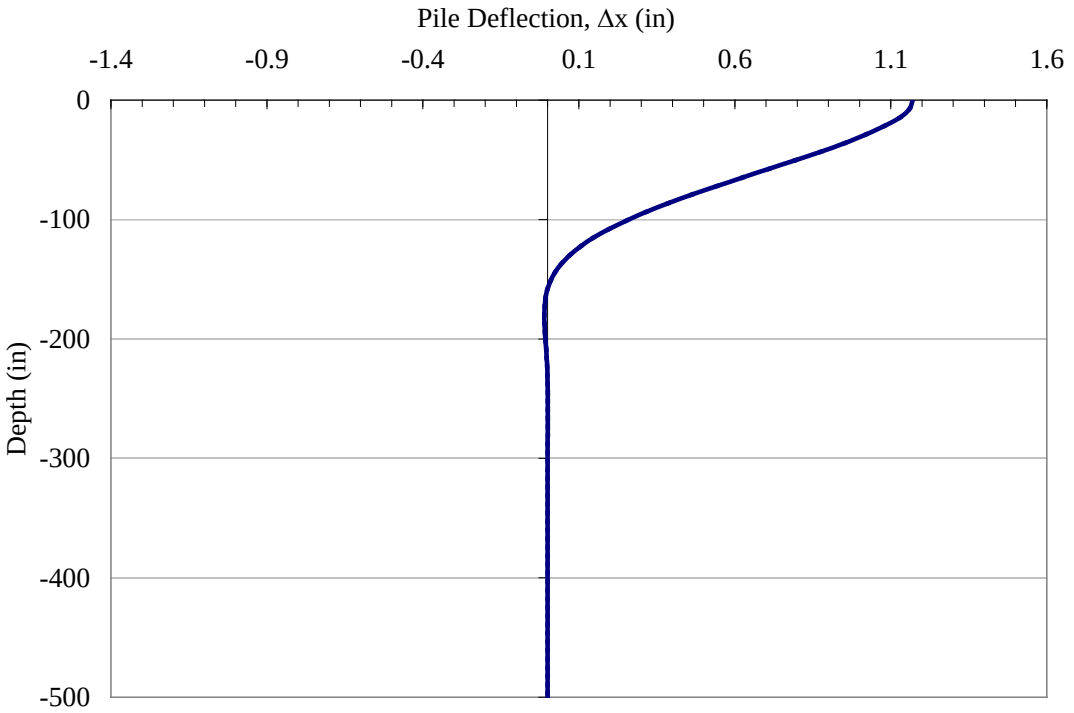

(a)

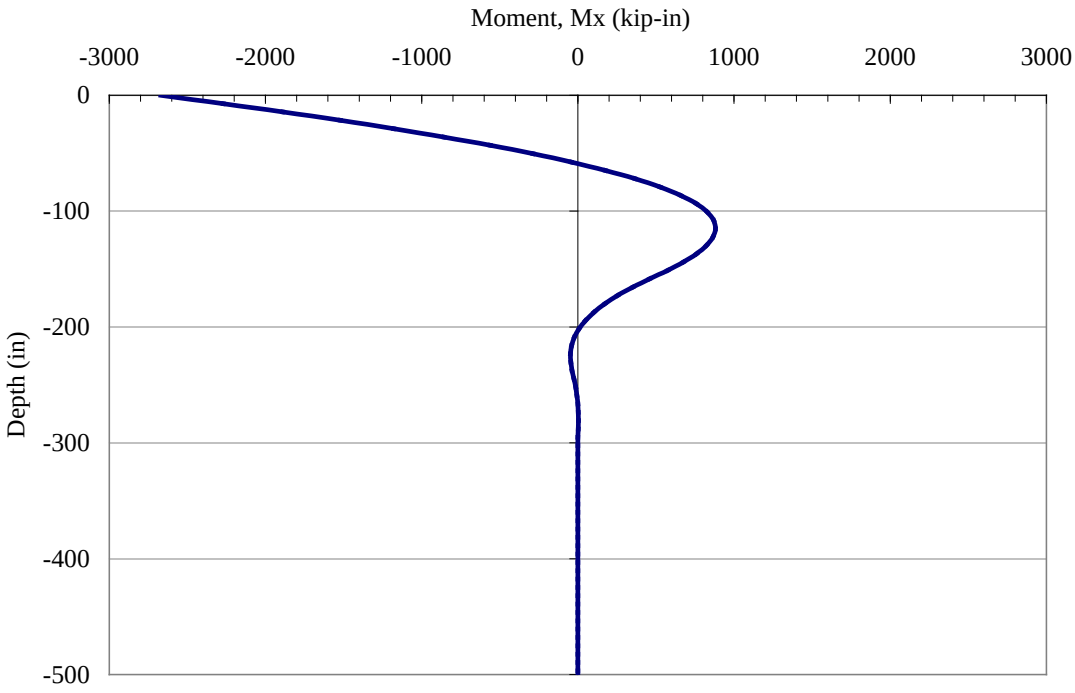

(b)

Figure 5-6 Pile deflection and moment about strong (x) axis when the moment at top of pile reached M_{px} = 2,656.5 kip-in

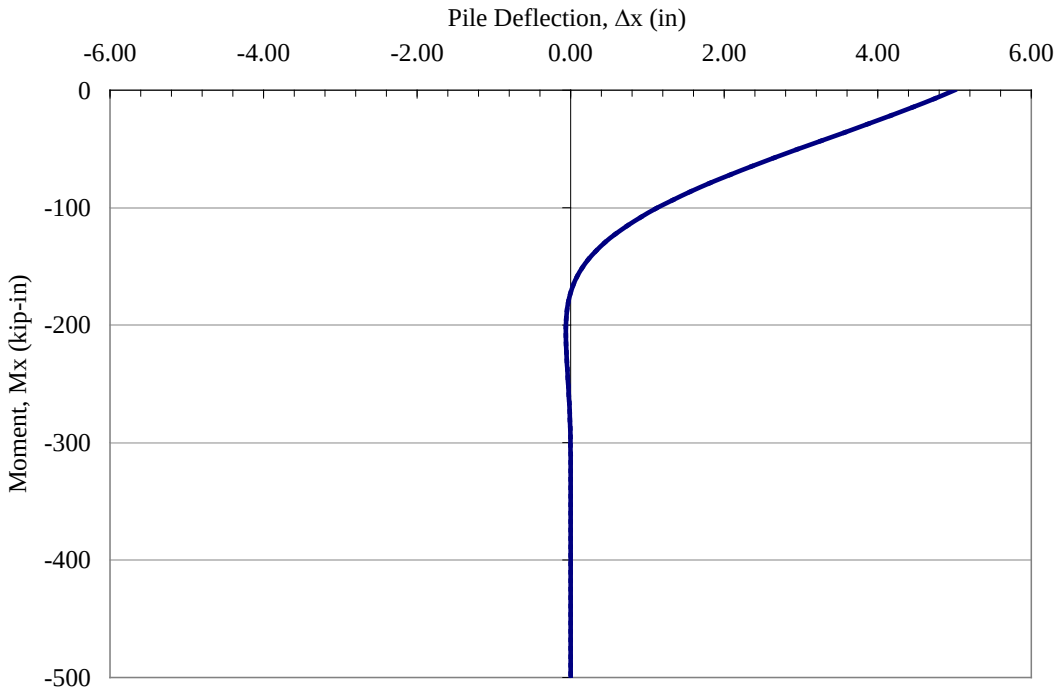

(a)

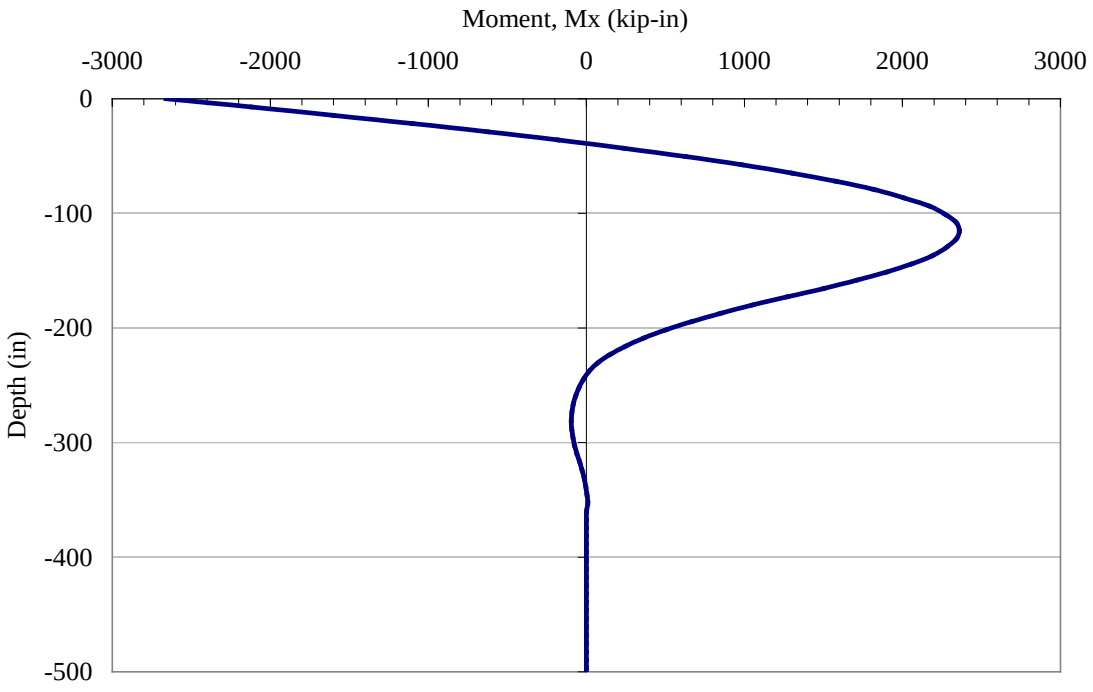

(b)

Figure 5-7 Pile deflection and moment about the strong (x) axis when the deflection at top of pile Δ_x = 5 in.

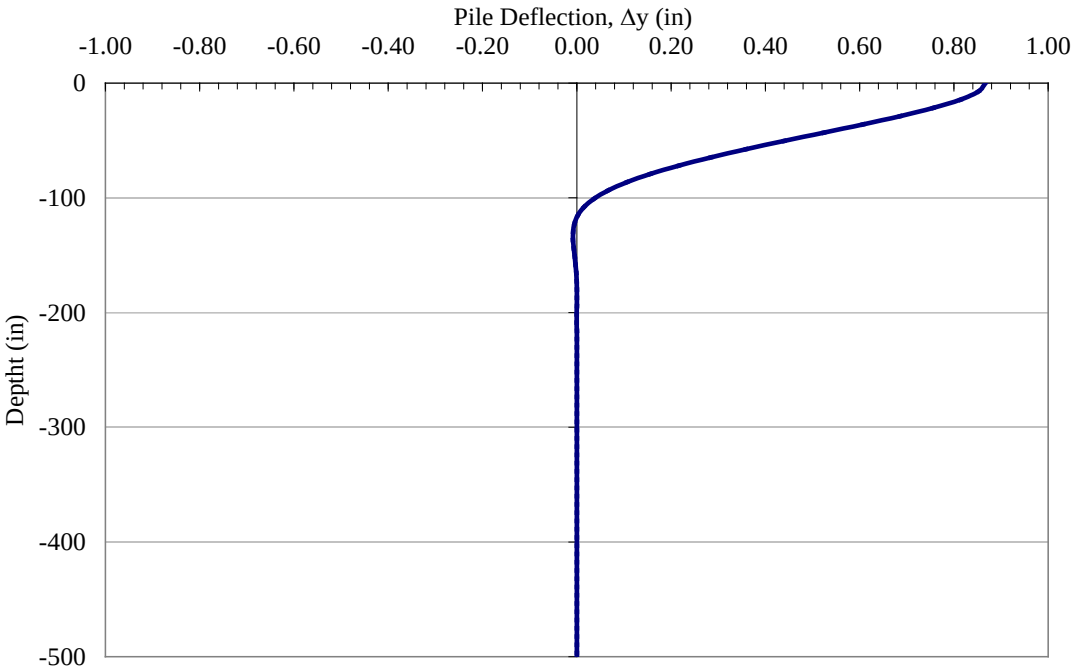

(a)

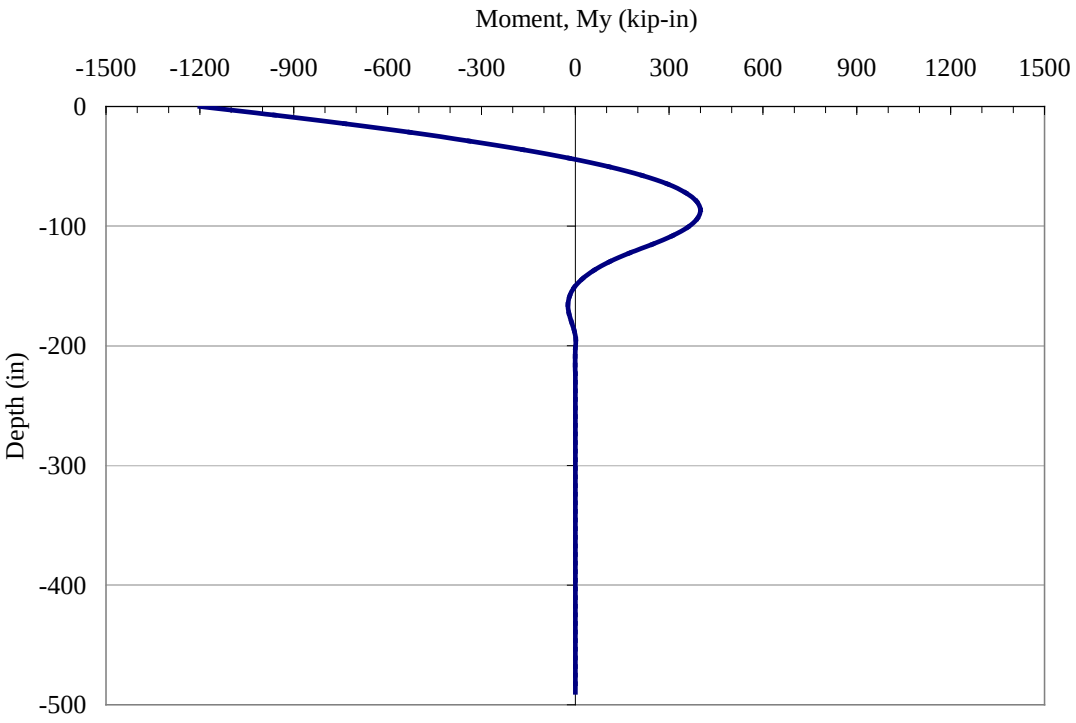

(b)

Figure 5-8 Pile deflection and moment about weak (y) axis when the moment at top of pile reached M_{py} = 1,199 kip-in

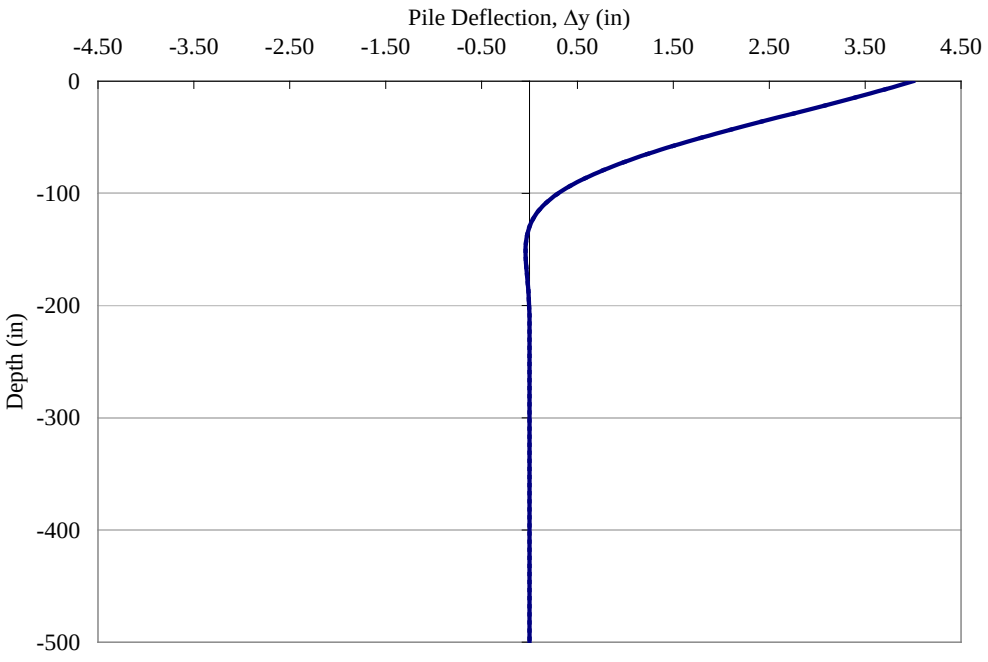

(a)

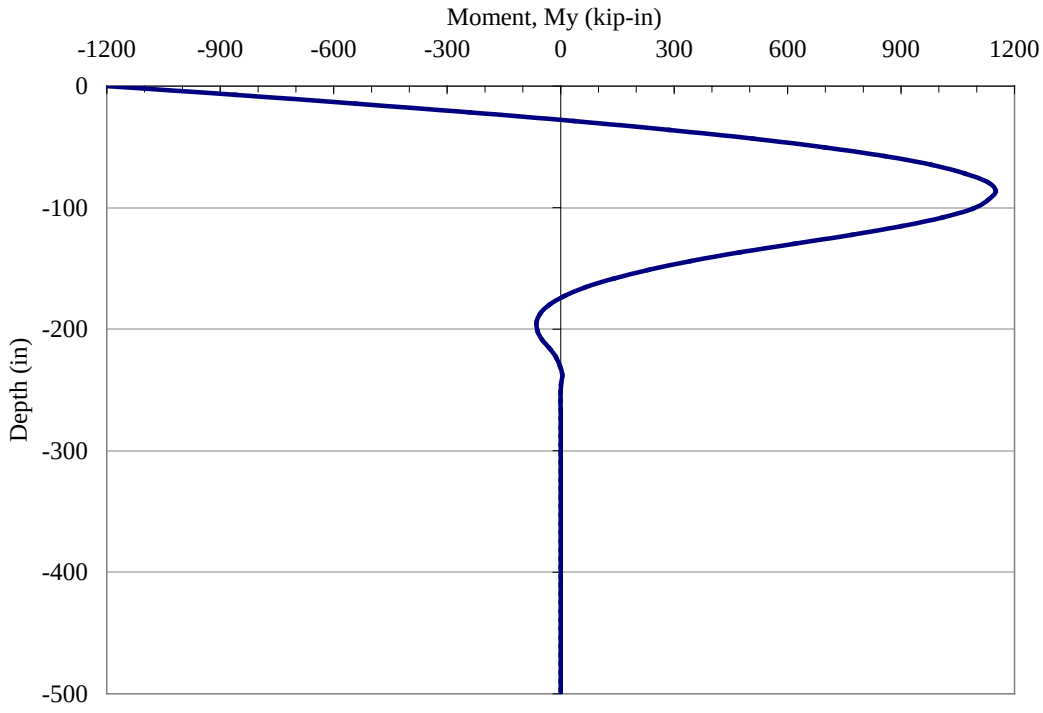

(b)

Figure 5-9 Pile deflection and moment about the weak (y) axis when the deflection at top of pile Δ_y = 4 in

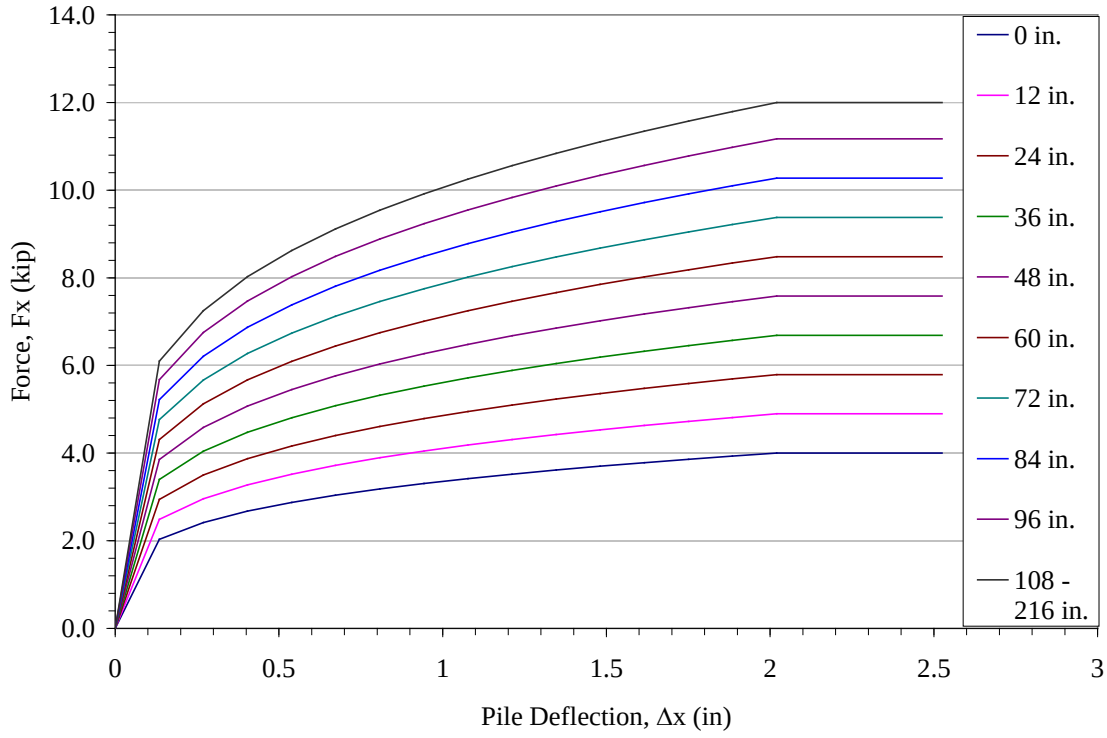

Figure 5-10 *p-y* springs along the strong (x) axis

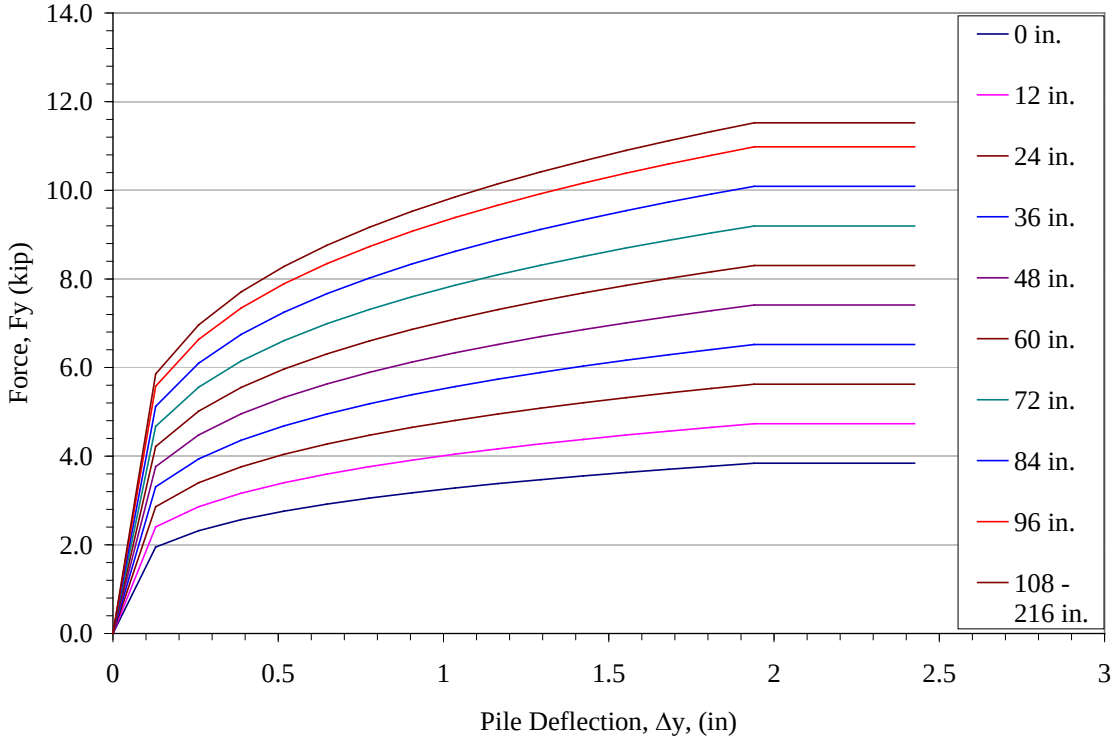

Figure 5-11 *p-y* springs along the weak (y) axis

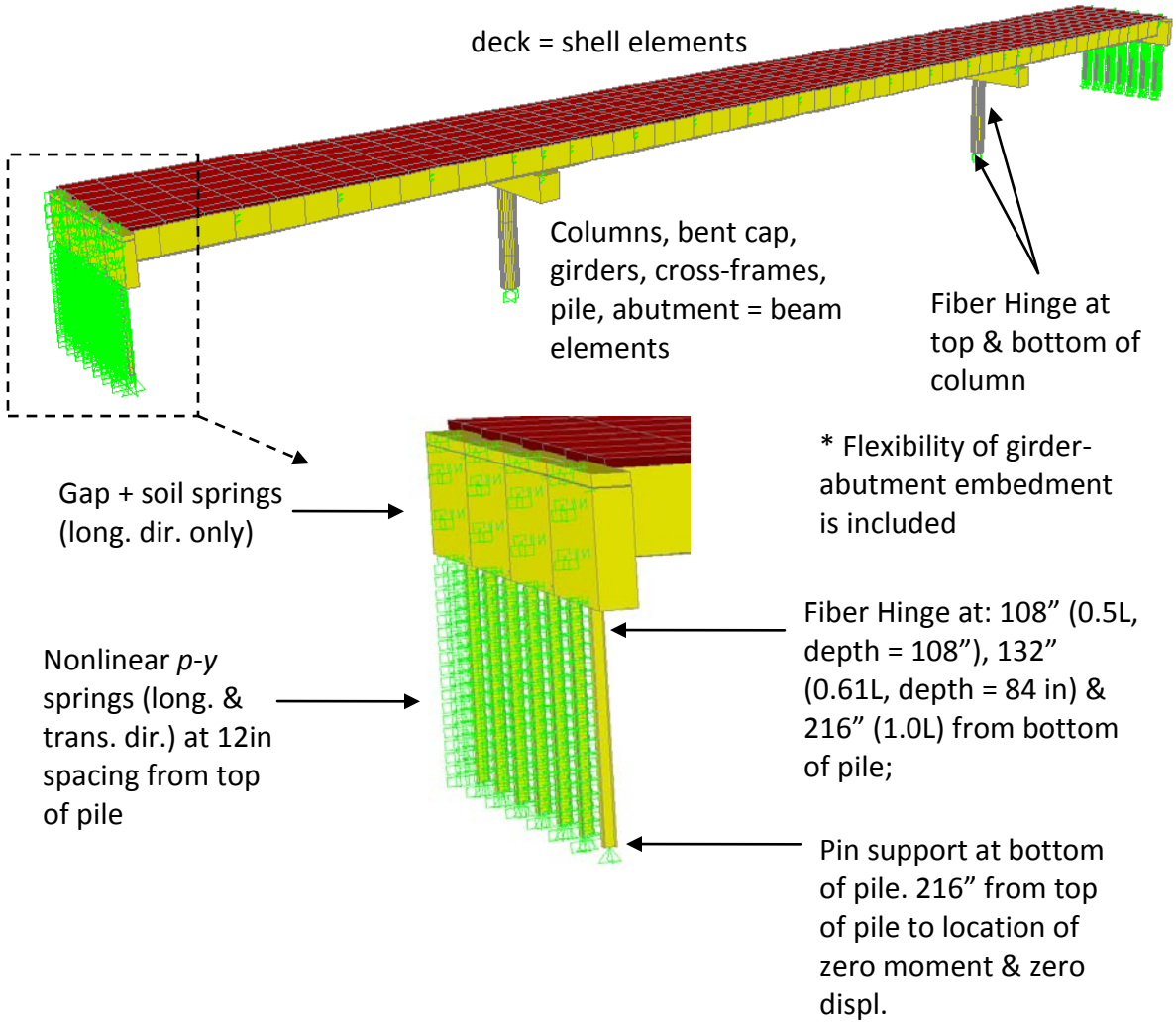

Figure 5-12 Finite element model of the example bridge

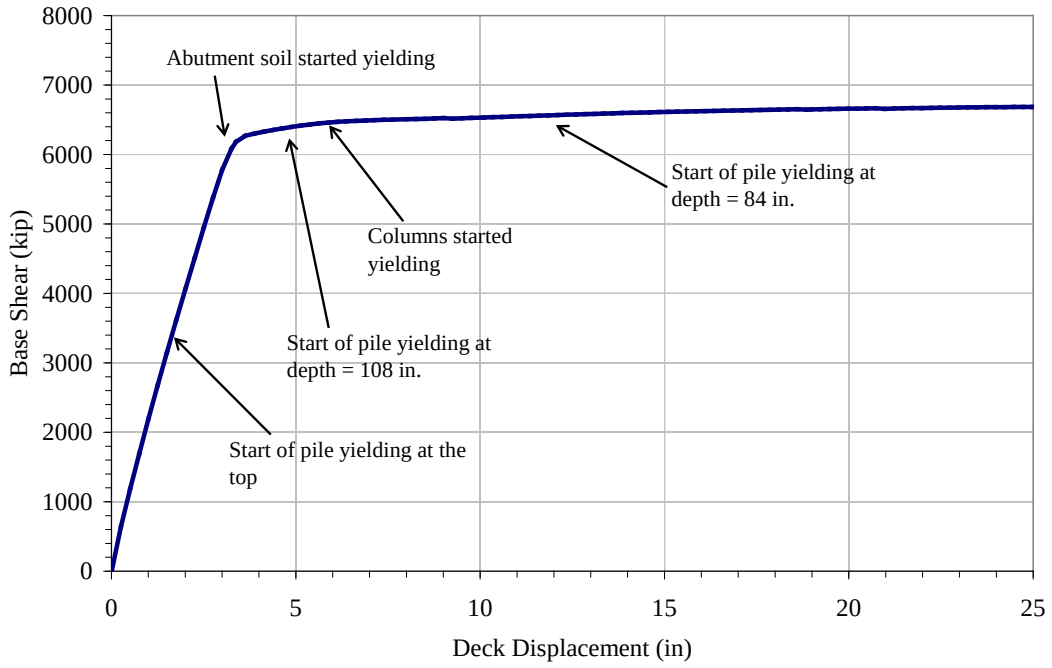

Figure 5-13 Total base shear versus deck displacement in the longitudinal direction from the 5th mode pushover

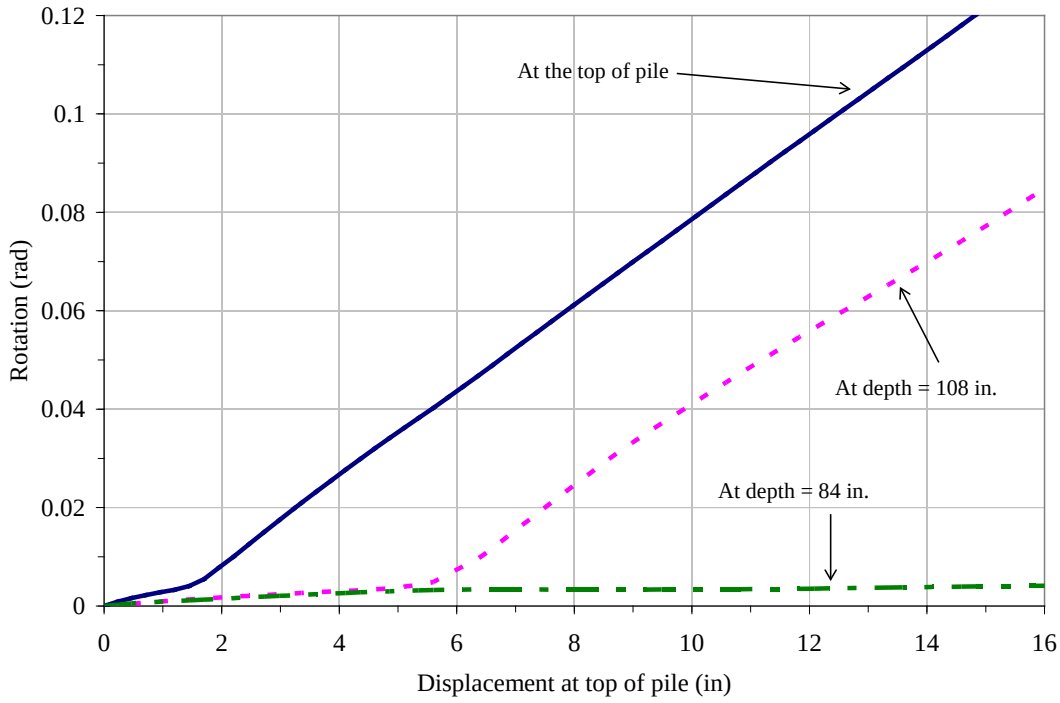

Figure 5-14 Pile fiber hinge rotation versus displacement at top of pile in the longitudinal direction from the 5th mode pushover

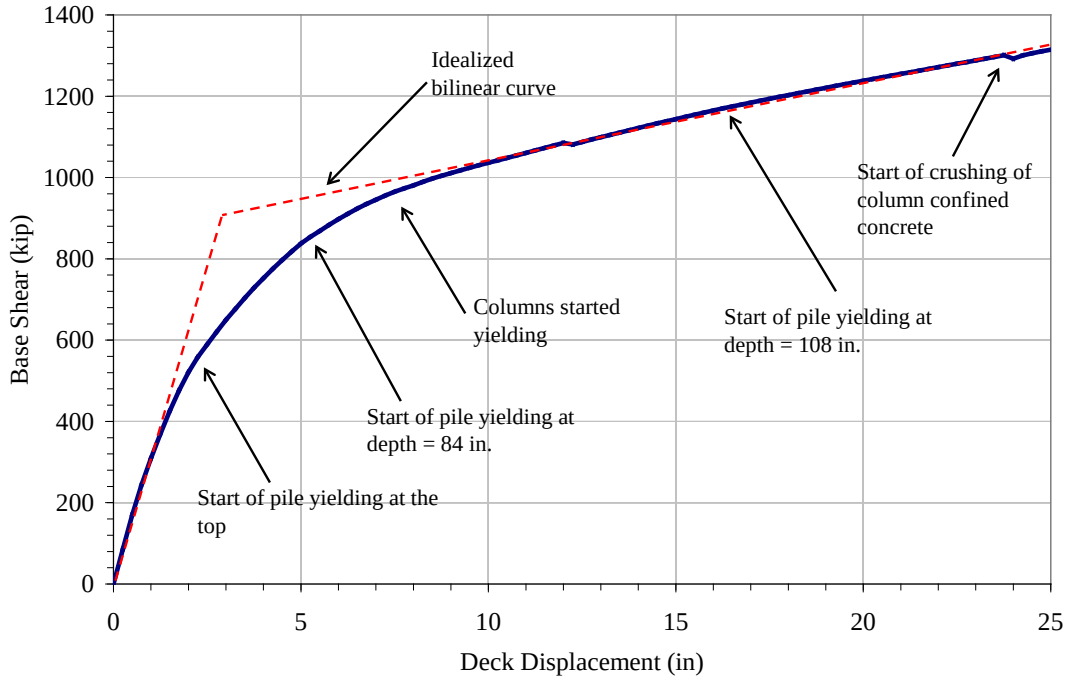

Figure 5-15 Total base shear versus deck displacement in the transverse direction from the 1st mode pushover

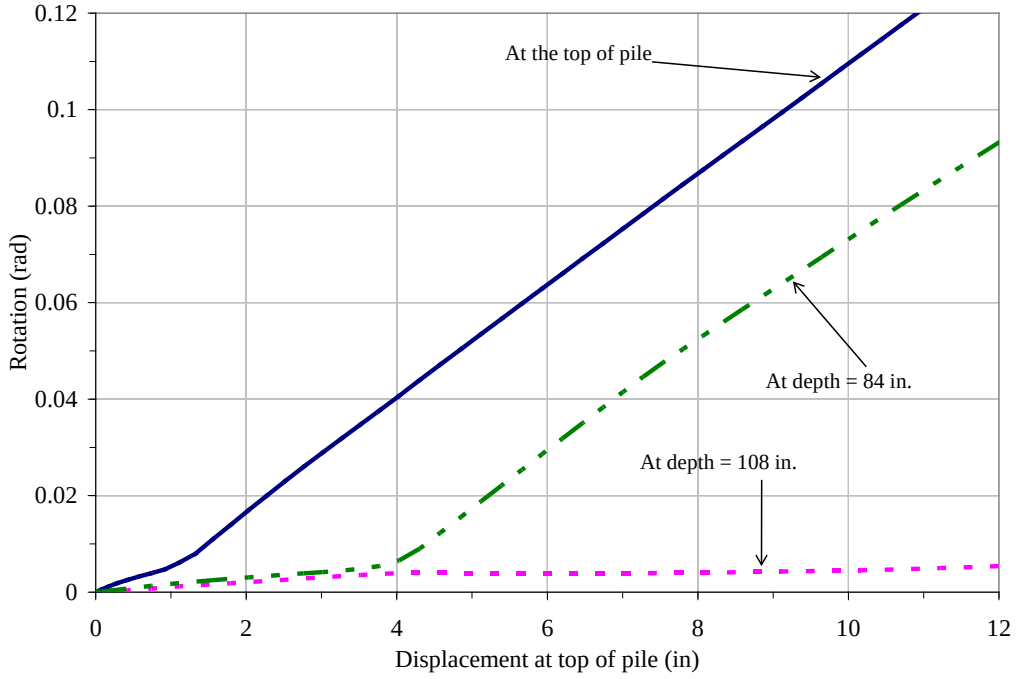

Figure 5-16 Pile fiber hinge rotation versus displacement at top of pile in the transverse direction from the 1st mode pushover

Chapter 6 SUMMARY AND CONCLUSIONS

6.1 SUMMARY AND CONCLUSIONS

Local and global computational models were developed to study the seismic response characteristics of steel bridges with integral abutments. A finite element model of a typical girder-abutment connection was using the computer program ADINA. The analysis of this connection was used to establish the stiffness properties (3 translations and 3 rotations) of nonlinear springs that define the connection flexibility. These springs can be used in global 3D models to represent the complex interaction of the girder-abutment connection. The global 3D models were then used to determine the effect of girder-abutment connection flexibility, abutment-soil interaction, and soil-pile interaction on the dynamic characteristics of integral abutment bridges. The global 3D models were also used to establish the seismic load path and seismic response characteristics of integral abutment bridges. Finally, seismic design guidelines were proposed based on the findings of this study and based on available experimental research. Equations for the design of girder-abutment and pile-abutment connections and for evaluating the system damping were developed. A design example was provided to illustrate the application of the design guidelines.

A 3D finite element model of a typical girder-abutment connection was developed to establish the stiffness properties of the nonlinear springs used to represent the connection flexibility. These springs, along with springs that define the abutment-soil and soil-pile interactions, were utilized in global 3D bridge computational models to determine their effect on the overall bridge structural dynamics. This investigation has shown that the typical girder embedment length is insufficient to ensure a rigid connection. It was shown that the connection flexibility increased the vibration period of the main transverse translation mode up to 50%. As such, a procedure for calculating the minimum required girder-abutment embedment length to achieve a rigid connection was developed.

The seismic load paths in the longitudinal and transverse directions of a three-span integral abutment bridge were determined using pushover analysis for the dominant translational modes. In the longitudinal direction, a large percentage (72%) of the seismic force was resisted by the abutment-soil passive resistance. In the transverse direction, the overall response was governed by the soil-pile interaction. About 40% of the transverse seismic force was resisted by the soil-pile interaction for each abutment. This shows that the columns in integral abutment bridges were subjected to low seismic forces, thus limiting their damage during seismic events.

A limited investigation on the effect of skew was conducted on a single-span bridge with integral abutments to determine the effect of skew on the dynamic properties and seismic load path. Three models were developed: a) no skew, b) 45-degree skew, and c) 60-degree skew. The results of the analyses showed that the variation of the skew angle caused significant changes in the bridge dynamic characteristics in terms of periods and mode shapes. It was also

shown that the translational modes in the skew bridge are highly coupled between the longitudinal and the transverse translations.

The effectiveness of steel bridges with integral abutments in high seismic zones was also investigated. Three global computational models of three span bridges were developed: (a) integral abutment bridge with piles that have strong axis parallel to abutment axis (3SIAB-PSA), (b) integral abutment bridge with pile strong axis perpendicular to abutment axis (3SIAB-PWA), and (c) seat-type abutment bridge (3SSAB). Nonlinear time history analyses were performed using a suite of artificially generated ground motions matching the AASHTO design spectrum.

The following observations and conclusions were made based on the comparison of the responses of 3SIAB-PSA and 3SIAB-PWA:

- The 3SIAB-PSA performed better than 3SIAB-PWA in terms of the nonlinear response of piles. Thus, the pile strong axis should be oriented parallel to the abutment axis in seismic zones.

- Due to the pile axis orientation, the abutments in 3SIAB-PWA were stiffer in the transverse direction than those in 3SIAB-PSA. This increased the seismic demands at the abutments of 3SIAB-PWA.

- The pile axis orientation was insignificant in the longitudinal direction because this response was dominated by the abutment-soil interaction.

The following observations and conclusions were made based on the comparison of the responses of the integral abutment bridges (3SIAB-PSA and 3SIAB-PWA) and the seat-type abutment bridge (3SSAB):

- The seismic performances of the integral abutment bridges were better than the seat-type abutment bridge in terms of overall displacements and column forces.

- Large displacements were observed in 3SSAB in the longitudinal and transverse directions. The longitudinal displacement in 3SSAB was almost twice the displacement of the integral abutment bridges. Thus, a relatively large seat width should be provided for the seat type bridge due to these large displacements.

- In 3SSAB, all of the seismic forces in the transverse direction were resisted by the columns only. Thus, these columns will experience large inelastic activity (damage) after an earthquake which may require their replacement or bridge removal after severe ground motions.

Seismic design guidelines were developed based on the analytical investigations and available experimental research. The guidelines include the calculation of the embedment lengths, evaluation of pile displacement capacity, and system damping. In addition, guidelines for analytical modeling of the nonlinear response of steel piles were presented. A pile

displacement capacity that produces 10% radian rotation is recommended based on the available experimental research. It was noted that because of the confinement provided by the soil, the piles can sustain large ductility demand as long as the pile has sufficient embedment length into the abutment.

It was shown that a typical girder-abutment connection introduces flexibility in the system, and sufficient embedment length is required to make the rigid connection assumption valid. Thus, equations for determining the required minimum embedment length of steel girders into the abutment to ensure connection rigidity were proposed. These equations were also used to determine the embedment length of piles into the abutment to develop their plastic flexural capacity.

A procedure for evaluating the system level damping was developed. This procedure accounts for the yielding and inelastic response of various components such as abutment-soil interaction, soil-pile interaction, pile inelasticity, and column inelasticity. The system level damping was evaluated in the main longitudinal and transverse translation modes based on pushover analysis. The calculated damping should be applied to these two modes only while performing response spectrum analysis. A detailed example is presented in a step-by-step procedure to illustrate the use of the recommended design guidelines.

6.2 RECOMMENDATIONS FOR FUTURE INVESTIGATIONS

Integral abutment bridges present conditions for abutment-soil-pile-structure interaction that require consistent and reliable procedures for assessing effective system damping. Although the present study introduces a procedure to approximate system-level damping that utilizes push-over response, various types of contributors to effective system damping like soil radiation damping should be investigated. The effective system damping is not a constant value but rather a variable which may be a function of acceleration, velocity, and displacement response of a given structural system.

A more comprehensive analytical model of the bridge system that considers the inertia effect of the abutment soil must be developed. Also, further investigation through detailed finite element analysis of the connection with different embedment lengths and girder flange widths, similar to the model presented in this report, is needed to verify the influence of embedment length on the connection flexibility. This investigation will establish relationship between typical embedment lengths and certain bridge parameters like span length, number of girders, and number of piles.

Experimental investigation on integral bridge abutment as a system should be established. Experiments similar to seat-type abutment tests (Maroney 1995) are needed for integral bridge abutments to better assess the subsystem cyclic response of integral abutments under large cyclic deformations.

REFERENCES

Abendroth, R.E., and Greimann, L.F. (2005). Field Testing of Integral Abutments. Final Report. Center for Transportation Research and Education, Iowa State University, June 2005.

ADINA (2008). *Automatic Dynamic Incremental Nonlinear Analysis (ADINA)*, ADINA R & D, Inc., Watertown, MA, www.adina.com.

Arockiasamy, M., Butrieng, N.; and Sivakumar, M. (2004). "State-of-the-Art of Integral Abutment Bridges: Design and Practice", ASCE Journal of Bridge Engineering, 9(5), 497-506.

California Department of Transportation. (1992). *PEQIT Report – Highway Bridge Damage - Petrolia Earthquakes No. 1, No. 2, No. 3. of April 25-26, 1992*, California Department of Transportation, Sacramento California.

Astaneh-Asl, A., Bolt, B., McMullin, K.M., Donikian, R.R., Modjtahedi, D., and Cho, S. (1994). "Seismic Performance of Steel Bridges during the 1994 Northridge Earthquake." *Report UCB/CE-STEEL-94/01*, Department of Civil Engineering, University of California at Berkeley, Berkeley, CA

Astaneh-Asl, A. and Ravat, S., 1998. "Cyclic Behavior and Seismic Design of Steel H-Piles," *Report No. UCB/CEE-98-01*, Department of Civil and Environamental Engineering, University of California, Berkeley, CA.

Bruneau, M., Wilson, J.W., and Tremblay, R. (1996). "Performance of Steel Bridges during the 1995 Hyogoken-Nanbu (Kobe, Japan) Earthquake." *Canadian J. of Civil Eng.*, 23(3), 678-713.

Burdette, E. G., J. H. Deatherage, and D. W. Goodpasture. (2000). Behavior of Laterally Loaded Piles Supporting Bridge Abutments – Phase I. Final Report. Center for Transportation Research, University of Tennessee, Knoxville, July 2000.

Burdette, E. G., J. H. Deatherage, and D. W. Goodpasture. (2007). Behavior of Laterally Loaded Piles Supporting Bridge Abutments – Phase II. Final Report. Center for Transportation Research, University of Tennessee, Knoxville, January 2007.

Burdette, E.G., Ingram, E.E., Tidwell, J.B., Goodpasture, D.W., Deatherage, J.H., and Howard, S.C. (2004). "Behavior of Integral Abutments Supported by Steel H-Piles." *Transportation Research Record: Journal of the Transportation Research Board, No. 1892*, National Research Council, Washington, D.C., 2004, pp. 24–28.

Burke, M. P., Jr. (1993). "Integral bridges: Attributes and limitations." *Transportation Research Record. 1393*, National Research Council, Washington, D.C., 1–8.

Caltrans SDC (2006). "Seismic Design Criteria." Version 1.4, California Department of Transportation, Sacramento, CA.

Civjan, S.A., Bonczar, C., Breña, S.F., DeJong, J., and Crovo, D. (2007). "Integral Abutment Bridge Behavior: Parametric Analysis of a Massachusetts Bridge." *ASCE Journal of Bridge Engineering*, 12(1), 64-71.

Computers and Structures, Inc. (2008). SAP2000, Version 12.0.1, Integrated Structural Analysis and Design Software, Berkeley, CA.

Conboy, D. W., and Stoothoff, E. J. (2005). "Integral abutment design and construction: The New England experience." *Proceedings of the Integral Abutment and Jointless Bridges 2005 Conference*, Federal Highway Administration, 50–60, Baltimore, Mar. 2005.

Dehne, Y. and Hassiotis, S. (2003). "Seismic Analysis Of Integral Abutment Bridge Scotch Road I-95 Project." Proceedings of the ASCE 16th Engineering Mechanics Conference, University of Washington, Seattle, July, 2003.

England, G.L., Tsang, N.C.M., and Bush, D.I. (2000). Integral Bridges – A Fundamental Approach to The Time-Temperature Loading Problem, Imperial College and The Highway Agency, U.K., Thomas Telford, 2000.

Faraji, S., Ting, J.M., Crovo, D.S. and Ernst, H. (2001). "Nonlinear Analysis Of Integral Bridges: Finite-Element Model." ASCE Journal of Geotechnical and Geoenvironmental Engineering, 127(5), 454-461.

Federal Highway Administration (FHWA), (2003a). Comprehensive Design Example for Prestressed Concrete (PSC) Girder Superstructure Bridge with Commentary (in US Customary Units), FHWA Report No. FHWA NHI-04-043, November 2003.

Federal Highway Administration (FHWA), (2003b). LRFD Design Example for Steel Girder Superstucture Bridge with Commentary, FHWA Report No. FHWA NHI-04-041, December 2003.

Federal Emergency Management Agency, 2000. *FEMA 356: Prestandard and Commentary for the Seismic Rehabilitation of Buildings*., Washington, D.C.

Fennem, J.L., Laman, J.A., and Linzell, D.G. (2005). "Predicted and Measured Response of an Integral Abutment Bridge." ASCE Journal of Bridge Engineering, 10(6), 666-677.

Gasparini, D.A. and Vanmarcke, E.H., (1976). SIMQKE, Department of Civil Engineering, Massachusetts Institute of Technology, Cambridge, MA.

Goel, R.K. (1997). "Earthquake Characteristics of Bridges with Integral Abutments." Journal of Structural Engineering, 123(11), 1435-1443.

Hassiotis, S., Khodair, Y., Roman, E., and Dehne, Y. (2006). Evaluation of Integral Abutments. Final Report, FHWA-NJ-2005-025, Department of Civil, Environmental and Ocean Engineering, Stevens Institute of Technology ,NJ.

Hoppe, E. J. and Gomez, J. P. (1996). Field study of an integral backwall bridge, Virginia Transportation Research Council, VTRC 97-R7, October 1996.

Ingram, E.E., Burdette, E.G., Goodpasture, D.W., and Deatherage, J.H. (2003). "Evaluation of Applicability of Typical Column Design Equations to Steel H-Piles Supporting Integral Abutments." AISC Engineering Journal, First Quarter, 50-58.

Itani A. and Sedarat, H. (2000). Seismic Analysis of the AISI Design Examples of Steel Highway Bridges, CCEER 00-08, November 2000.

Khodair, Y.A., and Hassiotis, S. (2005). "Analysis of soil–pile interaction in integral abutment." Journal of Computers and Geotechnics, Elsevier, 32, 201–209.

Kunin, J., and Alampalli, S. (2000). "Integral abutment bridges: Current practice in United States and Canada." Journal of Performance of Constructed Facilities, 14(3), 104–111.

Maroney, B.H. (1995). *Large Scale Bridge Abutment Tests to Determine Stiffness and Ultimate Strength under Seismic Loading*, Ph.D. Dissertation, University of California, Davis.

Maruri, R., and Petro, S. (2005). "Survey Results." *Proceedings of the Integral Abutment and Jointless Bridges 2005*, Federal Highway Administration, 12-29, Baltimore, Mar. 2005.

Mistry, V.C. (2000). "Integral Abutment and Jointless Bridges." Proceedings of the Conference of High Performance Steel Bridge, Baltimore, Maryland (http://www.nabro.unl.edu/articles/index.asp).

Shamsabadi, A. and Kapuskar, M. (2010) "Nonlinear Soil-Abutment-Foundation-Structure Interaction Analysis of Skewed Bridges Subjected to Near-Field Ground Motions." *Journal of the Transportation Research Board*, No. 2202, Transportation Research Board of the National Academies, Washington, D.C., 192-205.

Soltani, A. A., and Kukreti, A. R. (1992). "Performance evaluation of integral abutment bridges." *Transportation Research Record. 1371*, National Research Council, Washington D.C., 17–25.

Wang, S-T. and Reese, L.C. (1993). "COM624P – Laterally Loaded Pile Analysis Program for the Microcomputer, Version 2.0." *Report No. FHWA-SA-91-048*, Federal Highway Administration (FHWA), Washington D.C.

Wasserman, E. P., and Walker, J. J. (1996). Integral Abutments for Steel Bridges. In *Highway Structures Design Handbook, Vol 2.* Chicago: American Iron Steel Institue.

Yannotti, A.P., Alampalli, S.A., and White II, H.L. (2006). "New York State Department of Transportation's Experience with Integral Abutment Bridges", Proceedings of the International Workshop on the Bridges with Integral Abutment – Topics of Relevance for the INTAB Project, Lulea University of Technology, 5-12, Sweden, Oct. 2006.

APPENDIX A

Comparison of Fiber and PMM Hinge Nonlinear Response

The nonlinearity of frame elements can be represented by link elements, PMM (axial load – biaxial moment interaction) hinge, or fiber hinge. The link elements consist of predefined uncoupled force-deformation curves. The PMM hinge also consists of predefined force-deformation curves but with coupled axial load - biaxial moment behavior. In fiber hinge, the section is divided into axial fibers and each fiber is defined with cross-sectional area and stress-strain curve. The coupled axial load and biaxial moments are calculated by integrating the stresses in each fiber in the section. Therefore, the most accurate of the three is the fiber hinge but at large computational effort. Discussed below is the comparison of the response of a frame with PMM and fiber hinges.

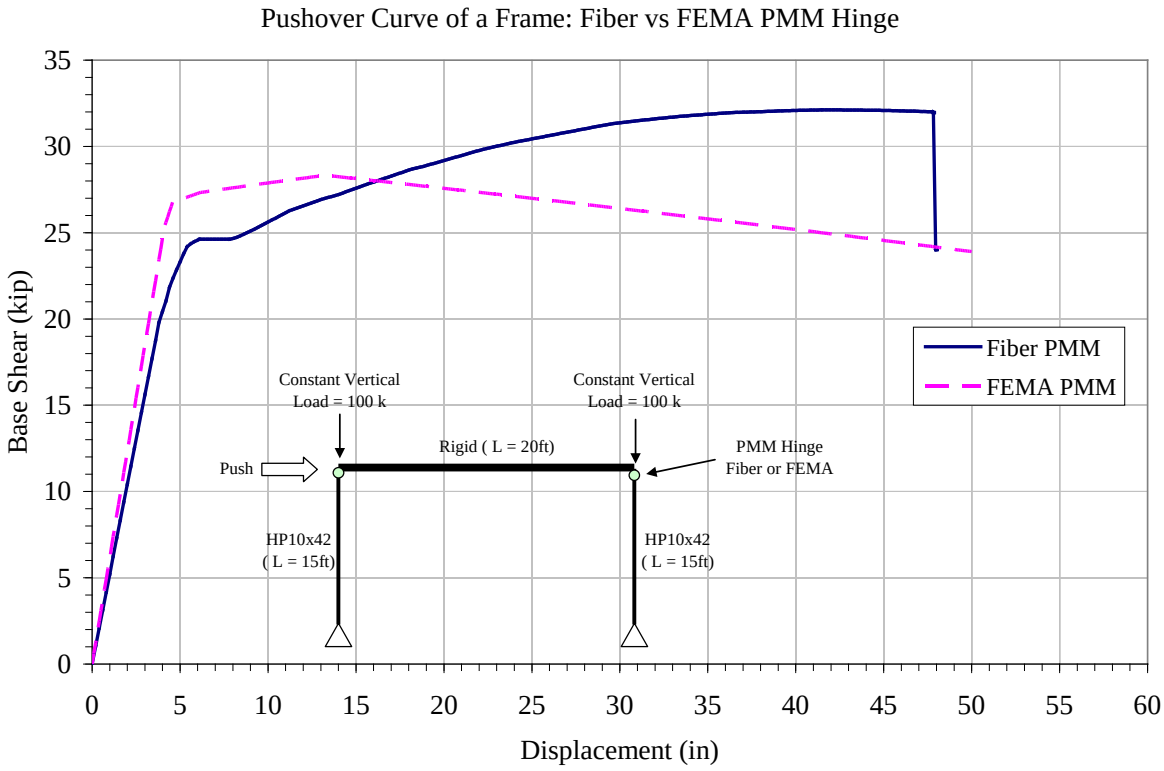

Two one-bay frames were modeled in SAP2000v14 with similar geometry and sections as shown. One frame is with FEMA PMM (axial load – biaxial moment interaction) hinge assigned at the top of the column. The other is with Fiber PMM hinge assigned at the top of the column. A nonlinear static pushover was performed on each frame to understand how SAP handles these types of PMM hinges. A constant vertical loads of 100 kips was applied as shown during the pushover analysis.

Effective yield in the frame with Fiber PMM hinge occurred at a displacement of about 6 in. (4% drift) and a base shear of about 25 kips. The ultimate point was reached at a displacement of

about 48 in. (27% drift) and a base shear of about 32 kips. After the ultimate point was reached, the curve drops as shown due to loss of load carrying capacity of the columns.

In the frame with FEMA PMM hinge, yielding was reached at a displacement of about 5 in. (3% drift) and a base shear of about 27 kips. This yield displacement can be calculated as follows:

$$\theta_y = \frac{ZF_{ye}L}{3EI} = \frac{48.3*55*180}{3*29000*210} = 0.03rad$$
$$\Delta_y = \theta_y L = 0.03*180 = 5in$$

The ultimate displacement depends on a specified plastic rotation θ_p, and in the case of FEMA PMM hinge, it depends on the *b/t* ratio of the flange and web. In this case, the ultimate point is reached at a displacement of 13.5 in. and a base shear of 28 kips. After the ultimate point is reached, the curve is expected to drop (similar to that in the pushover curve of the frame with Fiber PMM hinge). However, as shown, the curve continues on a constant negative gradual slope and tends to continue at a much larger displacement.

Based on the above comparison, the Fiber PMM hinge better represents the behavior after yielding. It can capture the sudden drop in the pushover curve after the ultimate point is reached.

Why use Fiber PMM hinge to represent inelasticity in piles?

- A specified PMM hinge requires manual input of plastic rotation and axial load – biaxial moment interaction values which can be tedious. In the case where the FEMA PMM hinge is specified, SAP automatically calculates these interaction values. The plastic rotation is calculated from Table 5-6 of the FEMA 356 document. This plastic rotation, however, may not be applicable to piles. For example, for HP10x42, the plastic rotation is about $4\theta_y$. Tests conducted on this type of pile show that a larger plastic rotation can be achieved as long as there is sufficient embedment length.
- SAP does not seem to follow the specified backbone curve of a PMM hinge. In the pushover curve shown, it tends to continue on a constant negative gradual slope and not on a steep drop as specified. The Fiber PMM hinge, on the other hand, captures the steep drop in the pushover curve after the ultimate point was reached.
- Tests have shown that piles can undergo large plastic rotations before fracture because of the confinement provided by the soil. In this regard, a Fiber PMM hinge is more suitable than a regular PMM hinge where plastic rotation needs to be specified.